AD_____

Award Number: W81XWH-10-2-0087

TITLE: Mobile Gait Analysis System for Lower Limb Amputee High-Level Activity Rehabilitation

PRINCIPAL INVESTIGATOR: Boyd M. Evans, III, Ph.D.

CONTRACTING ORGANIZATION: UT-Battelle, LLC
Oak Ridge, TN 37830-8050

REPORT DATE: September 2013

TYPE OF REPORT: Annual

PREPARED FOR: U.S. Army Medical Research and Materiel Command
Fort Detrick, Maryland 21702-5012

REPORT DOCUMENTATION PAGE

Form Approved
OMB No. 0704-0188

1. REPORT DATE	2. REPORT TYPE	3. DATES COVERED
September 2013	Annual	1 September 2012 – 31 August 2013

4. TITLE AND SUBTITLE

Mobile Gait Analysis System for Lower Limb Amputee High-Level Activity Rehabilitation

5a. CONTRACT NUMBER

5b. GRANT NUMBER
W81XWH-10-2-0087

5c. PROGRAM ELEMENT NUMBER

6. AUTHOR(S)

Boyd Evans, III, Ethan Farquhar, Andrzej Nycz, Nance Ericson, Martin Pusch, Jason Wilken

E-Mail: farquhare@ornl.gov

5d. PROJECT NUMBER

5e. TASK NUMBER

5f. WORK UNIT NUMBER

7. PERFORMING ORGANIZATION NAME(S) AND ADDRESS(ES)

UT-Battelle, LLC
Oak Ridge, TN 37830-8050

8. PERFORMING ORGANIZATION REPORT NUMBER

9. SPONSORING / MONITORING AGENCY NAME(S) AND ADDRESS(ES)
U.S. Army Medical Research and Materiel Command
Fort Detrick, Maryland 21702-5012

10. SPONSOR/MONITOR'S ACRONYM(S)

11. SPONSOR/MONITOR'S REPORT NUMBER(S)

12. DISTRIBUTION / AVAILABILITY STATEMENT
Approved for Public Release; Distribution Unlimited

13. SUPPLEMENTARY NOTES

14. ABSTRACT

The goal of this research is to develop a mobile gait analysis system (MGAS) for soldiers with lower limb prosthetics to enable improved prosthetic fit, alignment, training, and ultimately re-introduction into pre-injury activities. The system measures the ground reaction forces on the prosthetic foot and determines joint angles and limb segment positions during activities taking place outside of a conventional gait analysis laboratory. This year a number of activities were completed, all focused on verifying the system concept on patients at the CFI. The Mobile Ground Reaction Force Sensor was designed and two systems were constructed and successfully tested in patient studies at the CFI. Otto Bock's most recent 'smart pylon' force/moment sensor design also demonstrated good accuracy in patient tests. Inertial Measurement Units (IMUs) were constructed, patient data collected at CFI, and algorithms applied producing data having good agreement with the CFI gait lab data. These patient tests (3 performed this year under approved CFI IRB) also demonstrate complete simultaneous functioning of all patient worn MGAS system components, further validating this system concept. Efforts next year will focus on further improvement of system accuracy, reliability, ergonomics, and signal processing, enabling collection of meaningful clinical data. Ultimately, this research will promote much improved prosthetic personalization and use, resulting in improved patient outcomes.

15. SUBJECT TERMS
Motion Analysis, Motion Tracking, Force Sensor, Inertial Measurement Unit, Prosthetics, Wounded Warriors

16. SECURITY CLASSIFICATION OF:			17. LIMITATION OF ABSTRACT	18. NUMBER OF PAGES	19a. NAME OF RESPONSIBLE PERSON
a. REPORT	b. ABSTRACT	c. THIS PAGE			USAMRMC
U	U	U	UU	186	19b. TELEPHONE NUMBER *(include area code)*

Table of Contents

Commonly Used Acronyms and Terms

Ab/Ad	Abduction/Adduction
AP	Anterior/Posterior
b	Bit
CFI	Center for the Intrepid
deg	Degrees
F/M	Force/Moment
FEA	Finite Element Analysis
Flex/Ext	Flexion/Extension
g	Acceleration due to gravity, equal to 9.81 m/s^2
GRF	Ground Reaction Forces
IMU	Inertial Measurement Unit consists of accelerometers and gyroscopes
IRB	Institutional Review Board
Int/Ext	Internal/External Rotation
ISO	International Organization for Standardization
Kinematics	Motion of limb segments
Kinetics	External and interactive forces, moments and torques of limb segments during motion
LED	Light Emitting Diode
m	Meters
MEMS	Micro-Electro-Mechanical Systems
MGAS	Mobile Gait Analysis System
ML	Medial/Lateral
OB	Ottobock. Health Care
ORNL	Oak Ridge National Laboratory
ORP	Office of Research Protection
Pylon	Part of the internal structure of the prosthetic device
Pyramid Adapter	Adapter which connects the socket to the lower part of the TT prosthetic device and allows for orientation and alignment adjustment
PT	Physical Therapy
RMSE	Root Mean Squared Error
s	Second
SDK	Software development kit
SI	Superior/Inferior
Socket	The part of the prosthetic device which interfaces with the amputees limb
TT	Trans-Tibial
DCU	Data Collection Unit

Introduction

The goal of this project is to leverage recent advances in motion sensing and microprocessor technology for improving the function and fit of amputee prosthetics as well as providing new, highly accessible and versatile tools for clinicians to use in rehabilitation techniques for amputees. In order to meet these goals, we have evaluated the current state of the art in motion sensing microchips also known as inertial measurement units (IMUs). The latest IMUs typically incorporate Micro-Electromechanical system (MEMS) elements that perform the functions of both a three-axis accelerometer and a three-axis gyroscope. Neither of these devices alone can adequately characterize the motion produced during gait; however, when the signals of both are combined using advanced techniques called sensor fusion algorithms including Kalman filtering and its variants, an accurate measure of motion can be obtained.
In order to measure both the motions (kinematics) and calculate joint and prosthetic interface forces (kinetics), forces must be measured somewhere in the biomechanical system. This is typically accomplished using a floor-mounted force plate in a gait laboratory. In order to make our system compact, portable and versatile, a force/moment (F/M) measuring system which can be mounted under the shoe has been developed along with an F/M-measuring adapter which can be mounted within the prosthetic device between the socket and prosthesis. These sensors measure the kinetics of the affected and unaffected limb in the lower leg amputee. Combining these F/M measurements with camera-less motion capture made possible using IMUs and data fusion algorithms provides a complete picture of patient/subject biomechanics, acquired using a system that has the benefit of being utilized anywhere.

The motivation of this research is to help return our highly-trained, professional soldiers to the highest level of activity following injury. The vast majority of servicemen and women undergoing amputation procedures are under 25 years of age [1], and expect to return to an active lifestyle as shown in Figure 1. Other than traumatic amputation, amputation due to vascular disease, primarily diabetes, is performed in the Veterans Health Administration at a rate of ~5,000 amputations per year [1]. Return to activity following amputation is critical to minimize further disease progression. A soldier's ability to remain active is dependent not only on the prosthetic technology but also on their rehabilitation, training and how well the prosthetic is "aligned" or "fit" to their unique physiology. The intended application of this system is to improve and streamline the fitting process.

An ill-fitting or misaligned prosthetic can result in asymmetric gait [4, 5], which leads to more energy expenditure, injury and chronic conditions in the intact or affected leg [6-8]. Quantitative gait analysis is used in many clinical and research areas [9-18]. But is also be used in the evaluation of prosthetic devices used by patients with amputation of the lower extremity [19-21]. Gait labs, however, are constrained to permanent lab spaces, are not readily available to every clinician or prosthetist, are typically in high demand and expensive. It is our goal for the MGAS to give the prosthetist or clinician instant feedback about patient biomechanics and quality of a prosthetic fit. It will also be useful as a research tool as, with a more affordable and accessible system, more data becomes available to researchers and designers.

Significant progress has been made since the last annual report. New sensing hardware has been developed and tested. Improved software and motion analysis algorithms have been developed as well. Finally, three data collection sessions have been carried out. The data were analyzed and compared with the Center for the Intrepid results showing strong agreement. Plans are underway for more data collections in the following months.

Body

Task 1: Establish System Design

Establishing a system design is a combined effort between engineers at Oak Ridge National Laboratory (ORNL) (Oak Ridge, TN, USA), Otto Bock Healthcare, Inc. (OB) (Duderstadt, Germany) and clinicians from the Center for the Intrepid (CFI) at Brooke Army Medical Center at Fort Sam, TX (San Antonio, TX, USA). An initial meeting was held at the Center for the Intrepid February 15, 2011, along with teleconference meetings since that time, regarding the clinical and practical needs for this system. The actual design and production of the system at ORNL has resulted in several changes to the system design from the original laid out in these 2011 meetings.

1a: Clinical Staff Input:

Input from clinicians at CFI has been sought on a continuing basis in order for the MGAS to be clinically useful and successful. Their input is essential in ensuring that the MGAS system and all aspects of its use are user friendly and provide clinically relevant data. Our initial focus is on achieving high quality data over making a portable or inexpensive system. There will be two tiers of data, engineering data and clinical data, and one of the challenges for this project is turning the "raw" engineering data into clinically relevant data that is easy to quickly interpret. The system and all of its components should be lightweight and compact. The system needs to be quickly and easily attached to the subject and initialized, and the system should operate on battery power for a minimum of 1 hour. The goal of the software interface design to enhance the existing skillset and instrumentation of the typical prosthetist. The system should also be rugged enough to withstand normal wear and tear and be able to handle average outdoor conditions.

1b: Establish System Specifications:

Overall System:

In order to accurately characterize subject gait motion, the MGAS will have 5 to 8 IMUs. One attached to each body segment including the pelvis, thigh, shank and foot and possibly trunk (Figure 1). Each IMU consists of a three-axis accelerometer and three-axis gyroscope. Each will have a power source, onboard chip to handle data collection, conditioning, storage and wireless communication to the host PC or tablet at 200 Hz.

A custom F/M sensor, referred to as a "smart pylon" developed by OB will replace the normal pylon used to adjust a lower leg prosthetic in 6 degrees of freedom. The smart pylon will be able to detect forces and moments in the prosthetic and will have an IMU associated with it, a powersource (battery), data collection, microcontroller and antenna.

The F/M foot sensor will detect ground reaction forces (GRFs) in three dimensions on the intact limb and consists of a forefoot and heel sensor. Each force sensor (10 in the forefoot and 7 in the heel) measures forces resulting in 16 channels of 16 bit force data. One IMU will be

associated with each the forefoot and heel sensors adding 12 more channels of 16 bit data. The force sensors and foot sensor IMUs will be both powered by the same power source and microcontroller that controls the data acquistion and transmission to the host PC. For the initial prototype, the antenna, battery, IMU and microcontroller are on an outside package attached to the top of the shoe, however, the goal is to eventually have all of the electronics in the foot sensor package that attaches to the bottom of the foot. The foot sensor unit (including force sensors and foot IMUs) and each segment IMU unit has its own power source, microcontroller, SD memory card and wireless communication. These devices transmit the data over Bluetooth to the host PC or tablet.

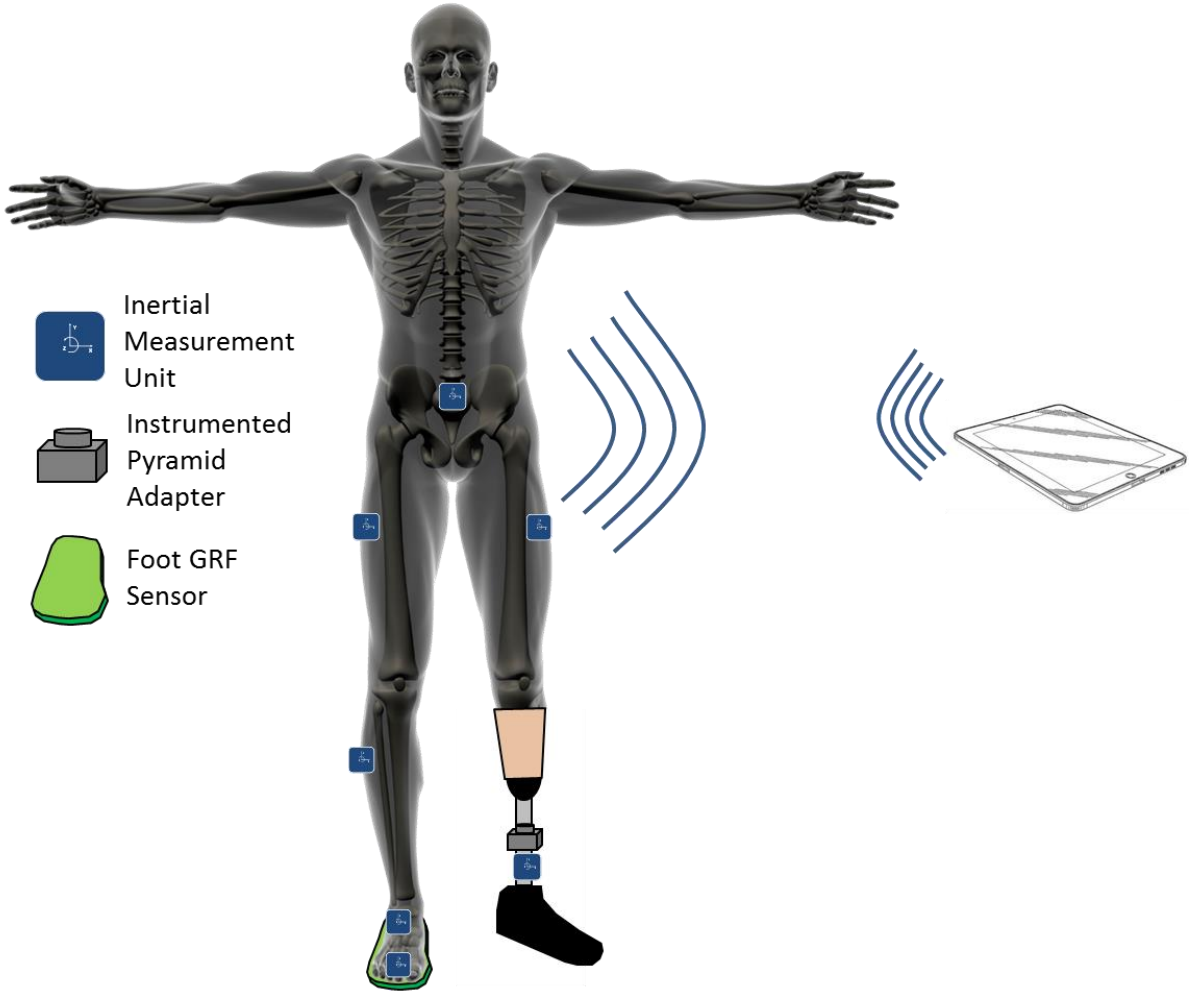

Figure 1: Overall summary of mobile gait analysis system architecture.

IMUs:

Accelerometers: Accelerometers included in IMUs detect acceleration in three axes. In most cases this consists of three single axis accelerometers aligned orthogonal to each other. There are various types and designs of accelerometers. One type is called a dynamic accelerometer which only picks up acceleration associated with movement. Another uses a mass to determine acceleration. This type can detect the direction of gravity. The direction of gravity can be used, along with trigonometry, to determine the pitch and roll orientations of the IMU. We are interested in the angle of limb segments, therefore a mass based accelerometer is needed.

MEMS accelerometers have become higher quality and more affordable over the past several years driven by the smart phone and videogame industries. For our application, the accelerometer needs to detect >6 g of acceleration, have low noise and have sufficient resolution, in the mg range. The accelerometers currently being utilized are of providing measurements up to ±16g with 16bits of resolution (~500µg/bit).

Gyroscopes: MEMS Gyroscopes are similar to accelerometers in that they generally consist of three uniaxial gyroscopes aligned orthogonally. Gyroscopes detect angular rate and use the Coriolis Effect to detect changes in angle. The gyroscope needs to have sufficient range, between 300 °/s and 600 °/s or higher, and have low noise, good stability and high resolution. In order to determine angle from angular rate, numerical integration is necessary. Over time, errant signals can cause the angular measurements to drift, so angular walk and drift are a concern resulting in significant errors in angle calculations from gyroscopes over time. Signal conditioning and software algorithms are used to address these issues. The gyroscopes used in this work are able to measure the angular velocity up to ±2000 °/s with 16bits of resolution (~ 61 m°/s).

Signal Conditioning and Algorithm: As mentioned earlier, for this device to be beneficial to both researchers and clinicians there will be two levels of data, engineering data and clinical data. Engineering data consists of the data from the IMUs and F/M sensors and also that data transformed into joint angles and joint forces and torques. The software associated with MGAS will take this data and give the clinician information they can use immediately to get more insight into existing prosthesis fit or alignment issues, help in deciding how to adjust a prosthetic or evaluate a prosthetic or fit to decide which is better. Both of these modalities have their individual challenges.

Engineering Data: MEMs IMUs, although readily available, inexpensive and relatively good quality, still contain substantial noise for the purposes of this project. The data is filtered using a low pass filter (LPF). Although for the initial prototype this is done in post-processing, the LPF is applied on board the IMU units and before the data is sent wirelessly to the DCU. To turn the IMU data into joint angle data the LPF filtered data is passed through a Kalman filter [22]. Kalman filters come in various types (e.g. traditional, extended, unscented, etc.) [23] and the algorithm for this application can be designed in many different ways [24-31]. The Kalman filter takes two noisy signals and combines them using covariance data about the measurement signal, noise and process to get better results than the two signals independently. This is advantageous for us since an errant signal and angular walk associated with gyroscopes can cause errors during integration of the angular rate signals. It can also be challenging to isolate the gravity signals from accelerometers which are also subject to noise. Combining data from accelerometers and gyroscopes with a Kalman filter can provide accurate joint angle results.

Clinical Data: Extracting meaningful clinical data from joint angle data and joint force/torque data requires the application of a second algorithm. This will also involve a GUI which will display this data to the clinician. Development of this algorithm and clinical interface will begin after prototypes are developed and sufficient amounts of patient data are collected.

Furthermore, the software should provide "recommendations" to optimize the prosthetic alignment by highlighting issues that are brought to light by the data analysis so that the prosthetist can use judgment to act accordingly. Therefore, it is required to investigate alignment variations of transtibial prosthetics and how they relate to changes in the gait pattern.

Initial Position Calibration: The IMUs when initially placed on the lower limbs will not necessarily be aligned with anatomical axes of the limb segments. There will be an offset between the IMU angle output and the physiological angle. One proposed method to match the IMU orientation to the physiological orientation using the Microsoft Kinect® Sensor (Microsoft, Corp., Redmond, WA, USA) was described in the 2012 report. Initial tests have found that the accuracy of the Kinect does not meet the requirements to accurately determine 3D position and orientation.

A second proposed method to find the initial position of the sensors involved using a calibration station to assist an optical-based technique with position determination. The test showed the accuracy of the system can reach 1mm under laboratory conditions. More work is underway concerning angular calibration. This method was described in details in the 2012 report.
Another method currently under investigation is based on self-calibration. In this method the subject performs a few simple, short and predefined activities. The orientation and position of the sensors are calculated based on the body and predefined motion constraints. It can be combined with the optical method or self-sufficient if the results are satisfactory. The main advantage is minimum to none usage of extra hardware and cost. The first results are expected by the end of November 2013.

Smart Pylon Specifications

More information on the design and testing results for the Smart Pylon are shown in Task 5.

- The F/M Sensor shall temporarily replace 4R72=32 Modular adapter (Figure 2)
- Time spent during a clinical fitting, including measurement and action steps based on measurement shall not exceed one hour (as the measurement takes time it must speed up the fitting process to stay within the given time frame).
- In several cases it might be necessary to perform a continuous data acquisition exceeding the fitting time. Therefore the storage capabilities and the power supply should allow for F/M data and inertial sensor data for eight to ten hours.
- Possibilities for the mobile ground reaction force sensor were shared, especially considering the comparison to gait lab and to mobile F/M sensors within a prostheses.

Figure 2: 4R72=32 Modular Adapter

Foot Sensor:

It was decided that the foot sensor would detect GRF in three directions and contain an IMU in both the heel section and toe section in order to track the sensor orientation relative to the shank and thigh segments. A two component system is used with one component measuring heel forces and orientation while the second measures forefoot forces. These will communicate wirelessly to the DCU and the data will be used to determine joint torques and moments in the healthy leg. This data along with the smart pylon force data and segment orientation data will be used to determine metrics to determine quality of fit and the adjustments need in a prosthetic to improve performance.

1c: Initial Protocol Development

The clinicians at CFI have developed an initial protocol for testing the validity of the mobile gait analysis system and this protocol has been approved by their Institutional Review Board (IRB). The testing consists of comparing the MGAS results to the 26 camera optoelectronic motion capture system (Motion Capture, Corp., Santa Rosa, CA, USA) at CFI. Fourteen (14) control subjects, 21 patients and 14 clinicians will be used in the study for data collection and for clinical feedback. The clinicians will be asked to set up/use the mobile gait analysis device and the subjects/patients will perform five trials of three activities, normal walking, stair ascent and 10 degree incline walking. Data will be collected to determine the error of the motion analysis system compared to the 26 camera system but also data will be collected on the clinician feedback.

Task 2: Orientation Module

The orientation module consists of the IMU sensor system used to determine orientation of the limb segments and joint angles.

2a: Orientation Component Selection

The component selection process was described in the 2011 annual report and also in conference proceedings included in Appendix 1. The team selected the Invensense MPU-6000 for the orientation sensor units from several chips tested. This chip was chosen for its size, low power consumption, price, ease of implementation and performance. This chip can be bought from commercial sources for approximately $10. Its performance was as good as or better than devices up to 50 times its cost.

2b: Prototype Electronics and Data

To reduce the design costs, a commercially available computer on module (COM) device was selected to act as the main controller for this system. (A Gumstix Overo FireStorm; www.gumstix.com) This device runs the Linux operating system and is Bluetooth, WiFi and SD card enabled. The COM system also has an open expansion header that allows for the creation and integration of custom expansion cards. ORNL designed such a custom expansion card to suit the needs of the MGAS. The first generation of the expansion board was designed and fabricated in 2012 and described in the annual report. See the manuscript tin Appendix 2 has more details. It included the IMU chip, USB connectivity, the connectors necessary to connect to and power the F/M foot sensors, battery management and an integrated Bluetooth antenna. A second generation expansion card was designed and fabricated (Figure 3) for the COM system which expanded the board features system with an on/off switch, additional separate overcurrent protection for the charging ports, battery power input, heel power output and toe power output. The system can power the foot sensor using the data cable lines (Figure 4). The previous system required a dedicated power line.

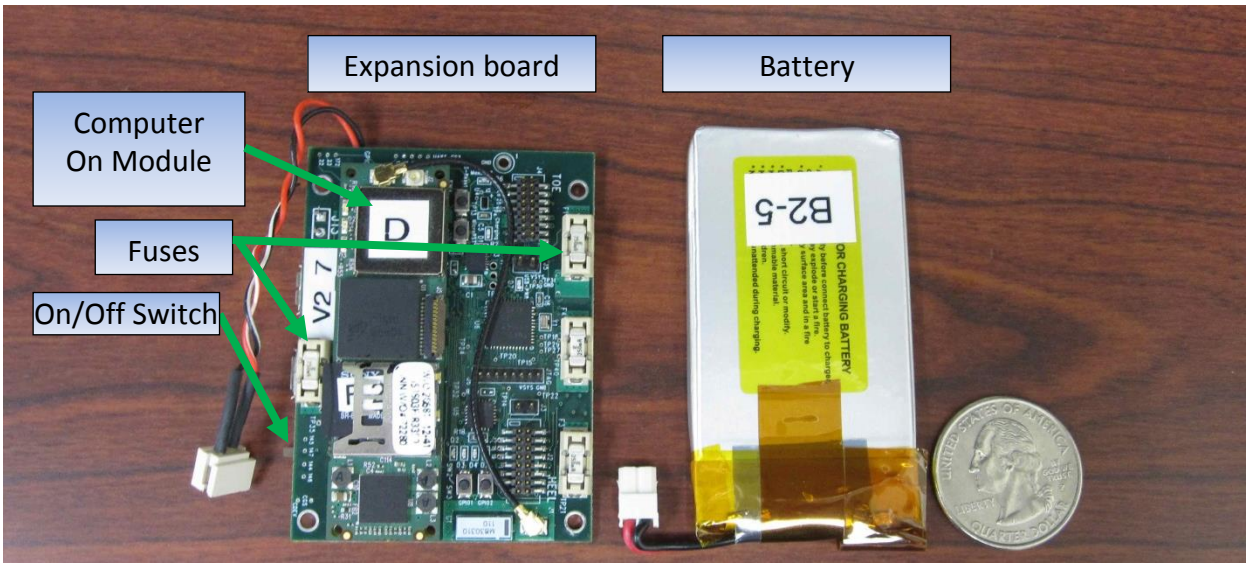

Figure 3 Expansion board with the Computer On Board and the battery

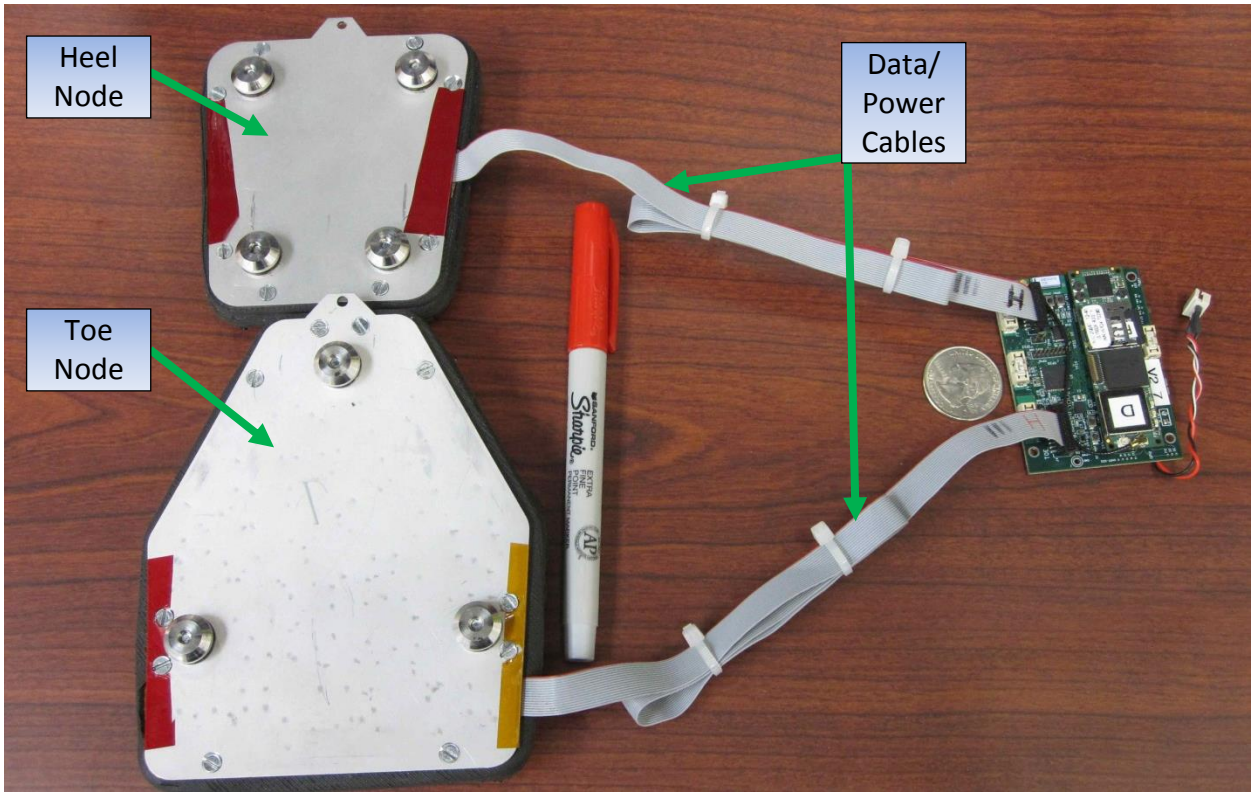

Figure 4. Expansion board connected to the foot sensor.

This decreased the system complexity and simplified the on-patient setup. Also, the battery board was removed from the design reducing system weight and volume. The battery is now secured in the enclosure and does not require a dedicated board. A new, smaller profile and weight battery was chosen to meet the needs of the device and effectively reduce the system weight.

The on-board software was augmented to allow for greater flexibility in the bi-directional Bluetooth communications. Also "user-friendly" features were added such as the ability to request the quality of the Bluetooth link, and the ability to time-synchronize the data of the multiple independent asynchronous sensor units. Previously, the data had to be synchronized in tedious post-processing analysis. The sensor units, themselves, now have the ability to provide the information needed to synchronize over while collecting live data.

2c/2f: Evaluation in Robotics Lab and Results Analysis

The robot was used to evaluate and select different commercially available IMUs, develop the extended Kalman filter (EKF) sensor fusion algorithm and to calibrate the sensors. The robot has proven to be an extremely useful tool during the development of this system. To evaluate the sensor fusion algorithm, the robot was programmed to move like a human leg using actual biomechanical data collected at CFI. The selected sensor and data fusion algorithm was accurate to within 0.5 degrees root mean squared error (RMSE) during simulated human motion on the robot (Figure 5 and Figure 6).

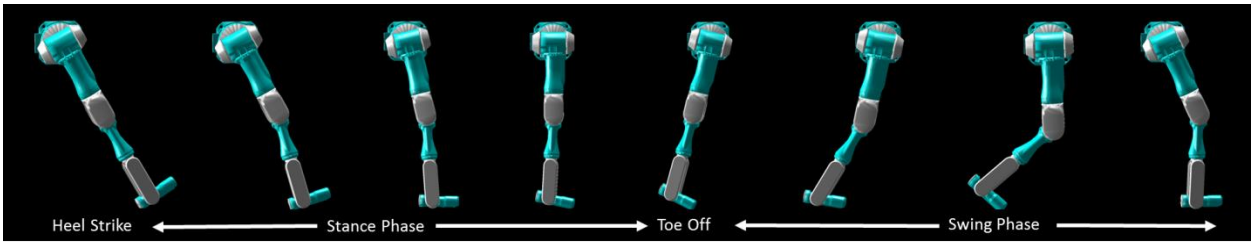

Figure 5: Image sequence of an animation of the robot moving through simulated human walking.

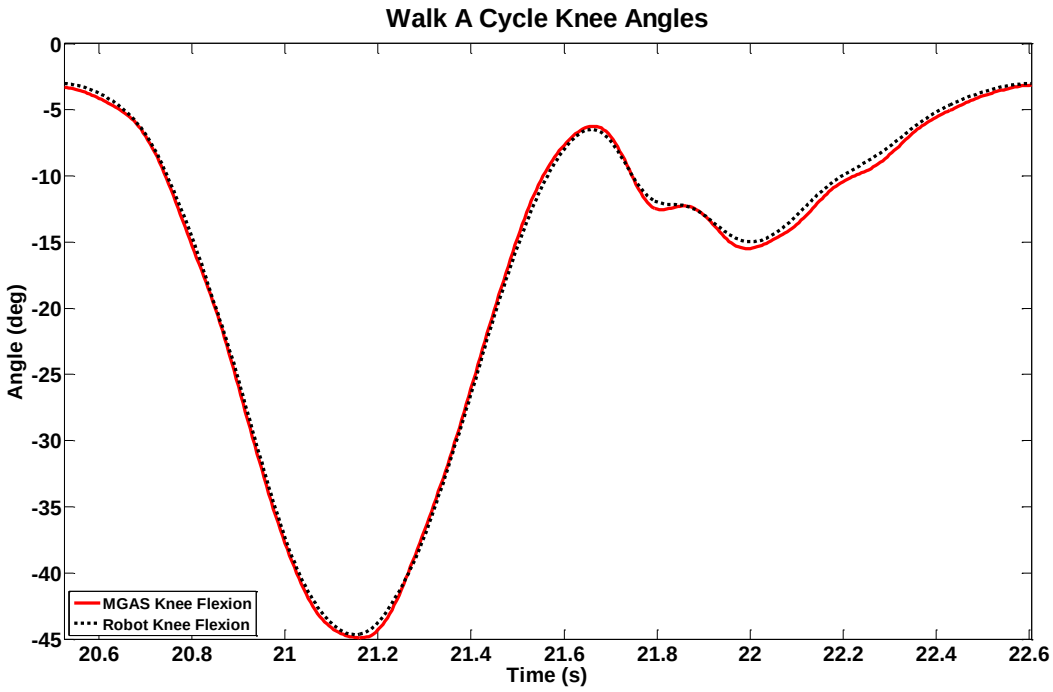

Figure 6: Comparison of knee angle from an example gait cycle from IMU data and sensor fusion algorithm and the actual robot motion according to encoders on the robot.

See manuscripts in Appendix 1 for more details on the IMU selection and initial results from the EKF in Appendix 2.

2d: Sensor Gait Lab Evaluation

The required IRB approval from all sites and subsequent approval from the Office of Research Protection (ORP) was received in the second week of August, 2012. During the week of August 27th, two ORNL team members traveled to San Antonio to evaluate the MGAS orientation and force measurement system against the camera based system at Center for the Intrepid on one healthy subject. The MGAS system test included the shoe force sensor and an IMU sensor on the shank and thigh. The initial results show that flexion orientations are within 2 degrees RMSE, (see Figure 7-Figure 9). The results from the MGAS foot force/moment sensor were within 10% of CFI's gait lab force plate in all three directions (Figure 10).

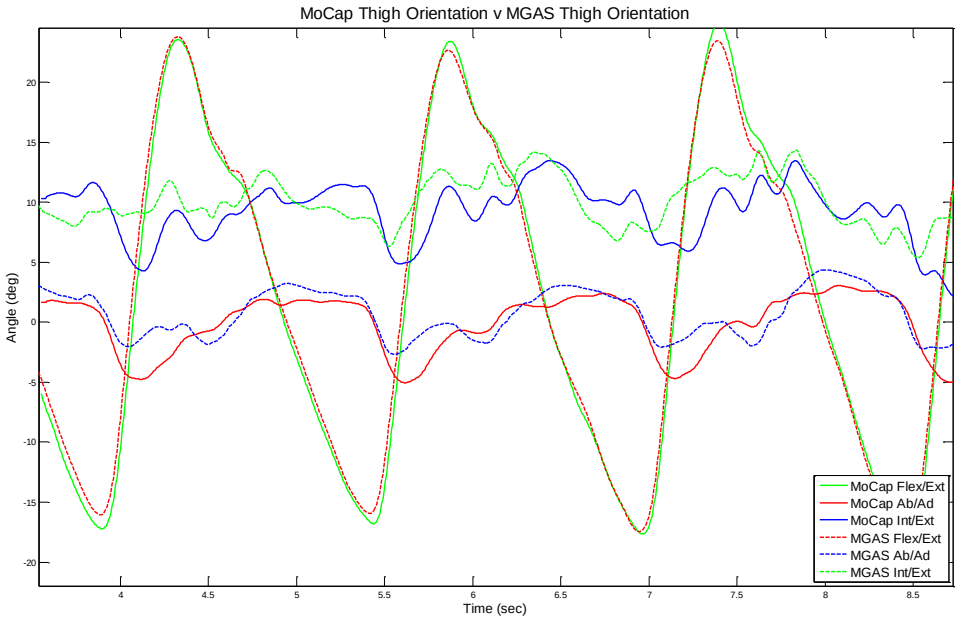

Figure 7: Thigh orientation comparison between the MGAS system currently being developed for this project and the motion capture system (MoCap) at CFI, currently regarded as the gold standard in human motion capture. RMSE value for flexion is 0.9 degrees.

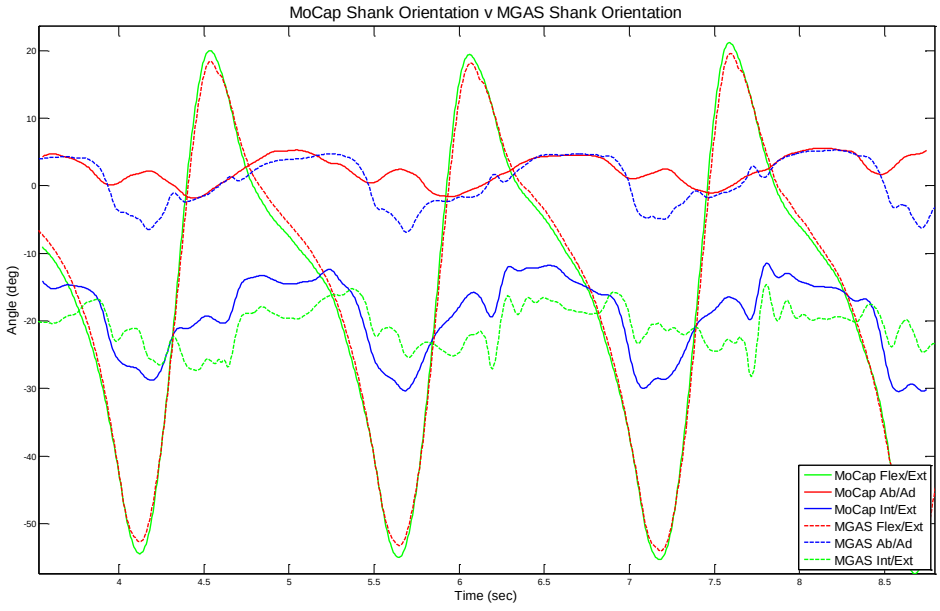

Figure 8: Shank orientation comparison between the MGAS system currently being developed for this project and the motion capture system (MoCap) at CFI. RMSE value for flexion is 1.2 degrees.

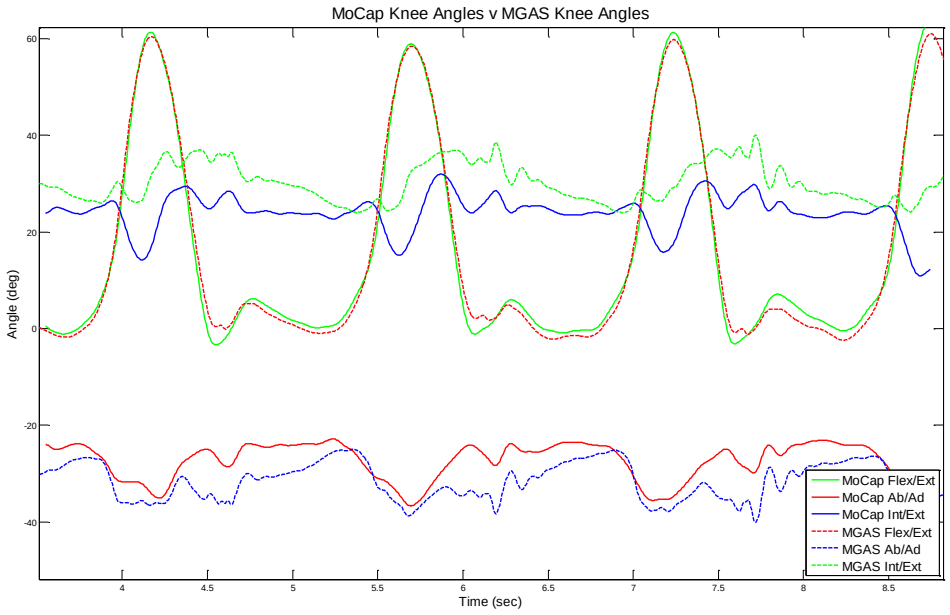

Figure 9: Knee orientation comparison between the MGAS system currently being developed for this project and the motion capture system (MoCap) at CFI. RMSE value for flexion is 1.5 degrees.

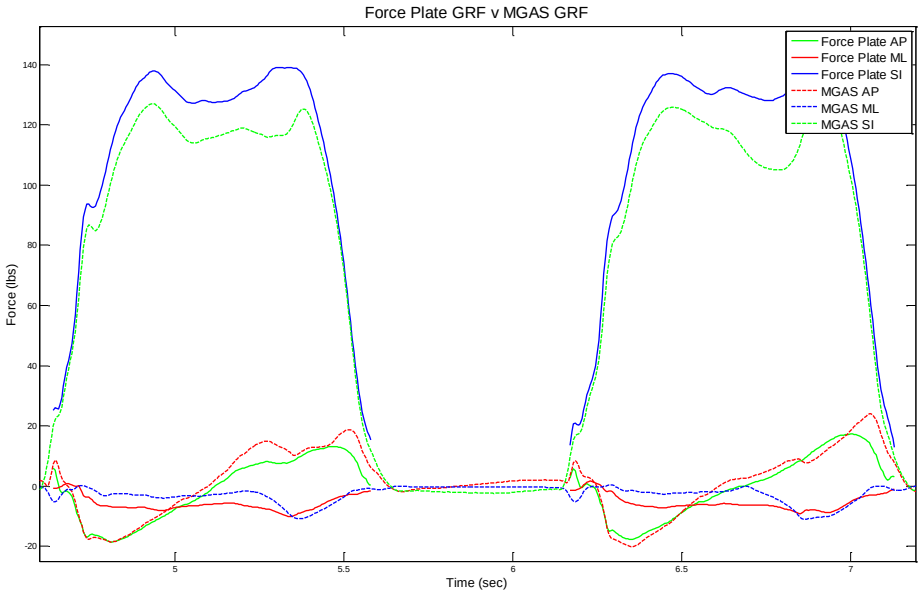

Figure 10: GRF comparison between MGAS foot sensor and the force plate at CFI.

The initial sensor evaluation is now considered finalized. The results are within expected limits. Further improvements are executed with the progress of task 8.

2e: Initial System Packaging

The first generation of the system packaging is described in a previous annual report. Since the last report the second generation of enclosures for the sensor units was designed (Figure 11

and Figure 13) using Solidworks (Dassault Systèmes SolidWorks Corp. Waltham, MA USA) and printed in plastic on a Dimension Elite 3D rapid manufacturing system (Stratasys Corporation, Eden Prairie, MN, USA). The enclosures can be secured to subject segments using Velcro or a double sided tape in the case of the presence of additional fixtures (Figure 14). The main features of the new system enclosures are:

- Decreased weight 115 to ~65 g. Velcro not included.
- Decreased height from 38 to 22mm (25mm for the foot version).
- Minor decrease in depth and length.
- Decreased number of assembly parts.
- Visibility of system status LEDs.
- Direct access to charging ports and on/off switches and reset buttons.
- Expansion board cover with a double quick lock/unlock feature.
- Ability to access and change the battery in the field within a few seconds (Figure 15).
- Ability to access the expansion boards without affecting the system functionality.
- Improved wire strain relief.
- Three components: main body, battery cover and expansion board cover.
- Quick system assembly.

Due to the wiring and connectors required between the foot sensors and the DCU, the enclosure has two lid versions reflecting the added height and wire strain relief requirement. All other elements are the same (Figure 12 and Figure 13). This allows for using the DCUs for different roles by changing only the plastic covers and plugging the cables. The decreased number of cables (compared to the previous versions) improves the ergonomics, the aesthetics, and the robustness of the current DCU (Figure 16-Figure 17).

Figure 11. DCU unit mounted in the enclosure.

Figure 12. Regular and foot enclosure comparison. Top view.

Figure 13. Regular and foot box height comparison.

Figure 14. DCU with a mounting strap.

Figure 15. DCU- battery access.

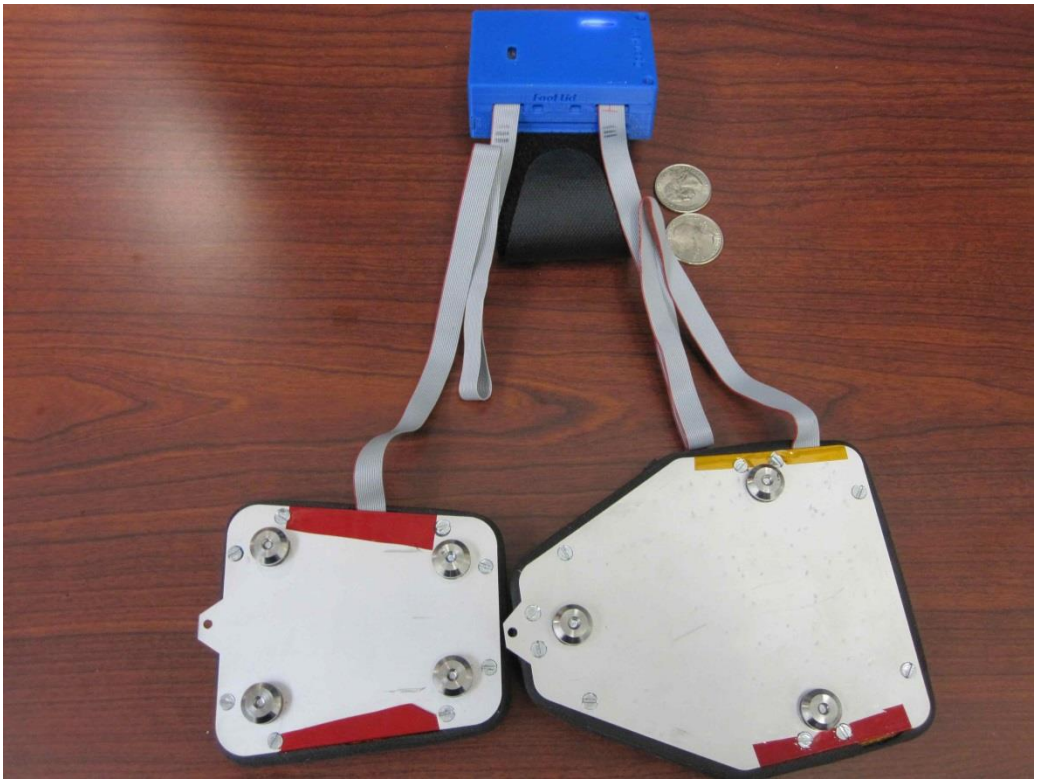

Figure 16. DCU connected to the foot sensors.

Figure 17. DCU and foot sensor on the shoe. DCU unit mounts on the lower shank.

The IMU system developed by Otto Bock consists of 5 five inertial sensors wired together on a belt/strap structure with a central DCU Unit (Figure 18).

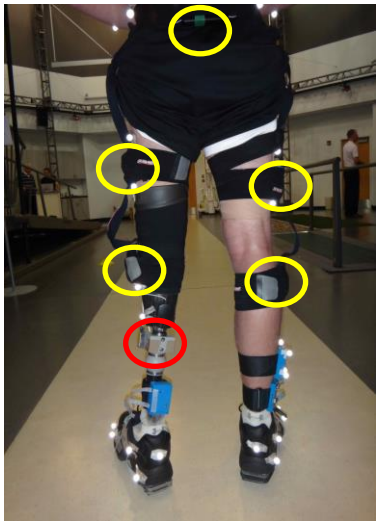

Figure 18.OB IMU strapping system (yellow) and F/M sensor (red).

Task 3: Wireless Communication

Although other methods were discussed, the team decided on Bluetooth (IEEE 802.15.1) as the wireless protocol since the 2011 annual report. We can now turn system data collection on and off wirelessly, and collect the data over this wireless link. The data is also stored on the on-board SD memory card incorporated in each sensor for backup purposes. Ultimately, the goal is to transmit all of the data wirelessly.

Ottobock is also developing a system which uses Bluetooth/Wi-Fi communication for both their transtibial Smart Pylon sensor and an inertial orientation sensor system which they are developing concurrently. When testing began with patients with transtibial prosthetics the data from the system being developed at ORNL and the system being developed at Ottobock was collected simultaneously without major issues. Optimization of the online transmission of the inertial signals was also performed to increase reliability and range.

While the Bluetooth wireless radios provide for a limited range, it has currently been adequate for the MGAS. However, if needed, Wi-Fi (IEEE 802.11.b/g/n) is available and could be incorporated with minimal effort. There would be a significant power consumption trade-off though.

Task 4: Modification of the Smart Pylon force/moment load measuring system

This task has been performed at OB. Testing consists of iterative design phases with finite element analysis (FEA) and physical testing after each design phase. Ottobock has gone through several iterations to this point and performed the necessary testing.

4a: Modification of Smart Pylon for prosthesis fit, alignment and gait training purposes

Two different design approaches were derived from the trans-femoral (TF) design which was available when the project began (Figure 19 and Figure 20). The TF Sensor shows a pyramid adapter on top, whereas a pyramid receiver is preferred for transtibial (TT) prostheses, and the durability of this design is limited because the TF design is designed to be mounted above the knee for activities of daily use. The “Large” 70mm design is based on the functional principles of the TF design, but has been increased in size and equipped with a double pyramid receiver. The dimensions are optimized for durability combined with appropriate strain distribution to acquire the loading data with appropriate resolution and accuracy.

A different design approach, using four independent structures around the two separated pyramid receivers offers not only smaller overall dimensions, but also the potential for measurement independence from the internal stress of the original design. This internal stress was caused by pressure on the pyramids, acting through the torque of the adjustment screws, as opposed to external stress, which is the parameter to be measured. The optimization of this improved structure has been the basis of all subsequent iterations.

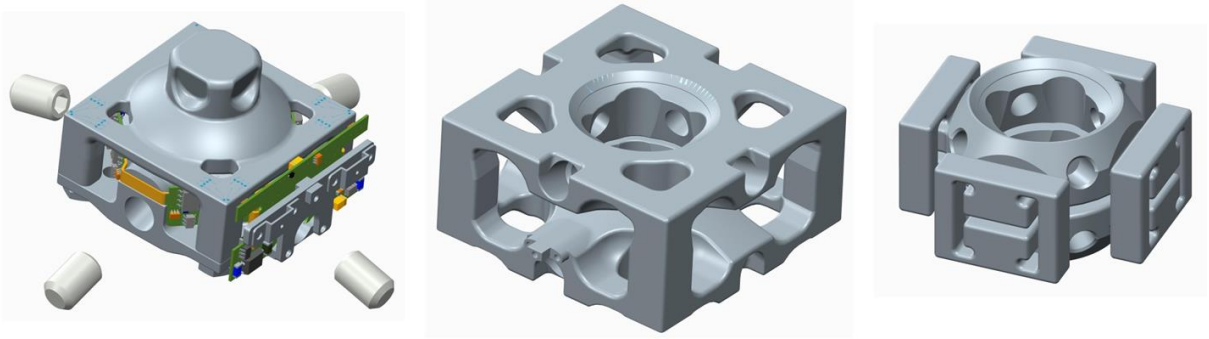

Figure 19. **Initial TF design** **"Large" 70mm wide design** **4 independent frames**

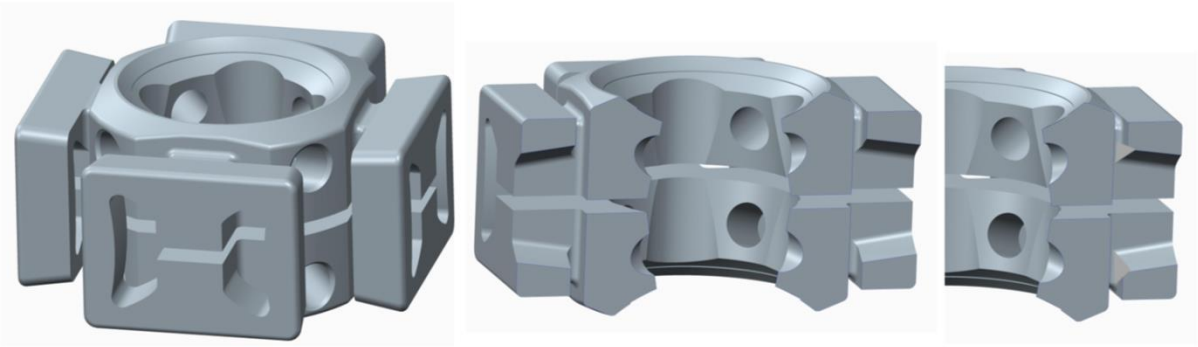

Figure 20. **Additional tilted plane** **Tilted plane inside the frame** **Additional chamfer**

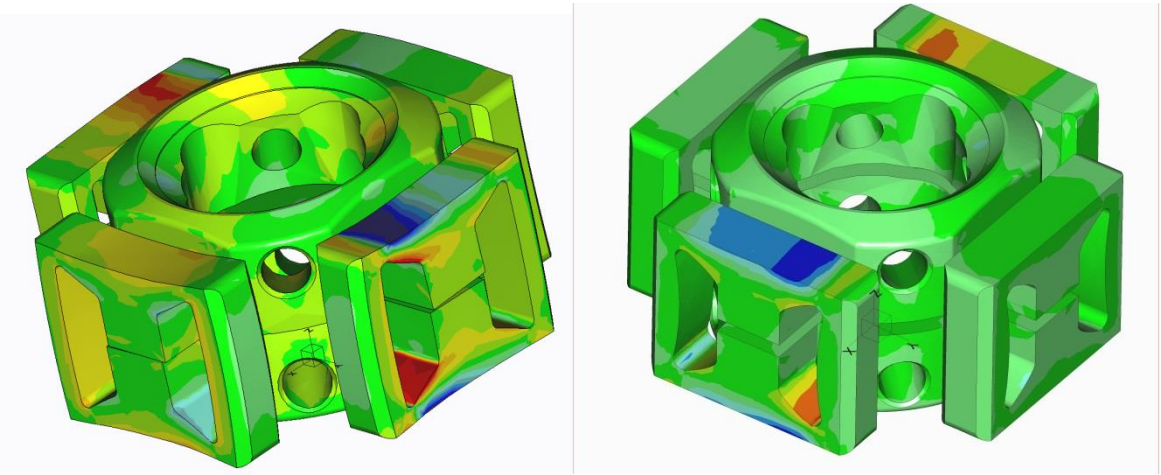

Figure 21. Finite Element Analysis examples

The smaller design still requires quite strong bearing elements, and so carving the intricate piece during fabrication became increasingly complex. The goal was to eliminate any final manual work in the difficult to access gaps since reproducibility is critical for reliability and durability. The further the design was optimized, the more complex the manufacturing process became, requiring specialized custom tools.

A series of F/M sensor frames have been produced and tested cyclically. Carefully increasing wall thickness, optimizing thickness distribution and shaping structures to reduce stress in related areas have all made iterative increases in the maximum cycle numbers – eventually achieving about 500,000 cycles before failure. For higher efficiency of the optimization process of the F/M sensor, FEA (Figure 21) and CAD now are performed within the same lab, so the effect of design changes on stress distribution is seen much faster and closing the iterative design loop is more effective.

The second to last modification (June 2013) shows a tilted plane in which the wall thickness ramps from a thinner inner surface to a thicker outer surface, which leads to a relief of the inner surface and an improved strain distribution for strain acquisition. This modification, in combination with the previous optimizations, achieved 1.117 million cycles.

In the most recent design, using a five axis carving method, a chamfer was carved along a gap which previously was not accessible by any tool, reducing the highest strain and achieving more than 3 million test cycles, thereby finally passing the industry standard cyclic test for durability. Further F/M sensor frames based on the recent design will be fabricated to verify the repeatability of the cyclic test result. If the next device also passes, functionalization (implementation of strain gauges and signal conditioning, etc.) will be the next step.

4b/4c: Integration of orientation measuring system from Task 2 and Wireless Data transmission system

Ottobock has designed a Bluetooth enabled orientation measurement system and will incorporate the data from the “smart pylon” device into it.

Task 5: Prosthetic component design safety

Task 5 is being conducted by Otto Bock in conjunction with Task 4.

5a: FEA modeling of design:

FEA modeling is incorporated throughout the iterative design process for this device. The latest design has gone through FEA analysis and was tested in laboratory settings in October, 2012 and on-patient in 2013 data collection sessions. See Task 4a.

5b: Mechanical testing:

As the ISO 10328 standard is based on the regular use of the tested components, the extraordinary loading conditions of the highly trained professional soldiers are covered by temporarily restricting the maximum bodyweight of the users to 100kg, whereas the device is tested to 175kg. Real data acquired under these conditions will allow the team to determine the basic constraints for a final design capable of performing data acquisition for soldiers of higher body weight. As the F/M sensor is driven with low voltage the mechanical risk is the only one at present which is covered by the structural strength test of ISO 10328.

Five of the large TT Smart Pylon F/M sensors were assembled and tested (Figure 22). These results were detailed in the 2011 Annual Report for this project. Currently, as described in Task 4, the lessons learned from these tests have been incorporated into newer versions of the large Smart Pylon and the design of the smaller, optimized pylon. This smaller optimized design was manufactured and tested in October 2012.

Figure 22: Test setup for smart pylon F/M sensors

Task 6: Mobile Ground Reaction Force Sensor

6a: Overall Design Requirements

- It was decided that the F/M foot GRF sensor for the healthy leg must be able to detect forces and moments in all three six axes.
- There will be a sensor for both the forefoot and heel.
- The sensor must be lightweight and less than a half inch thick so as not to affect the movement or gait patterns of the subject.
- The goal is that the design will have enough room in the underfoot module for electronics including an IMU, wireless transmission hardware and power source.
- For initial designs, it is satisfactory for some of the electronics to be worn on the shoe.
- The sensor will be environmentally sealed to prevent damage from normal amounts of wear and environmental/weather conditions.
- Desirable to be able to modularly swap out components (strain gauges, load cells, IMU) in case one fails.

6b: Load Cell Detailed Design
The foot F/M sensor was designed at ORNL.

The forefoot and heel sensors were designed in such a way that the vertical and shear forces could be isolated without the measurement of one loading mode affecting another. It was also designed to follow the shape of the sole of a size 10 1/2 athletic shoe with guides to limit slip between the sensor and the shoe sole. The sensors are 12 mm thick and the forefoot and heel sensors weigh ~170 grams and ~120 grams, respectively. This falls within reasonable limits which were determined not to affect the gait patterns of subjects. Some additional height is added for environmental sealing and to provide a high friction contact with the ground.

The design was also optimized to allow for as much room as possible within the cavity of the frame for the electronics and power supply. Currently, all of the filtering and sampling circuitry is contained within these cavities; however, the batteries and control circuitry are not.

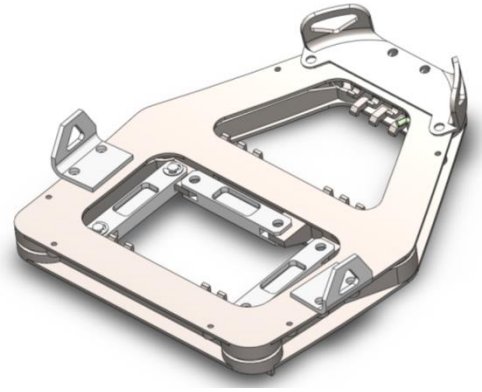

Figure 23: Forefoot sensor design
~170g and 12mm added height

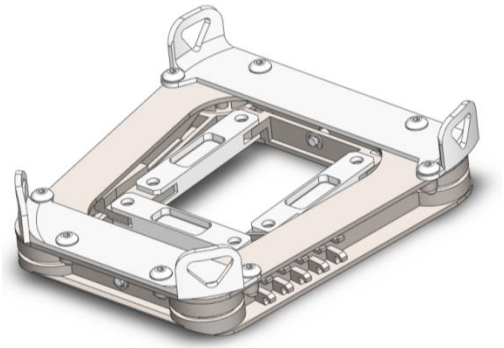

Figure 24: Heel sensor design
~120g and 12mm added height

6c: Footwear attachment system

An initial attachment system was developed using nylon straps. This attachment system works similar to the bindings found on crampons worn by mountaineers. However, after receiving feedback from subjects in early tests, it was determined that the strap system did not give the feeling of being securely attached. This was a significant concern, so a new attachment method was sought. `

Since the last report two new versions of the attachment system have been designed, fabricated and tested. The second generation utilized a thermoplastic material formed to fit the shoe shape (Figure 25). This system was also not satisfactory to users. This is due to added bulkiness and an inability to predict prior to a test the morphology of the shoe of the patient. Shoes that were smaller at the toe left large gaps between the shoe and the thermoplastic cup. Again, this method did not feel secure to the wearer, and added to measurement error because the sensor had room to move around on the shoe of the wearer.

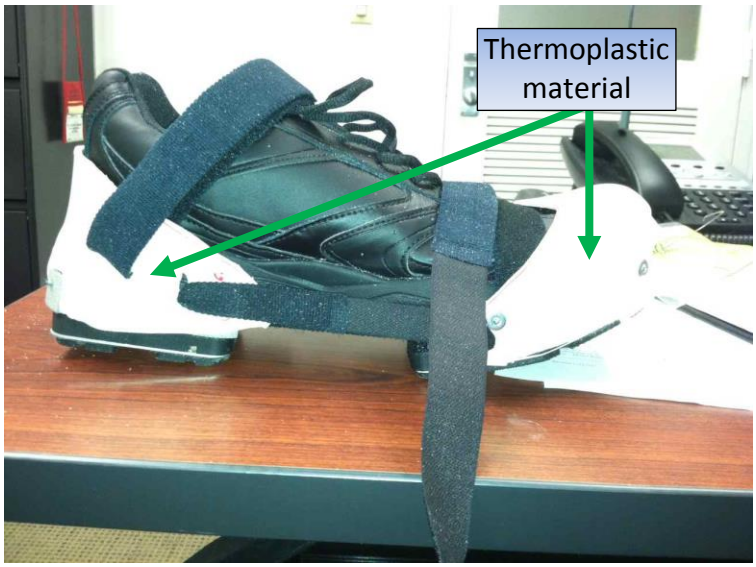

Figure 25 Binding system with a thermoplastic material.

Due to system bulkiness and the inability to provide repeatable, fast, comfortable and secure mounting without affecting the force measurement a third generation was developed (Figure 26). The new design requires shoe modifications and thus, a set of modified shoes was prepared covering sizes from 8 to 12 for the current tests. New modified shoes can be easily and quickly obtained without significant costs. The modification includes the removal of a portion of the sole thickness and the attachment of mounting plates. The sensor segments are equipped with matching mount support points.

The new design features are:

- Added rigidity
- Very fast mounting
- Repeatability of the mounting process
- Decreased system complexity
- Increased security for the patient
- Aesthetics

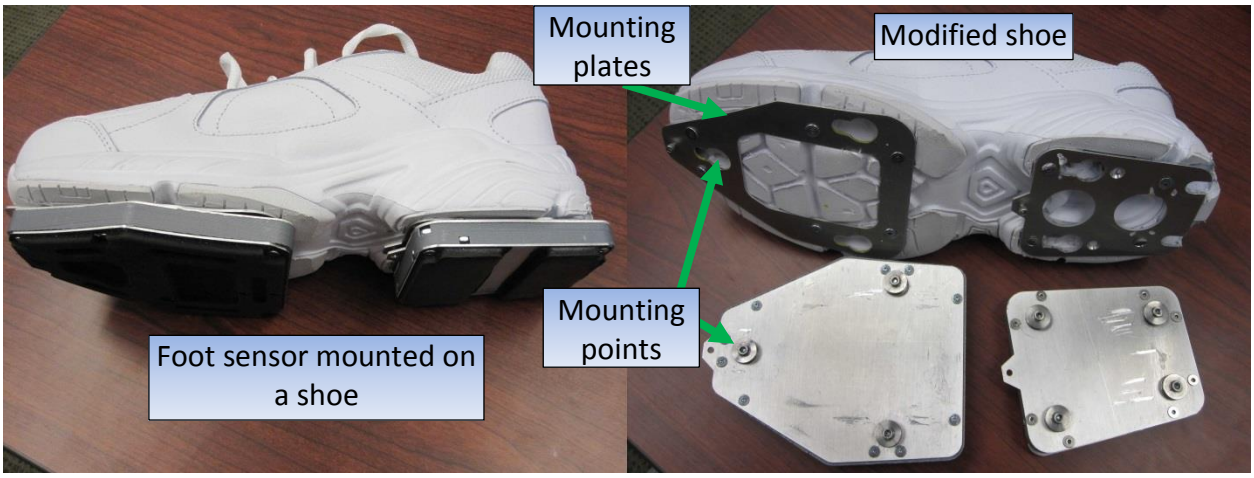

Currently, this mounting method is considered successful. The only drawback is the use of shoes that the patients are not used to wearing. Further testing will be required to determine if this interferes with patient gait.

6d/6f: Signal Conditioning and Electronics and Data Acquisition System

The Ground Force Reaction Sensor is composed of two sensor modules; one dedicated to each the heel and toe portions of the system. The toe sensor unit has 6 strain gauge button sensors for measuring the z-axis forces, and 3 strain gauge sensors for measuring lateral forces, for a total of 9 sensors. The heel sensor unit is comprised of 4 strain gauge button sensors (for z-axis force sensing) and 3 lateral force strain gauge sensors. Each of these units also has an inertial measurement unit (IMU) and other support circuitry. The operation of these two sensor units is controlled by the foot processor unit, which also supplies power. A simplified block diagram of these modules is shown below (Figure 27).

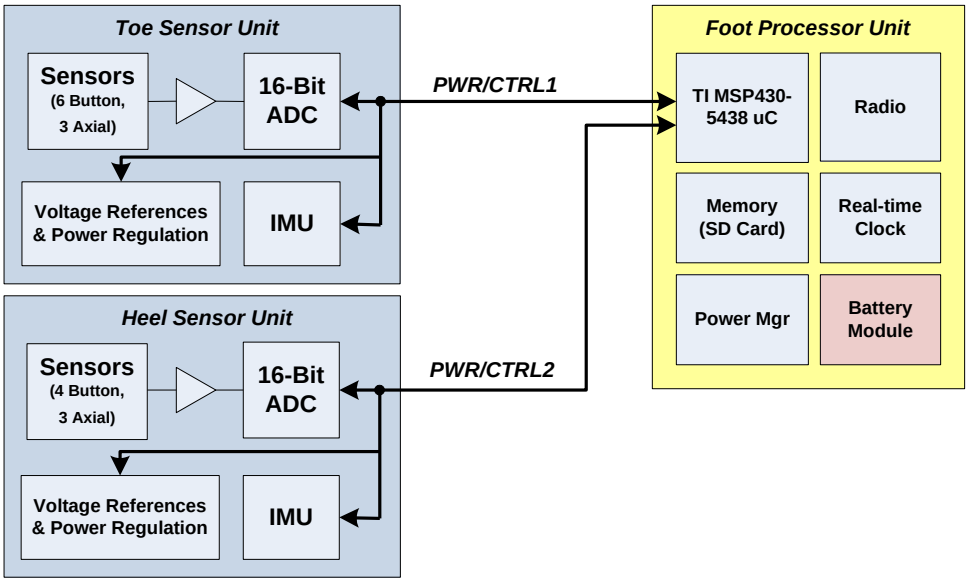

Figure 27 Ground Force Reaction Sensor electronics modules.

Each sensor requires a dedicated instrumentation channel for excitation of the Wheatstone bridge and for amplifying and conditioning the sensor output signals. A block diagram of the instrumentation channel is shown in Figure 28. A bridge amplifier provides gain to the differential input signal and a 2nd-order Sallen Key filter (Butterworth filter characteristic, f_{3dB}=20Hz) reduces the signal noise bandwidth via low pass filtering prior to digitization.

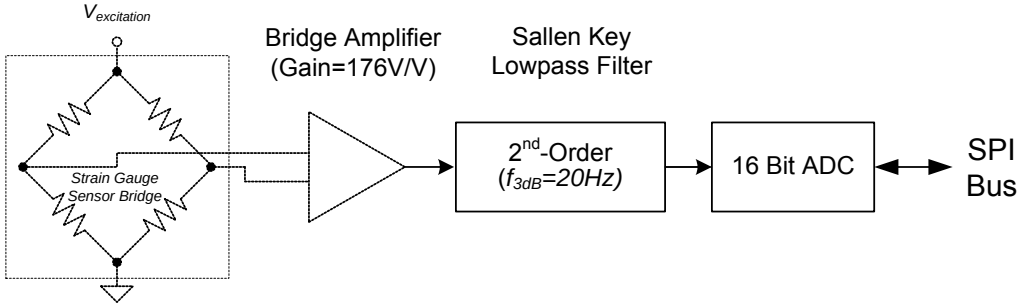

Figure 28 Ground Force Reaction Sensor electronics modules.

A common electronics board (sensor interface board –SIB) was designed to meet the needs of both the heel and toe sensor units. The printed circuit board area required for implementing the SIB was minimized by using dual channel integrated circuits for the preamplifier (AD8426, Analog Devices Inc.) and the low-pass filter amplifier (AD8607, Analog Devices Inc.) resulting in 5 dual electronic channels per board. Two multichannel 16-bit analog-to-digital converters (AD7689, AD7682, Analog Devices Inc.) were employed for digitizing the sensor outputs, and were controlled by the foot processor unit using a 4-wire serial interface (SPI standard). Other support electronics were required including multiple voltage regulators and a voltage reference for both the ADC and for setting the mid-point voltage of the signal processing frontend. The integrated circuits were carefully selected to allow maximum signal swing from 3V and 3.3V power, each regulated from the 3.7V provided by the Li battery pack. Highly miniaturized

connectors and passive components were also used to minimize the board area. A photograph of the sensor interface board is shown in Figure 29. Assembled heel and toe modules, each having a sensor interface board is shown in Figure 30.

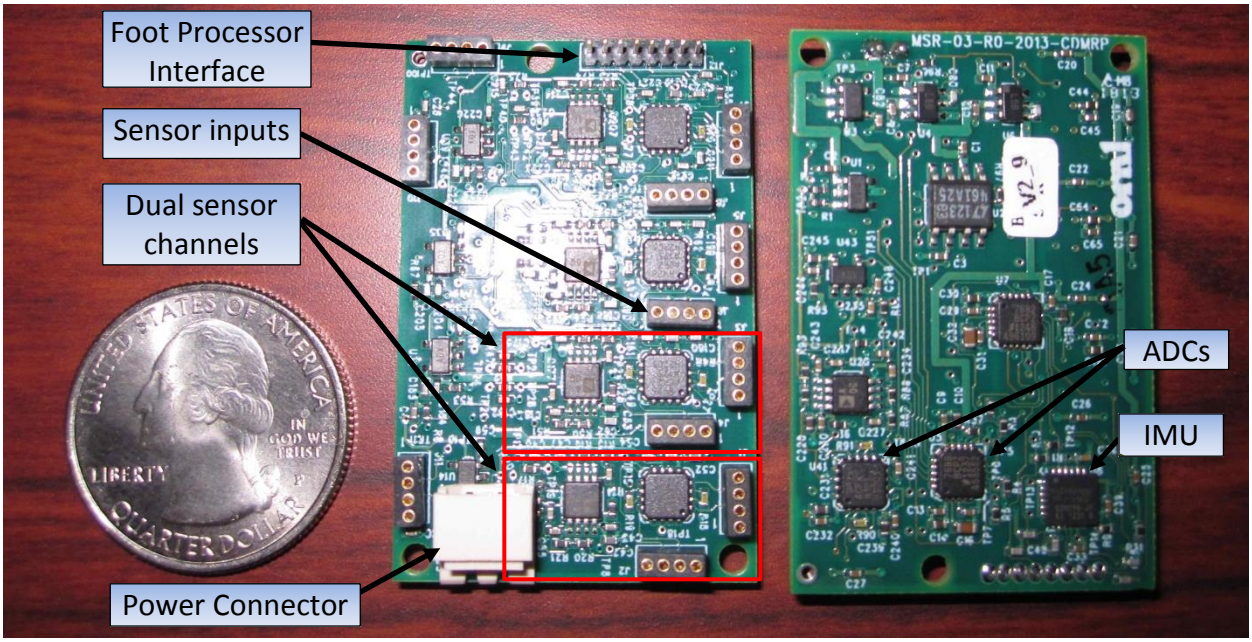

Figure 29 ORNL Sensor Interface Board used in the heel and toe portions of the foot sensor.

More details can be found in Appendix 2.

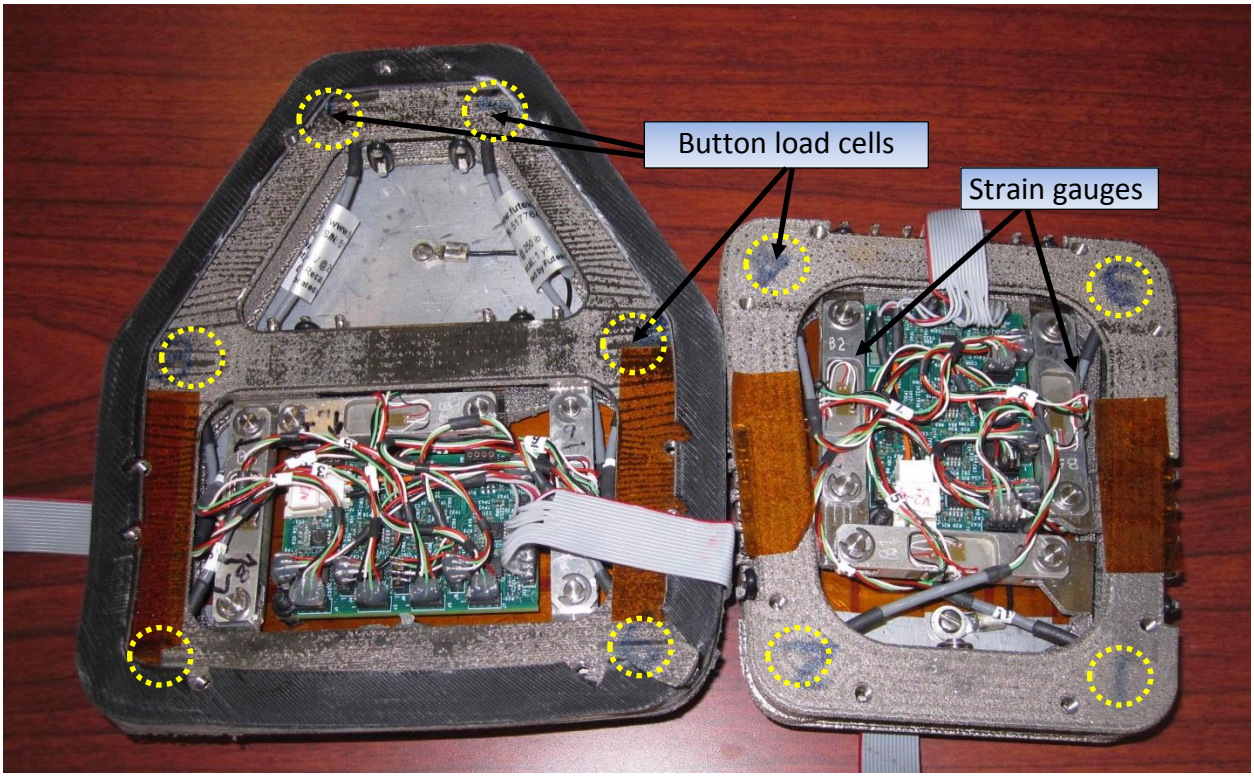

Figure 30 Sensor interface board mounted and wired in the foot sensor assemblies – Toe module (left) and heel module (right).

6e/6g: Prototype fabrication

Prototypes of both sensors have been fabricated using a titanium rapid prototyping process (Figure 31 and Figure 32). Environmental sealing, electronics integration, cabling and shoe attachment methodologies (6c) have been fabricated and tested. All design criteria outlined in 6a and 6b were met. Initial testing of the shoe sensor against an embedded force plate has been performed. Two fully functional sets (two toe nodes and two heel nodes) of foot sensors have been manufactured, assembled and tested. Static load tests showed measurement error to be below 3% of body weight.

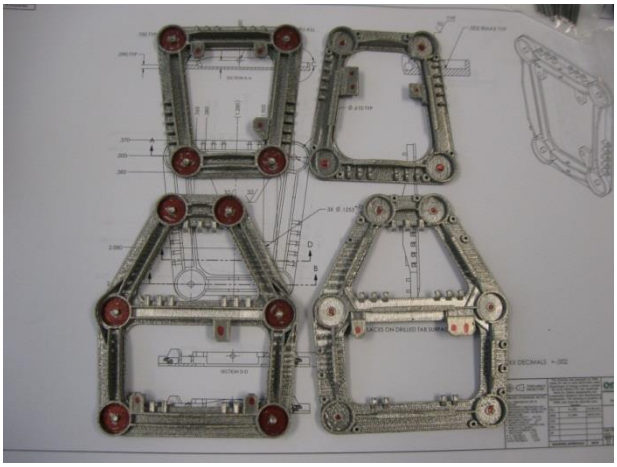

Figure 31: Prototypes of the heel (top) and forefoot (bottom) force sensor housings.

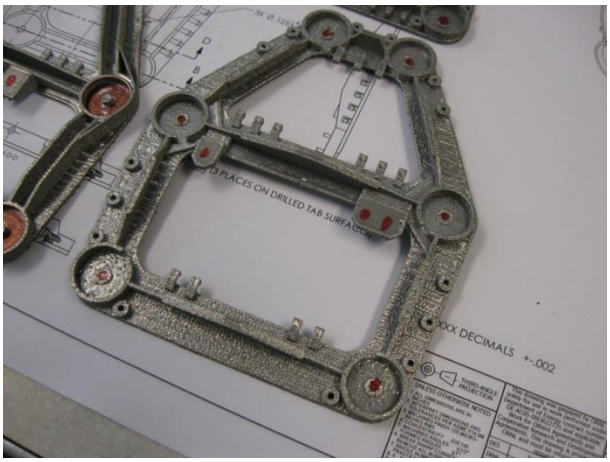

Figure 32: Close up of one of the two halves of the forefoot sensor housing.

Task 7: Software interface development

Software has been developed to post-process the data stored on the SD cards at each sensor node or the data transmitted via Bluetooth. Currently a GUI which can start and stop the data collection and display real time data channels including IMU and force data has been developed. The interface will continue to be developed. As more of the algorithm and software including the extended Kalman filter is embedded into the hardware, the software will be a window into what is being measured and calculated on the device. This will be a focus of the team once the system is validated, then clinical feedback from clinicians will be crucial to make an interface that is intuitive, powerful and displays meaningful data that will have immediate clinical impact.

Currently, two software systems are being developed by the respective engineering groups. This will be consolidated over the coming year into a single system. However, as the hardware systems are being developed, the engineers responsible for those systems are also developing the needed tools to operate and control their respective systems.

The ORNL system incorporates a GUI programmed in the Python programming language. It was picked because python is available on all major operating systems available today (Windows, Linux, MAC). This gives a great deal of flexibility in deploying this software to systems that are familiar to clinicians. The ORNL GUI provides for connecting to the various Bluetooth sensor nodes, as well as controlling basic low-level parameters of the sensor nodes. (Figure 33)

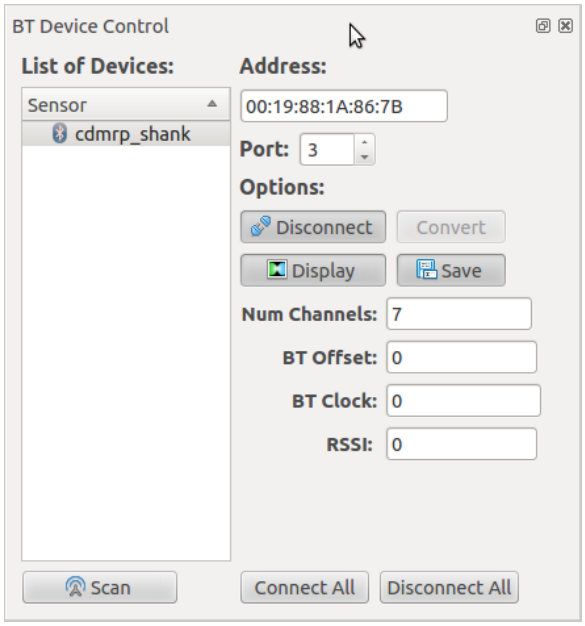

Figure 33 ORNL GUI, Bluetooth Control screen

It also provides the ability to control the starting and stopping of a collection event, including the name synchronization of storage files on all of the nodes involved in a particular collection event. (Figure 34)

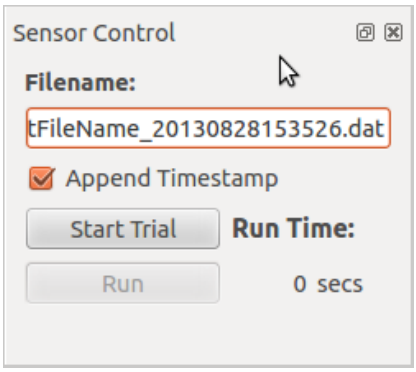

Figure 34 ORNL GUI Collection Event Control Screen

Lastly, the ORNL GUI provides the ability to view data from any available channel from any connected sensor in real time. This allows the user to see how things are behaving right now in the system. Currently this data is unprocessed, but future improvements will include the ability to see processed data in real time. (Figure 35)

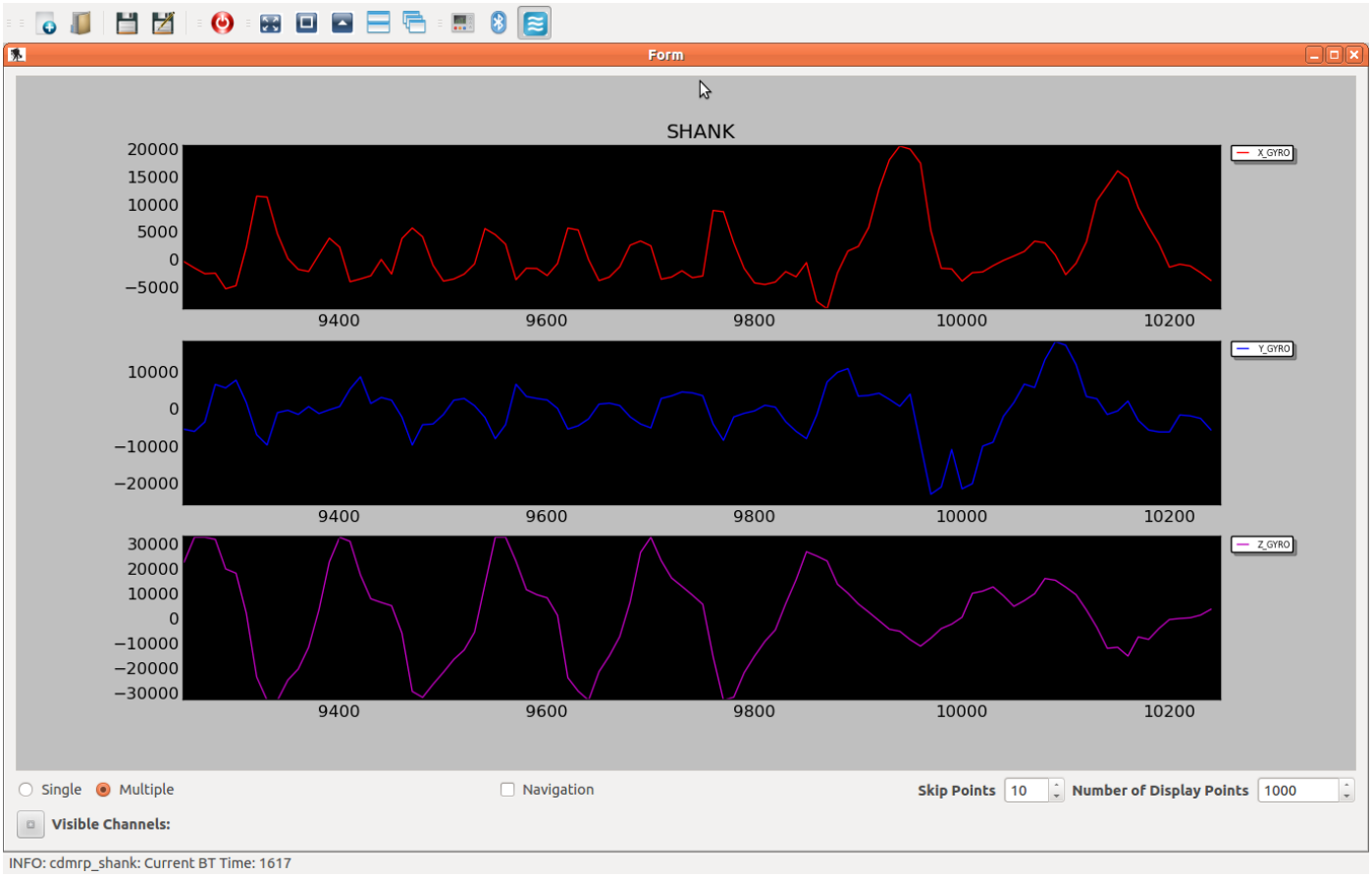

Figure 35 ORNL GUI Example data screen showing data from 3 channels of 1 particular sensor (Shank)

Within the last year, the Ottobock GUI system has also been extended with analysis software, which processes the limb segment orientations and facilitates interpretation of the data. The software incorporates a gait cycle detection algorithm, a gait cycle analyzer, an auto-calibration procedure and a user interface.

Figure 36 shows the software user interface. The left side contains controls to operate the measurement system, edit patient data and to save and load measurements. The right side displays plots of several detected gait cycles (knee angle in this case). Below the knee angle plot, the gait analyzer provides its results.

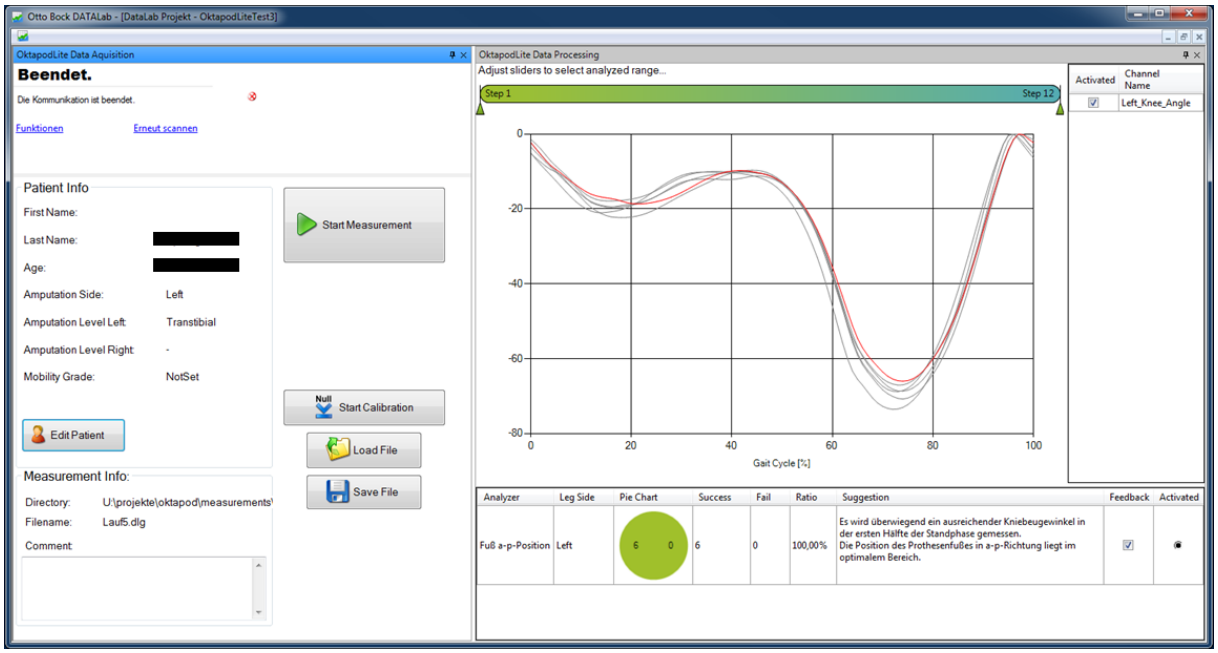

Figure 36. Analysis software user interface.

The gait cycle detection algorithm works solely on received segment orientations and does not depend on any force or acceleration data. Detected gait cycles are immediately plotted to the screen and serve as a basis to investigate and optimize the prosthetic alignment.

A simple gait analyzer has been designed to evaluate the foot AP position of a transtibial amputee, as it is an important optimization parameter during the fitting process. In order to identify a “good”” AP position, the shape of the knee angle curve is compared to a physiological curve shape.

Previously, the thigh and shank sensors were required to be strictly aligned to the sagittal plane. An auto-calibration procedure has been implemented in order to relax this constraint. The rotational shift about the limb long axis is automatically determined during the first three to five steps of a measurement trial.
The next steps will be to implement improvements of the analysis software. So far, the gait cycle detection algorithm works exclusively for ground level walking, but it is desirable to extend its detection capabilities to ramp and stairs

All F/M Octapod sensor data was made visible with the DataLab software (Figure 37), transformed to anatomical landmarks and exported to be further analyzed biomechanically.

Figure 37. Data sequence F/M Sensor during gait lab measurements.

Task 8: Evaluation of prototype device during clinical assessment/training

Up to this date, the data was collected on three (3) amputee patients and three (3) control subjects. Data collection was performed on a healthy/control subject the week of August 27th 2012, December 10th 2012, Jan 14th 2013 and July 8th 2013. During the last visit, two (2) amputee patients and one (1) control subject participated in the evaluation.

The amputee patients were three different unilateral trans-tibial subjects and they each performed different activities. It is believed, considering the current progress and system reliability, that during the next visit more subjects can participate in the evaluation This evaluation will be used to improve the accuracy of the results from the MGAS system compared to camera based biomechanical analysis systems. The evaluation also involves feedback from clinicians on the ease of use and validity of incorporating this system in their day to day practice.

In order to compare the data obtained from the MGAS and the CFI gait lab the patient was instrumented with the MGAS sensors and gait lab markers (Figure 38).

Figure 38. Control Subject instrumented with sensors and markers.

The data was synchronized using force plate signal from both systems. Three different measurement systems were compared ORNL vs. CFI and OB vs. CFI. The results were transformed to match the CFI coordinate frame. At this point the major interest was in the following parameters:

- Thigh orientation
- Shank Orientation
- Knee angle
- Foot orientation
- Ground reaction forces
- Sagittal moments.

For the three subjects 5-6 trials were performed for three different walking speeds (Froude 1, 3 and 5) on level ground and 2, 2 and 6 measurements with normal and slow speeds on slopes (5° and 10°) and none, 3 and 2 measurements on stairs.

The shank, thigh and knee orientation errors for the whole system obtained using the Mobile Gait Analysis System was approximately 1 deg. (Figures 35-37). The internal/external rotations errors were <3.5deg.

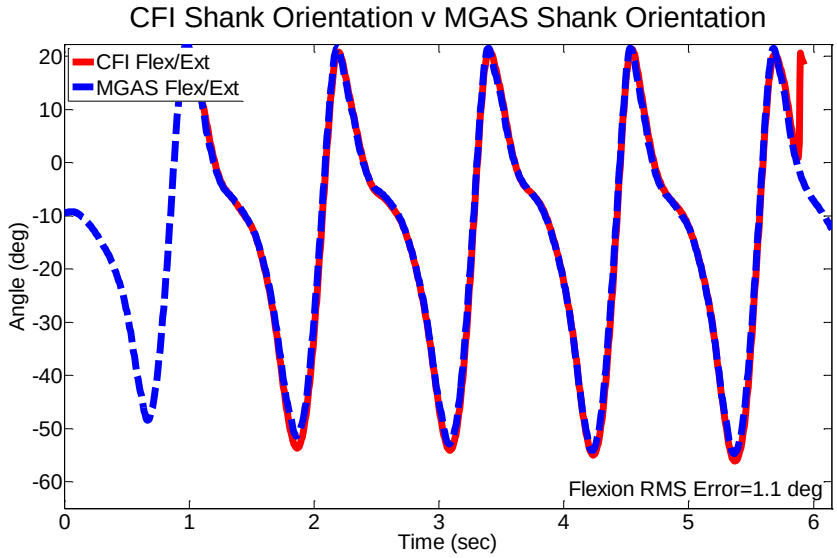

Figure 39 Shank orientation comparison - MGAS vs CFI.

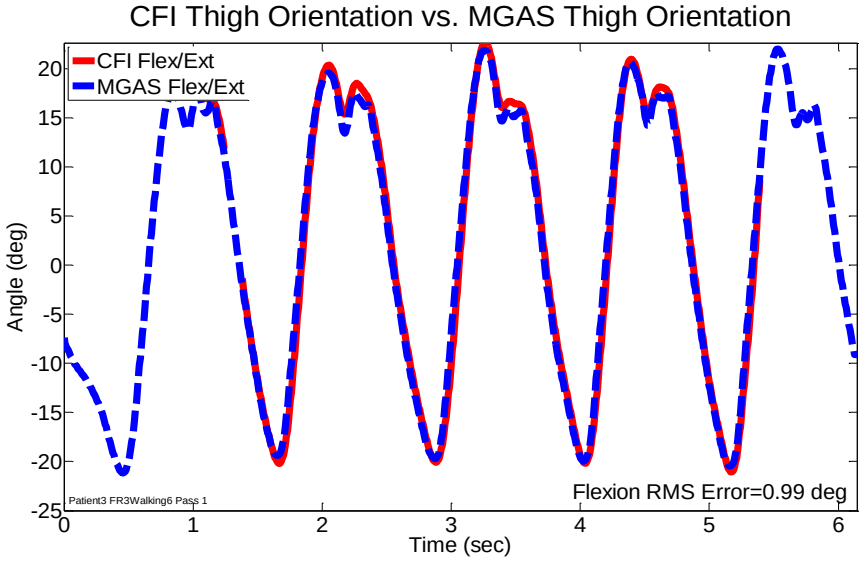

Figure 40. Thigh orientation comparison - MGAS vs. CFI.

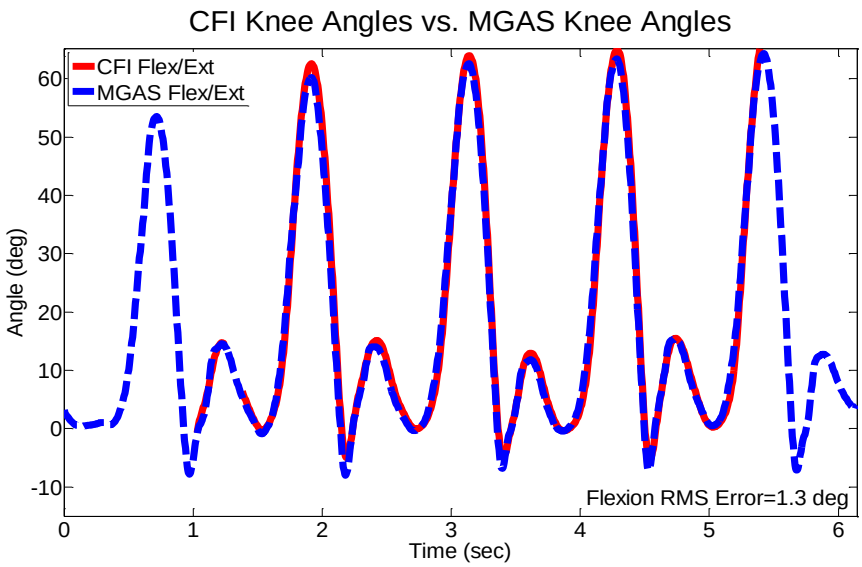

Figure 41. Knee orientation comparison - MGAS vs. CFI.

The foot orientation was harder to compare due to differences in kinematic models. The CFI foot model is a single body link with an ankle joint. The ORNL foot model is more complex and comprises of heel segment and toe segment with an ankle joint. A three degree of freedom spherical joint constraints the heel and toe. Based on the obtained orientation curves the CFI foot model is closer to the toe segment of the ORNL foot model (Figure 42). Note that this does not represent a problem, merely a difference in the way that the models are constructed.

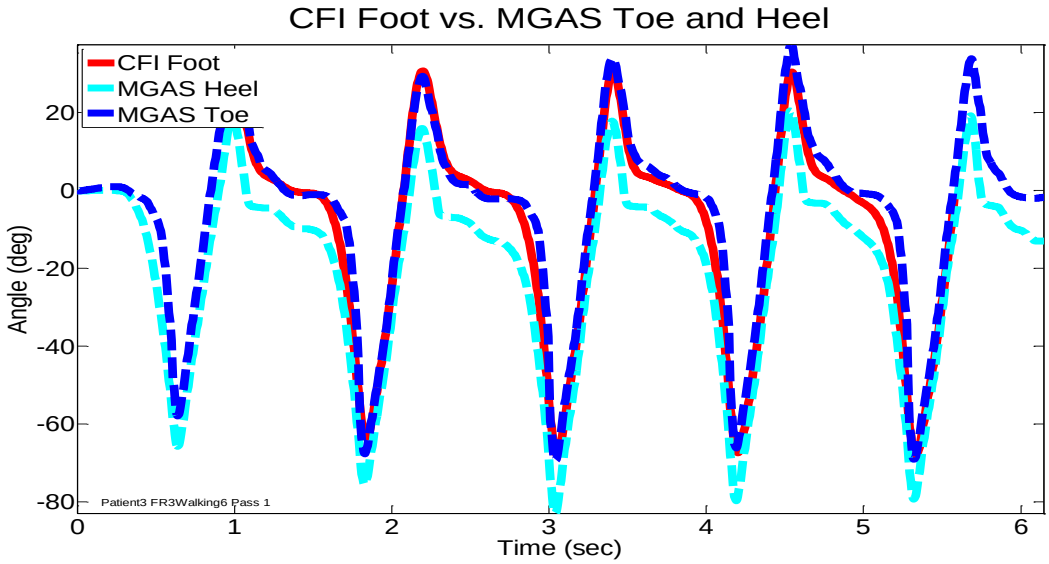

Figure 42. Foot orientation comparison - MGAS vs. CFI.

The foot force data shows excellent curve shape matching but indicates an amplitude disagreement (Figure 43). The reason for that has been identified as a mechanical assembly error, with a portion of the force being transferred around the load cells responsible for the measurement. This has been resolved, and in-lab testing now shows agreement to within 3% of body weight. Thus, it is expected that the next force data collection errors should be consistent with that 3% error.

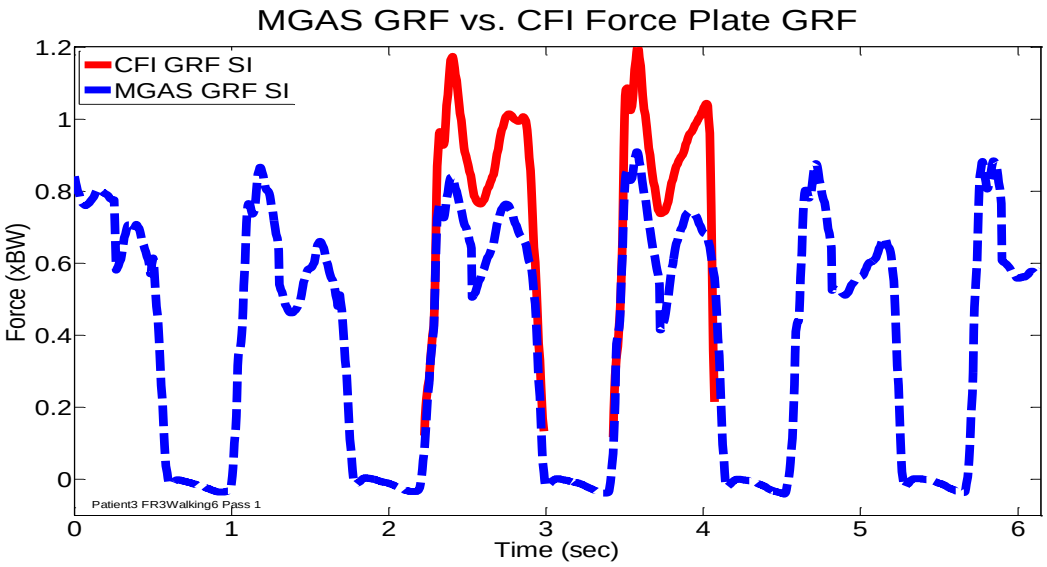

Figure 43 Ground Reaction Force data comparison - MGAS vs. CFI.

The calculated ankle angle is presented in Figure 44, and demonstrates excellent data agreement with CFI's calculated angle with an RMS error of 2.4°. These results can be further improved if the foot models used by MGAS and CFI are unified.

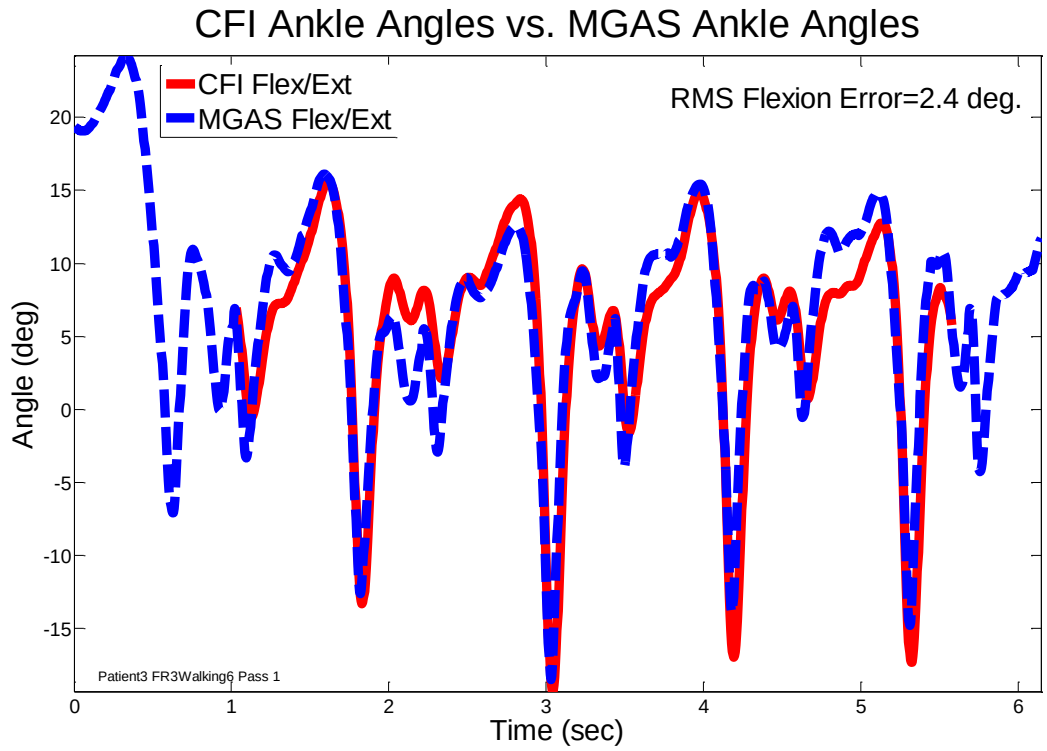

Figure 44 Ankle orientation comparison - CFI vs. MGAS

In order to facilitate the gait analysis, several post processing tools are under development. For example gait analysis is very often visualized using normalized gait cycles. Software has been developed to rapidly display this type of information (Figure 45).

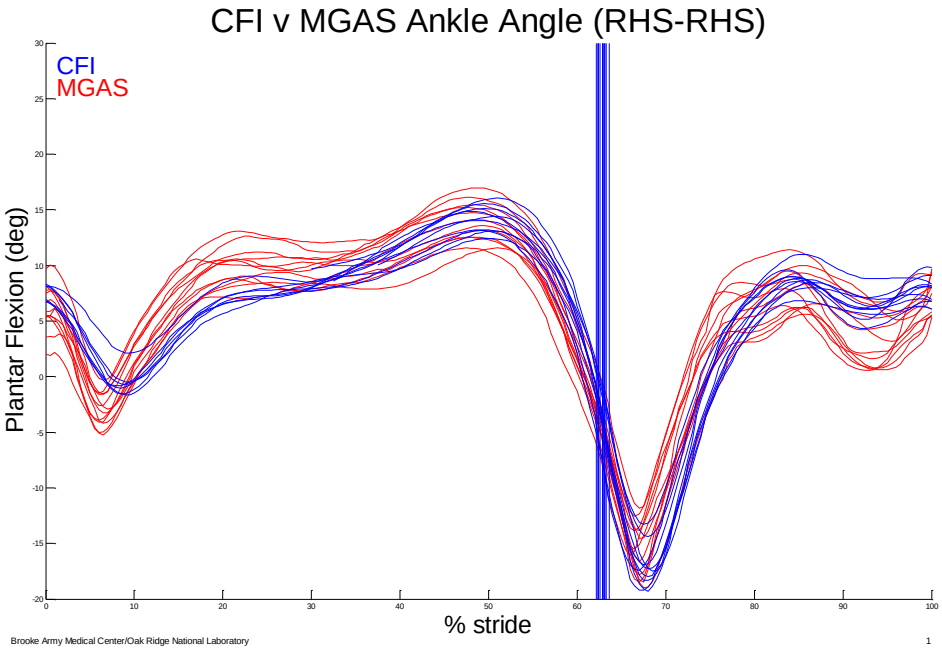

Figure 45 Gait analysis with normalized gait cycles. Ankle cycles presented.

Another type of assisting function under development is foot orientation with force load animation. The walking cycle can be slowed down or stopped and watched frame by frame (Figure 46).

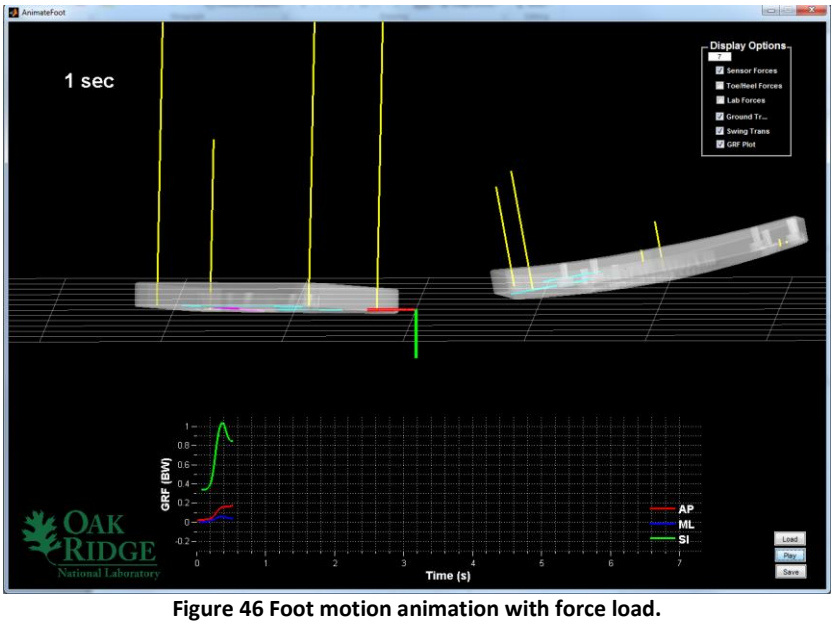

Figure 46 Foot motion animation with force load.

An initial inverse dynamic model was also developed. It calculates joint moments and powers. A sample is presented in Figure 47.

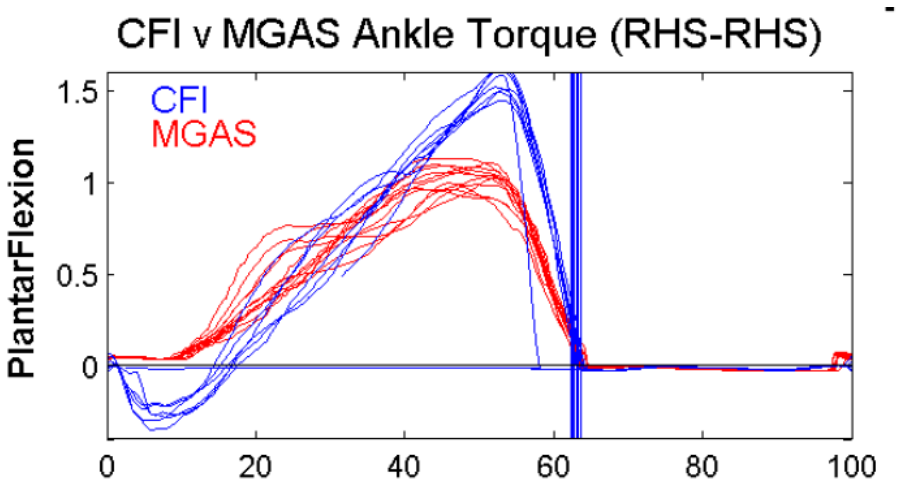

Figure 47 Inverse dynamic calculated for the Ankle. Initial Results.

During measurement sessions at the CFI gait laboratory, the accuracy of the OB inertial measurement system was also verified. Figure 48 through Figure 50 show a comparison of simultaneously recorded shank, thigh and knee angles. Although both systems were not aligned to the same coordinate frame, the signals match very well.

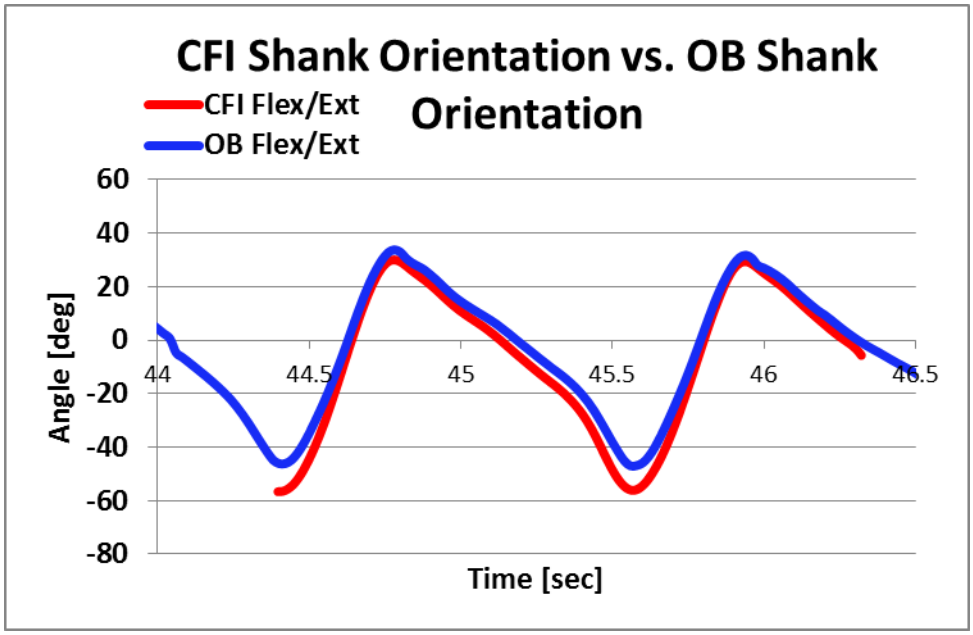

Figure 48 OB Shank orientation comparison - OB vs. CFI.

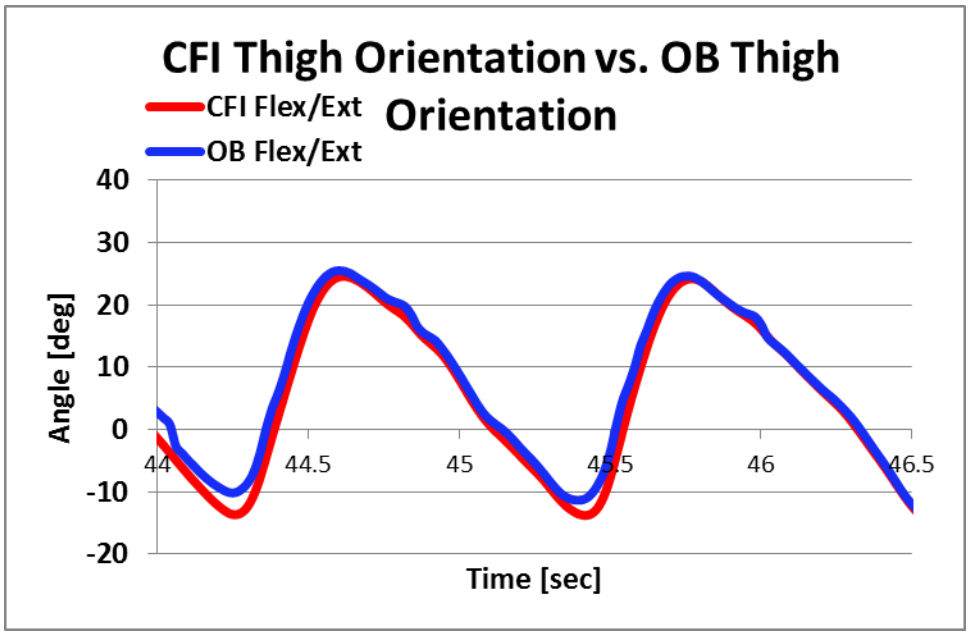

Figure 49 OB Thigh orientation comparison - OB vs. CFI.

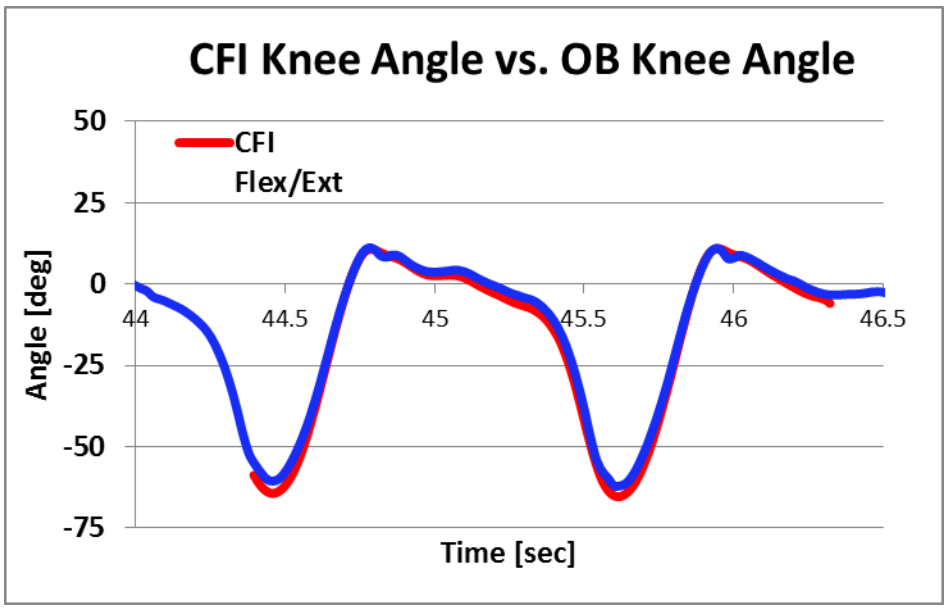

Figure 50 OB Knee orientation comparison - OB vs. CFI.

The CFI's MOCAP data was calculated to match the position of the Octapod F/M Sensor which was recorded via virtual markers. A data comparison of the two systems was then performed for this position. As an example the vertical ground reaction force and the sagittal moment at the Octapod position are shown in Figure 51 and Figure 52.

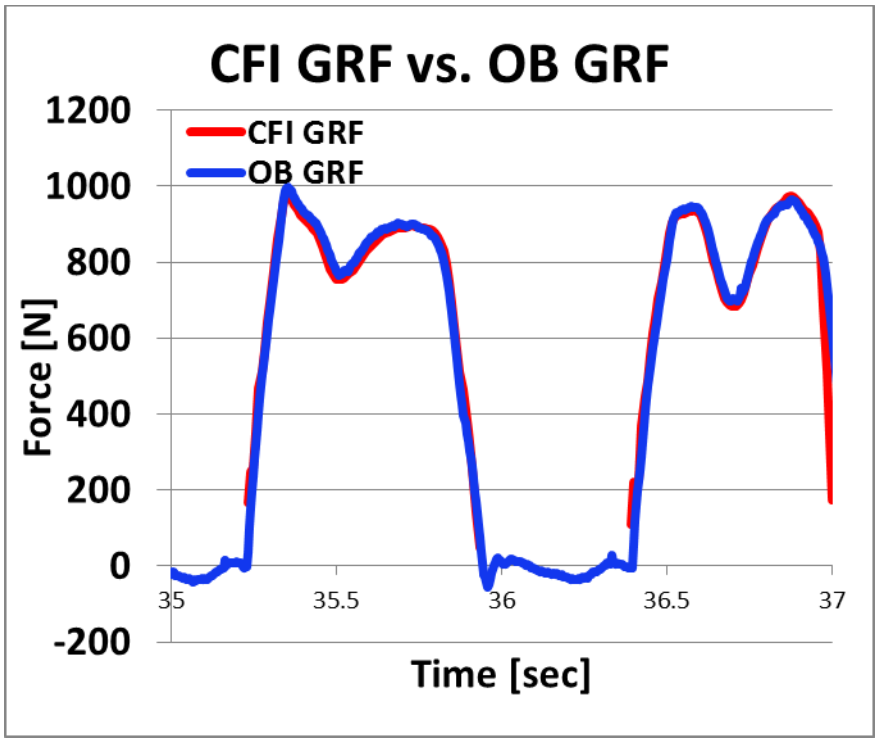

Figure 51 Vertical force comparison CFI vs. OB Octapod.

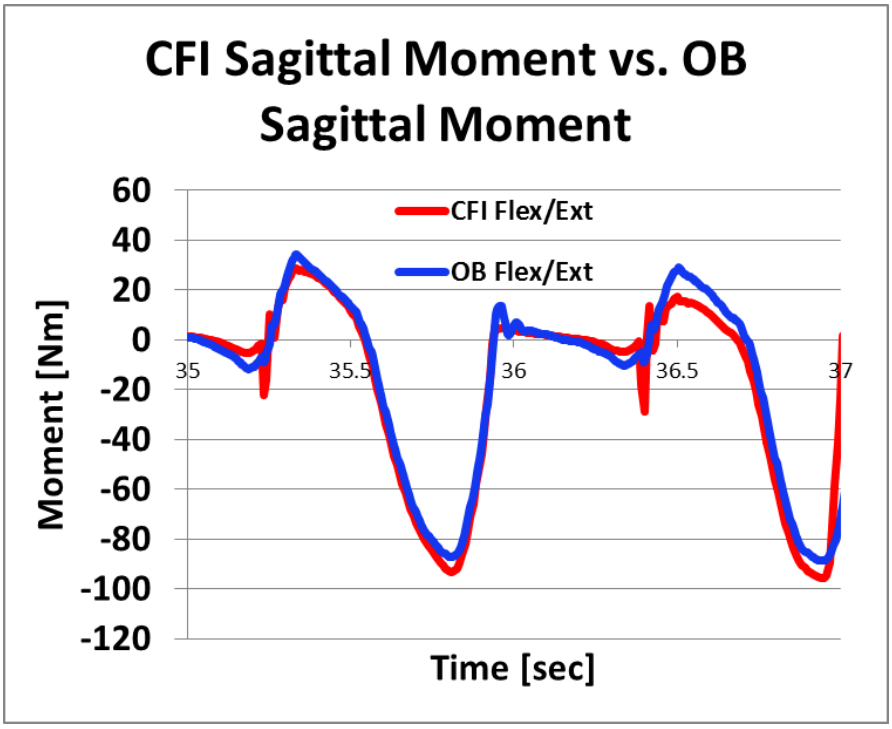

Figure 52 Sagittal moment comparison CFI vs. OB Octapod.

It is clear that the vertical force data matches very well, while the moment data is also a close match. However, it is affected by a small transformation error observed in the second step.

During the last MGAS trials at the CFI, all mechanical and electrical components performed according to initial requirements. The current battery power system provides at least 4 hours of continuous operation with some sensors capable of running up to 16 hours. This is well above the requirement of 1 hour. Additionally, ergonomic factors were substantially improved decreasing the time for patient setup. Further, decreased weight, volume and cabling resulted in a better more comfortable experience for both the patient and the clinician.

Improvements are expected in the coming year regarding the presentation of clinically meaningful data to users. Additional data collection and prosthesis adjustment sessions are necessary to bridge the gap between acquired raw unprocessed data and the desired processed data that has high relevance to the clinician or prosthetist.

Task 9: Develop activity performance criteria

The activities best performed to garner clinically meaningful data will be determined as the prototype is tested and data analyzed. Currently, the activities measured are over-ground walking at various speeds, incline walking and stair climbing.

Sample interpretations of the F/M sensor data (acquired at CFI when the first subject used the system) are given below. These are based only on non-statistically acquired data - verification will require more data from different subjects. However, it can already be shown that the mobile F/M sensor and the inertial sensor provide information which can be related to known results of Gait-Lab data.

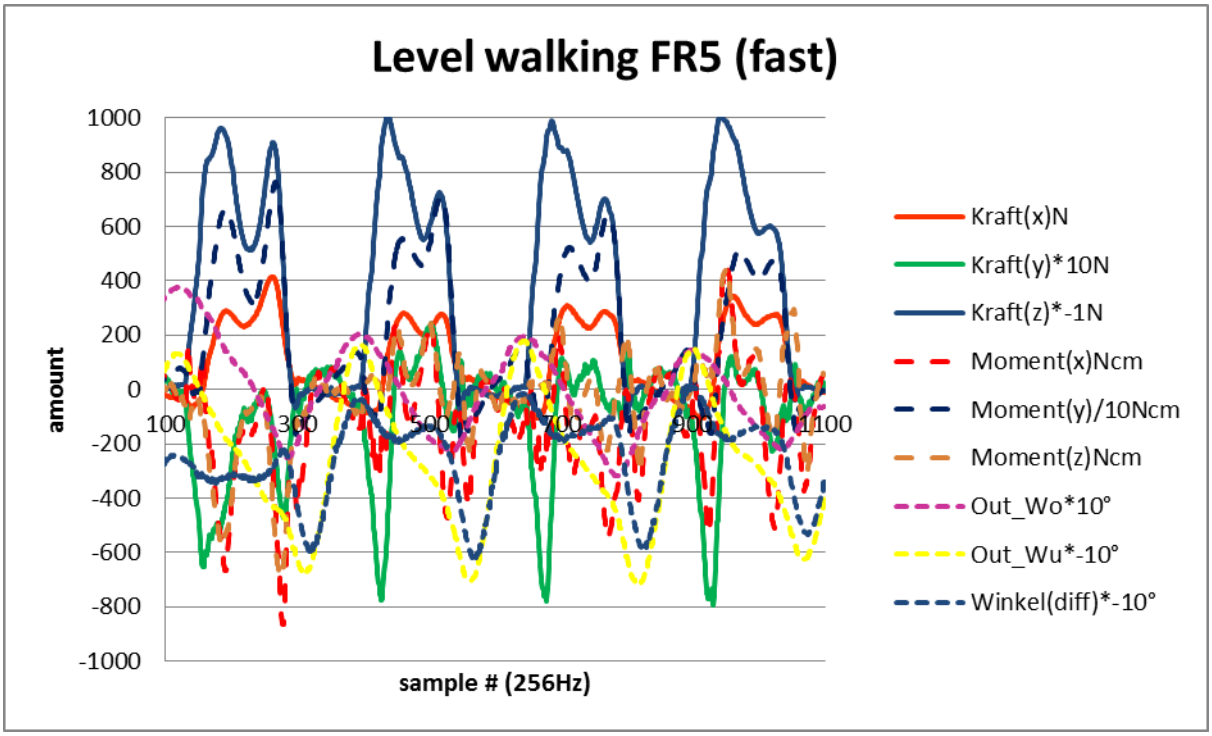

Figure 53 Level Walking Froude 5 ("Kraft" = Force, "Winkel" = Angle).

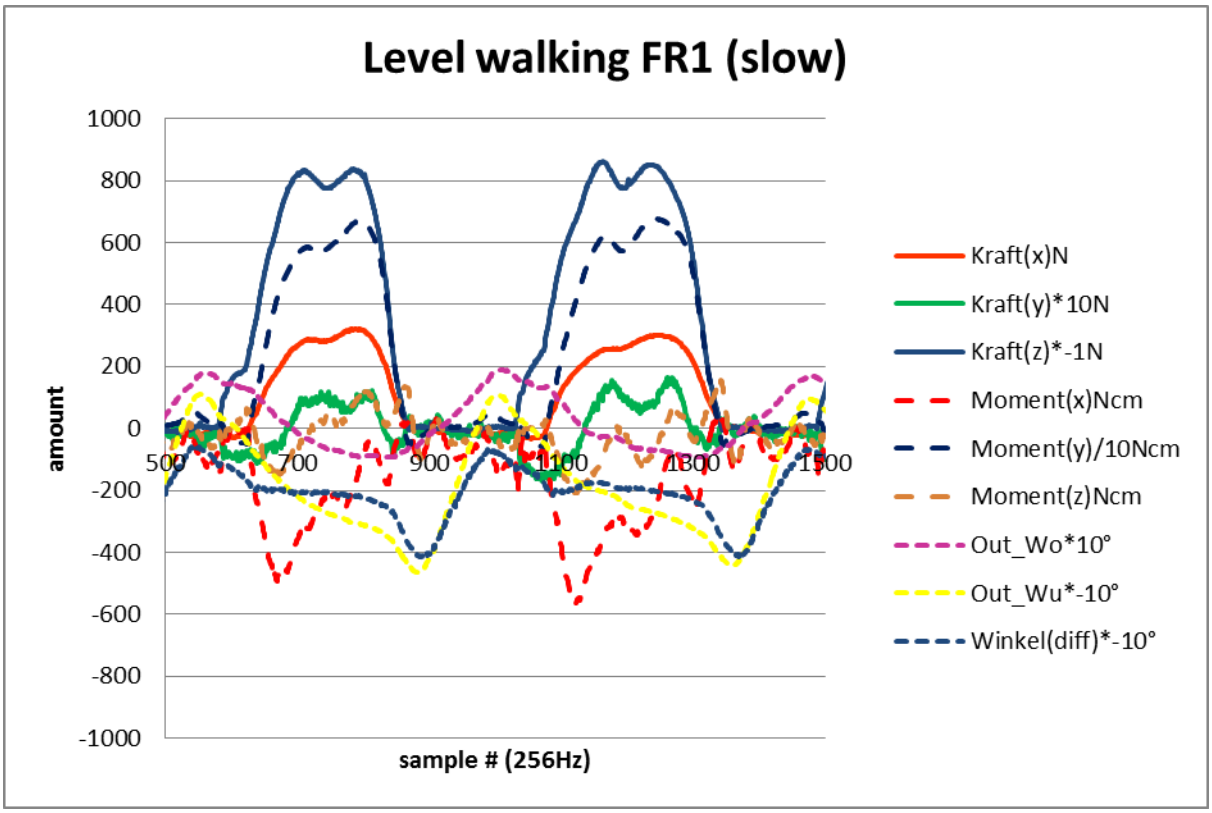

Figure 54 Level walking Froude 1 ("Kraft" = Force, "Winkel" = Angle).

Figure 53 and Figure 54 show the same subject with fast and slow walking on level ground. Fz (vertical) shows increased peaks when walking faster. Both orthogonal forces must be considered carefully as the F/M Sensor was positioned below the residual limb and changed in its orientation for alignment purposes. Nevertheless, the Fy peak at heel strike, walking fast, is remarkably different in comparison to walking slow. This indicates that the movement in frontal plane in both situations is also of interest (and a future task). It also gives motivation to continue testing with varying walking speeds, because opposing signal characteristics of different walking speeds indicate certain areas for optimization. A mobile system therefore is ideal because the subject can change walking velocity during a single sequence of steps (not typically performed in the lab, where feedback information for a constant reliable walking velocity is supplied to the subject).

Pre-flexion of the knee (dark blue dashed line) is visible in slow walking, but while walking fast, the knee starts to flex when Fz develops in stance. When walking fast, knee flexion reverses close to mid-stance. However, while walking slowly, the flexion angle achieved at heel load remains level.

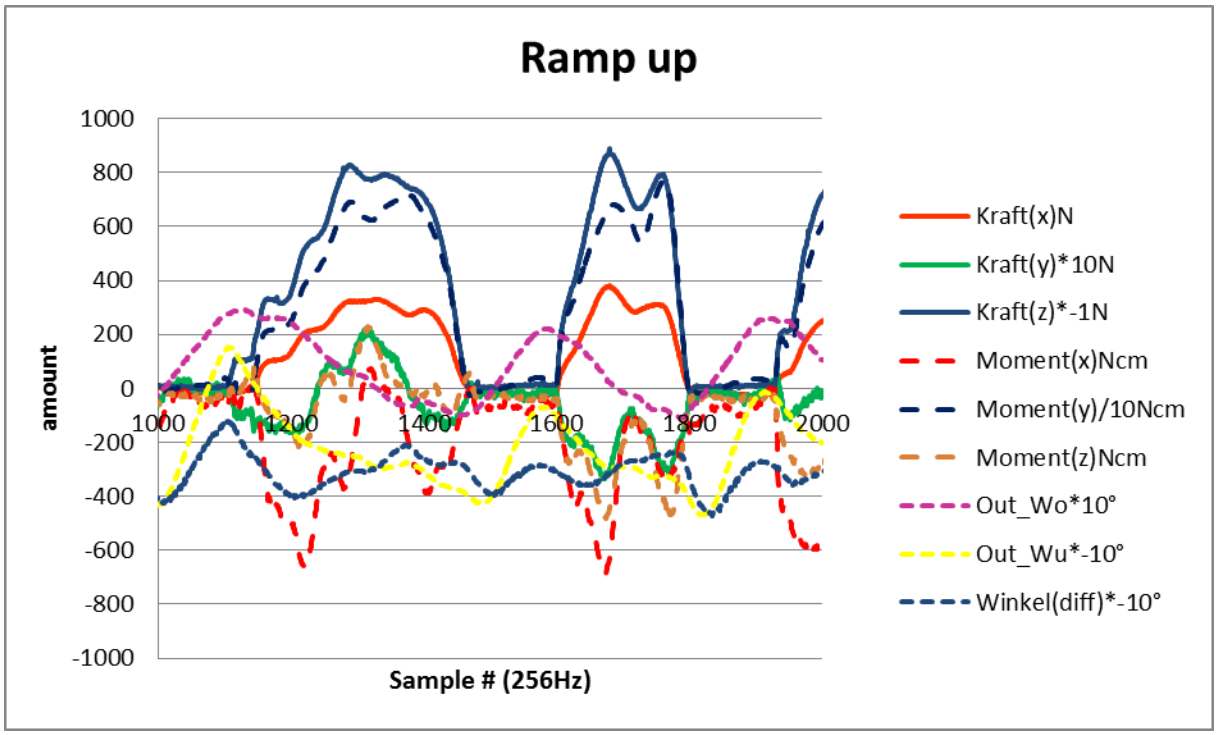

Figure 55 Ramp Up ("Kraft" = Force, "Winkel" = Angle).

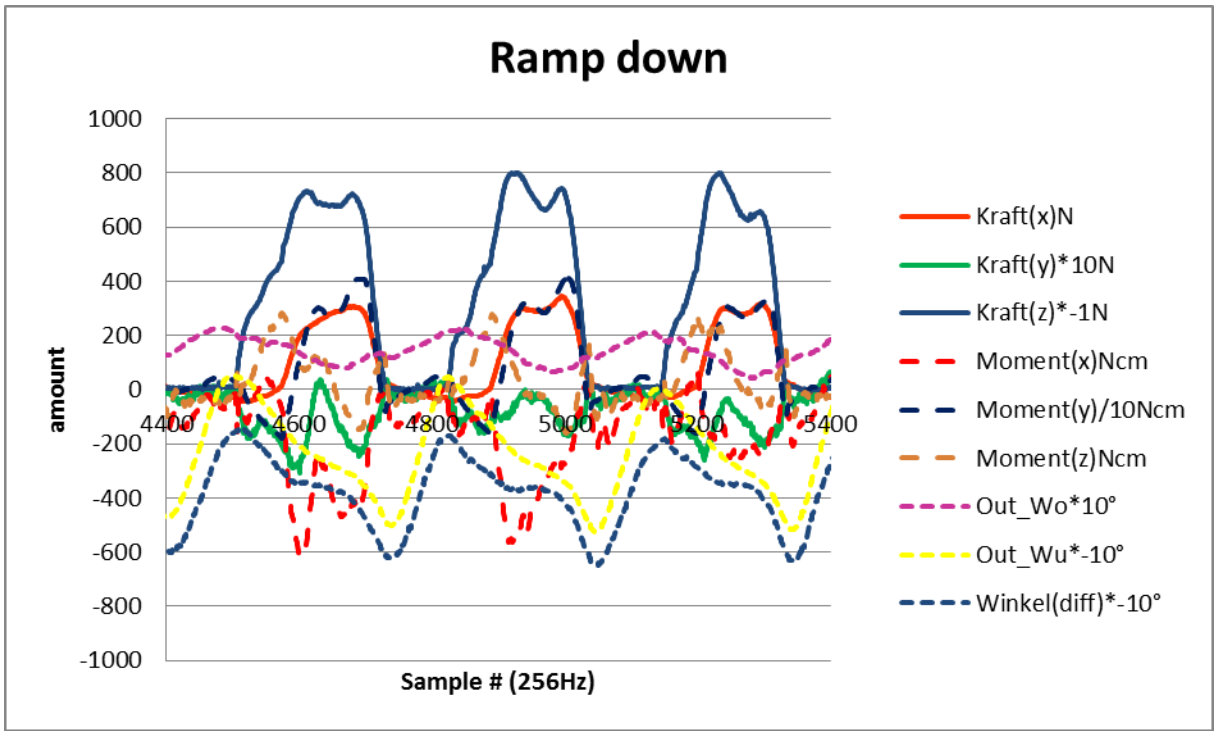

Figure 56 Ramp Down ("Kraft" = Force, "Winkel" = Angle).

The knee angle (Figure 55) shows a lower angular range, because the subject walks up the ramp by tilting the thigh and shank forward simultaneously (pink and yellow dashed lines). When walking down the ramp

(Figure 56) the thigh shows a lower range of motion and the shank a higher range. This comparison shows the subject's ability in a preferred knee angular direction of motion.

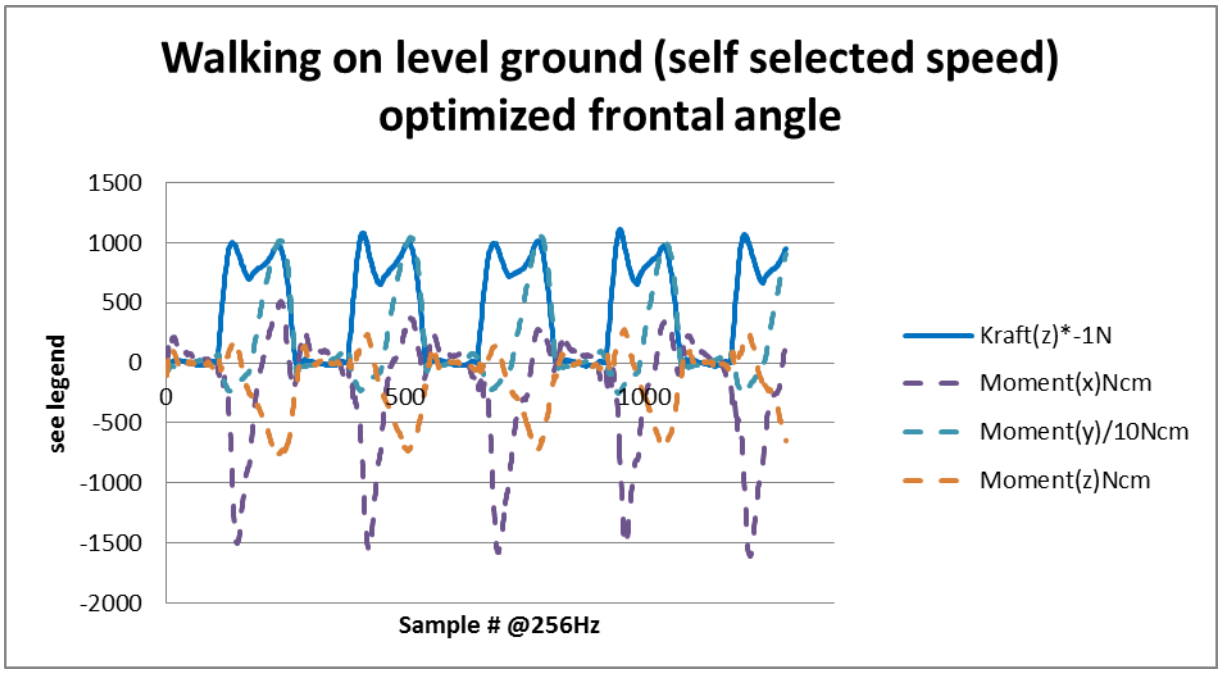

Figure 57 Level ground walking, Self-selected Speed ("Kraft" = Force).

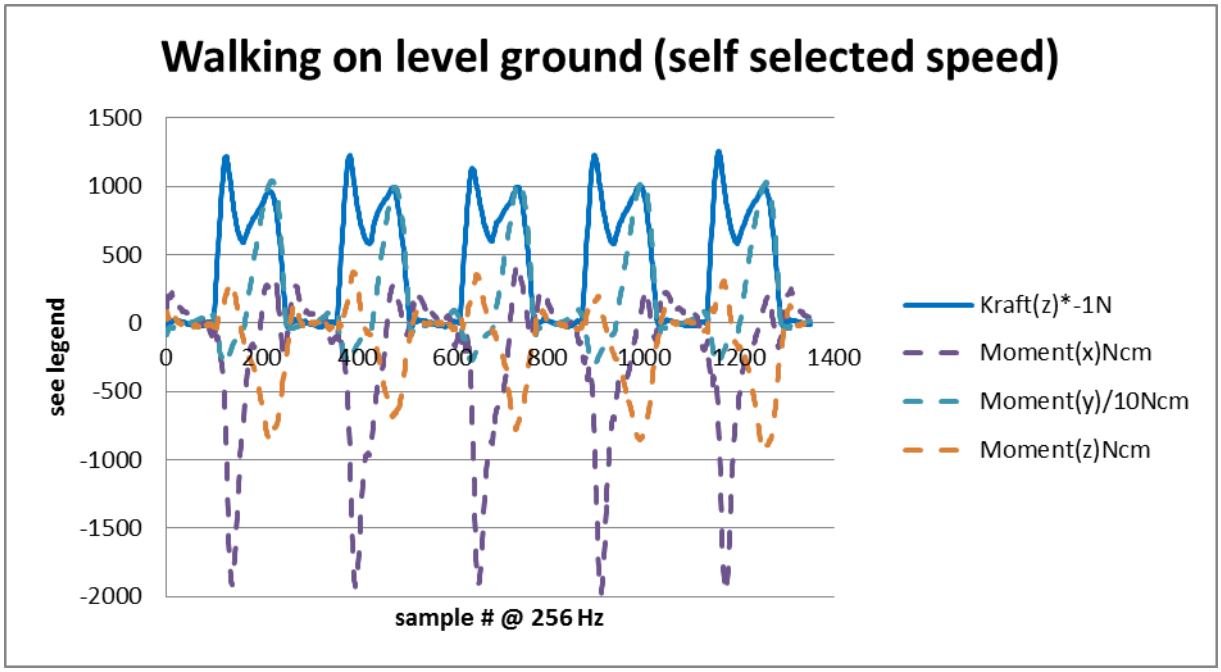

Figure 58 Level ground walking, Self-selected Speed ("Kraft" = Force).

Acquiring F/M data after every iterative step of optimization, in which the prosthetist optimizes based on experience, expertise and by visual and patient feedback. The results in Figure 57 and Figure 58 clearly show, for one subject, the effect with regards to the frontal moment: as the foot is shifted in the frontal plane to reduce the visible angular motion of the knee, the moment in this plane decreases by about 25%.

As Fz (vertical force) is also decreasing, it becomes obvious that a modification in the foot position causes less stress to the knee, but not necessarily by directly shortening the active lever-arm.

This example, seen with the second of three subjects for whom the data is now available, shows the complexity of the data acquired and the need for statistically relevant data on more subjects.

Task 10: Optimization of system durability for clinical implementation

During the most recent visit to the CFI, three subjects wore the MGAS components and performed ground level, slope and stair walking activities. Each subject had the system on approximately four (4) hours. No major mechanical issues were identified. Since the previous report the foot sensor was tuned to remove mechanical noises and provide improved mounting. More details available in task 6c.

Also the wireless communication was improved and no connection interruptions were observed. More work needs to be done in the area of data download performance and initial connection establishment. It is also believed that more data may be required concerning high level activities to finalize the design.

As problems arise during testing and during use in the "clinical" environment these adjustments will be made.

Task 11: Collection of activity data using multiple alignment configurations with comparison to opto-electric (camera based) motion capture system

This will be performed once all healthy/control subject data has been collected and the prototype system which meets the demands of the clinician is completed.

Task 12: Use data to determine metrics to indicate positive patient biomechanics factors and indicate successful prosthesis fit and alignment

This will be performed using data collected in Task 11.

Task 13: Develop 4 fully functional units

This task will begin once Tasks 1 through 12 are completed.

Task 14: Reintroduce final system in clinic

This task will follow task 13.

Task 15: Direct use in patient setup and alignment for multiple patients

This will occur concurrently with Task 14.

Key Research Accomplishments

- The system requirements and the initial system architecture for the MGAS have been established.
- Testing of different IMU units has been performed to determine sensor and signal quality and efficacy in determining joint angles.
- Algorithms to calculate joint angles from acceleration and angular rate signals from IMUs have been developed. This will be an ongoing process but with current methods, the system provides accuracy compared to the gold standard motion analysis methods of better than 2 degrees RMSE.
- Design iterations and testing of the "smart pylon" have been completed
- The design of the foot sensor prototype mechanical and electronic components has been completed and fabrication of device and associated electronics completed.
- Data acquisition and wireless transmission devices and software have been designed, fabricated, implemented and tested during data collection at Center for the Intrepid.
- A protocol for the testing and validation of the MGAS system has been established and the IRB approved.
- Data has been successfully collected from the first three TT amputee patients and three control subjects.
- A second generation of the electronics has been designed, fabricated and tested
- The electronics reliability has been greatly improved.
- A safe, secure, reliable and quick mounting system has been designed, implemented, and successfully evaluated.
- Significant improvements have been achieved in system weight, volume, attachment and assembly complexity of the system components.
- Patient comfort has been improved in wearing the system components
- Preliminary ground work on providing clinically meaningful data has begun

Reportable Outcomes

- One post-doc, three Science Undergraduate Laboratory Internship (SULI) positions and a project which won first prize in the Siemens Competition in Math, Science and Technology by two Oak Ridge High School (Oak Ridge, TN) students has been supported as a result of this grant.
- A paper was presented at the 2nd Annual Future of Instrumentation International Workshop November 7-8, 2011. (Appendix 1)
  http://www.ornl.gov/sci/ees/mssed/futureinstruments/index.shtml
- A podium presentation was made at MHSRS August 13-16, 2012 and a manuscript submitted which, if accepted, will be published in Military Medicine. (Appendix 2)
  https://www.ataccc.org/
- A Patent application has been filed on the titanium foot sensor system (Appendix 3).
- A patent application has been filed on the MGAS electronics system (Appendix 4).
- A podium presentation was made at the 1st Annual ORNL Post-Doc Symposium, 2013.
- A podium presentation was made at MHSRS August 12-15, 2013.

Conclusions

Significant progress has been made on the Mobile Gait Analysis System in the past year. The electronics and software have each had the benefit of going through significant revisions to correct errors and improve the robustness and feature completeness of the various systems.

At this point the majority of the electronics, hardware, and software are complete along with the wireless data transmission protocols. This represents a giant leap forward that should facilitate the on-going collection and analysis of patient data. Continuing software work will need to be done to enhance collection and analysis, however, the basic functionality of all major components of the system are in place and functional.

To date, data has been collected from 3 control subjects and 3 amputee patients, and initial results are proving to be exceedingly promising.

Significant early delays for data collection were the result of delays in the IRB and ORP approval process. The delay in data collection put the team significantly behind schedule for some of this project's milestones.

We anticipate several more trips to CFI in the coming year to collect data and to further improve upon analysis methodologies. The data from these results will be used to further improve the system and provide meaningful "clinical data". This clinical data will improve the method in which clinicians personalize prosthetics and train patients while also improving clinical results.

References

1. Gawande A. Notes of a Surgeon Casualties of War — Military Care for the Wounded from Iraq and Afghanistan. N Engl J Med. 2004 351;24. 2473-2475.
2. Mayfield JA, Reiber GE, Maynard C, Czerniecki JM, Caps MT, Sangeorzan BJ. Survival following lower-limb amputation in a veteran population. Journal of Rehabilitation Research and Development. May/June 2001. (38) 3. 341–345.
3. U.S. Department of Health and Human Services, AHRQ, Agency for Healthcare Research and Quality. National Healthcare Quality Report, 2007. http://www.ahrq.gov/qual/nhqr07/Chap2.htm. Accessed Oct. 7, 2008.
4. Reiber GE. Who Is At Risk of Limb Loss And What To Do About It? Journal of Rehabilitation Research and Development. Nov. 1994. (31) 4. 357-362.
5. Schmalz T, Blumentritt S, Jarasch R. Energy expenditure and biomechanical characteristics of lower limb amputee gait: the influence of prosthetic alignment and different prosthetic components. Gait Posture. 2002 Dec;16(3):255-63.
6. Schmalz T, Blumentritt S, Jarasch R. Energy expenditure and biomechanical characteristics of lower limb amputee gait: the influence of prosthetic alignment and different prosthetic components. Gait Posture. 2007 Feb;25(2):267-78.
7. Kulkarni J, Gaine WJ, Buckley JG, Rankine JJ, Adams J. Chronic low back pain in traumatic lower limb amputees. Clin Rehabil. 2005. Jan;19(1):81-6. Kulkarni J, Adams J, Thomas E, Silman A. Association between amputation, arthritis and osteopenia in British male war veterans with major lower limb amputations. Clin Rehabil. 1998 Aug;12(4):348-53.
8. Nolan L, Wit A, Dudzinski K, Lees A, Lake M, Wychowanski. Adjustments in gait symmetry with walking speed in trans-femoral and trans-tibial amputees. Gait and Posture. 2003. 17: 142-151.
9. Vickers DR, Palk C, McIntosh AS, Beatty KT. Elderly unilateral transtibial amputee gait on an inclined walkway: A biomechanical analysis, Gait & Posture. 2007, doi:10.1016/j.gaitpost.2007.06.08.
10. Miff SC, Childress DS, Gard SA, Meier MR, Hansen AH. Temporal symmetries during gait initiation and termination in nondisabled ambulators and in people with unilateral transtibial limb loss. J. Rehab. Res. and Dev. 2005:42 (2), 175-182.
11. Quesada PM, Pitkin M, Colvin J. Biomechanical Evaluation of a Prototype Foot/Ankle Prosthesis. IEEE Trans. on Rehab. Eng. 2000:8(1), 156-159.
12. Buckley JG, ODriscoll D, Bennett SJ. Postural Sway and Active Balance Performance in Highly Active Lower-Limb Amputees. Am. J. Physical Medicine and Rehabilitation. 2002:81(1), 13-20.
13. Schmalz T, Blumentritt, Marx B. Biomechanical analysis of stair ambulation in lower limb amputees. Gait & Posture. 2007:25, 267-278.
14. Gard SA. Use of Quantitave Gait Analysis for the Evaluation of Prosthetic Walking Performance. J. Prosthetics and Orthotics. 2006:18(1S) 93.
15. Hofstad CJ, van der Linde H, Nienhuis B, Eng M, Weerdesteyn V, Duysens J, Geurts AC. High Failure Rates When Avoiding Obstacles During Treadmill Walking in Patients With a Transtibial Amputation. Arch Phys Med Rehabil. 2006:87, 1115-1122.
16. Ebrahimzadeh MH, Rajabie MT. Long-term Outcomes of Patients Undergoing War-related Amputations of the Foot and Ankle. J Foot Ankle Surg. 2007:46(6), 429-433.

17. Dennis DA, Komistek RD, Mahfouz MR, Outten JT, Sharma A. Mobile-bearing total knee arthroplasty: do the polyethylene bearings rotate? Clin Orthop Relat Res. 2005:440, 88-95.
18. Han TR, Chung SG, Hi S. Gait Patterns of Transtibial Amputee Patients Walking Indoors Barefoot. Am J Phys Med Rehabil. 2003:82(2), 96-100.
19. Dou P, Jia X, Suo S, Wang R, Zhang M. Pressure distribution at the stump/socket interface in transtibial amputees during walking on stairs, slope and non-flat road. Clinical Biomechanics. 2006:21, 1067-1073.
20. Segal AD, Orendurff MS, Klute GK, McDowell ML, Pecoraro JA, Shofer J, Czerniecki JM. Kinematic and kinetic comparisons of transfemoral amputee gait using C-Leg and Mauch SNS prosthetic knees. J. of Rehabil Res and Dev. 2006: 43(7), 857-870.
21. Lee WCC, Zhang M, Chan PPY, Boone DA. Gait Analysis of Low-Cost Flexible-Shank Transtibial Prosthesis. IEEE Trans on Neural Systems and Rehabilitation Engineering. 2006: 14(3), 370-377.
22. Kalman, R.E. A new Approach to linear filtering and prediction problems. Journal of Basic Engineering. 1960: 82 (Series D), 35-45.
23. Cui, C.K., Chen, G., 1999. Kalman Filtering: with Real Time Applications, 3rd ed. Springer, Berlin, Germany.
24. Favre, J., et al.,. Ambulatory measurement of 3D knee joint angle. Journal of Biomechanics. 2008: 41 (5), 1029–1035.
25. Luinge, H.J., Veltink, P.H.. Measuring orientation of human body segments using miniature gyroscopes and accelerometers. Medical and Biological Engineering and Computing. 2005: 43 (2), 273–282.
26. Favre, J., et al. Quaternion-based fusion of gyroscopes and accelero- meters to improve 3D angle measurement. Electronics Letters. 2006: 42 (11), 612–614.
27. Boonstra, M.C., et al. The accuracy of measuring the kinematics of rising from a chair with accelerometers and gyroscopes. Journal of Biomechanics. 2006: 39, 354–358.
28. Kavanagh, J.J., Menz, H.B. Accelerometry: a technique for quantifying movement patterns during walking. Gait Posture. 2008: 28 (1), 1–15.
29. Cutti AG, Giovanardi A, Rocchi L et al. Ambulatory measurement of shoulder and elbow kinematics through inertial and magnetic sensors. Med Biol Eng Comput. 2008: 46(2), 169–178
30. O'Donovan KJ, Kamnik R, O'Keeffe DT et al. An inertial and magnetic sensor based technique for joint angle measurement. J Biomech. 2007: 40,2604–2611
31. Cooper, G., Sheret, I., McMillian, L., Siliverdis, K., Sha, N., Hodgins, D., Kenney, L., Howard, D. Inertial sensor-based knee flexion/extension angle estimation. J. Biomech. 2009: 42, 1678-1685.

Appendicies

Appendix 1: Manuscript Submitted to FIIW 2011

Appendix 2: Manuscript Submitted to MHSRS 2012

Appendix 3: Patent Application for Wearable Foot Sensor

Appendix 4: Patent Application for MGAS Electronics System

A Mobile Motion Analysis System Using Inertial Sensors for Analysis of Lower Limb Prosthetics

John Kyle P. Mueller, Boyd M. Evans, III, M. Nance Ericson, Ethan Farquhar, Randall Lind
Measurement Science and Systems Engineering Division
Oak Ridge National Laboratory
Oak Ridge, TN, USA
muellerjp@ornl.gov

Kevin Kelley, Martin Pusch, Timo Von Marcard
Otto Bock Healthcare Products
Dunderstadt, Germany

Jason M. Wilken
Military Performance Lab
Center for the Intrepid-Brooke Army Medical Center
Fort Sam Houston, TX

Abstract— **Soldiers returning from the global war on terror requiring lower leg prosthetics generally have different concerns and requirements than the typical lower leg amputee. These subjects are usually young, wish to remain active and often desire to return to active military duty. As such, they demand higher performance from their prosthetics, but are at risk for chronic injury and joint conditions in their unaffected limb. Motion analysis is a valuable tool in assessing the performance of new and existing prosthetic technologies as well as the methods in fitting these devices to both maximize performance and minimize risk of injury for the individual soldier. We are developing a mobile, low-cost motion analysis system using inertial measurement units (IMUs) and two custom force sensors that detect ground reaction forces and moments on both the unaffected limb and prosthesis. IMUs were tested on a robot programmed to simulate human gait motion. An algorithm which uses a kinematic model of the robot and an extended Kalman filter (EKF) was used to convert the rates and accelerations from the gyro and accelerometer into joint angles. Compared to encoder data from the robot, which was considered the ground truth in this experiment, the inertial measurement system had a RMSE of <1.0 degree. Collecting kinematic and kinetic data without the restrictions and expense of a motion analysis lab could help researchers, designers and prosthetists advance prosthesis technology and customize devices for individuals. Ultimately, these improvements will result in better prosthetic performance for the military population.**

Keywords - Prosthetic, Motion Analysis, Inertial Measurement Unit, Ground Reaction Force Sensor

I. INTRODUCTION

Since the global war on terror began 10 years ago, the United States military has made great strides in how it treats wounded soldiers on the battlefield as well as in the hours and days following a soldier's injury. Although this has resulted in a decrease in mortality among the wounded, it has left thousands of soldiers and veterans with conditions like lower leg amputations which require long term care. Before their injuries, lower leg amputees in the military population were young, athletic and in top physical condition [1]. For this reason, most military patients want to remain active and in some cases return to active military duty. The likelihood of these patients returning to an active lifestyle for an extended period of time is dependent upon prosthesis fit and function, and the patient's acclimation to the device. One symptom of an ill-fitting or poorly functioning prosthetic device is asymmetric gait [2]. Asymmetric gait over extended periods of time can contribute to the development of overuse injury and chronic conditions like arthritis in the patient's healthy leg. One method for quantifying movement asymmetries and its effect on joint kinematics and kinetics is computerized motion analysis. In general, motion analysis requires access to gait labs which require a large open space. These facilities are not readily available, are expensive and are in high demand. The fitting of a prosthesis is also an iterative and ongoing process which means multiple gait lab analyses are needed to get the best results. It also requires patient testing be performed in a controlled lab environment, which may not represent normal performance of daily activities. Our objective is to develop a relatively inexpensive, portable, camera-less, motion analysis system using portable force sensors and inertial measurement units (IMUs) that can give prosthetists or therapists instant biomechanical information and feedback regarding prosthetic performance and fit on individual soldiers.

Funding provided by Department of Defense Congressionally Directed Medical Research Programs Funding Opportunity Number: W81XWH-09-PRORP-TDA

Oak Ridge National Laboratory (ORNL) is managed by UT Battelle, LLC for the U. S. Department of Energy under Contract No. DE-AC05-00OR22725.

II. MATERIALS AND METHODS

A. Robot Testing

A Mitsubishi Heavy Industry (Tokyo, Japan) PA-107C robot arm was employed for testing different prepackaged IMUs. Initial tests using a calibrated digital level showed that the encoder (joint angle) data from the robot was accurate to

within 0.2 degrees. The IMU system is intended to attain accuracy within one degree, therefore the encoder data is used as the gold standard in this experiment. The robot was run through repeatable motions several times while simultaneously recording the encoder data from the robot with the gyroscope and accelerometer data from the IMUs (Fig. 1).

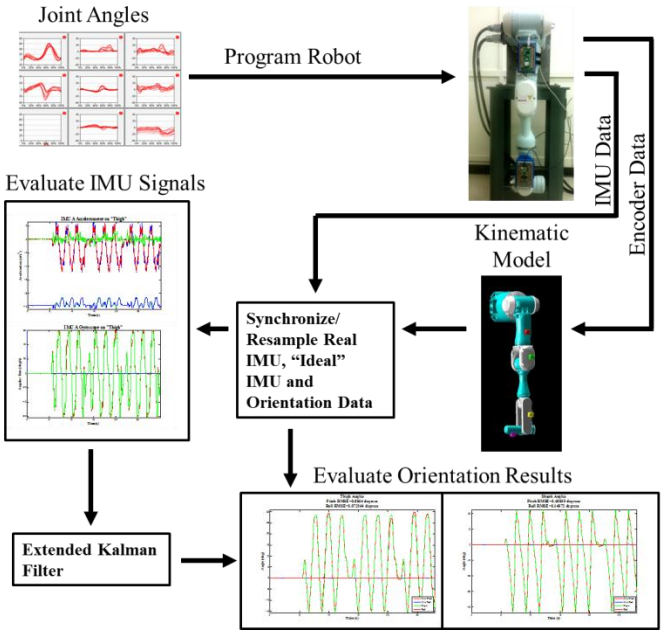

Figure 1: Flow chart describing the methods in this study including taking data from gait analysis to program the robot and using the encoder data to evaluate IMU and EKF results.

The robot was programmed to simulate the motion of a human leg using joint angle data from gait analyses of a healthy subject. Since the human leg has nine rotational degrees of freedom (DOF) including the hip, knee and ankle while the robot can only represent six, three DOF are excluded. The angles represented by the robot included hip flexion/extension, hip abduction/adduction, knee flexion/extension, knee abduction/adduction, knee internal/external rotation and foot flexion/extension. For this study the IMUs were tested with the robot only articulating at the hip and knee in flexion/extension (2D Gait). An IMU was attached to the "thigh" and "shank" segments of the robot. The goal was to determine the orientation of the segments and the angle between them, or the "knee" angle (no IMU was placed on the "foot" in tests presented here).

IMUs were attached to the robot segments using custom holders designed to put the IMUs in the same place for each trial (Fig. 1). The positions of the IMUs relative to the robot segments, needed for the kinematic model, were measured by hand.

B. *Kinematic Model and IMU Signals*

A kinematic model of the PA-10 was created (Fig. 1). The position and orientation of the IMUs relative to the robot segments, the robot joint angle data, and the robot segment lengths were the inputs for the model. The outputs were the position and orientation of the IMUs as well as calculated accelerometer and gyroscope "signals" used as the ground truth when determining the accuracy of the IMU signals. The calculated IMU data was used to synchronize IMUs, evaluate IMU performance and develop the algorithm used to calculate joint angles from IMU data (Fig. 1).

Two IMUs from leading manufacturers, IMU A and IMU B, which included three axis accelerometers and gyroscopes were tested. IMU A was designed for commercial/industrial use and IMU B was designed for consumer use (phones and video game controllers). The sensors were calibrated using the manufacturer provided software and instructions. Any signal conditioning, including filtering, was left at the default settings. The joint position signals from the robot and the IMU signals were simultaneously collected during the trials. IMU A was sampled at 167 Hz and IMU B at 187 Hz. To easily compare and work with data from two asynchronous systems, the data from the kinematic model and both types of IMUs were synchronized and resampled at 150 Hz using linear interpolation, resulting in easily comparable, synchronized data sets.

C. *Algorithm to Determine Joint Angles*

Segment (robotic "shank" and "thigh") pitch and roll angles were calculated by estimating the direction of gravity using the accelerometer signals. The gyroscope signals can be integrated to determine pitch, roll and yaw (heading). However, these calculations are subject to drift and noise which cause increasing error as the signal is integrated over time. Individually, these respective angle calculations are inaccurate.

An extended Kalman filter (EKF) [3] was developed to fuse the accelerometer and gyroscope data. The method is a modification of an algorithm presented in Cooper et al. [4]. The filter used a 14-element state vector (1)

$$x = \begin{bmatrix} v_{\text{int}} \\ a_{\text{int}} \\ \omega_{body} \\ b_{gyr} \\ r \\ p \end{bmatrix} \tag{1}$$

where v_{int} and a_{int} are velocity and acceleration in three axes transformed to an intermediate reference frame, ω_{IMU} and b_{gyr} are the gyroscope signals and the gyroscope bias in three axes, and r and p are roll and pitch of the segment. The intermediate reference frame is initially aligned with the laboratory reference frame but rotates about the gravity vector and is propagated outside of the EKF. The rotations from the laboratory frame to the IMU frames are represented using direction cosine matrices so pitch and roll rotations can be isolated while rotations about the gravity vector are ignored.

The velocity at step k+1, in the intermediate frame are found by numerically integrating a_{int} (2) over timestep Δt.

$$v_{\text{int},k+1} = v_{\text{int},k} + a_{\text{int},k}\Delta t \,. \quad (2)$$

Accelerations, angular rates and angular biases are modeled by using the value at the previous time step, adding noise, w^a, w^ω, w^{gyr} to acceleration, gyroscopes and bias and, for the acceleration model subtracting a factor multiplied by velocity, γv_p, to stabilize the velocity calculation (3)

$$\begin{aligned} a_{\text{int},k+1} &= a_{\text{int},k} + w_k^a - \gamma v_{p,k} \\ w_{body,k+1} &= \omega_{body,k} + w_k^\omega \\ b_{gyr,k+1} &= b_{gyr,k} + w_k^{gyr} \end{aligned} \quad . \quad (3)$$

Angles of the segments in the lab frame were calculated by transforming the gyroscope signals to the lab frame (4)

$$\begin{aligned} \dot{r} &= \omega_x + \left(\omega_z \cos r + \omega_y \sin r\right)\tan p \\ \dot{p} &= \left(\omega_y \cos r - \omega_z \sin r\right) \\ \dot{y} &= \left(\omega_z \cos r + \omega_y \sin r\right)\sec p \end{aligned} \quad (4)$$

representing the time derivative of roll, pitch and yaw, $\dot{r}$, $\dot{p}$ and $\dot{y}$, then numerically integrating the angular velocities (5)

$$\begin{aligned} r_{k+1} &= r_k + \dot{r}_k \Delta t \\ p_{k+1} &= p_k + \dot{p}_k \Delta t \,. \\ y_{k+1} &= y_k + \dot{y}_k \Delta t \end{aligned} \quad (5)$$

Here, y is yaw, which is not included in the EKF state equations and represents the rotation of the intermediate frame about the gravity vector.

The measurement vector (6) consists of the three signals from the accelerometer, a_{IMU}, three signals from the gyroscope in the IMU frame and any drift associated with the gyroscope, w_{IMU} and b_{gyr}. An estimate of roll and pitch, r_{est} and p_{est}, respectively, using the acceleration signals and the direction of gravity are calculated and entered to the filter in the measurement vector, v_k,

$$v_k = \begin{pmatrix} a_{IMU,k} \\ \omega_{IMU,k} + b_{gyr,k} \\ r_{est} \\ p_{est} \end{pmatrix} + w_k^{meas}, \quad (6)$$

where w_k^{meas} is the measurement noise at time *k*.

The process covariances were calculated using the ideal signals calculated with the kinematic model of the robot. Only covariances for a_{int}, ω_{body}, and b_{gyr} were used. All other covariances were set to zero. The measurement covariances were optimized so that the algorithm "listened" to the gyroscopes more closely than the accelerometer and estimated angle measurements.

The knee angle was found by subtracting the pitch angles of the "thigh" and "shank" segments of the robot. The segment orientation results from the EKF were compared to the orientations from the kinematic model. Only orientation data from the 2D Gait trials is reported in this study.

D. Foot Sensor and System Architecture

A prototype for a portable, attachable foot force/moment (F/M) sensor is currently under development. There is a separate sensor for the forefoot and heel and the design is such that measuring the shear portion in the ground reaction forces (GRF) will not affect the vertical GRF measurement. A "smart pylon" or F/M sensor for the prosthetic is also currently undergoing testing along with the electronic system that will wirelessly collect the F/M data and the IMU data from each of the lower leg segments once this system is ready for testing on human subjects.

III. RESULTS

A. IMU signals

By inspection, the accelerometers appeared noisier and less stable than the gyroscopes for both IMUs during the trial, an example of which can be seen in Figure 2. The IMU B accelerometer and gyroscope both appeared noisier than the IMU A equivalent. The gyroscope also appeared to match the calculated IMU data better than the accelerometer signals.

IMU B had higher root mean square error (RMSE) in both the gyroscope and accelerometer signals (Table 1). The accelerometer signal RMSE for IMU B ranged from 0.16 to 3.18 m/s^2 and the gyroscope RMSE ranged from 0.32 to 12.85 deg/s in all axes, with greater error typically occurring on the shank segment.

IMU A generally was less noisy and had lower RMSE than IMU B. The accelerometer RMSE for IMU B ranged from 0.10 to 1.88 m/s^2 with the gyroscope RMSE from 0.45 to 5.47 deg/s (Table 1). Similar to IMU B, typically greater error occurred on the shank segment.

B. Segment Orientation

The pitch RMSE for both the thigh and shank segments was 0.8 degrees and 0.5 degrees, respectively, when using IMU A. This translated to an error in the knee angle of slightly greater than 0.9 degrees. The EKF succeeded in limiting the amount of error caused by integrating the gyroscope signal and the roll values stayed close to 0.0 degrees.

IMU B resulted in RMSE values of 1.06 degrees and 2.04 degrees for the thigh and shank segments, respectively. This resulted in an RMSE of 2.2 degrees for the knee angle calculation.

IV. Discussion

The objective of this project is to develop a system which uses inertial sensors and portable F/M sensors to easily and inexpensively perform biomechanical analysis during the prosthetic fitting and training period. This study focuses on the development of the motion analysis portion of this system and the testing of different IMUs. The authors believe the comparison between a "commercial" (IMU A) and "consumer" (IMU B) IMU with the intent of determining segment orientation is unique to this paper.

Commercial IMUs are typically higher quality, less noisy and more expensive. Consumer IMUs are used in modern smart phones and video game controllers and are typically noisy but smaller in size, less power hungry and can be 1/50th the cost of commercial IMUs. Looking at the RMSE in Table 1, it is clear which sensor provides better performance. Imperfect synchronization between the IMU signals and the reference data, and the resampling process are two sources of error and probably increases the RMSE. Also a difference between the actual and simulated placement of the IMU in the kinematic model would lead to inaccuracies in the accelerometer data calculation from the kinematic model.

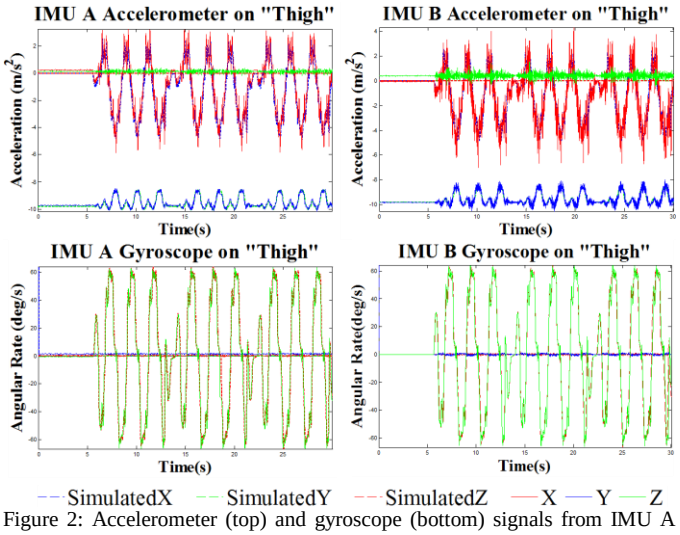

Figure 2: Accelerometer (top) and gyroscope (bottom) signals from IMU A (left) and IMU B (right) (solid lines) on the thigh segment of the robot during 2D Gait compared to calculated IMU signals (dashed lines) from the kinematic model.

TABLE 1: RMSE OF IMU DATA VS CALCULATED IMU DATA

		IMU	Accelerometer[a]			Gyroscope[b]		
			x	*y*	*z*	*x*	*y*	*z*
2D Gait	Thigh	A	0.45	0.10	0.15	0.45	1.42	3.19
		B	0.71	0.16	0.46	0.32	0.46	6.2
	Shank	A	1.88	0.30	0.35	0.82	2.02	5.47
		B	3.18	0.56	0.51	0.70	0.97	12.85

a.Accelerometer values are the RMSE in m/s^2

b.Gyroscope values are the RMSE in deg/s

The difference between the IMUs is also evident in the orientation results. The results of the commercial sensor are comparable to results from other authors who use gyroscopes and accelerometers to calculate knee angle [4,5]. Although the EKF did succeed in limiting drift of the pitch and roll values in the IMU B trial, it was not able to overcome the errors in the gyroscope/accelerometer signals to accurately find the peaks and minimums of the pitch values. This resulted in a motion profile that looked dissimilar to the real motion. However, the attractiveness of the cost and size of these sensors will drive continued development of algorithms, including EKFs, that can manage the limitations of these sensors.

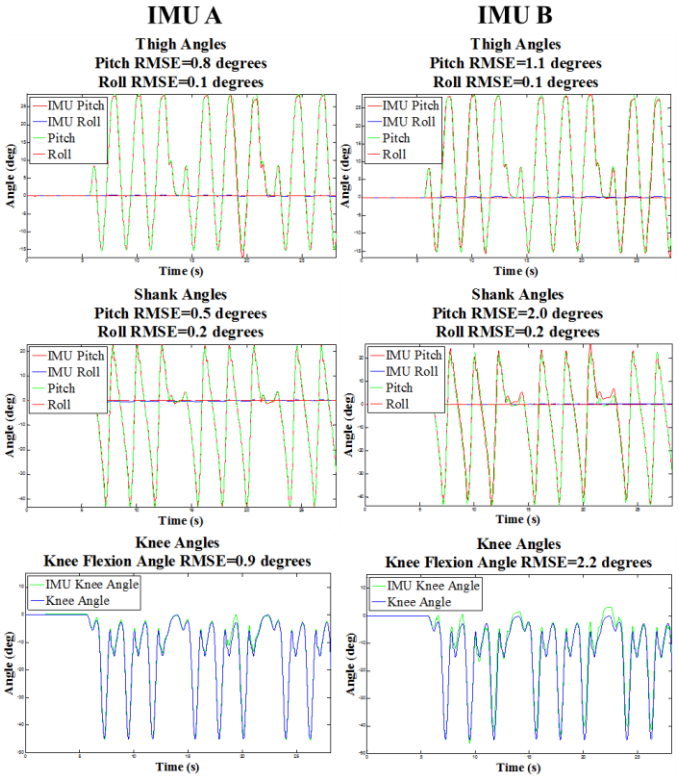

Figure 3: Orientation calculations using IMU A (left) and the IMU B (right) for the thigh (top), shank (middle) and knee angle (bottom) including the RMSE values compared to the actual orientation of the robot segments during 2D Gait simulation.

V. References

[1] Gawande A. Notes of a Surgeon Casualties of War — Military Care for the Wounded from Iraq and Afghanistan. N Engl J Med. 2004 351;24. 2473-2475.

[2] Schmalz T, Blumentritt S, Jarasch R. Energy expenditure and biomechanical characteristics of lower limb amputee gait: the influence of prosthetic alignment and different prosthetic components. Gait Posture. 2002 Dec;16(3):255-63.

[3] Cui, C.K., Chen, G., Kalman Filtering: with Real Time Applications, 3rd ed. Berlin: Springer, 1999.

[4] Cooper, G., Sheret, I., McMillian, L., Siliverdis, K., Sha, N., Hodgins, D., Kenney, L., Howard, D. Inertial sensor-based knee flexion/extension angle estimation. J. Biomech. 2009: 42, 1678-1685.

[5] Favre, J., et al.,. Ambulatory measurement of 3D knee joint angle. Journal of Biomechanics. 2008: 41 (5), 1029–1035.

Development of Mobile Gait Analysis System for Military Populations with Lower Limb Prosthetics

John Kyle P. Mueller, Boyd M. Evans, III, M. Nance Ericson, Ethan Farquhar, Randall Lind
Measurement Science and Systems Engineering Division
Oak Ridge National Laboratory
Oak Ridge, TN, USA
muellerjp@ornl.gov

Kevin Kelley, Martin Pusch
Otto Bock Healthcare Products
Dunderstadt, Germany

Jason M. Wilken
Military Performance Lab
Center for the Intrepid-Brooke Army Medical Center
Fort Sam Houston, TX

Abstract— **Military service members with amputations are unique within the general amputee population as they are highly active and demand better prosthesis performance. We present kinematic data from the development of a mobile gait analysis system designed to assess lower limb amputees outside of a motion analysis laboratory. The overall goal of this project is to develop a mobile gait analysis system (MGAS) which can improve, streamline and quantify the prosthetic fitting process, ultimately improving the clinical effectiveness of prosthetic devices for wounded warriors. The MGAS system will determine limb orientation and joint angles using inertial measurement units and ground reaction forces using a portable shoe sensor and an instrumented pyramid adapter in a lower leg prosthetic. The kinematic capabilities of this MGAS system were validated in this current study using a robot which simulates the motions of a human leg. An algorithm including an extended Kalman filter was developed to collect the IMU data, determine limb orientation and consequently knee angle. The MGAS system calculation of robotic "knee" angle was accurate to 0.5 degrees and 0.8 degrees for two different walking motion patterns and 0.4 degrees RMSE for a slow stair climb activity. Further clinical comparison is planned with a patient population in a motion analysis facility where the accuracy of the orientation of each segment, including the foot, and the GRF forces from the foot sensor can be determined.**

Keywords - Prosthetic, Motion Analysis, Inertial Measurement Unit, Ground Reaction Force Sensor, Wearable Sensors

I. INTRODUCTION

The advances made in battlefield treatment have resulted in a decrease in mortality among the wounded. Thousands of soldiers and veterans who survived their injuries now live with conditions like lower leg amputations which require long term, lifelong care. The unique population of military amputees consists of young, athletic patients in top physical condition [1]. These patients stay physically active and in some cases wish to remain on active military duty. A patient with the need for a prosthesis is more likely to return to an active lifestyle for an extended period of time with better prosthesis function. Asymmetric gait is a symptom of a poorly fit or functioning prosthetic [2]. Asymmetric gait can result in overuse injuries and other chronic pathologies like arthritis in the patient's healthy leg.

Asymmetric motion patterns and their effect on a patient's joint kinetics and kinematics can be quantified using motion analysis tools. In general, this requires access to gait labs which require a large open space, are not readily available, and are expensive and in high demand. The iterative nature of a prosthetic fitting would require multiple gait analysis sessions which is time and cost prohibitive. Also many activities of daily living (ADL) may not be represented in a controlled lab environment. The objective of this present study is to develop a relatively inexpensive, portable, camera-less motion analysis system using portable force sensors and inertial measurement units (IMUs) that can give prosthetists instant biomechanical information and feedback regarding prosthetic performance and fit on individual soldiers.

II. MATERIALS AND METHODS

A. Robot Testing

Prior to evaluating with clinical subjects, a Mitsubishi Heavy Industry (Tokyo, Japan) PA-107C robot arm was used to calibrate the IMUs and test the sensors and data processing algorithm. The robot was controlled with a personal computer which moved it through a repeatable motion sequence while simultaneously recording the encoder data. A separate personal computer recorded the gyroscope and accelerometer data from the IMUs (Figure 1).

The robot was programmed to simulate the motion of a human leg using joint angle data from gait analyses of a healthy subject. The human leg has nine rotational degrees of

Funding provided by Department of Defense Congressionally Directed Medical Research Programs Funding Opportunity Number: W81XWH-09-PRORP-TDA

Oak Ridge National Laboratory (ORNL) is managed by UT Battelle, LLC for the U. S. Department of Energy under Contract No. DE-AC05-00OR22725.

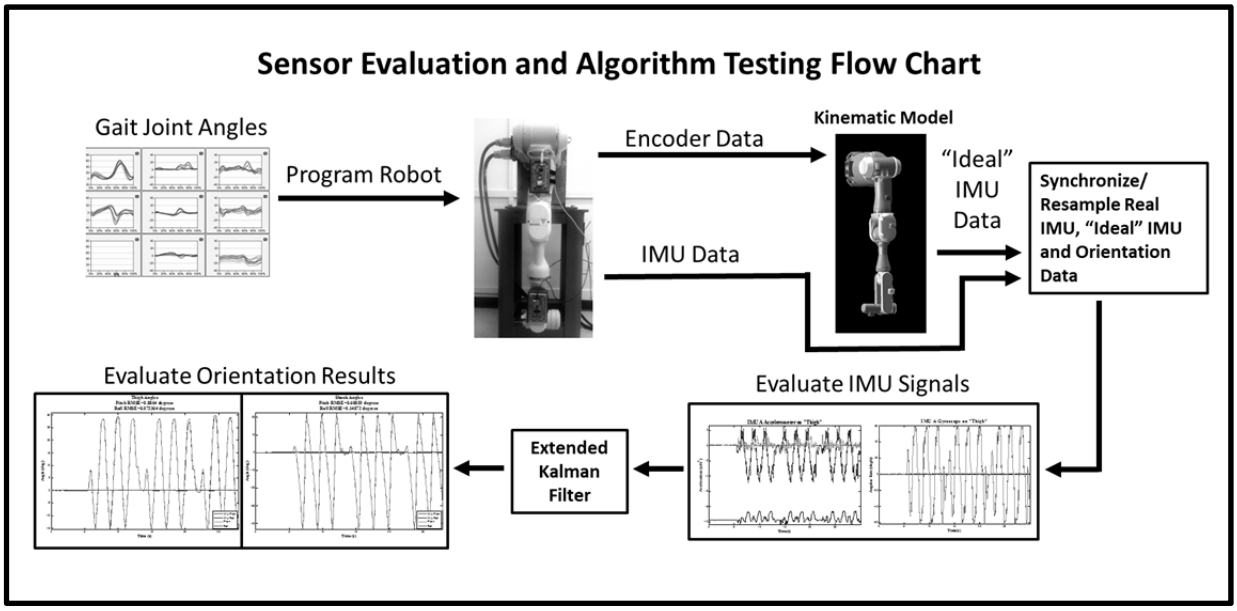

Figure 1: Flow chart describing the methods in this study including taking data from gait analysis to program the robot and using the encoder data to evaluate IMU and EKF results.

freedom (DOF) including the hip, knee and ankle while the robot can only represent six, thus, three DOF are excluded from the robot motion. The angles represented by the robot included hip flexion/extension, hip abduction/adduction, knee flexion/extension, abduction/adduction and internal/external rotation and foot flexion/extension. An IMU was attached to the "thigh" and "shank" segments of the robot. The goal was to determine the orientation of the segments and the angle between them, or the "knee" angle.

The motions evaluated for this study consist of two different walking patterns, Walking A (Figure 2) and Walking B, for the purposes of this study. Walking B is slightly faster than Walking A but simulates a smaller range of motion. The speed of the motions is limited by the capabilities of the robot arm. A slow stair climb motion was also simulated and called Stair Climb for the purposes of this study.

mean-squared-error (RMSE) between the MGAS orientation angles and the robot orientation angles were calculated.

B. Kinematic Model and IMU Signals

A mathematical model of the PA-10 was created using the Matlab (The Mathworks, Natick, MA) programming environment. The position and orientation of the IMUs relative to the robot segments, the robot joint angle data, and the robot segment lengths were the inputs for the model. The outputs were the position and orientation of the IMUs as well as calculated accelerometer and gyroscope "signals" used as the ground truth when determining the accuracy of the IMU signals. The calculated IMU data was used to synchronize the robot and IMU data, evaluate IMU performance and develop the algorithm used to calculate joint angles from IMU data (Fig. 1).

Leading up to this study, a range of IMU sensors were

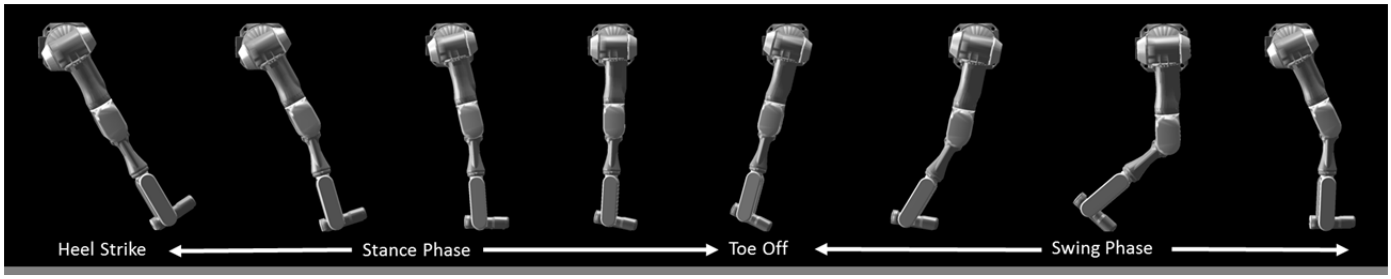

Figure 2: Sequence of images of robot kinematic model represented real robot motion.

IMUs were attached to the robot "thigh" and "shank" segments using custom holders designed to put the IMUs in the same place for each trial. For this study the IMU data was collected using a MSP430 (Texas Instruments, Inc., Dallas, TX) microcontroller and stored on a computer for post-processing using Matlab (The Mathworks, Inc. Natick, MA). Three trials were performed for all three activities. The root-

evaluated using the robotic procedure. One IMU chip that consists of an accelerometer and gyroscope was selected based on performance, cost, size, form factor, communication interface and ease of implementation. For future data collection and clinical testing, this chip was incorporated to an expansion board for a commercially available computer-on-module device that uses an ARM reduced instruction set processor that runs the Linux operating system, runs compiled

C++ code and incorporates wireless communication through Bluetooth and data storage with a micro SD card (Figure 3).

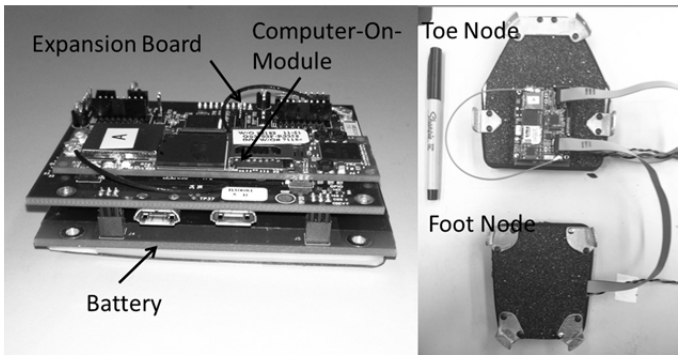

Figure 3: Computer-n-Module with expansion circuit board and battery for use on a limb segment (left) and the same board unit connected to the foot sensor.

The expansion board itself is designed for two applications. The first application is to control and manage data from a portable force/moment (F/M) foot sensor which is strapped to the bottom of the shoe (Figure 4). The foot sensor consists of a toe and heel nodes incorporating load cells that isolate loads in the cardinal directions to eliminate cross talk. Thse nodes are capable of very accurate force measurements in three dimensions that can be resolved to vertical (SI), anterior-posterior (AP) and medial-lateral (ML) ground reaction forces (GRF) and moments in each node. The toe and heel node each contain a circuit board consisting of signal conditioning and 16-bit (effective resolution of greater than 14.5 bits) analog to digital conversion (ADC) circuitry for 10 channels and the selected IMU sensor.

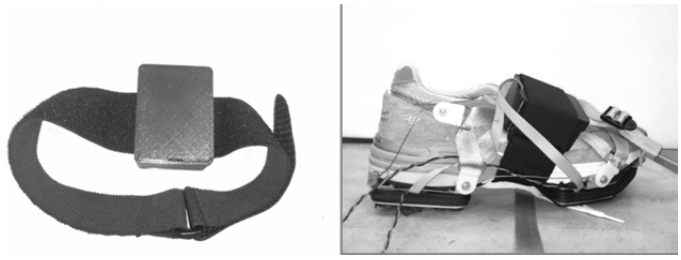

Figure 4: Enclosure and strap to attach inertial measurement unit to limb segment (left) and foot sensor attached to shoe (right).

A MSP430 microcontroller on the expansion board communicates to the ADC and IMU chips in the two sensor nodes and allows for on hardware timing to collect data at a consistent programmable 200 Hz sampling rate. The force and inertial data is read from the expansion board by the computer-on-module device and stored in the on-board SD card. A Lithium-Polymer battery provides power to the expansion board which, in turn, provides power to the computer-on-module device and the foot sensor circuitry. The Bluetooth and Wi-Fi capabilities of the computer-on-module allow for wireless control of the device and real-time data transmission to a host computer, tablet or phone.

The second application of the expansion board is as a limb segment (e.g. thigh, shank) IMU sensor (Figure 4). In this case the MSP430 microcontroller controls the IMU and on-hardware clock. The battery only powers the expansion board and computer-on-module device which has the same function as the foot sensor application but only stores and transmits inertial data from the IMU on the expansion board. In both cases the expansion board manages the battery charge/discharge with power management circuits. A means to charge the battery, and command line access to the computer-on-module device, is provided through micro-USB on the expansion board.

C. Algorithm to Determine Joint Angles

The accelerometer signals, were used to determine the direction of gravity in the IMU reference frame, thus giving an estimate of the pitch and roll of the segment that is especially accurate when the robot is moving slowly or still. The angular velocity signals from the gyroscope were integrated to determine pitch, roll and yaw (heading) starting from an initial orientation. These calculations are subject to drift and noise which cause increasing error as the signal is integrated over time making these measurements on their own inaccurate.

An extended Kalman filter (EKF) [3] was developed to fuse the accelerometer and gyroscope data. The algorithm was inspired, but modified from a method presented in Cooper et al. [4]. The current EKF uses a 14-element state vector (1)

$$x = \begin{bmatrix} v_{\text{int}} \\ a_{\text{int}} \\ \omega_{IMU} \\ b_{gyr} \\ r \\ p \end{bmatrix} \tag{1}$$

where v_{int} and a_{int} are three-dimensional vectors of velocity and acceleration, respectively, transformed to an intermediate reference frame. The vectors ω_{IMU} and b_{gyr} are three-dimensional and represent the gyroscope signals and gyroscope bias in the IMU frame, respectively. The variables r and p are scalars representing the roll and pitch of the segment in the intermediate reference frame. Roll, pitch and yaw correspond to orientation in the sagittal plane, coronal plane and transverse plane, respectively, in the case of the lower leg or robotic lower leg. Initially, the intermediate reference frame is aligned with the Newtonian, or "lab", reference frame but rotates about the vertical lab vector and is integrated outside of the EKF. The rotations from the laboratory frame to the IMU frames are represented using direction cosine matrices so pitch and roll rotations can be isolated while rotations about the gravity vector are ignored.

The measurement vector (2) consists of three accelerometer signals, a_{IMU}, and three gyroscope signals in the IMU frame and any drift associated with the gyroscope, w_{IMU} and b_{gyr}. An estimate of roll and pitch, r_{est} and p_{est}, respectively, using the acceleration signals and the direction of

gravity are calculated and entered to the filter in the measurement vector, v_k,

$$v_k = \begin{pmatrix} a_{IMU,k} \\ \omega_{IMU,k} + b_{gyr,k} \\ r_{est} \\ p_{est} \end{pmatrix}, \quad (2)$$

where w_k^{meas} is the measurement noise at time *k*.

The process covariances represents what kind of data the sensor is expected to see and was calculated using the ideal signals calculated with the kinematic model of the robot. Only covariances for a_{int}, ω_{body}, and b_{gyr} were used. All other covariances were set to zero. The measurement covariances were optimized so that the algorithm "listened" to the gyroscopes more closely than the accelerometer signals and estimated angle measurements.

The knee angle was calculated with the difference of the "thigh" and "shank" segments of the robot. The segment orientation results from the EKF were compared to the orientations from the kinematic model. The algorithm was run in post-processing for the current data.

D. Pylon Sensor and System Architecture

Along with the foot sensor mentioned earlier, a "smart pylon" or F/M sensor for a lower leg prostheses has been developed. This allows kinematic and kinetic evaluation of both the prosthetic and healthy limb.

The final design of the system will consist of seven IMUs, two from the foot sensor on the sound foot, one on the sound limb calf, two on each thighs, one on the trunk and one on the below the knee prosthesis. The data from these IMUs and the force data from the foot and adapter F/M sensors will be transmitted to a host device for data visulatization. Currently the EKF algorithm is run on a host computer in real time or during post processing. The computer-on-module devices have enough speed and power that they will be used to run the sensor fusion algorithms for their particular segments, allowing for real time calculation of segment orientation and joint powers and torques.

III. RESULTS

A. Limb Orientation

The IMU and algorithm which will be incorporated into the MGAS system had a sagittal angle RMSE of 0.5 degrees or less for all segment and angle calculations, except for one.

The average results of the six trials of Walk A, were the thigh segment pitch RMSE was 0.2 degrees (stdev=0.1 degrees), shank segment pitch RMSE was 0.5 degrees (stdev=0.0 degrees) and the knee flexion calculation RMSE was 0.5 degrees (stdev=0.1 degrees) with a max error of 1.5 degrees (stdev=0.2 degrees) of knee flexion (Figure 6-Figure 7). The RMSE of the out of sagittal plane angles were not calculated but by inspection are within one or two degrees throughout the trials.

The average results of the three trials of Walk B were the thigh segment pitch RMSE was 0.1 degrees (stdev=0.0 degrees), the shank segment pitch RMSE was 0.3 degrees (stdev=0.1 degrees) and the knee flexion RMSE was 0.8 degrees (stdev=0.2 degrees) (Figure 9-Figure 10). Similar to the Walk A data, by inspection the out of sagittal plane orientation data appeared to be within one or two degrees by visual inspection of the plots.

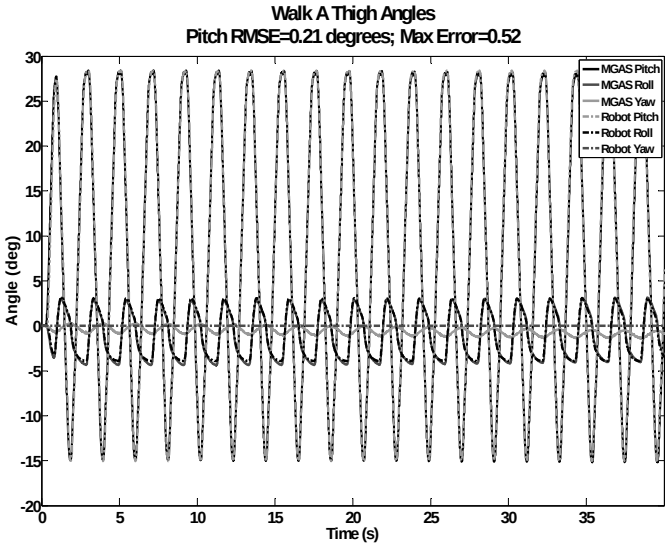

Figure 5: Sample trial of Walk A orientation angles from IMU data(MGAS values) and orientation angles calculated by the kinematic model (Robot values) for the "thigh" segment of the robot.

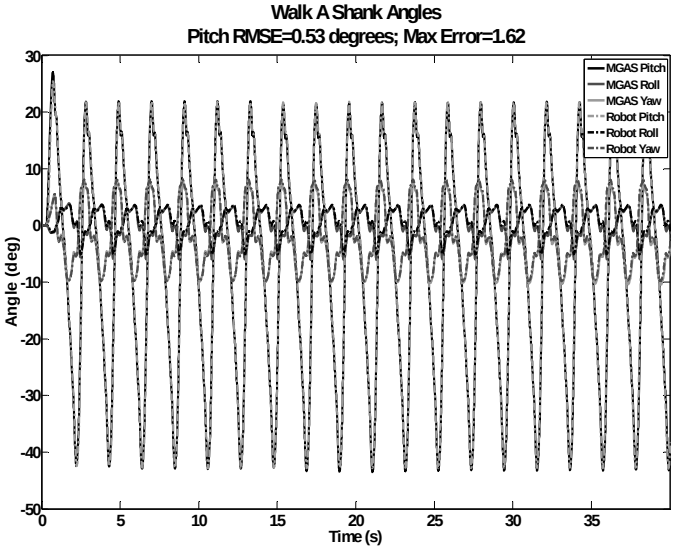

Figure 6: Sample trial of Walk A orientation angles from IMU data(MGAS values) and orientation angles calculated by the kinematic model (Robot values) for the "shank" segment of the robot. The pitch RMSE and maximum pitch angle error are also displayed for this trial.

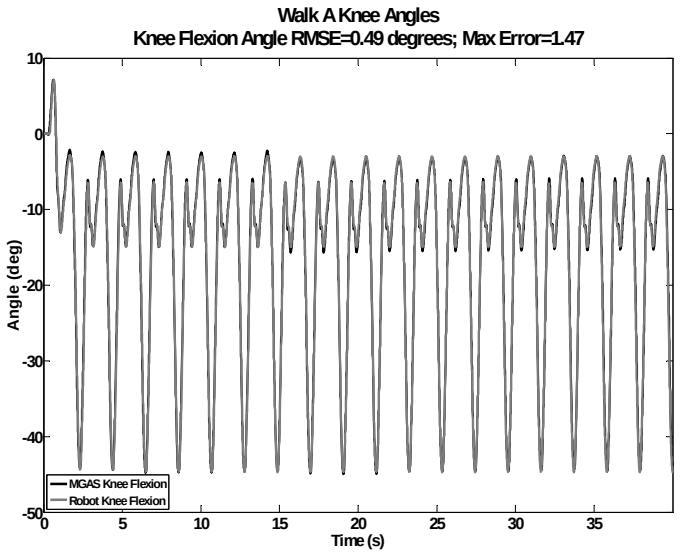

Figure 7: Sample trial of Walk A calculated knee flexion angles (MGAS values) and knee flexion angles calculated by the kinematic model (Robot values). The knee flexion RMSE and maximum knee flexion angle error are also displayed for this trial.

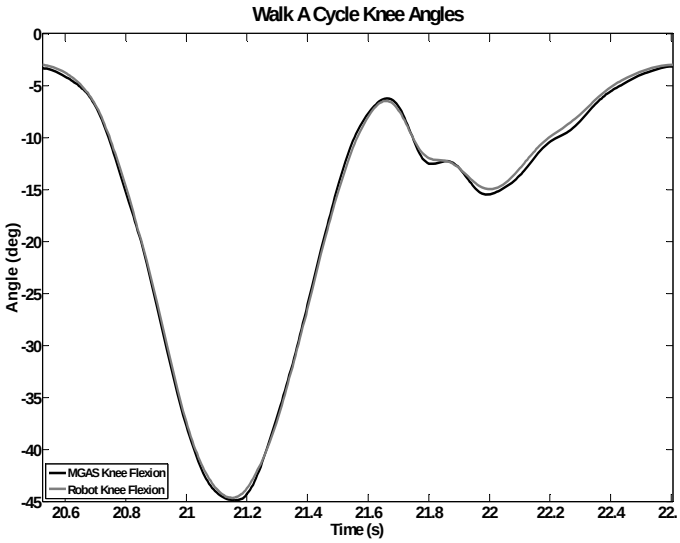

Figure 8: Sample trial of Walk A knee flexion angles from IMU data (MGAS values) and knee flexion angles from the kinematic model (Robot values) from one simulated gait cycle.

The average slow Stair Climb activity segment pitch RMSE for the thigh segment was 0.3 degrees (stdev=0.1 degrees), for the shank segment was 0.1 degrees (stdev=0.1 degrees) and for knee flexion 0.4 degrees (stdev=0.0 degrees) (Figure 11-Figure 12). Similar to the previous two activities the error of out of sagittal plane motion appeared to be within a few degrees by visual inspection of the data.

The average maximum knee flexion errors per trial were 1.5 degrees (stdev=0.2 degrees), 3.1 degrees (stdev=0.2 degrees) and 1.2 degrees (stdev=0.3 degrees) for Walk A, Walk B and Stair Climb activities, respectively (Figure 13).

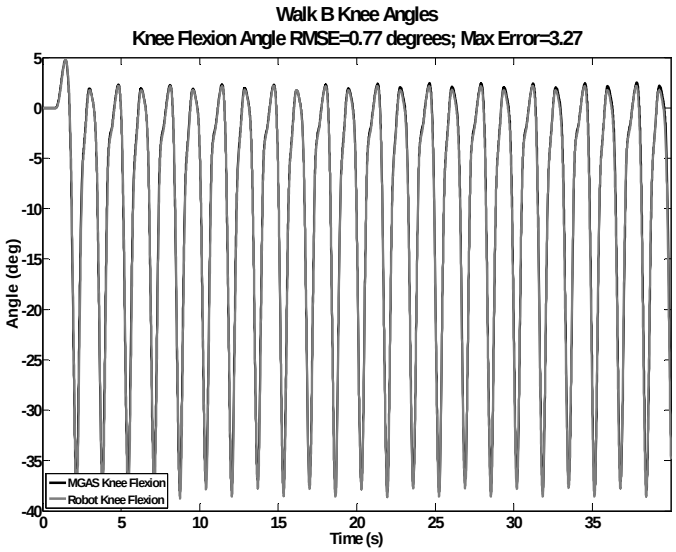

Figure 9: Sample trial of Walk B calculated knee flexion angles (MGAS values) and knee flexion angles calculated by the kinematic model (Robot values). The knee flexion RMSE and maximum knee flexion angle error are also displayed for this trial.

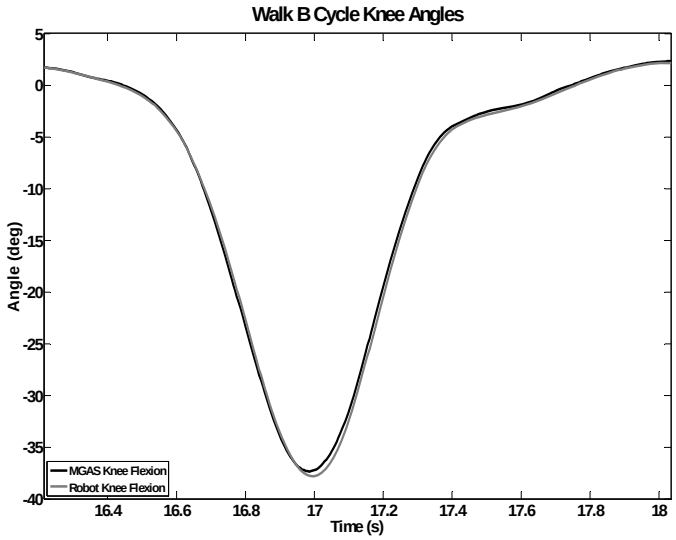

Figure 10: Sample trial of Walk B knee flexion angles from IMU data (MGAS values) and knee flexion angles from the kinematic model (Robot values) from one simulated gait cycle.

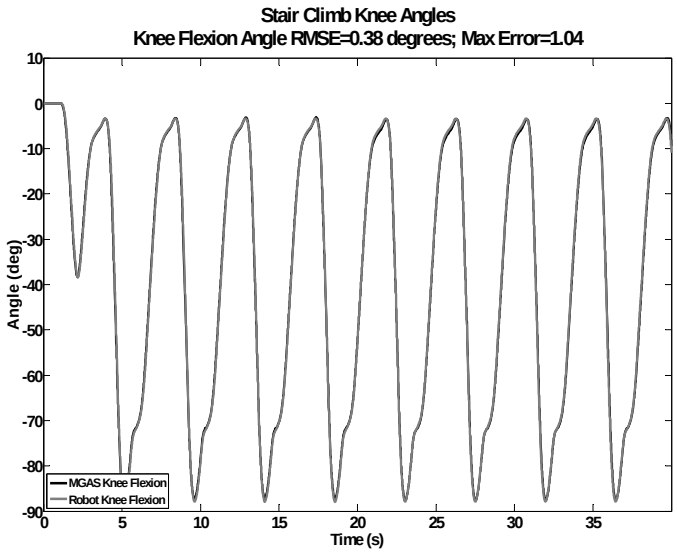

Figure 11: Sample trial of Stair Climb calculated knee flexion angles (MGAS values) and knee flexion angles calculated by the kinematic model (Robot values).

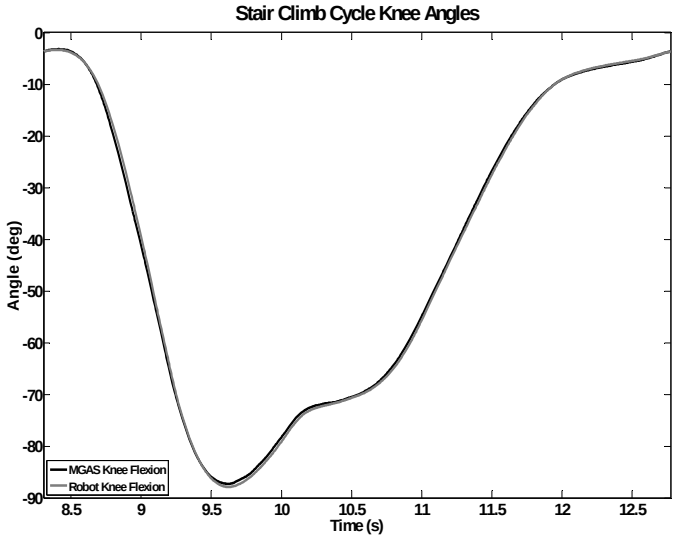

Figure 12: Sample trial of Stair Climb knee flexion angles from IMU data (MGAS values) and knee flexion angles from the kinematic model (Robot values) from one simulated gait cycle.

I. Discussion

This project's objective is to develop a portable, easy to use system to provide more information to prosthetists and clinicians and quantify the prosthetic fitting process. By employing portable F/M sensors, small inexpensive IMUs and data fusion algorithms the proposed system will provide data normally only available through gait analysis in a motion capture lab. This portable system will provide more data about the military amputee patient population and allow easier access to tools that could help improve the performance of lower limb prosthetics.

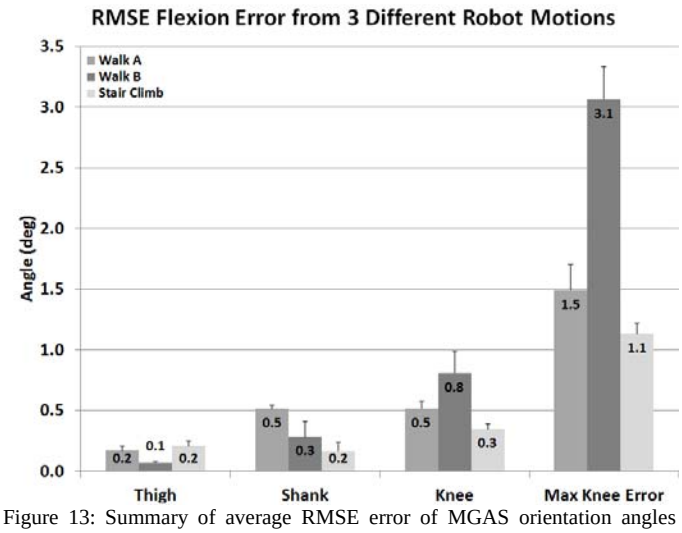

Figure 13: Summary of average RMSE error of MGAS orientation angles versus Robot Angles.

The focus of this current study is on the kinematics aspect of this project. The bench top testing reported here, using the robot leg to mimic a human leg, was essential in evaluation of different inertial sensors and in the development of the algorithm to extract sound orientation data from typical noisy and unstable accelerometer and gyroscope signals.

The results from these initial kinematic tests are promising. The RMSE values for sagittal plane orientations are within 1 degree RMSE, which was a loose goal set for the kinematic portion of the system. The out of sagittal plane motions are also accurate to within a few degrees. There is no additional reference for the yaw component of the limb orientation, therefore this calculation is dependent purely on the gyroscope signal and vulnerable to drift errors. This may be a factor in real world testing of the system when soft tissue artifact and inconsistent motion comes into play. However, we hypothesize that, with additional processing, a stable estimate of yaw orientation, or heading, can be made without the use of additional sensors such as magnetometers. By avoiding using magnetometers, the concern over ferrous perturbations is avoided and this system should work in any setting.

It is interesting that the error values for the thigh and shank segment during the Walk B activity were some of the lowest in the reported data. However, when these values were used to calculated knee angle, the average knee angle RMSE was the highest of the three activities. This is most likely due to inaccurate synchronization between the robot data and IMU data.

There are at least two caveats to the results reported here. The first is that there is a rigid connection between the IMUs and the robot segments. On human subjects, the goal is to track the orientation of the underlying bone, but skin and muscle artifact prevent this. However, camera-based motion analysis systems, considered the gold standard in gait analysis instrumentation, face the same issues.

The second caveat is the speed with which the activities presented were performed. From Figure 8, Figure 10 and Figure 12, a single gait cycle on the robot takes ~2 seconds, ~1.6 seconds and ~4.3 seconds for Walk A, Walk B and Stair Climb, respectively. A normal subject walking at a normal speed will complete a full gait cycle in ~1 second. The robot walking patterns are more like a very leisurely stroll. The motions used here were slower because of limitations of the robot arm. Validation testing in a clinical environment has been scheduled and will determine whether the accuracy of the system will hold up for faster and more complex motion patterns.

This study has shown that portable, inexpensive inertial sensors can be used to accurately track complicated repeated biomechanical motion. Incorporating this into the proposed MGAS will result in a tool that will give prosthetists, clinicians and researchers more information to improve the performance of lower leg prosthesis and the overall quality of life of our wounded warriors.

II. REFERENCES

[1] Gawande A. Notes of a Surgeon Casualties of War — Military Care for the Wounded from Iraq and Afghanistan. N Engl J Med. 2004 351;24. 2473-2475.

[2] Schmalz T, Blumentritt S, Jarasch R. Energy expenditure and biomechanical characteristics of lower limb amputee gait: the influence of prosthetic alignment and different prosthetic components. Gait Posture. 2002 Dec;16(3):255-63.

[3] Cui, C.K., Chen, G., Kalman Filtering: with Real Time Applications, 3rd ed. Berlin: Springer, 1999.

[4] Cooper, G., Sheret, I., McMillian, L., Siliverdis, K., Sha, N., Hodgins, D., Kenney, L., Howard, D. Inertial sensor-based knee flexion/extension angle estimation. J. Biomech. 2009: 42, 1678-1685.

[5] Favre, J., et al.,. Ambulatory measurement of 3D knee joint angle. Journal of Biomechanics. 2008: 41 (5), 1029–1035.

Title: Wearable Ground Reaction Force Foot Sensor
Inventor: Randall F. Lind
ORNL Docket Number: ID-2777

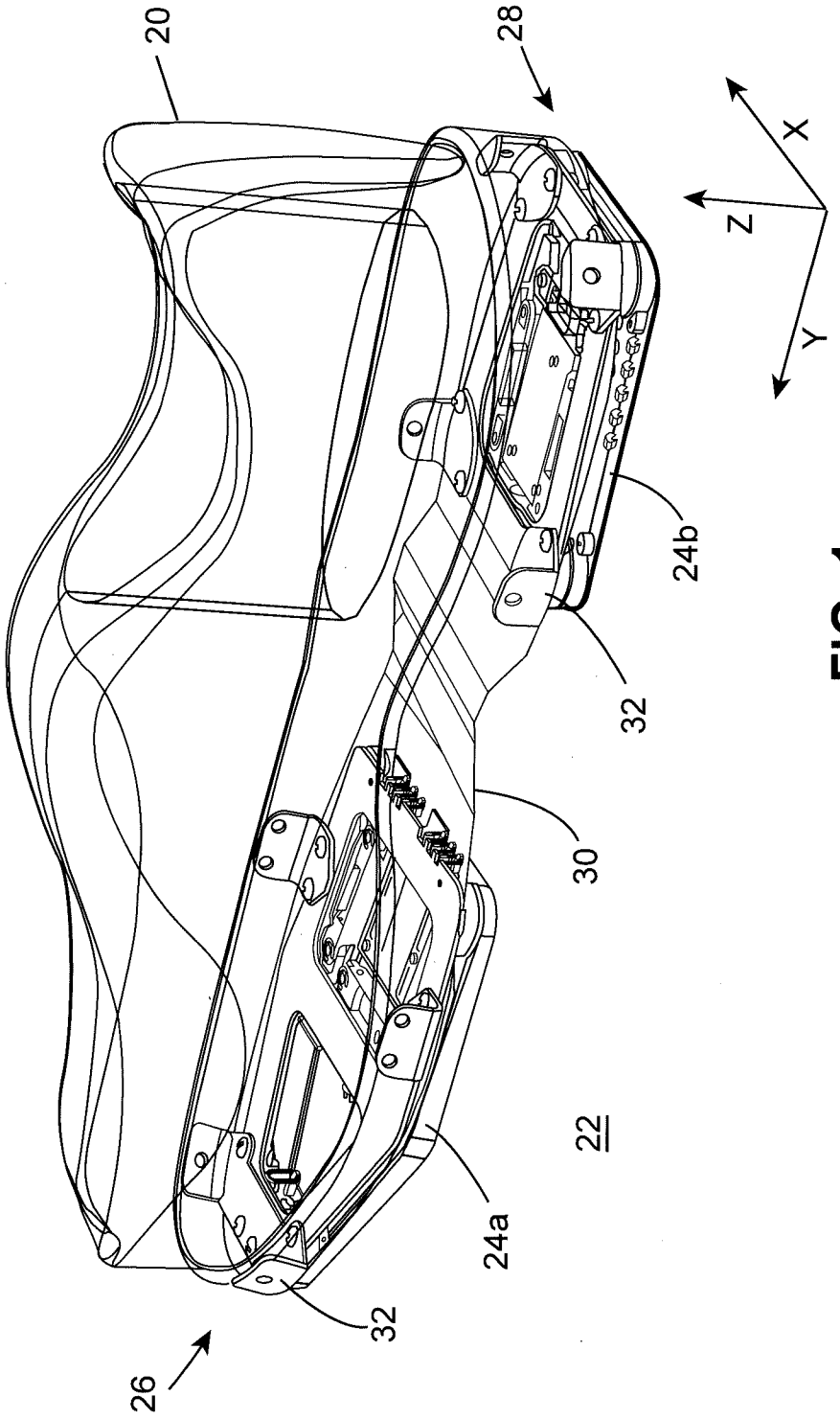

FIG. 1

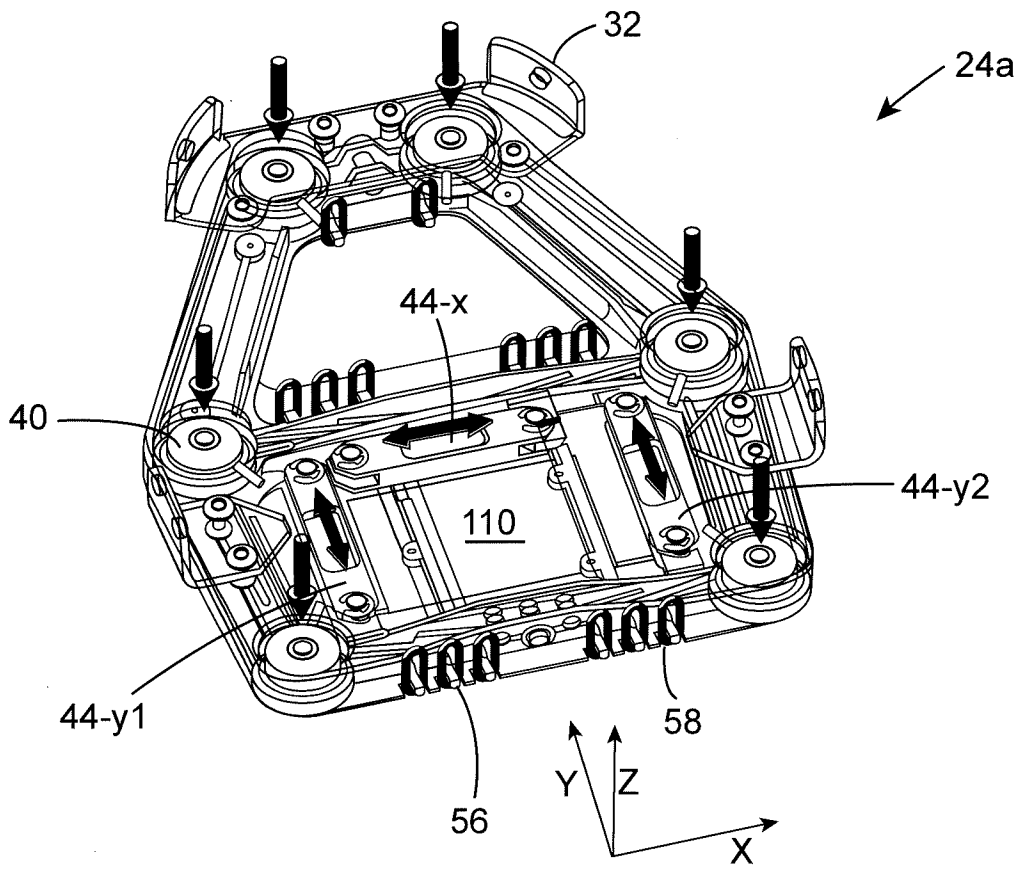

FIG. 2

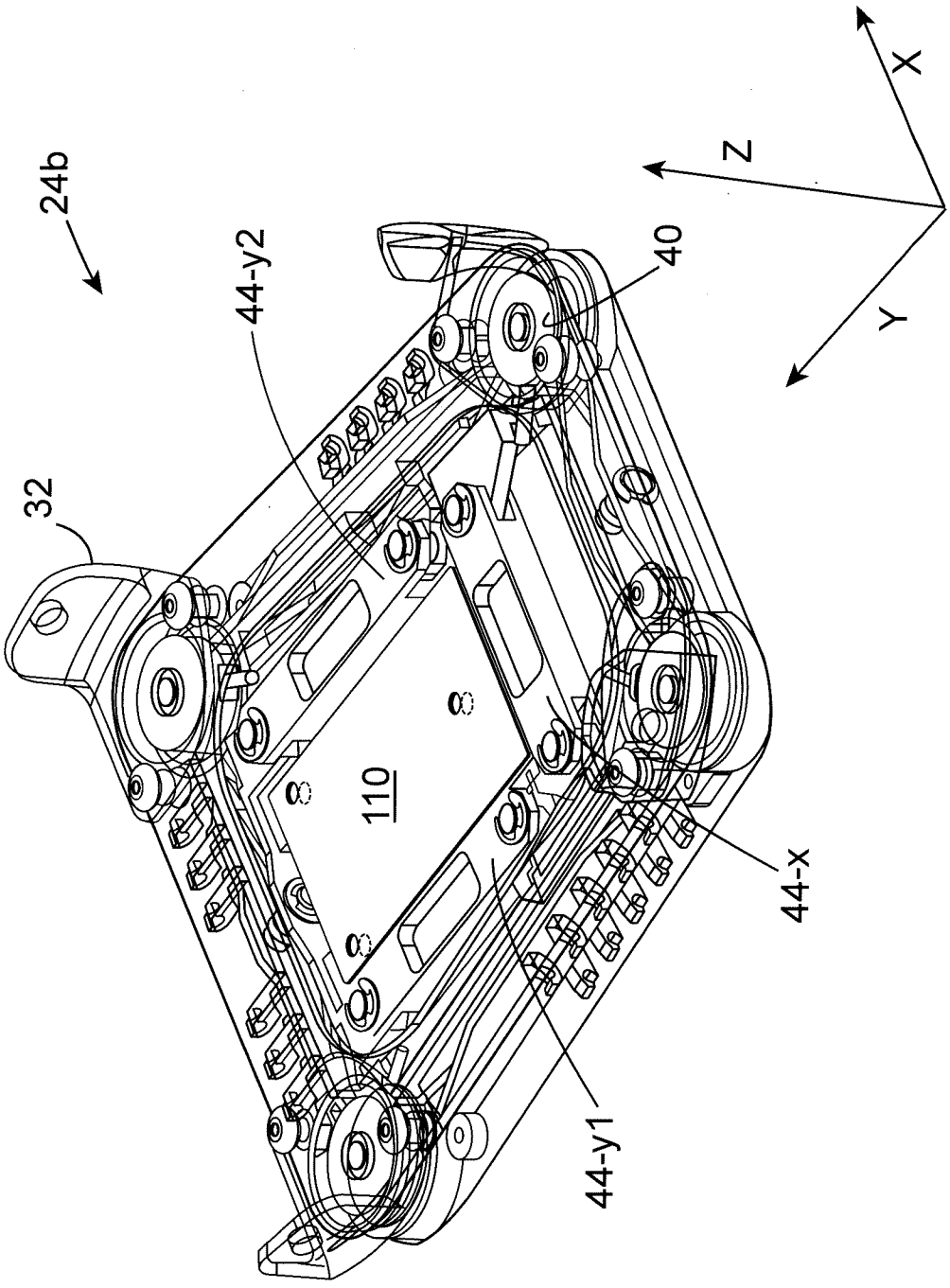

FIG. 3

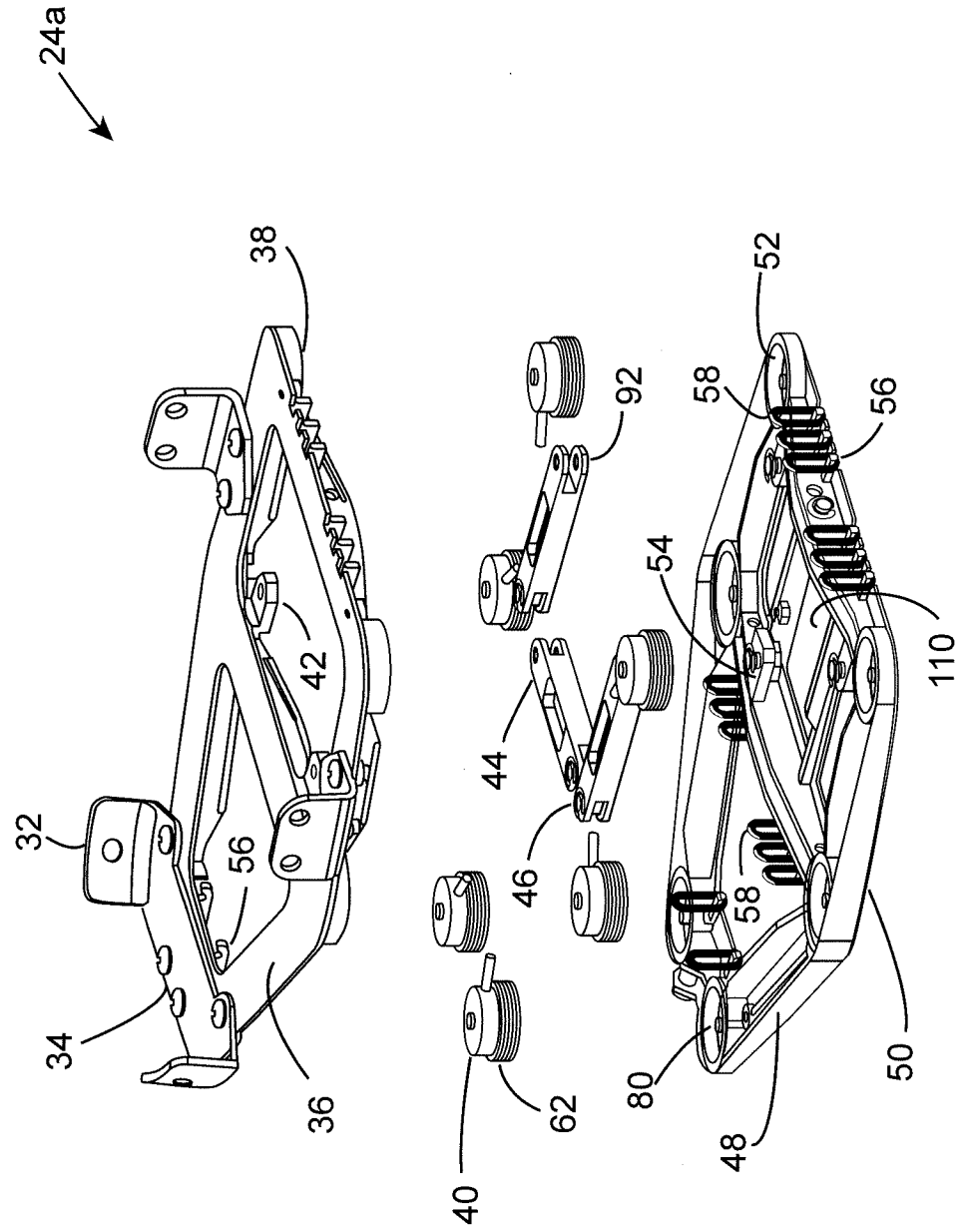

FIG. 4

Title: Wearable Ground Reaction Force Foot Sensor
Inventor: Randall F. Lind
ORNL Docket Number: ID-2777

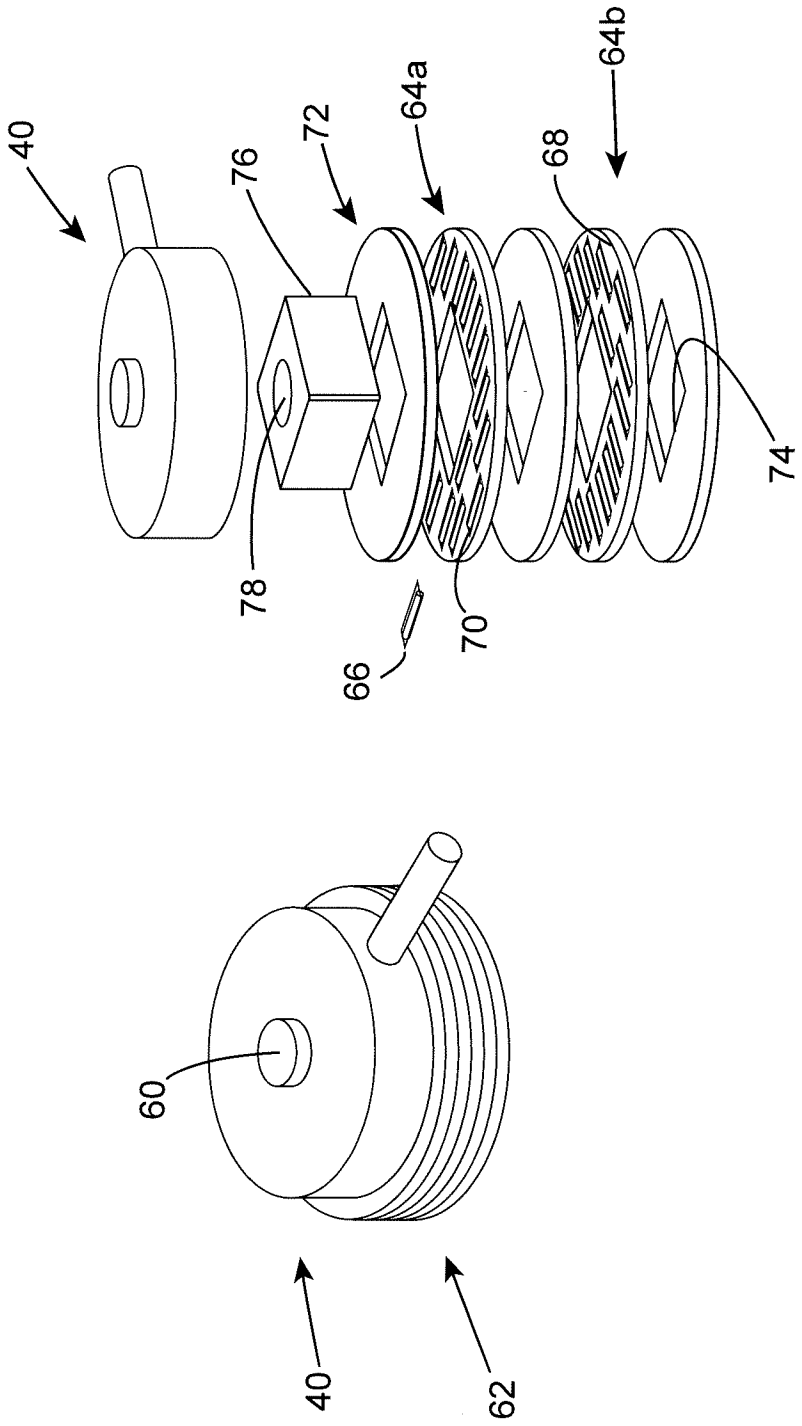

FIG. 5

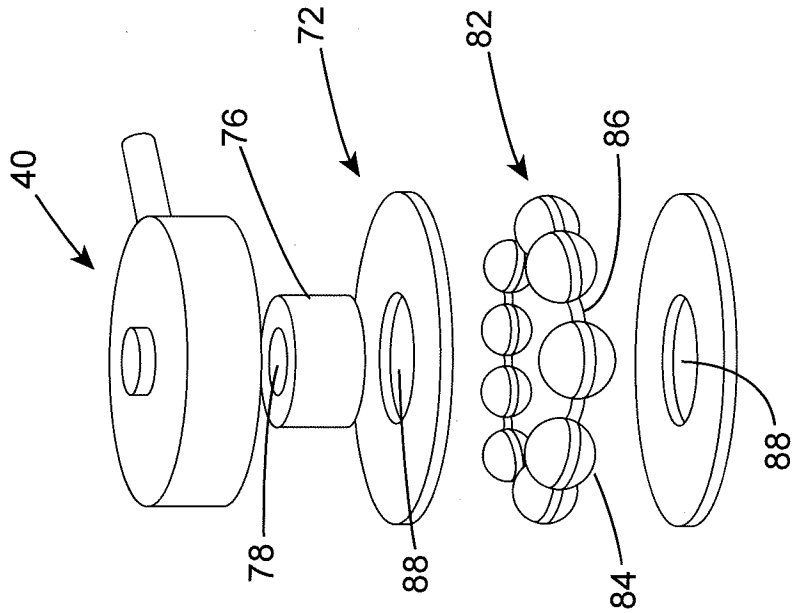

FIG. 6

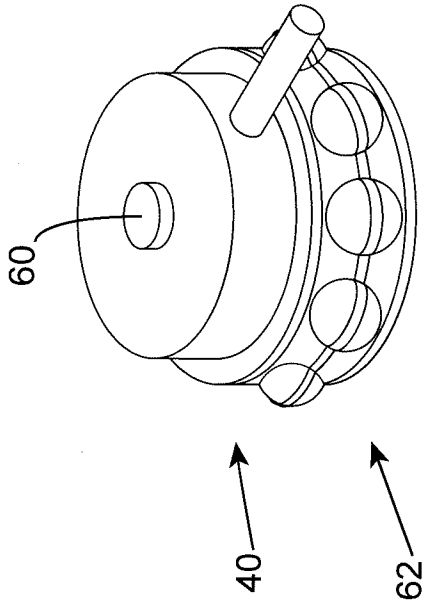

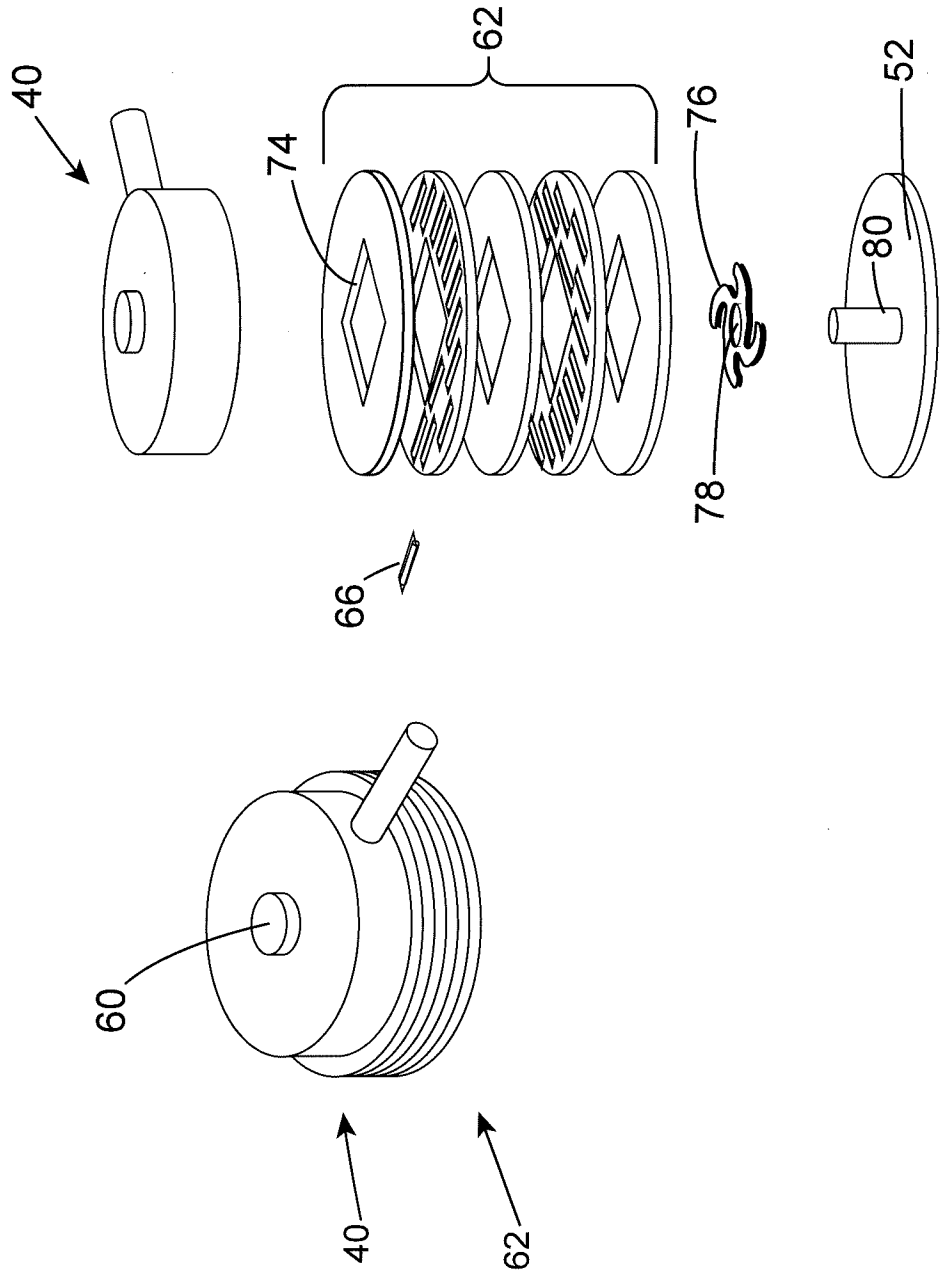

FIG. 7

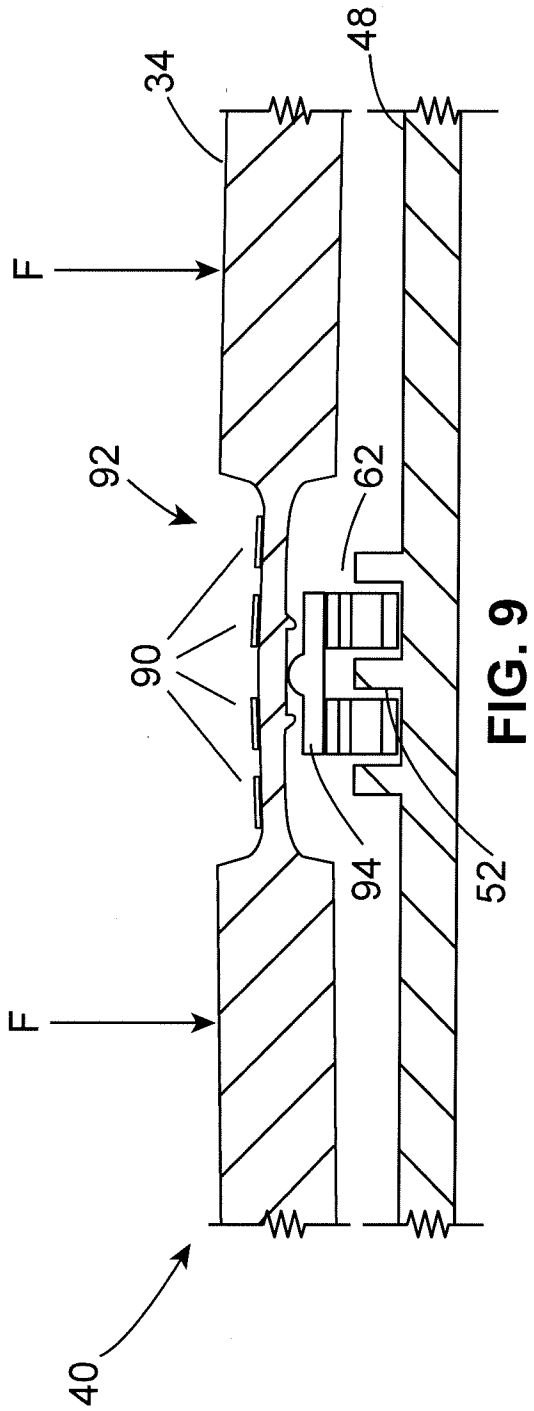

FIG. 9

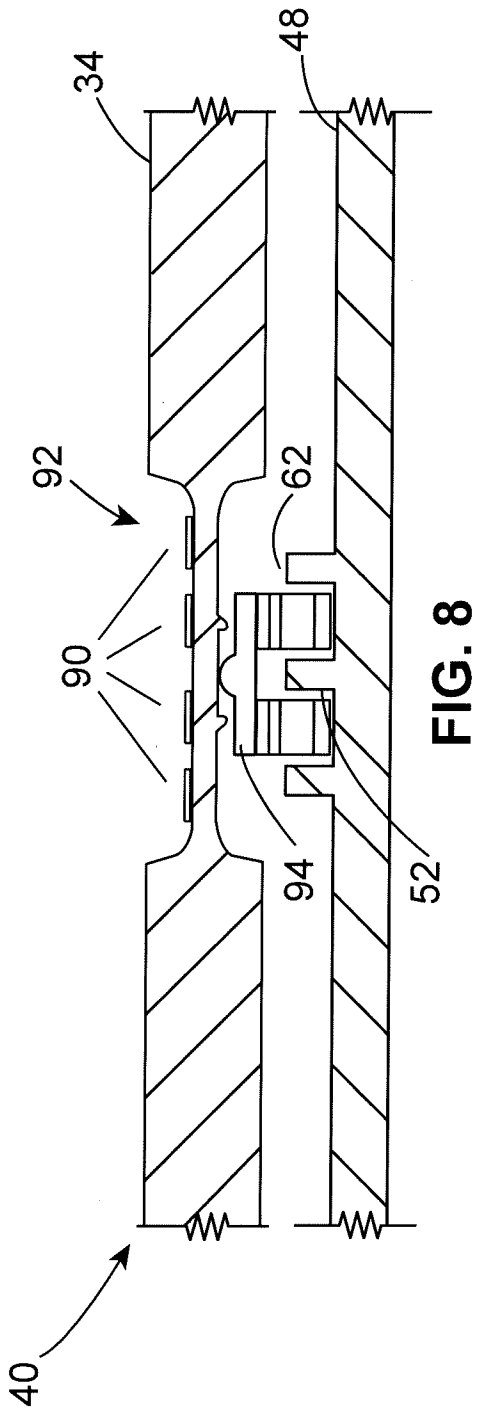

FIG. 8

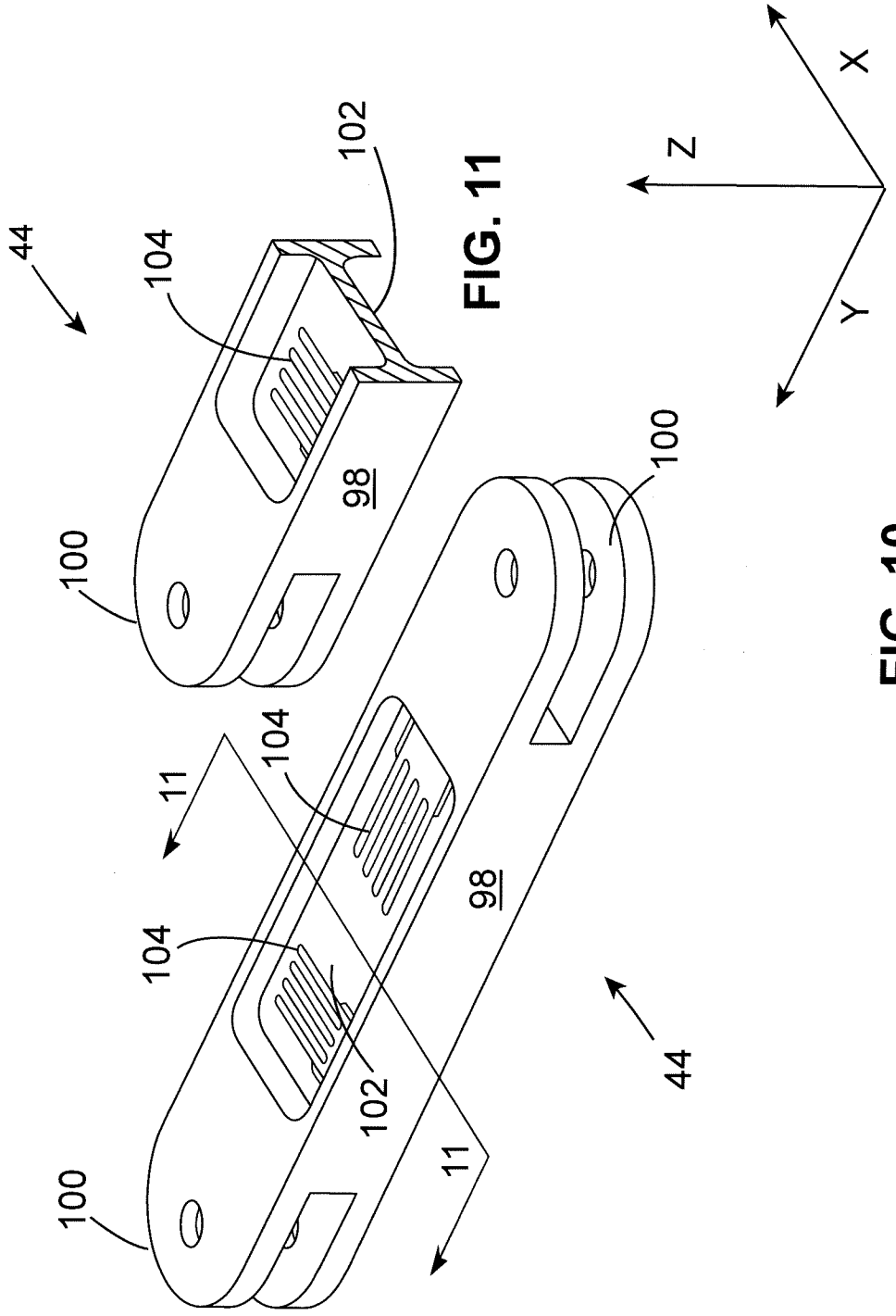

FIG. 11

FIG. 10

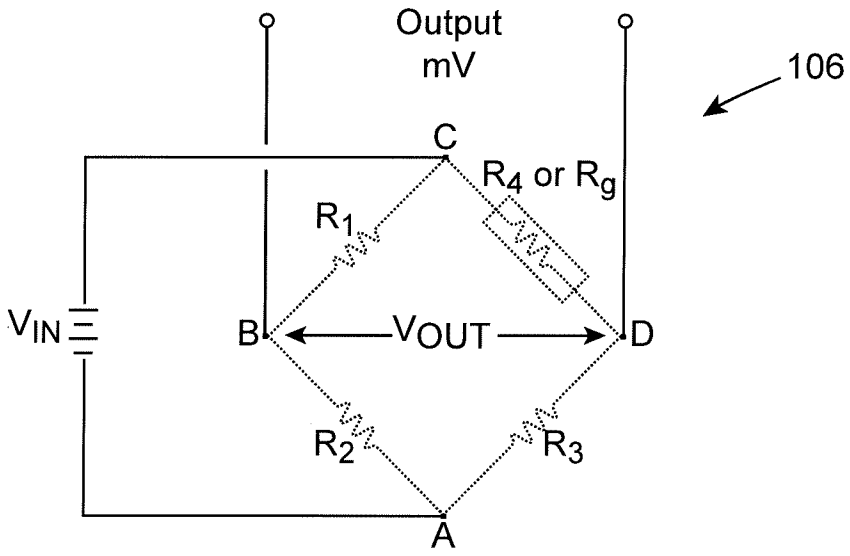

FIG. 12

Title: Wearable Ground Reaction Force Foot Sensor
Inventor: Randall F. Lind
ORNL Docket Number: ID-2777

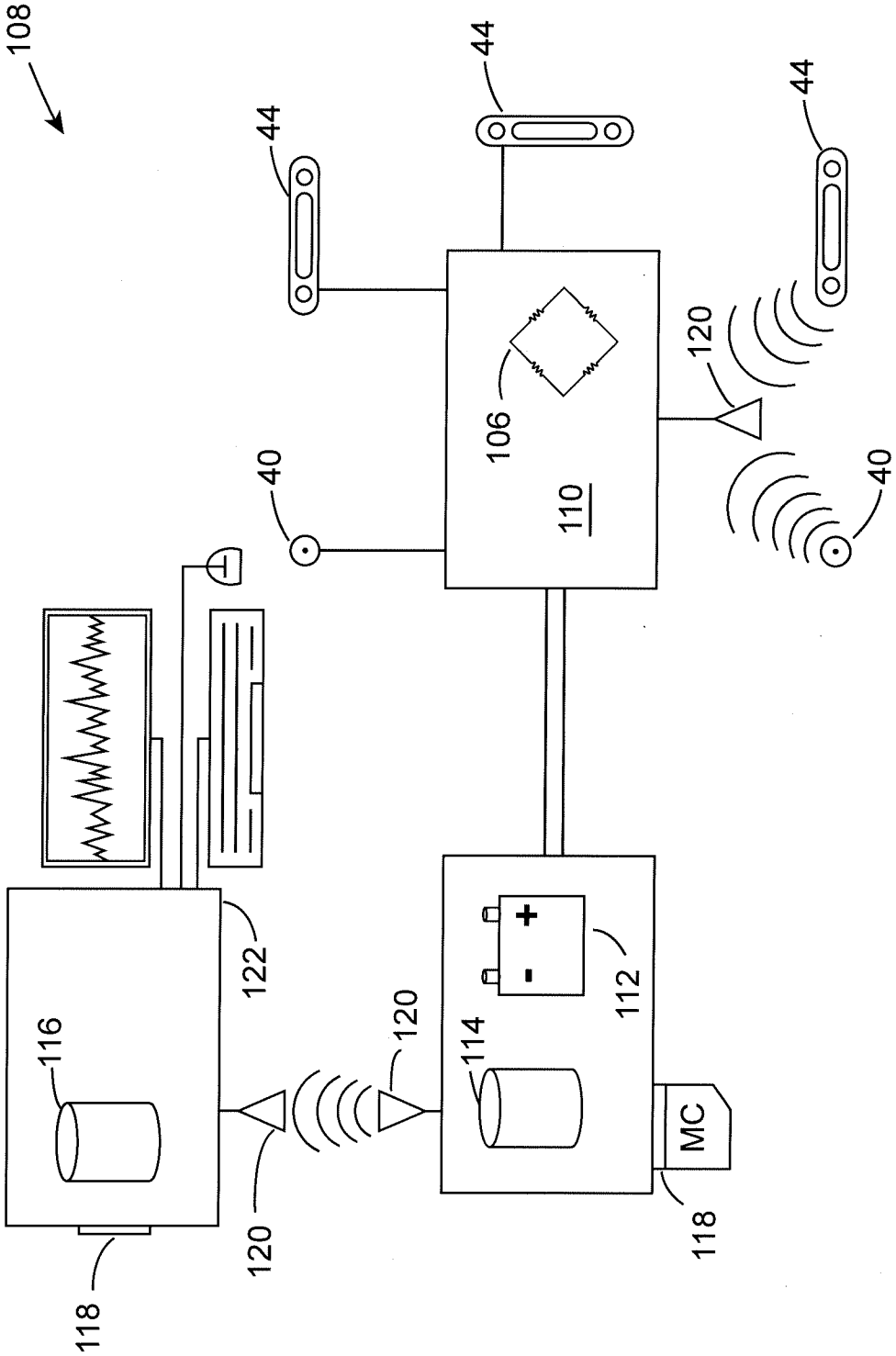

FIG. 13

TITLE

Wearable Ground Reaction Force Foot Sensor

CROSS-REFERENCE TO RELATED APPLICATIONS.

[0001] None.

STATEMENT REGARDING FEDERALLY SPONSORED RESEARCH AND DEVELOPMENT.

[0002] This invention was made with government support under Contract No. DE-AC05-00OR22725 awarded by the U.S. Department of Energy. The government has certain rights in the invention.

THE NAMES OF THE PARTIES TO A JOINT RESEARCH AGREEMENT

[0003] None.

BACKGROUND OF THE INVENTION

1. Field of the Invention

[0004] The present disclosure relates to force measurements and more specifically to a wearable sensor for measuring the reaction force of an article on a surface such as the ground.

2. Description of the Related Art

[0005] Gait analysis is the study of locomotion and is one method of analyzing the effects of various factors on ordinary movement. A subject's gait may be influenced by factors such as a stroke, spine misalignment, joint replacements, sports injuries, shoe fitment, and prosthetic limb fitment, among other things. With regard to prosthetic limb fitment, it's essential for a prosthetic limb to function properly once it's fitted to an amputee. In order for this to occur, the amputee's normal gait must be acquired and examined by a clinician, for use as a

baseline. The normal gait cycle includes several components and an issue with one or more components may cause the amputee to compensate for improper fitment and this can increase stress on joints and tendons. The normal gait of an amputee can be determined by measuring the ground force reaction forces in the unaffected limb.

[0006] Known gait analysis devices include potentiometers for measuring the flexion or extension angle of a prosthetic device, sensors for mounting outside a shoe, instrumented insoles, and pressure sensitive mats, which the subject walks on.

[0007] Despite the teachings of the current art, a ground force reaction sensor having a low profile, low mass, and minimal influence on the normal gait of a subject is needed.

BRIEF SUMMARY OF THE INVENTION

[0008] Disclosed are several examples of a ground force reaction sensor for use in a gait analysis of a subject. The ground may be any surface that can support the subject such as a tiled floor, a carpeted floor, a mat, a stair, or a stage for example, and the subject may be a human, an animal, or a machine (e.g., a robot).

[0009] According to an example, a ground reaction force sensor for an article such as a shoe includes: an upper force plate for contacting the article; a lower force plate for contacting the ground; a vertical load cell disposed between the plates for measuring the force acting on the cell in a direction that is substantially perpendicular to the ground; a horizontal load cell disposed between the plates for measuring the force acting on the cell in a direction that is substantially parallel to the ground, and with the load cells being mounted between the plates in a configuration that is substantially insensitive to off-axis forces imposed on them for improved load cell measurement accuracies.

BRIEF DESCRIPTION OF THE SEVERAL VIEWS OF THE DRAWINGS

[0010] The present ground force reaction sensor may be better understood with reference to the following drawings and detailed description. The components in the drawings are not necessarily drawn to scale, emphasis instead being placed upon illustrating principles. In the drawings, like referenced numerals refer to like parts throughout the different drawings unless otherwise specified.

[0011] Figure 1 is a perspective view of ground reaction force sensors installed on an article in accordance with an example of the present invention;

[0012] Figure 2 is a top, perspective view of a forefoot ground reaction force sensor in accordance with the example illustrated in Figure 1;

[0013] Figure 3 is a top, perspective view of a heel ground reaction force sensor in accordance with the example illustrated in Figure 1;

[0014] Figure 4 is a partially exploded view of the forefoot ground reaction force sensor in accordance with the example illustrated in Figure 2;

[0015] Figure 5 is an assembled view and an exploded view of a vertical load cell and bearing assembly in accordance with an example of the present invention;

[0016] Figure 6 is an assembled view and an exploded view of another vertical load cell and bearing assembly in accordance with another example of the present invention;

[0017] Figure 7 is an assembled view and an exploded view of another vertical load cell and bearing assembly in accordance with yet another example of the present invention;

[0018] Figure 8 is a partial sectional view of a vertical load cell and bearing assembly, in a first condition, in accordance with another example of the present invention;

[0019] Figure 9 is a partial sectional view of a vertical load cell and bearing assembly, in a second condition, in accordance with an example of the present invention;

[0020] Figure 10 is a perspective view of a horizontal load cell in accordance with an example of the present invention;

[0021] Figure 11 is a sectional view of the horizontal load cell taken along line 11-11of Figure 10;

[0022] Figure 12 is a schematic diagram of a Wheatstone bridge circuit in accordance with an example of the present invention; and

[0023] Figure 13 is a schematic diagram of an electronics module in accordance with an example of the present invention.

DETAILED DESCRIPTION OF THE INVENTION

[0024] Referring first to Figure 1, an article 20 such as a foot covering or shoe (shown), a prosthetic device, an animal's hoof, or a robotic limb, for example, transfers loads to the a surface such as the ground 22. The ground 22 extends parallel to a horizontal plane defined by an X-axis and a Y-axis. The ground 22 also extends perpendicular to first vertical plane defined by the X-axis and a Z-axis and a second vertical plane defined by the Y-axis and the Z-axis.

[0025] Exemplary ground reaction force sensors 24a, 24b may be attached to forefoot 26 and heal 28 regions at a bottom surface 30 of the article 20 by attachment means 32 such as tabs and fasteners (shown), bindings, straps, adhesives, and hook and loop fasteners, for example. In other examples, the sensors 24a, 24b are formed integrally with the article 20 during its manufacture. In yet other examples, the article 20 is modified, after its manufacture, by removing a vertical slice to compensate for the vertical thickness of the sensors 24a, 24b.

Please note that the sensors 24a, 24b have a very slim vertical profile in comparison to the article 20. The forefoot sensor 24a may also be slightly curved to conform to the shape of the forefoot portion 26, thus allowing for a more natural gait by the subject during analysis.

[0026] With reference to Figures 2-4, further details of the exemplary sensors 24a, 24b, which were designed and built at the Oak Ridge National Laboratory, will now be described in much greater detail. An upper force plate 34 includes an upper contact surface 36 for contacting the bottom surface 30 of the article 20. Upper pockets 38 receive vertical load cells 40 and upper clevises 42 receive horizontal load cells 44, which are rotationally affixed via vertically-oriented cylindrical pins 46. The pins 46 are retained by C-clips, cotter pins or other pin retention means. Please note that the upper force plate 34 includes only one upper clevis 42 for each horizontal load cell 44. In this example, three horizontal load cells were used 44-X, 44-Y1, and 44-Y2.

[0027] A lower force plate 48 includes a lower contact surface 50 for contacting the ground 22. Lower pockets 52 receive the vertical load cells 40 and lower clevises 54 receive the horizontal load cells 44, which are rotationally affixed via cylindrical pins 46 positioned vertically. Please note that the lower force plate 48 includes only one lower clevis 54 for each horizontal load cell 44.

[0028] The upper and lower force plates 34, 48 were formed using an additive manufacturing process that selectively solidifies metallic powder with an electron beam to form layers from a computer generated file, such as an STL file. In this example, the force plates 34, 48 were formed of a light-weight and high-strength Titanium Alloy using a system manufactured by Arcam AB of Gothenburg, Sweden. The force plates 34, 48 could also be formed of other light-weight and high-strength, metallic or nonmetallic, materials by stamping, forming, machining, molding, casting, or other known methods.

[0029] With the force plates 34, 48 assembled together, a horizontal load cell 44-X1 is affixed between the upper and lower clevises 42, 54 by pins 46 in a direction that is parallel to the X-axis and in the horizontal plane defined by the X-axis and the Y-axis. Additionally, two horizontal load cells 44-Y1, and 44-Y2 are affixed between the upper and lower clevises 42, 54 by pins 46 in a direction that is parallel to the Y-axis and in the horizontal plane defined by the X-axis and the Y-axis. The pins 46 assure that only substantially axial forces are transferred to the horizontal load cells 44-X, 44-Y1, and 44-Y2. By including at least three horizontal load cells 44-X, 44-Y1, and 44-Y2, the upper and lower force plates 34, 48 are inhibited from twisting and/or racking with respect to one another. Three horizontal load cells 44-X, 44-Y1, and 44-Y2, are also necessary in order to measure Fx, Fy and Mz (moment about a vertical Z-axis).

[0030] Protruding fingers 56 on each of the force plates 34, 48 retain elastomer bands 58, which secure the plates 34, 48 together and impose a slight compressive load on the vertical load cells 40. The elastomer bands 58 have a relatively low spring rate in comparison to the spring rate of the vertical load cells 40. This compressive load counteracts any potential tension loads that might occur as the upper force plate 34 is raised. The slight compressive load is simply zeroed out while processing the actual load data that is collected during the gait analysis on a computing device. An additional advantage of the elastomer bands 58 is their ability to provide unencumbered cleaning, inspection, service, and replacement of the various components of the sensors 24a, 24b.

[0031] Referring now to Figures 5-8, further details of the vertical load cells 40 will be described. The vertical load cells 40 used in the exemplary sensors 24a, 24b are subminiature load buttons having a 250 lb (113 kg) compression load capacity, model LLB250, and sold by FUTEK Advanced Sensor Technology, Inc., City of Irvine, California, USA, for example. The vertical load cells 40 include a crowned surface 60 to approximate a point loading

condition. This allows for slight flexing of the force plates 34, 48 with respect to each other without transmitting moment loads to the vertical load cells 40. In some examples, at least three vertical load cells 40 are used, in other examples, at least four vertical load cells 40 are used and in yet other examples, at least six vertical load cells 40 are used.

[0032] It is to be noted again that the upper force plate 34 and the lower force plate 48 are not rigidly attached to one another and that slight relative motion is necessary to measure the horizontal forces. The single axis, vertical load cells 40 are not sensitive to this off-axis loading. To ensure that the vertical load cells 40 only measure forces that are substantially perpendicular to the ground 22, a bearing assembly 62 is disposed between the vertical load cells 40 and a force plate 34, 48.

[0033] In the bearing assembly 62 example of Figure 5, a pair of roller-type bearings 64a, 64b each include a series of individual rollers 66 confined in a cage 68 having a number of through slots 70 that are sized to accept the rollers 66. The slots 70 in the example were formed by wire EDM; however, punching, stamping, laser cutting, water jet, or other forming techniques could similarly be used. Note that all of the rollers 66 in roller-type bearing 64a are aligned in a first direction that differs from a second direction of the rollers 66 in the roller-type bearing 64b. In this specific embodiment, the rollers 66 in roller-type bearing 64a are aligned in a direction that is perpendicular to the rollers 66 of roller-type bearing 64b. This perpendicular alignment ensures that the vertical load cells 40 are substantially insulated from all lateral and fore to aft loads. A hardened bearing plate 72 (e.g., stainless steel) is disposed between the two roller-type bearings 64a, 64b. In some examples, hardened bearing plates 72 are disposed on each side of the roller-type bearings 64a, 64b (shown). Roller-type bearings 64a and 64b are available from The Timken Company, 1835 Dueber Ave., S.W. Canton, Ohio 4470-2790, USA, for example.

[0034] The two roller-type bearings 64a, 64b and the hardened bearing plates 72 may each include a clocking feature 74 that interacts with a centering element 76 made of a resilient material (e.g., 40 durometer polyurethane elastomer). In this example, a square clocking feature 74 was used; however, other clocking features (e.g., asymmetric shape, spline, slot, offset pin, etc…) could also be used. The centering element 76 permits: a slight amount of unimpeded relative motion between the two roller-type bearings 64a and 64b and the bearing plates 72; permits a slight lateral movement between force plates 43 and 48; assures the two bearings 64a, 64b are orthogonal relative to each other; and assures the bearing plates 72 are concentric with one another and with the roller cages 68 after each loading cycle. The centering element 76 includes an aperture 78 for accepting a protruding pin 80 that is affixed in a pocket 38 or 52 of a force plate 34, 48. In one example, the pin 80 is affixed to the lower force plate 48 and the vertical load cell 40 contacts the upper force plate 34 (shown). In another example, the pin 80 is affixed to the upper force plate 34 and the vertical load cell 40 contacts the lower force plate 48. In another example, one of the roller-type bearings, 64a or 64b, is disposed above a vertical load cell 40 and the other of the roller-type bearings, 64a or 64b, is disposed below the vertical load cell 40.

[0035] In the bearing assembly 62 example of Figure 6, a ball-type bearing 82 includes a series of hardened steel balls 84 confined in a steel cage 86 designed for axial loading. These bearings are also known as thrust bearings. A hardened bearing plate 72 is disposed on each side of the ball-type bearing 82. The bearing plates 72 each include an aperture 88 that cooperates with a centering element 76, made of a resilient material (e.g., 40 durometer polyurethane elastomer), to ensure proper alignment of the bearing assembly 62. Please note that a clocking feature 74 is not shown in this example, because the balls 84 are free to rotate in any direction within the horizontal plane defined by the X-axis and Y-axis. Ball-type

bearings 82 are available from McMaster-Carr, 200 Aurora Industrial Parkway, Aurora, Ohio 44202-8087, USA, for example.

[0036] While each type of bearing assembly 62 will work in this application, the roller-type bearings 64a, 64b provide a superior load handling capability for their size and offer a relatively low vertical profile, which enhances the function of the sensors 24a, 24b and ensures nearly unencumbered motion during gait analysis.

[0037] In another example of a bearing assembly 62, as illustrated in Figure 7, an additional example of a centering element 76 is shown. In this example, the centering element has a series of compliant arms that mate with clocking features 74 as in the earlier example. An aperture 78 in the centering element 76 accepts a protruding pin 80 that is affixed in a pocket 38 or 52 of a force plate 34, 48. This centering element may be made of a resilient material (e.g., 40 durometer polyurethane elastomer); however, due to its compliant design, may also be made of a plastic or spring steel material for example. The centering element 76 permits: a slight amount of unimpeded relative motion between the two roller-type bearings 64a and 64b and the bearing plates 72; permits a slight lateral movement between force plates 43 and 48; assures the two bearings 64a, 64b are orthogonal relative to each other; and assures the bearing plates 72 are concentric with one another and with the roller cages 68 after each loading cycle.

[0038] Referring now to Figures 8-9, another example of a vertical load cell 40 is illustrated. In this example, the vertical load cell 40 is a series of individual strain gages 90 affixed to one of the upper or lower force plates 34, 48. Here, the four individual strain gages 90 react to the deflection of a force plate 34, 48 as a force F is applied. In this example, the upper force plate 34 has a beam shaped cross sectional portion 92 that is approximately 0.020 inches (0.508 mm) thick. A crowned plate 94 sits atop a bearing assembly 62and fits within a

pocket 52, as earlier described. When a force F is applied to the load plates 34, 48, the beam portion 92 deflects slightly, as shown in the condition of Figure 9, and the two inner strain gages 90 will be subjected to a tension load, while the two outer strain gages 90 will be subjected to a compression load. The sum of these four loads is indicative of the total vertical load on the load cell 40. In this example, the strain gages 90 are affixed directly to a force plate 34, 48, at the time of manufacture, instead of being a prefabricated component as in the earlier examples of Figures 5-7.

[0039] Referring now to Figures 10 and 11, further details of the horizontal load cells 44 will now be discussed. The horizontal load cells 44 have an I-beam shaped body 98 with clevis attachments 100 at each end for engaging clevises 42, 54 on the force plates 34, 48. In this example, the horizontal load cells 44 were machined from an aluminum alloy material, although other materials are also contemplated. A web portion 102 of the body 98 is approximately 0.020 inches (0.508 mm) thick and includes two strain gages 104 affixed on each side of the web portion 102. One strain gage 104 on each side is aligned parallel to the X-axis and one strain gage on each side is aligned parallel to the Y-axis. Strain gages 104 and associated hardware are available from Omega Engineering, Inc., One Omega Drive P.O. Box 4047, Stamford, Connecticut 06907-0047, USA, for example.

[0040] The strain gages 90, 104 are wired in a full Wheatstone bridge circuit 106 as illustrated in Figure 12, because of its ability to measure minute resistance changes in the strain gage 90, 104 wires. The full Wheatstone bridge has two fully active strain gages in the principal stress direction and two strain gages that will see the effect of Poisson's Ratio. The full bridge circuit 106 tends to cancel thermal and off-axis errors. The output voltage of the Wheatstone bridge is expressed in millivolts output per volt input. Wheatstone bridge circuits 106 are well known in the art of strain measurements and, although this specific circuit was illustrated in the example, other circuits may also be used.

[0041] Referring finally to Figure 13, a sensor electronics module 108 is shown. A printed circuit board (PCB) 110, located in each sensor 24a, 24b, acquires electronic signals from each of the vertical 40 and horizontal 44 load cells through directly wired or wireless connections as shown. The electronics module 108 also includes a power supply (e.g., battery) 112, and access to a local 114 and/or remote 116 data storage device. A local storage device 114 may include a hard drive, a memory card, a memory stick or other device that stores electronic load signals in the electronics module 108. A memory card slot 118 may be utilized with specialized cards and plug-in devices such as, for example, a wireless networking card, to expand the capabilities of functionality of the electronics module 108. The electronics module 108 may include a communications device 120 such as an antenna to facilitate connectivity and transfer of electronic data to the remote storage device 116 via one or more communication protocols such as: WiFi (WLAN); Bluetooth or other personal area network (PAN) standard; cellular communications; an infrared (IR) for communication via the Infrared Data association (IrDA) standard and/or any other communication standard known or yet to be developed. Once the acquired load data is communicated to and stored on the local 114 or remote 116 data storage device, it may be reviewed, manipulated, and further analyzed by a gait clinician using commercially available or custom coded software using, for example, a personal computing device 122.

[0042] While this disclosure describes and enables several examples of a wearable ground reaction force foot sensor, other examples and applications are contemplated. Accordingly, the invention is intended to embrace those alternatives, modifications, equivalents, and variations as fall within the broad scope of the appended claims. The technology disclosed and claimed herein may be available for licensing in specific fields of use by the assignee of record.

What is claimed is:

1. A wearable ground reaction force sensor for an article comprising:

an upper force plate for contacting a bottom surface of the article;

a lower force plate for contacting the ground;

a vertical load cell disposed between said plates for measuring a force acting on the cell in a direction that is substantially perpendicular to the ground;

a horizontal load cell disposed between said plates for measuring a force acting on the cell in a direction that is substantially parallel to the ground; and

wherein the load cells are mounted between the plates in a configuration that is substantially insensitive to off-axis forces imposed on them for improved load cell measurement accuracies.

2. The sensor of claim 1, wherein said horizontal load cell comprises a first and a second end, and wherein the first end is affixed to said upper force plate and the second end is affixed to said lower force plate by pin and clevis attachments for providing only substantially axial loading of the horizontal load cell.

3. The sensor of claim 1, further comprising:

a bearing disposed between said vertical load cell and a force plate for assuring only substantially axial loading of the vertical load cell.

4. The sensor of claim 3, wherein said bearing is a ball-type bearing having balls in a cage.

5. The sensor of claim 3, wherein said bearing is a roller-type bearing having rollers in a cage.

6. The sensor of claim 5, wherein said bearing comprises two roller-type bearings, each of said roller-type bearings having rollers aligned in one direction in a cage, and wherein the rollers of a first of said bearings are aligned in a first direction that differs from a second direction of the rollers of a second of said bearings.

7. The sensor of claim 6, wherein the rollers of the first of said bearings are aligned in a first direction that is perpendicular to the second direction of the rollers of said second bearings.

8. The sensor of claim 7, further comprising a bearing plate disposed between said two roller-type bearings.

9. The sensor of claim 8, wherein said two roller-type bearings and said bearing plate each have a clocking feature that cooperates with a centering element to ensure that said roller-type bearings and said bearing plate start out with a correct position and permits slight relative motion between said upper and lower force plates without adding any additional loading to said load cells.

10. The sensor of claim 10, wherein said centering element is made of an elastomer material.

11. The sensor of claim 10, wherein said centering element comprises an aperture for accepting a pin that extends from a force plate.

12. The sensor of claim 11, wherein the pin extends from said lower force plate.

13. The sensor of claim 10, comprising at least three vertical load cells and at least three horizontal load cells, and wherein two of said horizontal load cells are disposed in a direction that is perpendicular to the other one of said horizontal load cells.

14. The sensor of claim 11, comprising at least four vertical load cells and at least three horizontal load cells, and wherein two of said horizontal load cells are disposed in a direction that is perpendicular to the other one of said horizontal load cells.

15. The sensor of claim 12, comprising at least six vertical load cells and at least three horizontal load cells, and wherein two of said horizontal load cells are disposed in a direction that is perpendicular to the other one of said horizontal load cells.

16. The sensor of claim 1, further comprising an elastomer band affixed to said upper and said lower force plates, said band for providing a minimal compressive force between said force plates.

17. The sensor of claim 1, further comprising means for attaching the sensor to the article.

18. The sensor of claim 1, wherein said upper and lower force plates are made of a powdered titanium material using additive manufacturing.

19. The sensor of claim 1, further comprising an electronics module for accepting electronic signals from the load cells.

20. A wearable ground reaction force sensor for an article comprising:

an upper force plate for contacting a bottom surface of the article;

a lower force plate for contacting the ground;

a vertical load cell disposed on one of said plates for measuring a force acting on the cell in a direction that is substantially perpendicular to the ground;

a horizontal load cell disposed between said plates for measuring a force acting on the cell in a direction that is substantially parallel to the ground; and

wherein the load cells are mounted between the plates in a configuration that is substantially insensitive to off-axis forces imposed on them for improved load cell measurement accuracies.

ABSTRACT

[0043] Disclosed are several examples of a ground reaction force sensor for an article having an upper force plate for contacting the article, a lower force plate for contacting the ground, a vertical load cell disposed between the plates for measuring the force acting on the cell in a direction that is substantially perpendicular to the surface, a horizontal load cell disposed between the plates for measuring the force acting on the cell in a direction that is substantially parallel to the surface, and with the load cells being mounted between the plates in a configuration that is substantially insensitive to off-axis forces imposed on them for improved load cell measurement accuracies. Various other features and benefits are provided.

PTO/SB/14 (11-08)
Approved for use through 01/31/2014. OMB 0651-0032
U.S. Patent and Trademark Office; U.S. DEPARTMENT OF COMMERCE

Application Data Sheet 37 CFR 1.76	Attorney Docket Number	2777.0
	Application Number	
Title of Invention	Wearable Ground Reaction Force Foot Sensor	

The application data sheet is part of the provisional or nonprovisional application for which it is being submitted. The following form contains the bibliographic data arranged in a format specified by the United States Patent and Trademark Office as outlined in 37 CFR 1.76.
This document may be completed electronically and submitted to the Office in electronic format using the Electronic Filing System (EFS) or the document may be printed and included in a paper filed application.

Secrecy Order 37 CFR 5.2

☐ Portions or all of the application associated with this Application Data Sheet may fall under a Secrecy Order pursuant to 37 CFR 5.2 (Paper filers only. Applications that fall under Secrecy Order may not be filed electronically.)

Applicant Information:

Applicant 1 Remove

Applicant Authority ◉ Inventor ○ Legal Representative under 35 U.S.C. 117 ○ Party of Interest under 35 U.S.C. 118

Prefix	Given Name	Middle Name	Family Name	Suffix
	Randall	F.	Lind	

Residence Information (Select One) ◉ US Residency ○ Non US Residency ○ Active US Military Service

City	Loudon	State/Province	TN	Country of Residence [i]	US

Citizenship under 37 CFR 1.41(b) [i] US

Mailing Address of Applicant:

Address 1	350 Rivers Edge Drive		
Address 2			
City	Loudon	State/Province	TN
Postal Code	37774	Country[i]	US

All Inventors Must Be Listed - Additional Inventor Information blocks may be generated within this form by selecting the **Add** button. Add

Correspondence Information:

Enter either Customer Number or complete the Correspondence Information section below.
For further information see 37 CFR 1.33(a).

☐ **An Address is being provided for the correspondence Information of this application.**

Customer Number	24298		
Email Address	cinicl@ornl.gov	Add Email	Remove Email

Application Information:

Title of the Invention	Wearable Ground Reaction Force Foot Sensor		
Attorney Docket Number	2777.0	Small Entity Status Claimed	☒
Application Type	Nonprovisional		
Subject Matter	Utility		
Suggested Class (if any)		Sub Class (if any)	
Suggested Technology Center (if any)			
Total Number of Drawing Sheets (if any)	11	Suggested Figure for Publication (if any)	

PTO/SB/14 (11-08)
Approved for use through 01/31/2014. OMB 0651-0032
U.S. Patent and Trademark Office; U.S. DEPARTMENT OF COMMERCE

Application Data Sheet 37 CFR 1.76	Attorney Docket Number	2777.0
	Application Number	
Title of Invention	Wearable Ground Reaction Force Foot Sensor	

Publication Information:

☐	Request Early Publication (Fee required at time of Request 37 CFR 1.219)
☐	**Request Not to Publish.** I hereby request that the attached application not be published under 35 U.S.C. 122(b) and certify that the invention disclosed in the attached application **has not and will not** be the subject of an application filed in another country, or under a multilateral international agreement, that requires publication at eighteen months after filing.

Representative Information:

Representative information should be provided for all practitioners having a power of attorney in the application. Providing this information in the Application Data Sheet does not constitute a power of attorney in the application (see 37 CFR 1.32).
Enter either Customer Number or complete the Representative Name section below. If both sections are completed the Customer Number will be used for the Representative Information during processing.

Please Select One:	◉ Customer Number	○ US Patent Practitioner	○ Limited Recognition (37 CFR 11.9)
Customer Number	24298		

Domestic Benefit/National Stage Information:

This section allows for the applicant to either claim benefit under 35 U.S.C. 119(e), 120, 121, or 365(c) or indicate National Stage entry from a PCT application. Providing this information in the application data sheet constitutes the specific reference required by 35 U.S.C. 119(e) or 120, and 37 CFR 1.78(a)(2) or CFR 1.78(a)(4), and need not otherwise be made part of the specification.

Prior Application Status			Remove
Application Number	Continuity Type	Prior Application Number	Filing Date (YYYY-MM-DD)

Additional Domestic Benefit/National Stage Data may be generated within this form by selecting the **Add** button. Add

Foreign Priority Information:

This section allows for the applicant to claim benefit of foreign priority and to identify any prior foreign application for which priority is not claimed. Providing this information in the application data sheet constitutes the claim for priority as required by 35 U.S.C. 119(b) and 37 CFR 1.55(a).

Remove

Application Number	Country [i]	Parent Filing Date (YYYY-MM-DD)	Priority Claimed
			◉ Yes ○ No

Additional Foreign Priority Data may be generated within this form by selecting the **Add** button. Add

Assignee Information:

Providing this information in the application data sheet does not substitute for compliance with any requirement of part 3 of Title 37 of the CFR to have an assignment recorded in the Office.

Assignee 1 Remove

PTO/SB/14 (11-08)
Approved for use through 01/31/2014. OMB 0651-0032
U.S. Patent and Trademark Office; U.S. DEPARTMENT OF COMMERCE

Application Data Sheet 37 CFR 1.76	Attorney Docket Number	2777.0
	Application Number	
Title of Invention	Wearable Ground Reaction Force Foot Sensor	

If the Assignee is an Organization check here. ☒			
Organization Name	UT-Battelle, LLC		
Mailing Address Information:			
Address 1	One Bethel Valley Road		
Address 2	4500N, MS-6258		
City	Oak Ridge	**State/Province**	TN
Country [i]	US	Postal Code	37831
Phone Number	865-574-4179	Fax Number	865-574-0381
Email Address	cincl@ornl.gov		
Additional Assignee Data may be generated within this form by selecting the **Add** button.		Add	

Signature:

A signature of the applicant or representative is required in accordance with 37 CFR 1.33 and 10.18. Please see 37 CFR 1.4(d) for the form of the signature.

Signature	/Colin L. Cini/			Date (YYYY-MM-DD)	2012-07-12
First Name	Colin	Last Name	Cini	Registration Number	51563

This collection of information is required by 37 CFR 1.76. The information is required to obtain or retain a benefit by the public which is to file (and by the USPTO to process) an application. Confidentiality is governed by 35 U.S.C. 122 and 37 CFR 1.14. This collection is estimated to take 23 minutes to complete, including gathering, preparing, and submitting the completed application data sheet form to the USPTO. Time will vary depending upon the individual case. Any comments on the amount of time you require to complete this form and/or suggestions for reducing this burden, should be sent to the Chief Information Officer, U.S. Patent and Trademark Office, U.S. Department of Commerce, P.O. Box 1450, Alexandria, VA 22313-1450. DO NOT SEND FEES OR COMPLETED FORMS TO THIS ADDRESS. **SEND TO: Commissioner for Patents, P.O. Box 1450, Alexandria, VA 22313-1450.**

Privacy Act Statement

The Privacy Act of 1974 (P.L. 93-579) requires that you be given certain information in connection with your submission of the attached form related to a patent application or patent. Accordingly, pursuant to the requirements of the Act, please be advised that: (1) the general authority for the collection of this information is 35 U.S.C. 2(b)(2); (2) furnishing of the information solicited is voluntary; and (3) the principal purpose for which the information is used by the U.S. Patent and Trademark Office is to process and/or examine your submission related to a patent application or patent. If you do not furnish the requested information, the U.S. Patent and Trademark Office may not be able to process and/or examine your submission, which may result in termination of proceedings or abandonment of the application or expiration of the patent.

The information provided by you in this form will be subject to the following routine uses:

1. The information on this form will be treated confidentially to the extent allowed under the Freedom of Information Act (5 U.S.C. 552) and the Privacy Act (5 U.S.C. 552a). Records from this system of records may be disclosed to the Department of Justice to determine whether the Freedom of Information Act requires disclosure of these records.

2. A record from this system of records may be disclosed, as a routine use, in the course of presenting evidence to a court, magistrate, or administrative tribunal, including disclosures to opposing counsel in the course of settlement negotiations.

3. A record in this system of records may be disclosed, as a routine use, to a Member of Congress submitting a request involving an individual, to whom the record pertains, when the individual has requested assistance from the Member with respect to the subject matter of the record.

4. A record in this system of records may be disclosed, as a routine use, to a contractor of the Agency having need for the information in order to perform a contract. Recipients of information shall be required to comply with the requirements of the Privacy Act of 1974, as amended, pursuant to 5 U.S.C. 552a(m).

5. A record related to an International Application filed under the Patent Cooperation Treaty in this system of records may be disclosed, as a routine use, to the International Bureau of the World Intellectual Property Organization, pursuant to the Patent Cooperation Treaty.

6. A record in this system of records may be disclosed, as a routine use, to another federal agency for purposes of National Security review (35 U.S.C. 181) and for review pursuant to the Atomic Energy Act (42 U.S.C. 218(c)).

7. A record from this system of records may be disclosed, as a routine use, to the Administrator, General Services, or his/her designee, during an inspection of records conducted by GSA as part of that agency's responsibility to recommend improvements in records management practices and programs, under authority of 44 U.S.C. 2904 and 2906. Such disclosure shall be made in accordance with the GSA regulations governing inspection of records for this purpose, and any other relevant (i.e., GSA or Commerce) directive. Such disclosure shall not be used to make determinations about individuals.

8. A record from this system of records may be disclosed, as a routine use, to the public after either publication of the application pursuant to 35 U.S.C. 122(b) or issuance of a patent pursuant to 35 U.S.C. 151. Further, a record may be disclosed, subject to the limitations of 37 CFR 1.14, as a routine use, to the public if the record was filed in an application which became abandoned or in which the proceedings were terminated and which application is referenced by either a published application, an application open to public inspections or an issued patent.

9. A record from this system of records may be disclosed, as a routine use, to a Federal, State, or local law enforcement agency, if the USPTO becomes aware of a violation or potential violation of law or regulation.

Electronic Acknowledgement Receipt

EFS ID:	13232201
Application Number:	13547105
International Application Number:	
Confirmation Number:	8182
Title of Invention:	Wearable Ground Reaction Force Foot Sensor
First Named Inventor/Applicant Name:	Randall F. Lind
Customer Number:	24298
Filer:	Colin Lyle Cini/Karen Vance
Filer Authorized By:	Colin Lyle Cini
Attorney Docket Number:	
Receipt Date:	12-JUL-2012
Filing Date:	
Time Stamp:	09:48:47
Application Type:	Utility under 35 USC 111(a)

Payment information:

Submitted with Payment	yes
Payment Type	Deposit Account
Payment was successfully received in RAM	$530
RAM confirmation Number	10169
Deposit Account	131958
Authorized User	

The Director of the USPTO is hereby authorized to charge indicated fees and credit any overpayment as follows:

Charge any Additional Fees required under 37 C.F.R. Section 1.16 (National application filing, search, and examination fees)

Charge any Additional Fees required under 37 C.F.R. Section 1.17 (Patent application and reexamination processing fees)

Charge any Additional Fees required under 37 C.F.R. Section 1.19 (Document supply fees)

Charge any Additional Fees required under 37 C.F.R. Section 1.20 (Post Issuance fees)

Charge any Additional Fees required under 37 C.F.R. Section 1.21 (Miscellaneous fees and charges)

File Listing:

Document Number	Document Description	File Name	File Size(Bytes)/ Message Digest	Multi Part /.zip	Pages (if appl.)
1	Oath or Declaration filed	2777_DEC.pdf	60502 b3ba689055ec147407555322c18fb75fb413bcf0	no	2
Warnings:					
The page size in the PDF is too large. The pages should be 8.5 x 11 or A4. If this PDF is submitted, the pages will be resized upon entry into the Image File Wrapper and may affect subsequent processing					
Information:					
2		2777_Specification.pdf	157351 638042f55a5b31a5a70ab3b49387d2b0b4be038b	yes	15

Multipart Description/PDF files in .zip description

Document Description	Start	End
Specification	1	11
Claims	12	14
Abstract	15	15

Warnings:					
Information:					
3	Drawings-only black and white line drawings	2777_Figures.pdf	2351457 46364abf4b586998568bd80fe6bab09eb961c75e	no	11
Warnings:					
Information:					
4	Application Data Sheet	2777_ADS.pdf	1421012 01b635b4b80c4ce4f6c3473261612853121386ee	no	4
Warnings:					
Information:					
5	Fee Worksheet (SB06)	fee-info.pdf	32213 049eaffa87e29a8b8c29609d3fda34e373d4f913	no	2
Warnings:					
Information:					
		Total Files Size (in bytes):	4022535		

This Acknowledgement Receipt evidences receipt on the noted date by the USPTO of the indicated documents, characterized by the applicant, and including page counts, where applicable. It serves as evidence of receipt similar to a Post Card, as described in MPEP 503.

New Applications Under 35 U.S.C. 111

If a new application is being filed and the application includes the necessary components for a filing date (see 37 CFR 1.53(b)-(d) and MPEP 506), a Filing Receipt (37 CFR 1.54) will be issued in due course and the date shown on this Acknowledgement Receipt will establish the filing date of the application.

National Stage of an International Application under 35 U.S.C. 371

If a timely submission to enter the national stage of an international application is compliant with the conditions of 35 U.S.C. 371 and other applicable requirements a Form PCT/DO/EO/903 indicating acceptance of the application as a national stage submission under 35 U.S.C. 371 will be issued in addition to the Filing Receipt, in due course.

New International Application Filed with the USPTO as a Receiving Office

If a new international application is being filed and the international application includes the necessary components for an international filing date (see PCT Article 11 and MPEP 1810), a Notification of the International Application Number and of the International Filing Date (Form PCT/RO/105) will be issued in due course, subject to prescriptions concerning national security, and the date shown on this Acknowledgement Receipt will establish the international filing date of the application.

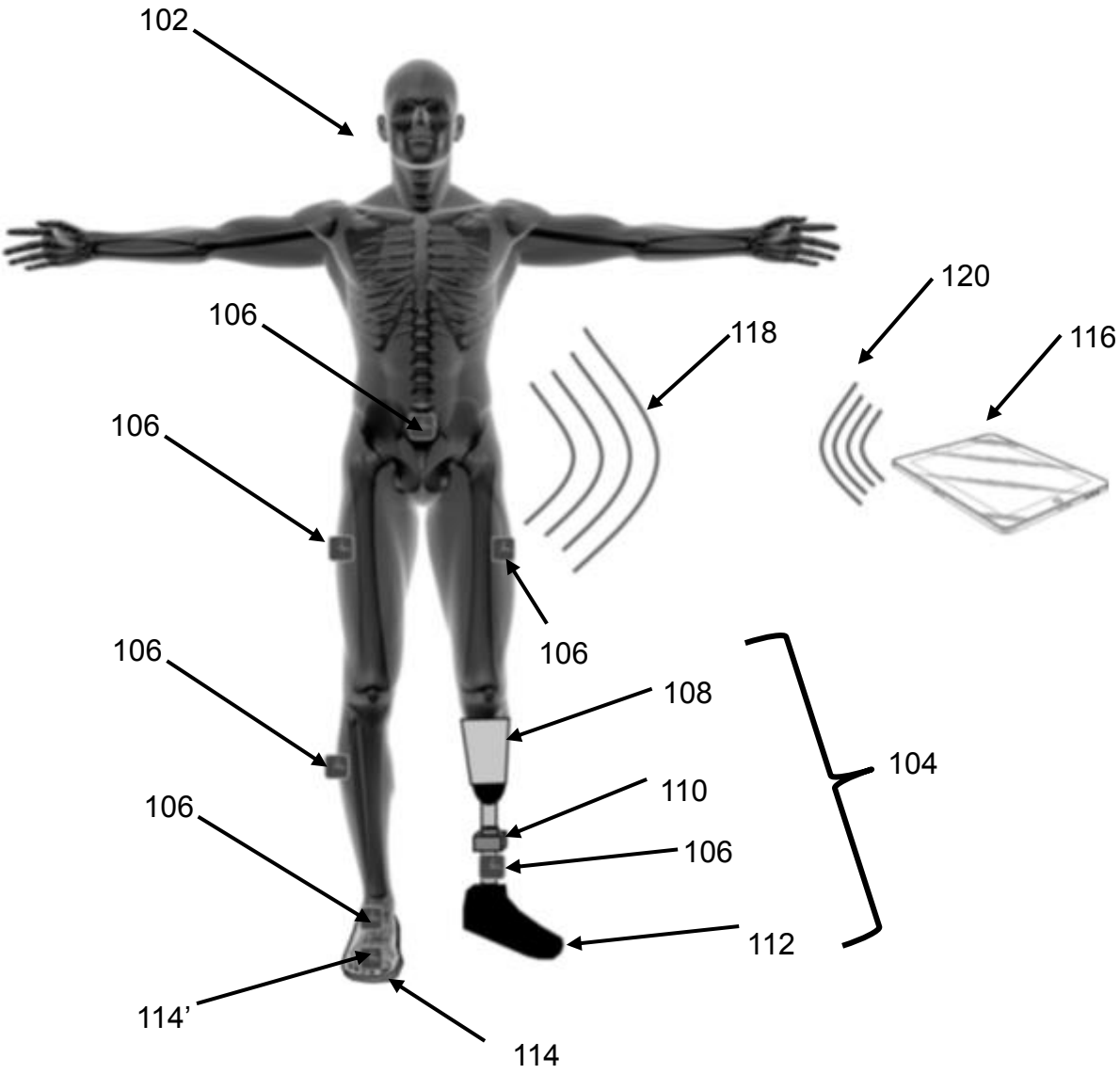
102
120
106
118
116
106
106
106
108
104
106
110
106
106
112
114'
114

FIG. 1 100

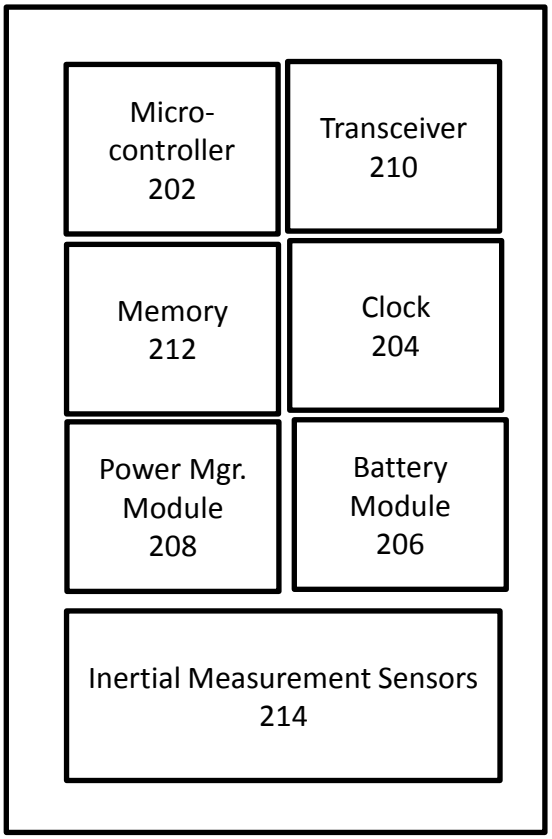
Micro-
controller
202
Transceiver
210
Memory
212
Clock
204
Power Mgr.
Module
208
Battery
Module
206
Inertial Measurement Sensors
214

FIG. 2
106

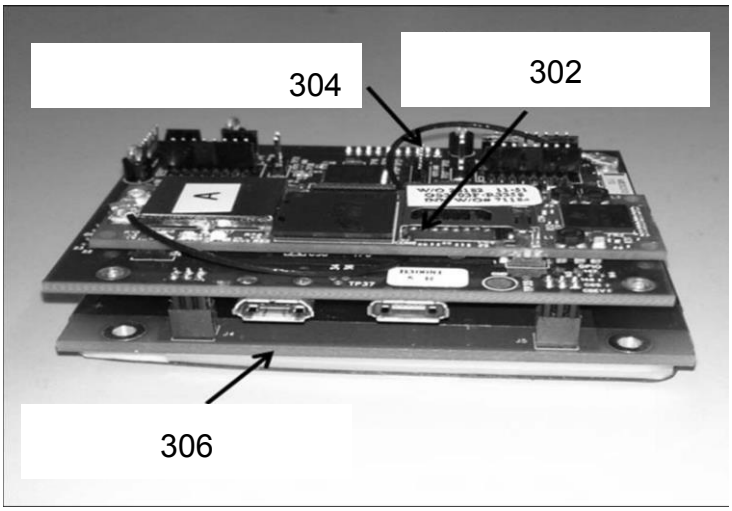

FIG. 3 106

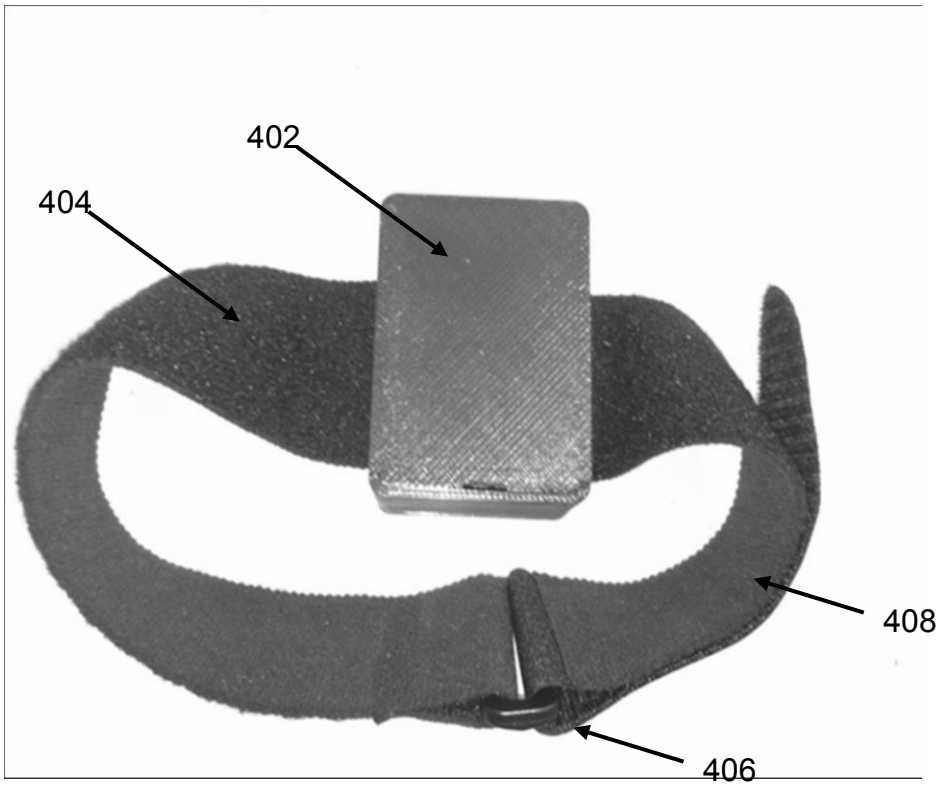

FIG. 4 106

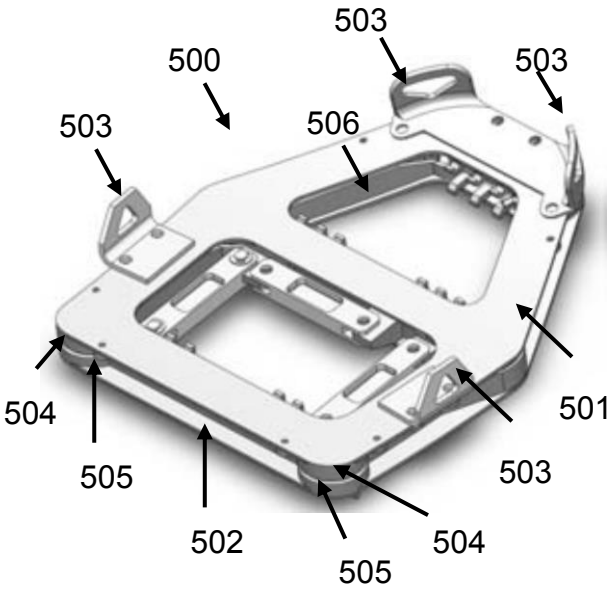

FIG. 5A

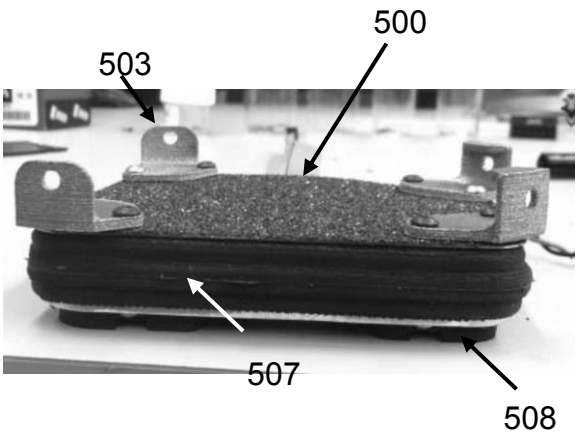

FIG. 5B

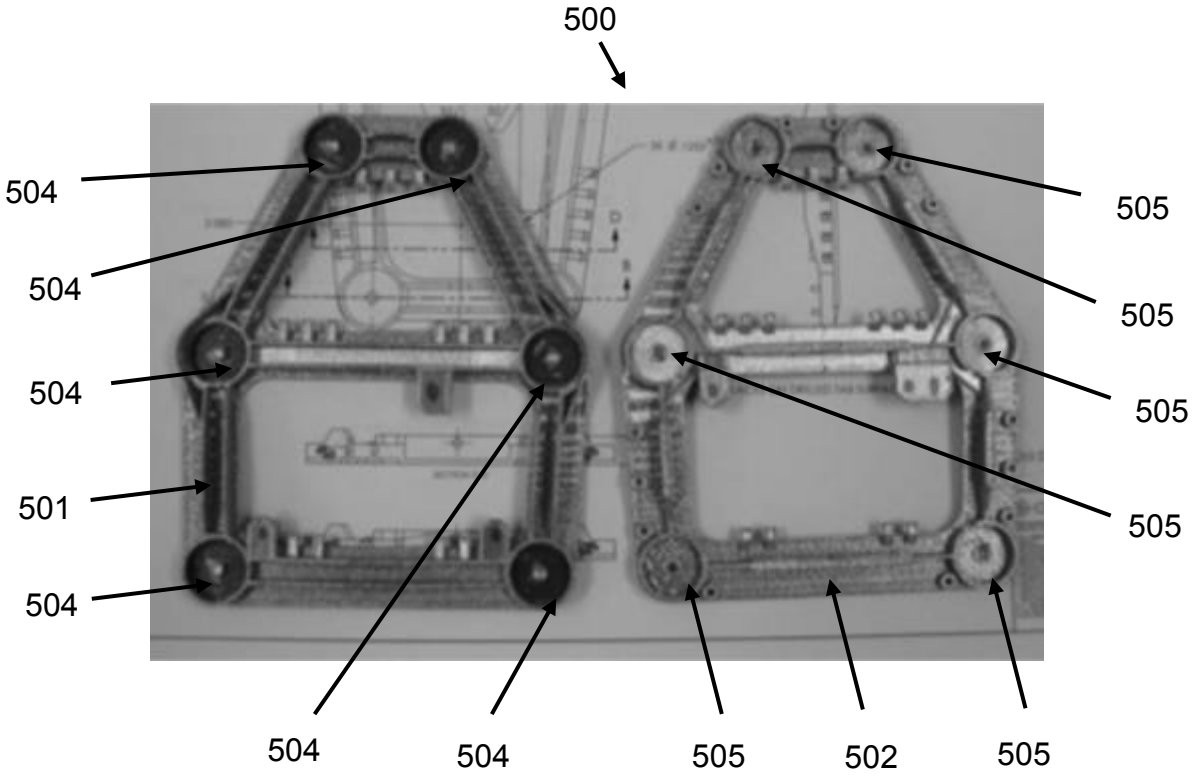

FIG. 5C

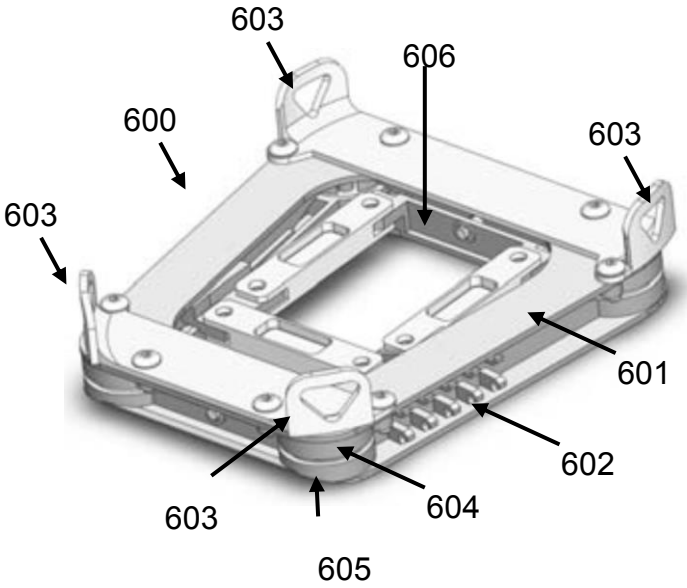

FIG. 6A

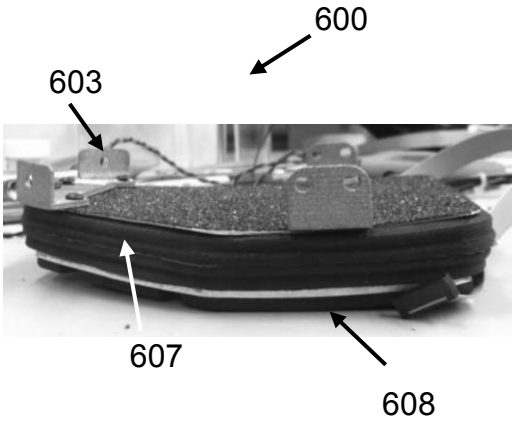

FIG. 6B

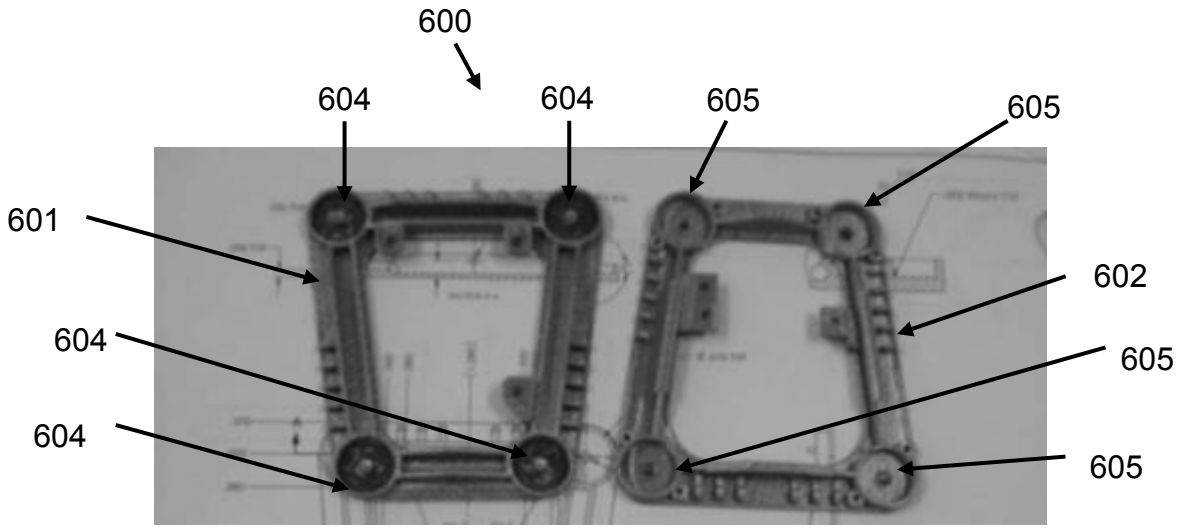

FIG. 6C

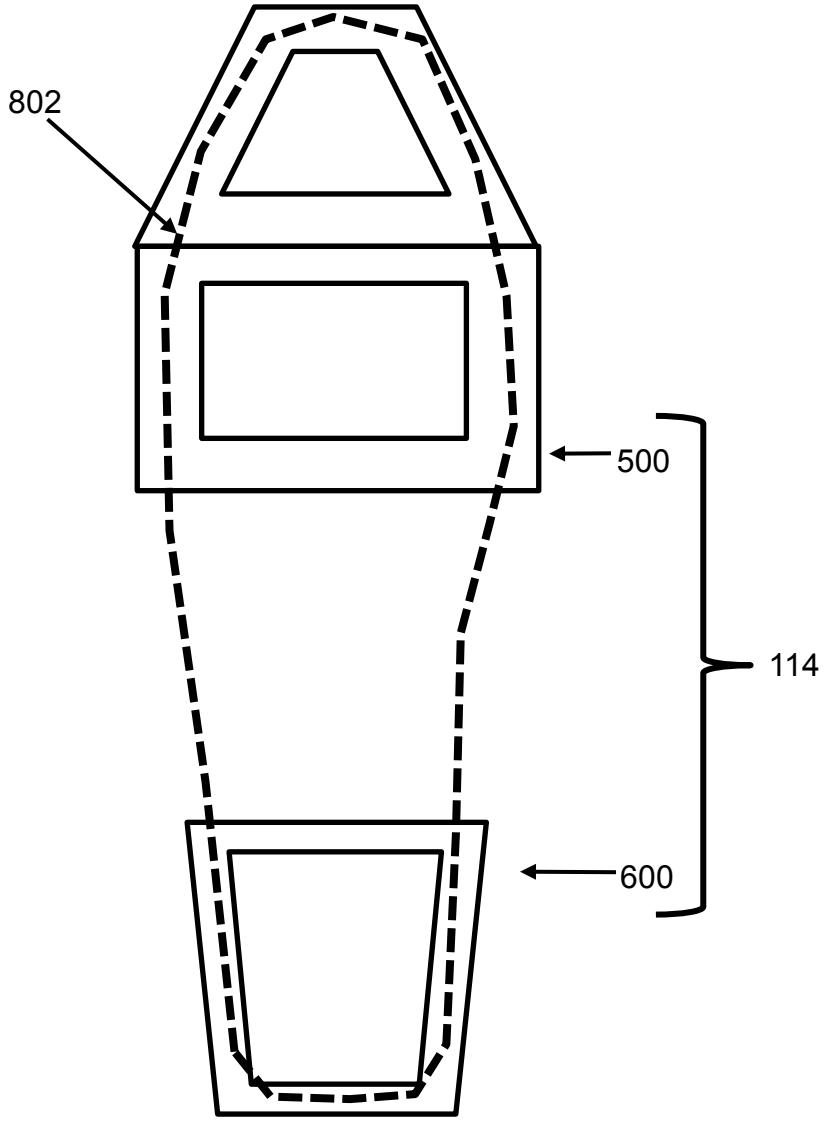

FIG. 7

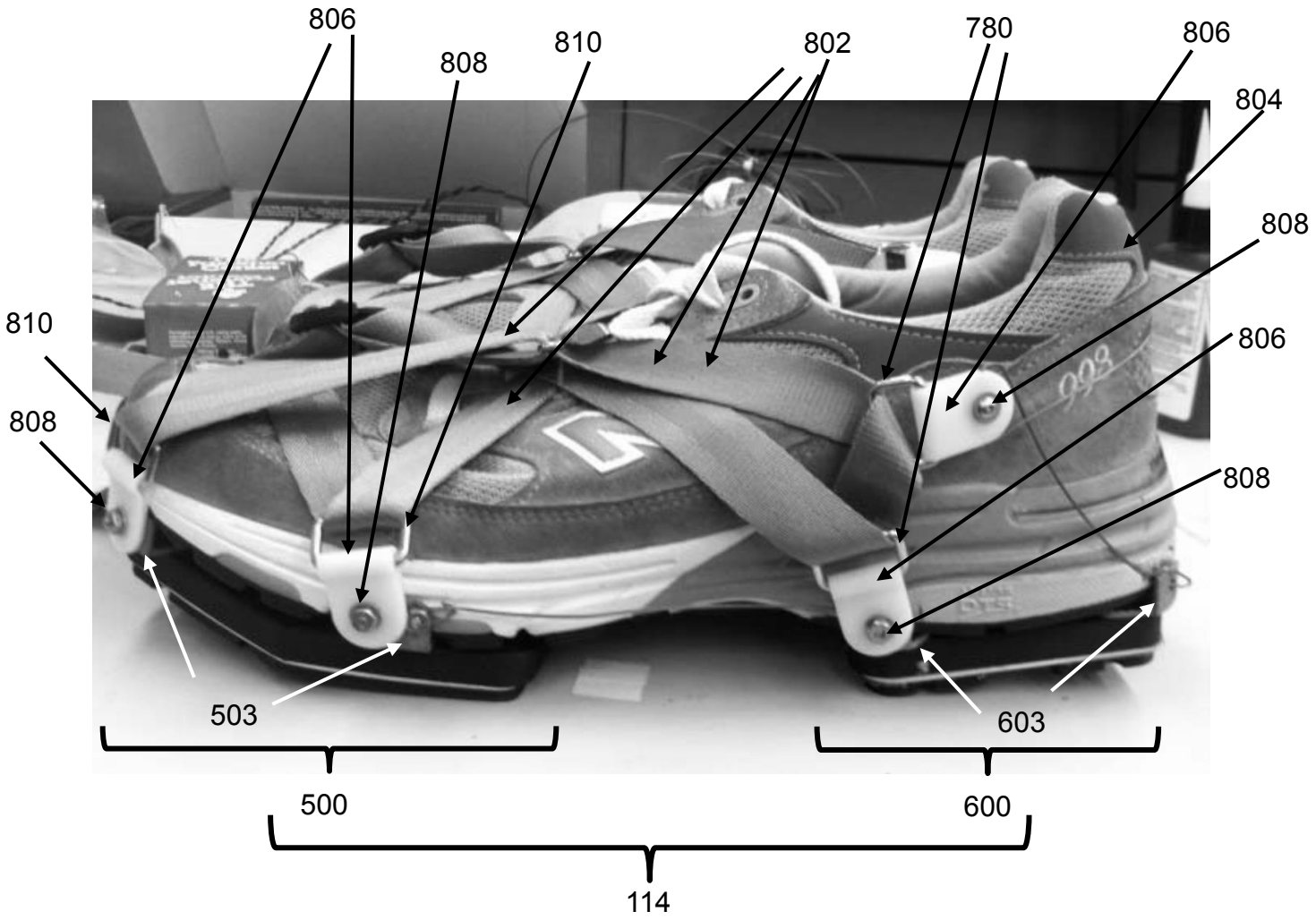
806
808
810
802
780
806
804
808
810
806
808
808
503
603
500
600
114

FIG. 8

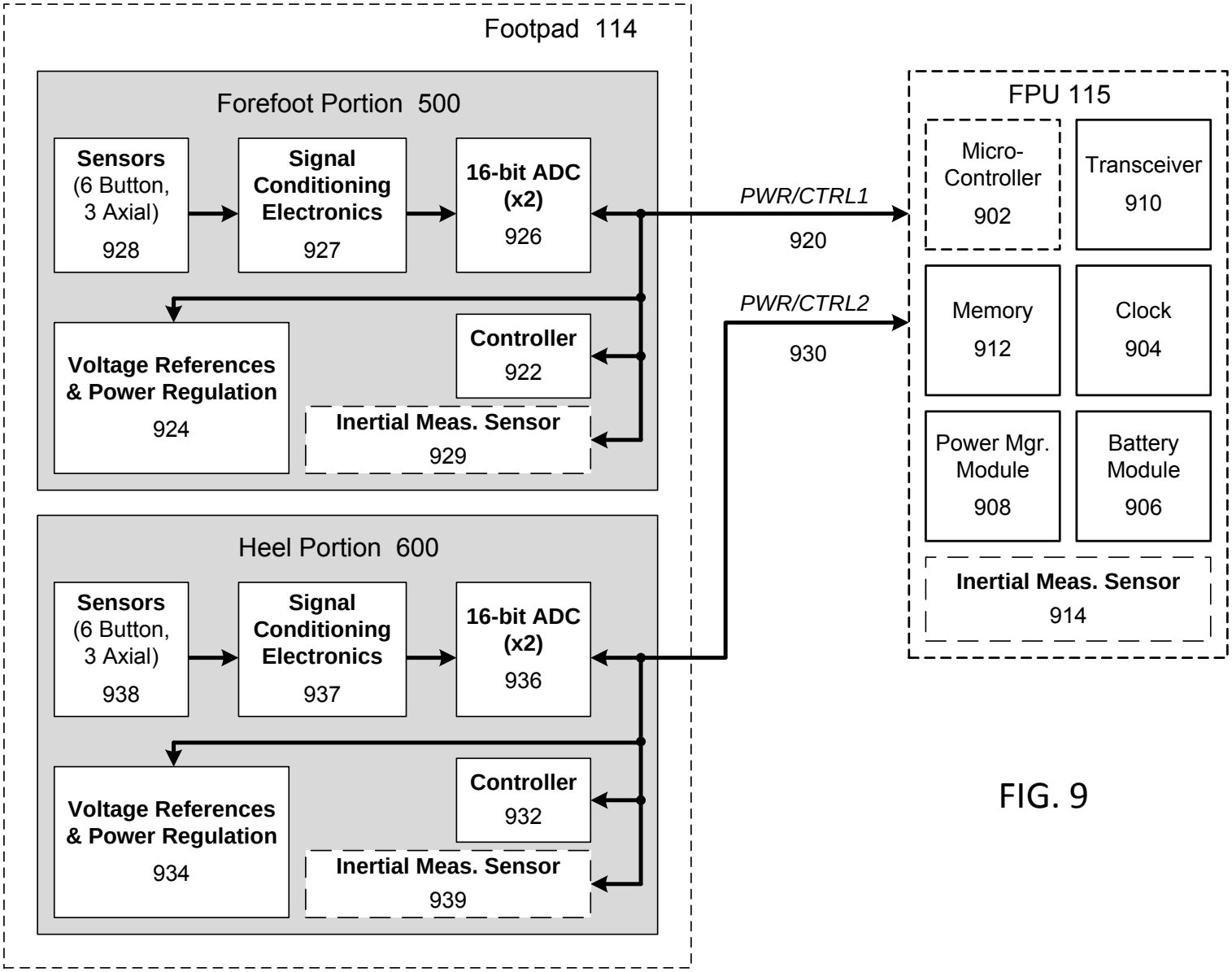
Footpad 114
Forefoot Portion 500
Sensors
(6 Button,
3 Axial)
928
Signal
Conditioning
Electronics
927
16-bit ADC
(x2)
926
Voltage References
& Power Regulation
924
Controller
922
Inertial Meas. Sensor
929
Heel Portion 600
Sensors
(6 Button,
3 Axial)
938
Signal
Conditioning
Electronics
937
16-bit ADC
(x2)
936
Voltage References
& Power Regulation
934
Controller
932
Inertial Meas. Sensor
939
PWR/CTRL1
920
PWR/CTRL2
930
FPU 115
Micro-
Controller
902
Transceiver
910
Memory
912
Clock
904
Power Mgr.
Module
908
Battery
Module
906
Inertial Meas. Sensor
914

FIG. 9

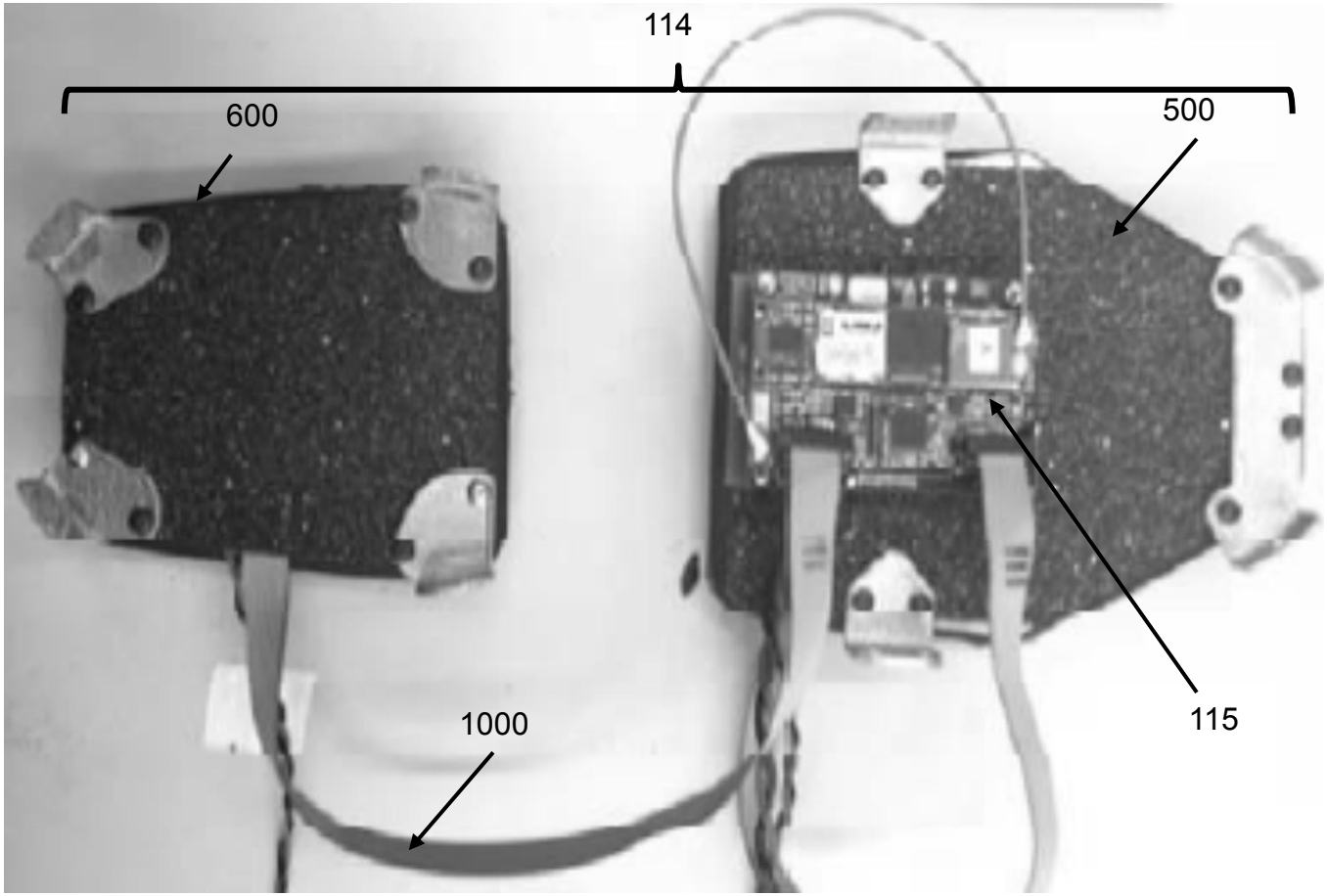

FIG. 10

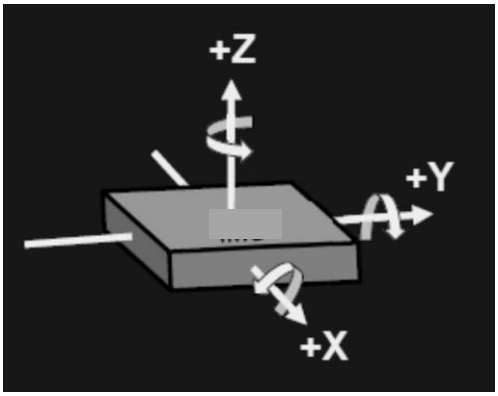

FIG. 11

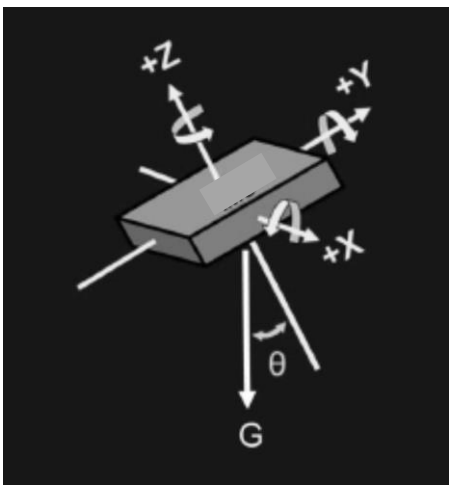

FIG. 12

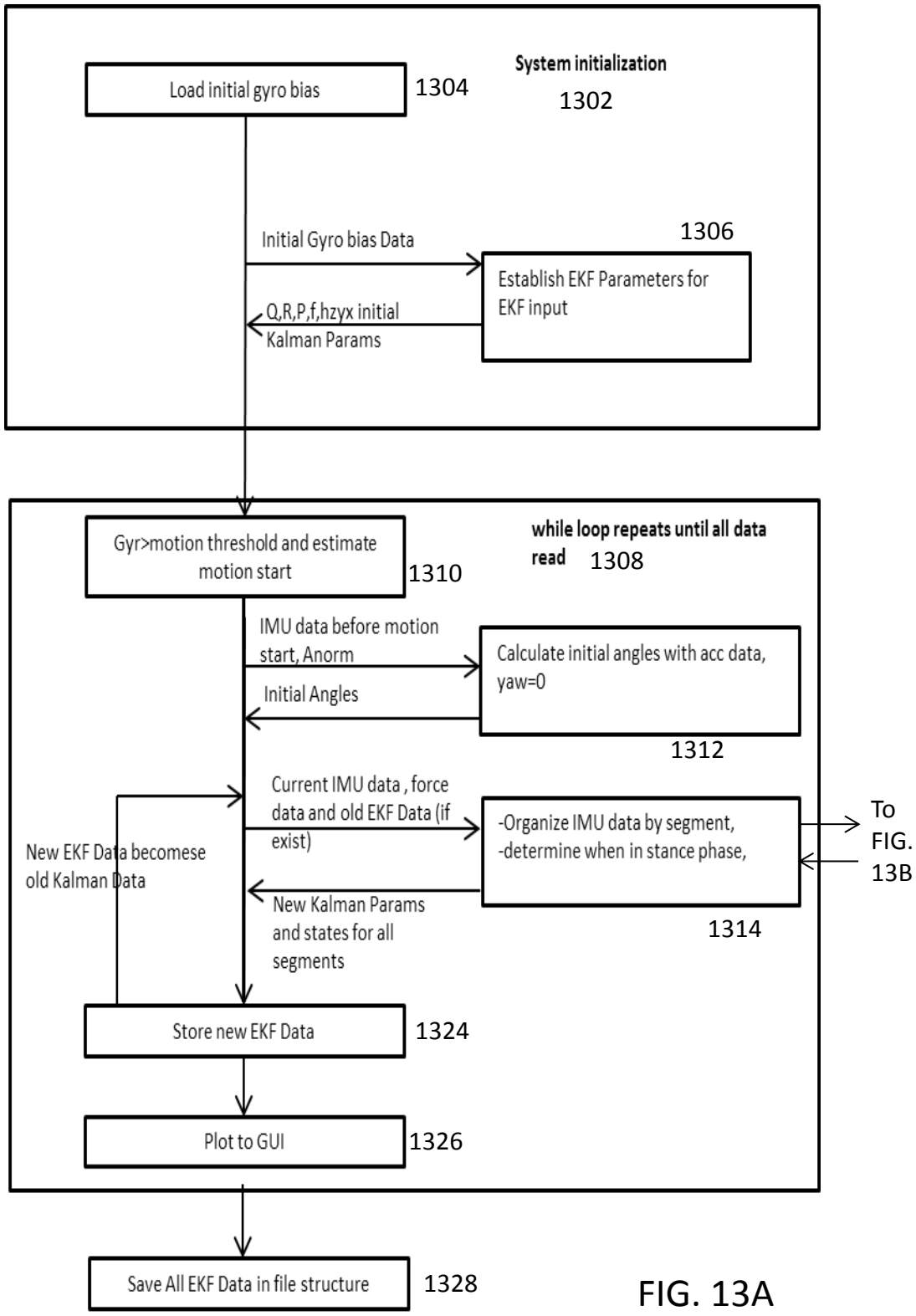
System initialization
1302
Load initial gyro bias
1304
Initial Gyro bias Data
1306
Establish EKF Parameters for EKF input
Q,R,P,f,hzyx initial Kalman Params
while loop repeats until all data read
1308
Gyr>motion threshold and estimate motion start
1310
IMU data before motion start, Anorm
Calculate initial angles with acc data, yaw=0
Initial Angles
1312
Current IMU data , force data and old EKF Data (if exist)
-Organize IMU data by segment,
-determine when in stance phase,
To FIG. 13B
New EKF Data becomese old Kalman Data
New Kalman Params and states for all segments
1314
Store new EKF Data
1324
Plot to GUI
1326
Save All EKF Data in file structure
1328

FIG. 13A

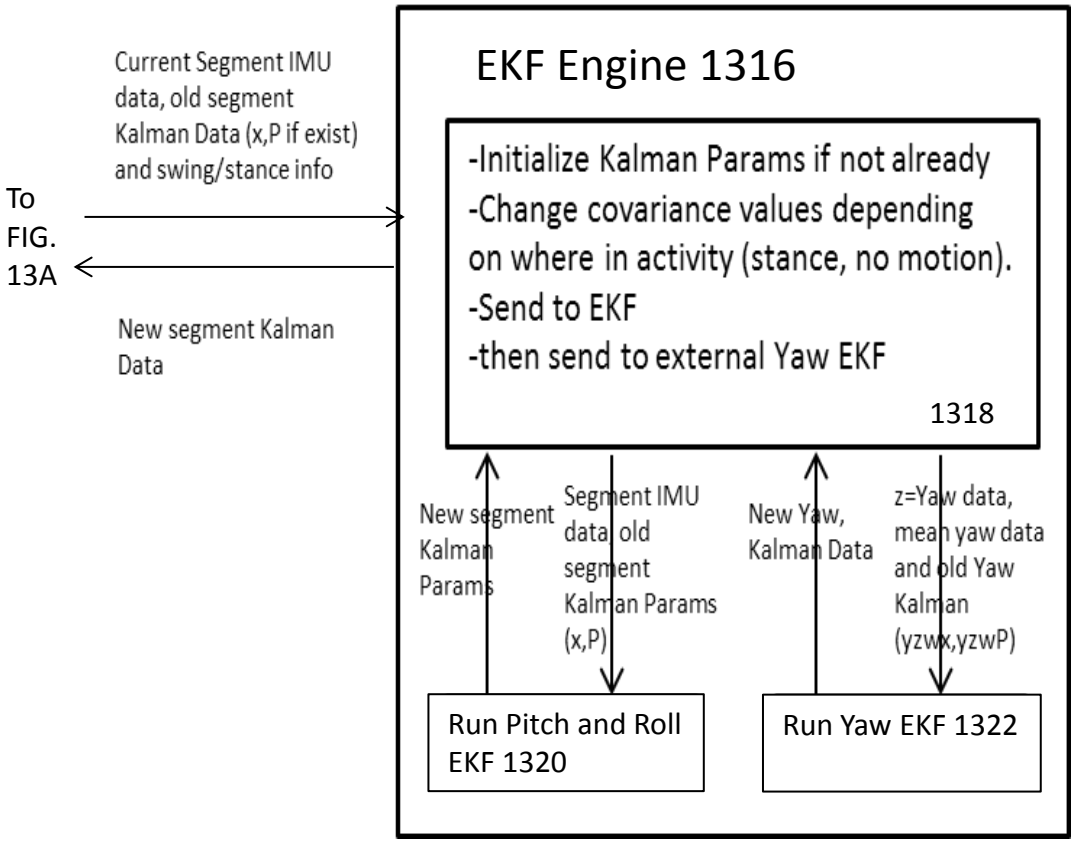
Current Segment IMU data, old segment Kalman Data (x,P if exist) and swing/stance info
To FIG. 13A
New segment Kalman Data
EKF Engine 1316
-Initialize Kalman Params if not already
-Change covariance values depending on where in activity (stance, no motion).
-Send to EKF
-then send to external Yaw EKF
1318
New segment Kalman Params
Segment IMU data, old segment Kalman Params (x,P)
New Yaw, Kalman Data
z=Yaw data, mean yaw data and old Yaw Kalman (yzwx,yzwP)
Run Pitch and Roll EKF 1320
Run Yaw EKF 1322

FIG. 13B

FIG. 14

1400

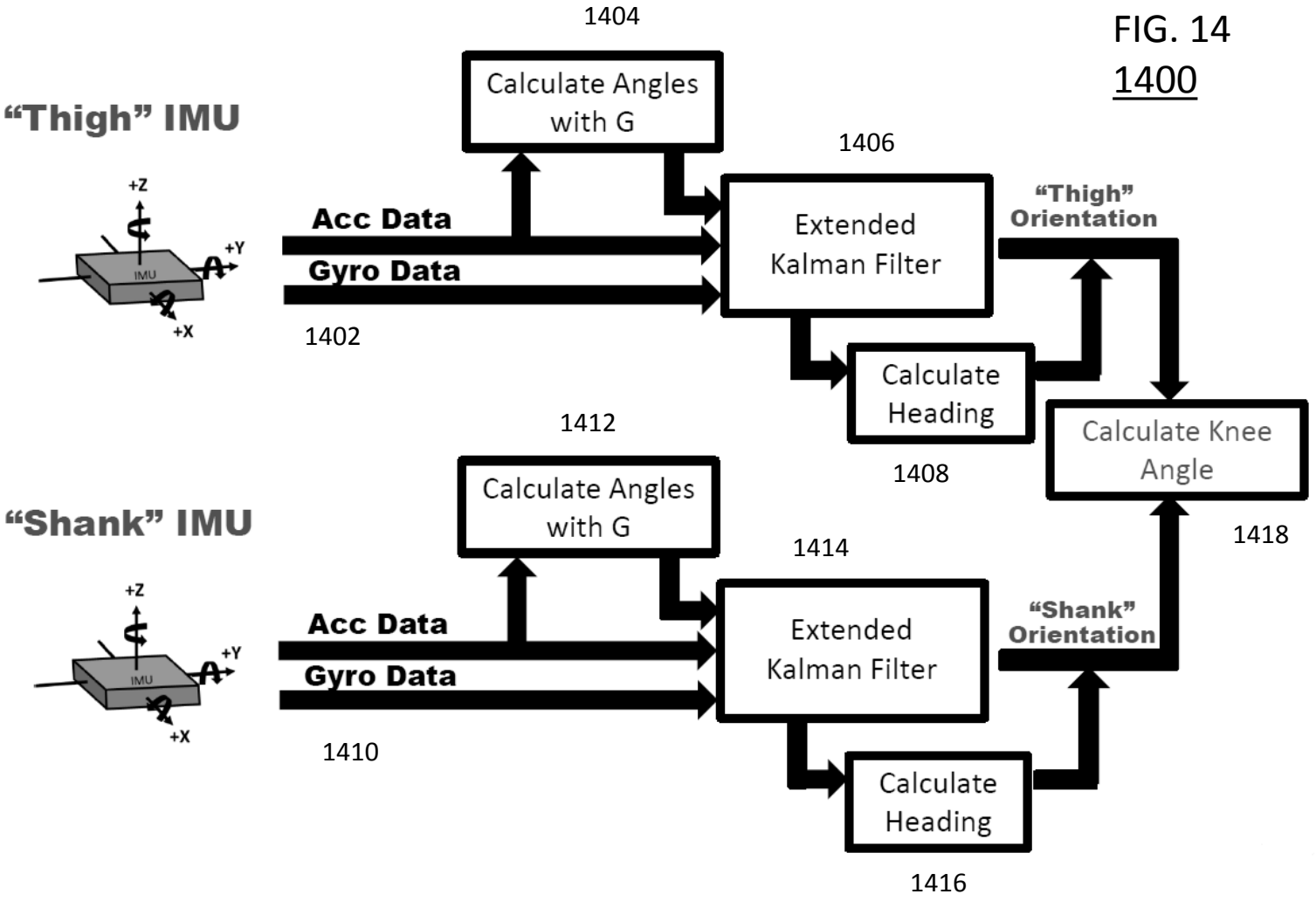
1404
Calculate Angles with G
"Thigh" IMU
+Z
+Y
+X
IMU
Acc Data
Gyro Data
1402
1406
Extended Kalman Filter
"Thigh" Orientation
Calculate Heading
1408
1412
Calculate Knee Angle
1418
"Shank" IMU
Calculate Angles with G
1414
Acc Data
Gyro Data
1410
Extended Kalman Filter
"Shank" Orientation
Calculate Heading
1416

FIG. 15

1500

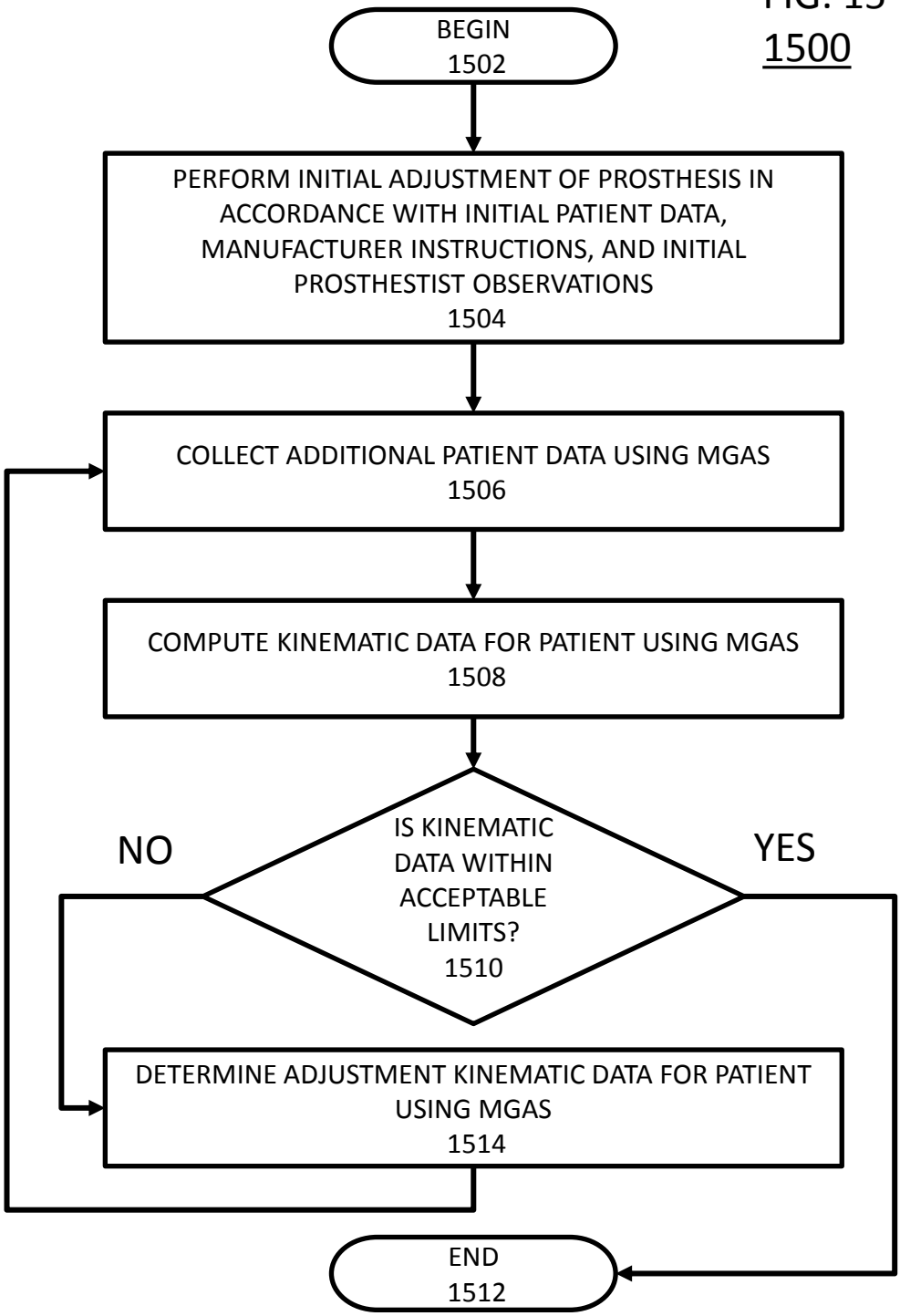
BEGIN
1502
PERFORM INITIAL ADJUSTMENT OF PROSTHESIS IN ACCORDANCE WITH INITIAL PATIENT DATA, MANUFACTURER INSTRUCTIONS, AND INITIAL PROSTHESTIST OBSERVATIONS
1504
COLLECT ADDITIONAL PATIENT DATA USING MGAS
1506
COMPUTE KINEMATIC DATA FOR PATIENT USING MGAS
1508
IS KINEMATIC DATA WITHIN ACCEPTABLE LIMITS?
1510
NO
YES
DETERMINE ADJUSTMENT KINEMATIC DATA FOR PATIENT USING MGAS
1514
END
1512

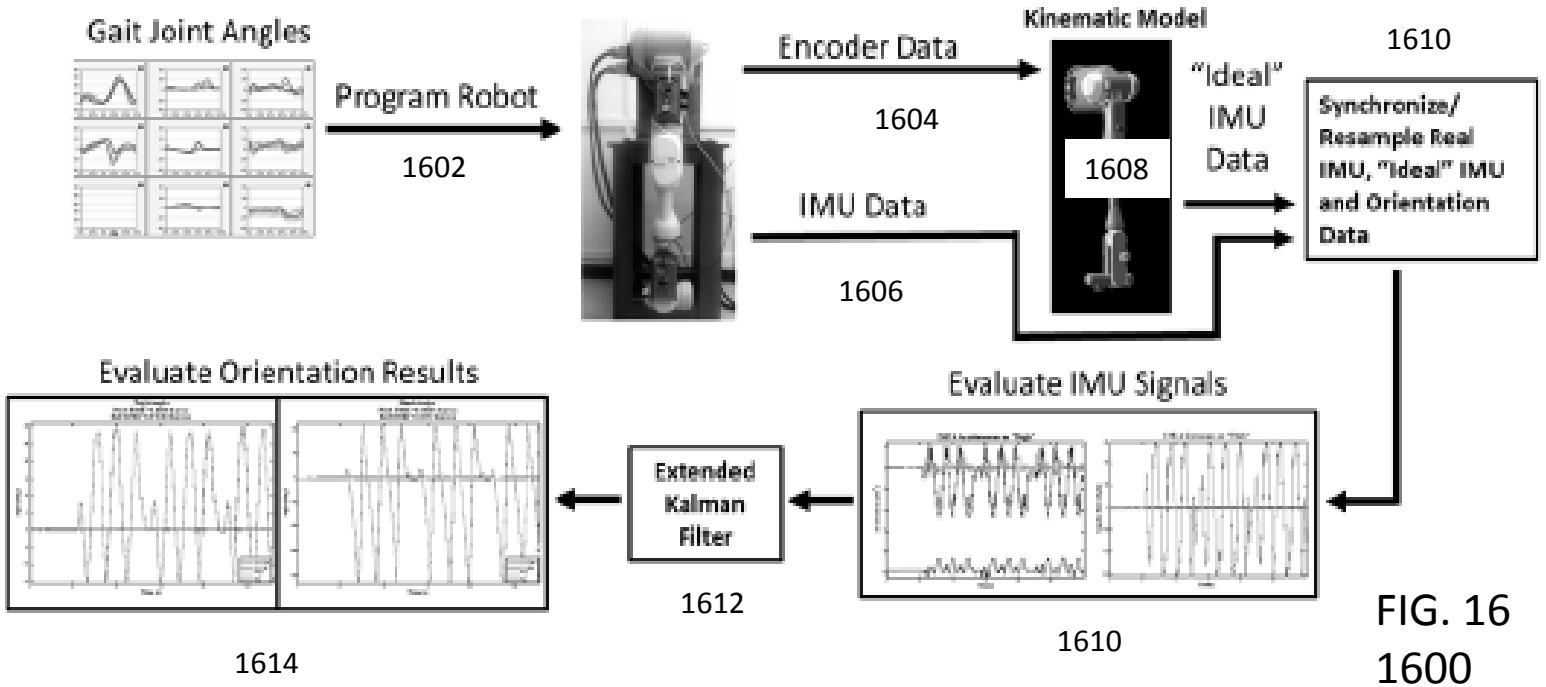
Gait Joint Angles
Program Robot
1602
Encoder Data
1604
IMU Data
1606
Kinematic Model
1608
"Ideal" IMU Data
1610
Synchronize/ Resample Real IMU, "Ideal" IMU and Orientation Data
Evaluate IMU Signals
1610
Extended Kalman Filter
1612
Evaluate Orientation Results
1614

FIG. 16
1600

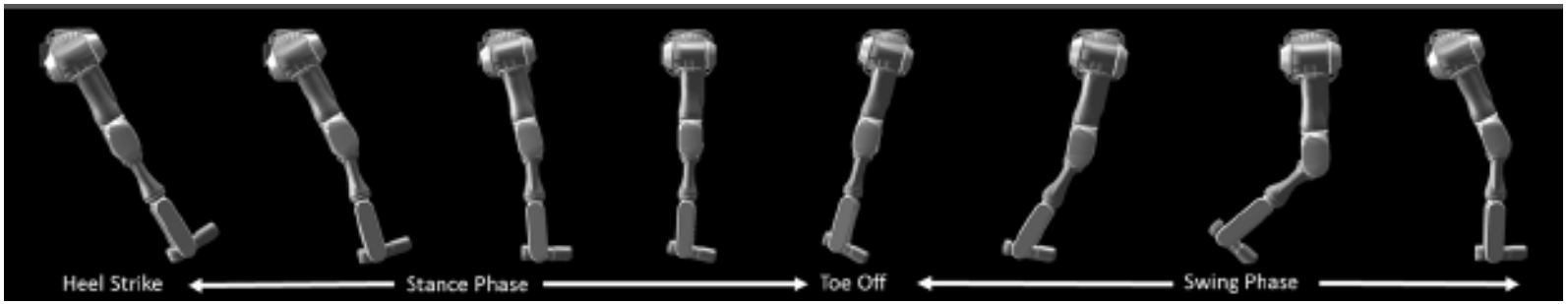

FIG. 17

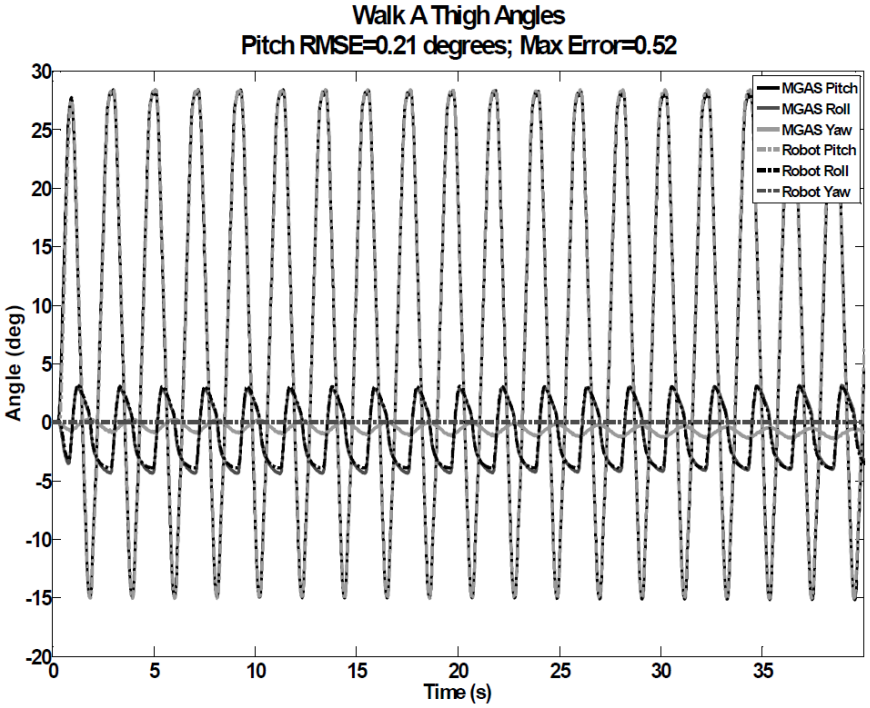
Walk A Thigh Angles
Pitch RMSE=0.21 degrees; Max Error=0.52
MGAS Pitch
MGAS Roll
MGAS Yaw
Robot Pitch
Robot Roll
Robot Yaw
Angle (deg)
Time (s)

FIG. 18

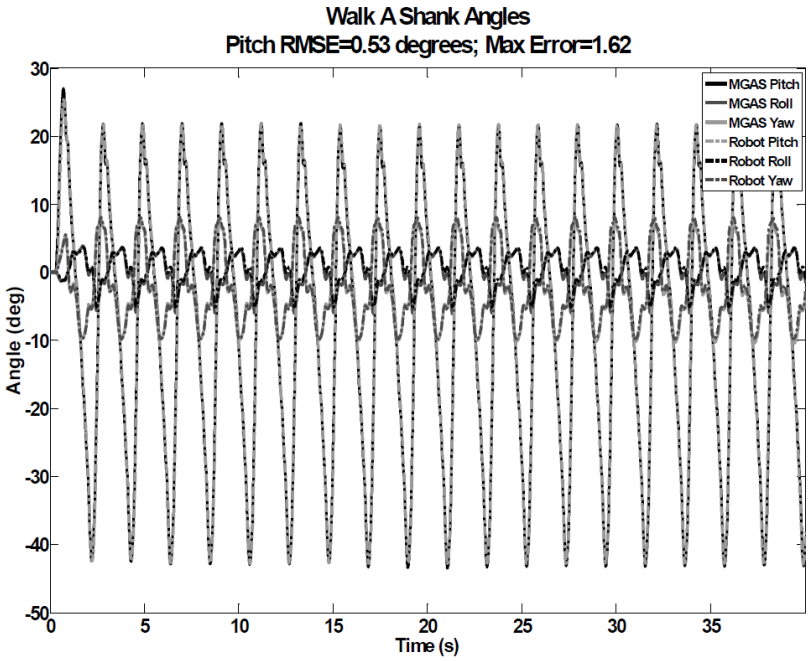
Walk A Shank Angles
Pitch RMSE=0.53 degrees; Max Error=1.62
MGAS Pitch
MGAS Roll
MGAS Yaw
Robot Pitch
Robot Roll
Robot Yaw
Angle (deg)
Time (s)

FIG. 19

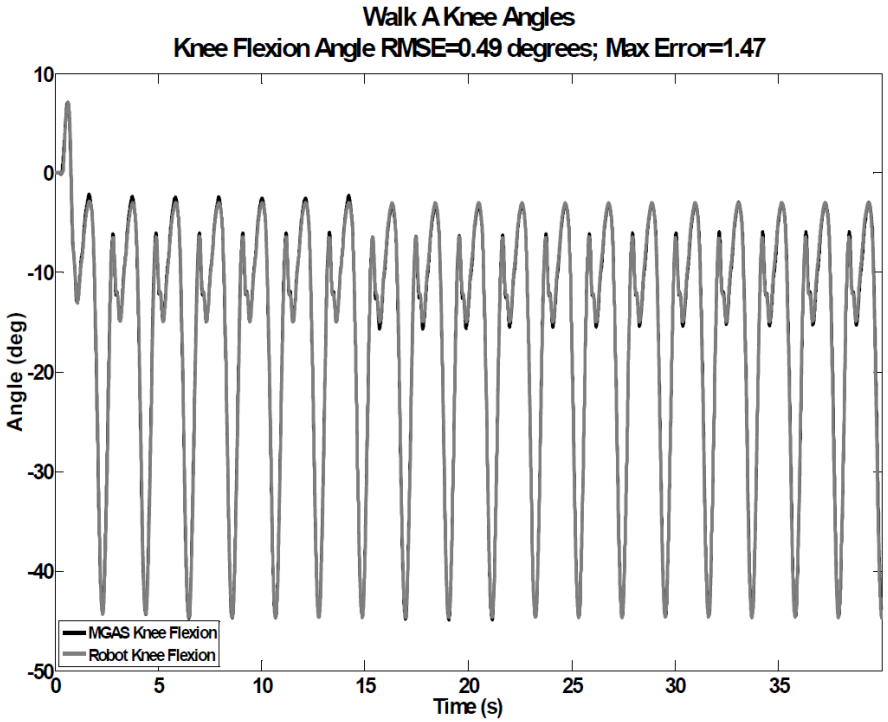
Walk A Knee Angles
Knee Flexion Angle RMSE=0.49 degrees; Max Error=1.47
Angle (deg)
Time (s)
MGAS Knee Flexion
Robot Knee Flexion

FIG. 20

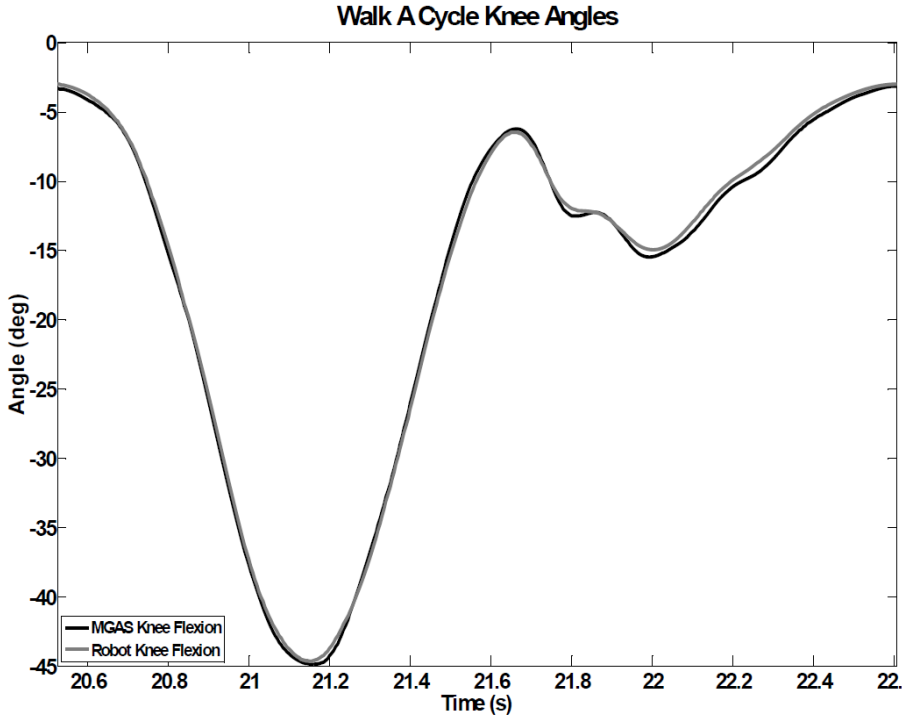
Walk A Cycle Knee Angles
Angle (deg)
Time (s)
MGAS Knee Flexion
Robot Knee Flexion

FIG. 21

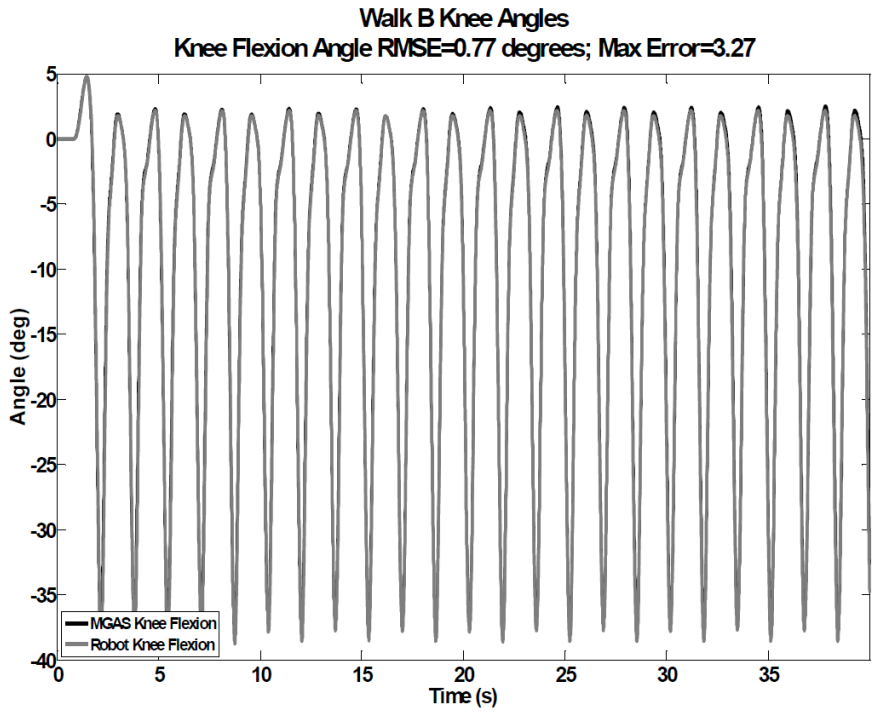
Walk B Knee Angles
Knee Flexion Angle RMSE=0.77 degrees; Max Error=3.27
Angle (deg)
Time (s)
MGAS Knee Flexion
Robot Knee Flexion

FIG. 22

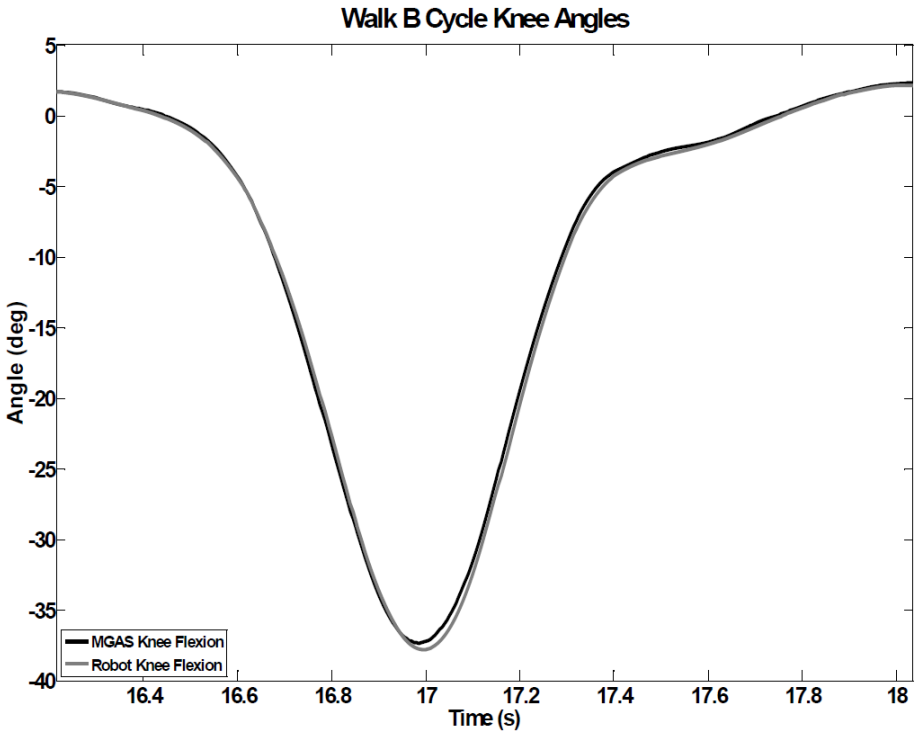
Walk B Cycle Knee Angles
Angle (deg)
Time (s)
MGAS Knee Flexion
Robot Knee Flexion

FIG. 23

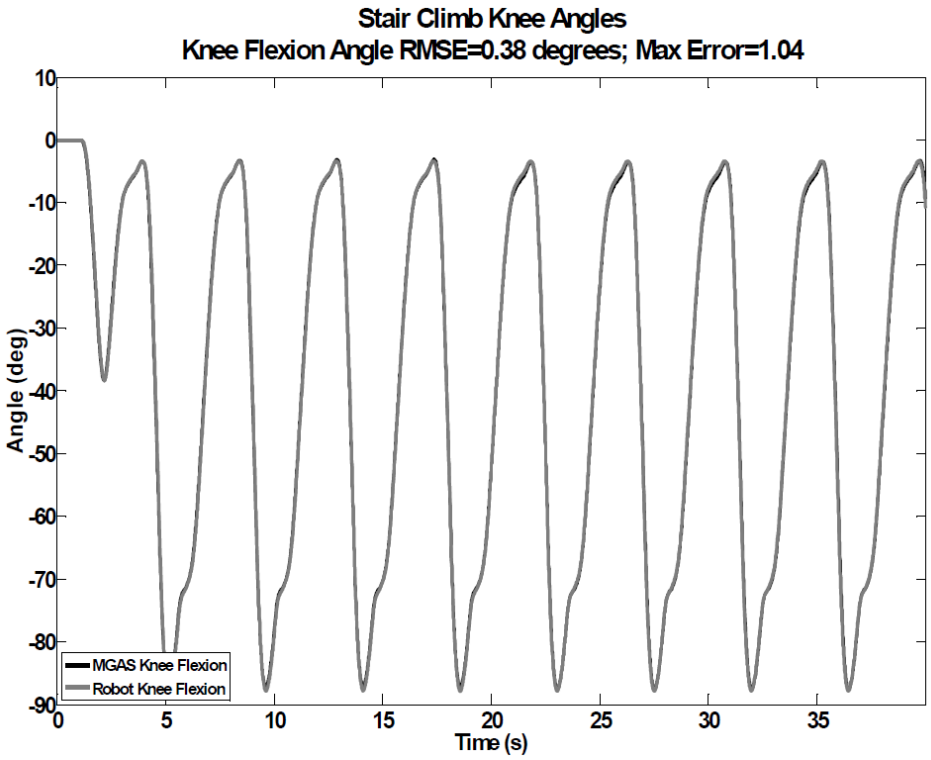
Stair Climb Knee Angles
Knee Flexion Angle RMSE=0.38 degrees; Max Error=1.04
Angle (deg)
Time (s)
MGAS Knee Flexion
Robot Knee Flexion

FIG. 24

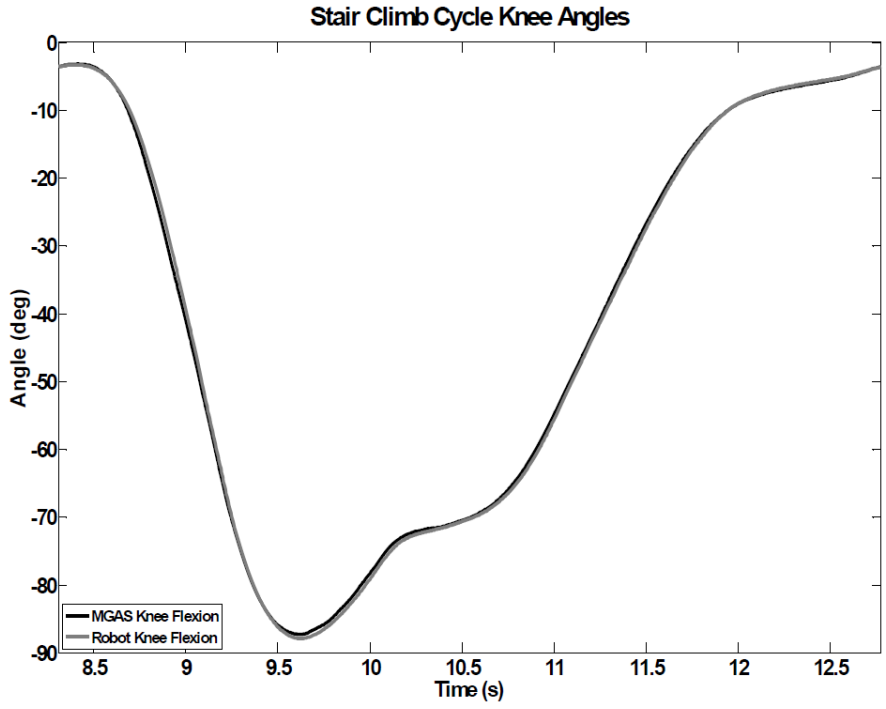
Stair Climb Cycle Knee Angles
Angle (deg)
Time (s)
MGAS Knee Flexion
Robot Knee Flexion

FIG. 25

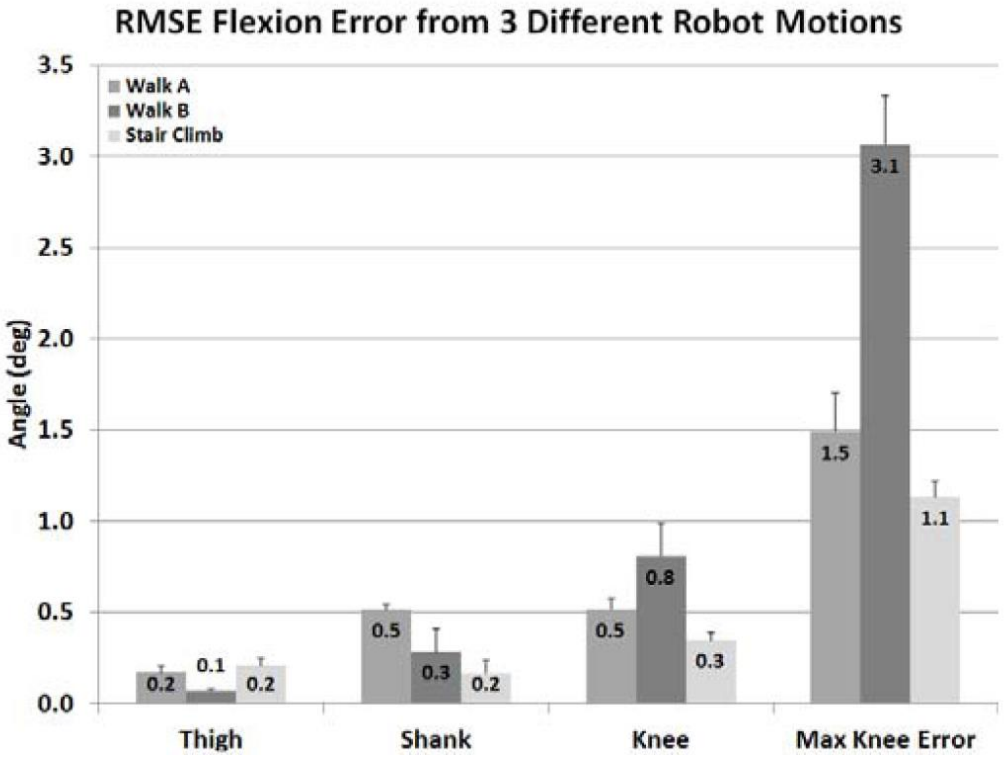
RMSE Flexion Error from 3 Different Robot Motions
Walk A
Walk B
Stair Climb
Angle (deg)
3.5
3.0
2.5
2.0
1.5
1.0
0.5
0.0
0.2
0.1
0.2
0.5
0.3
0.2
0.5
0.8
0.3
1.5
3.1
1.1
Thigh
Shank
Knee
Max Knee Error

FIG. 26

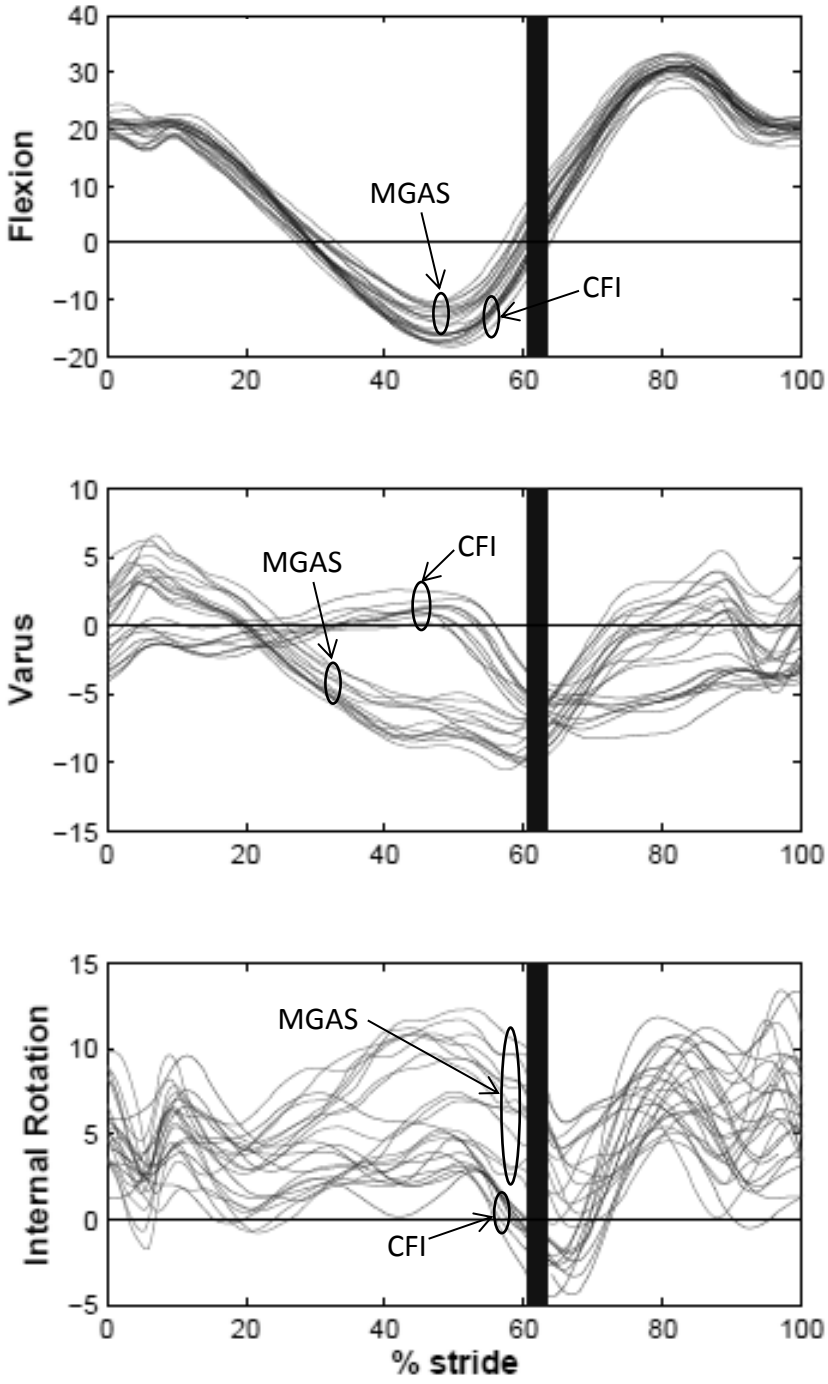
Flexion
MGAS
CFI
Varus
MGAS
CFI
Internal Rotation
MGAS
CFI
% stride

FIG. 27

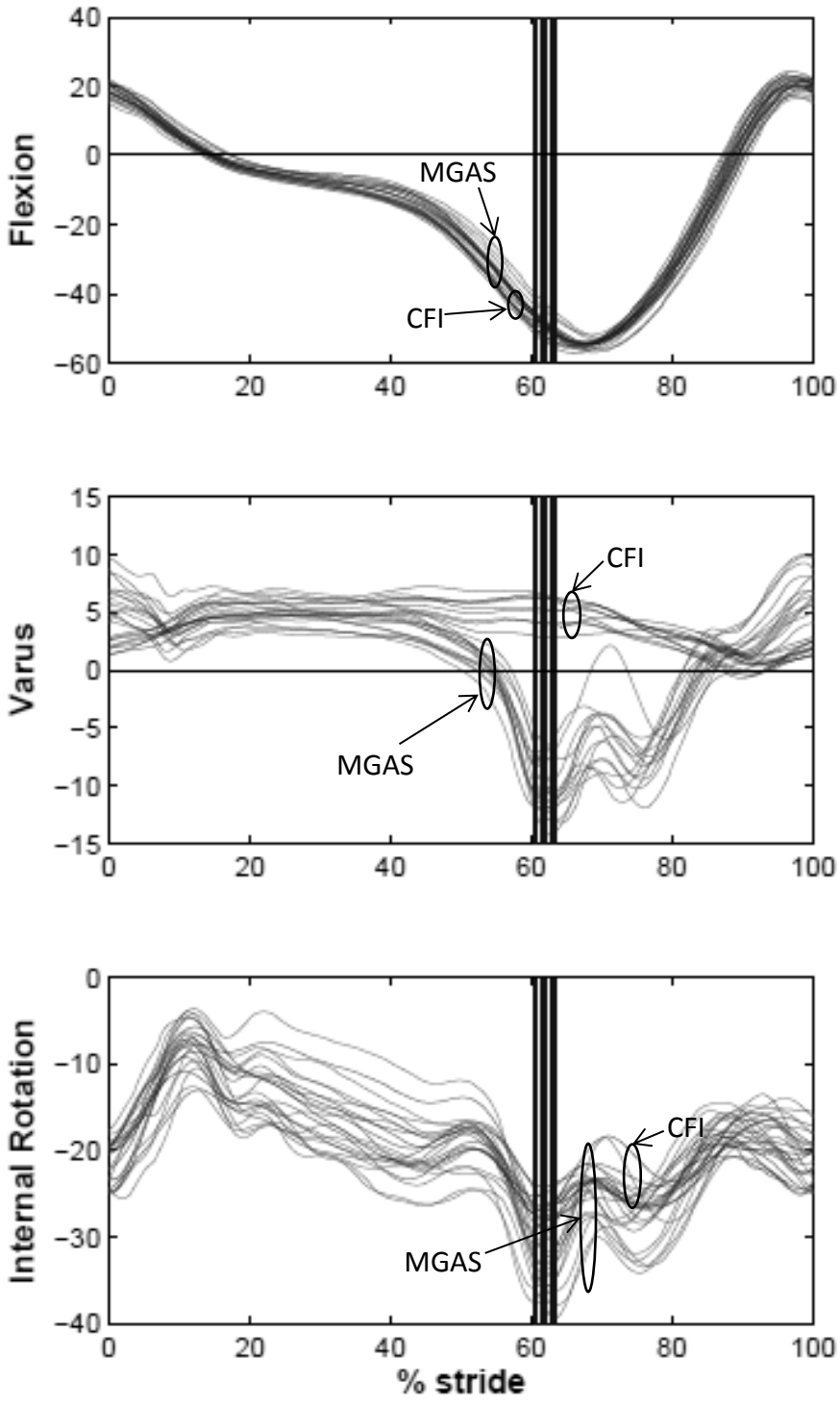
Flexion
40
20
0
−20
−40
−60
MGAS
CFI
0
20
40
60
80
100
Varus
15
10
5
0
−5
−10
−15
CFI
MGAS
Internal Rotation
0
−10
−20
−30
−40
CFI
MGAS
% stride

FIG. 28

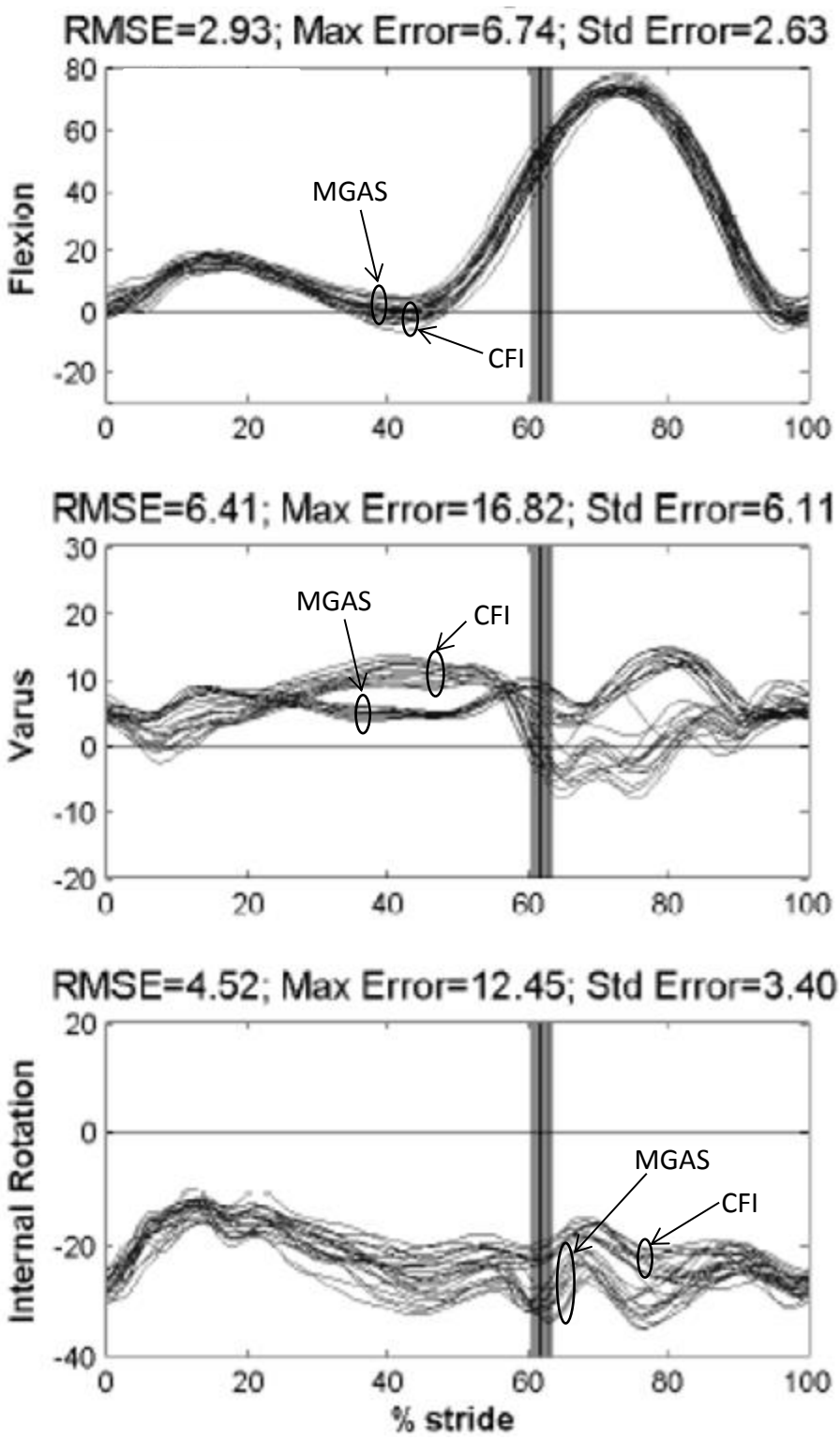
RMSE=2.93; Max Error=6.74; Std Error=2.63
Flexion
MGAS
CFI
RMSE=6.41; Max Error=16.82; Std Error=6.11
Varus
MGAS
CFI
RMSE=4.52; Max Error=12.45; Std Error=3.40
Internal Rotation
MGAS
CFI
% stride

FIG. 29

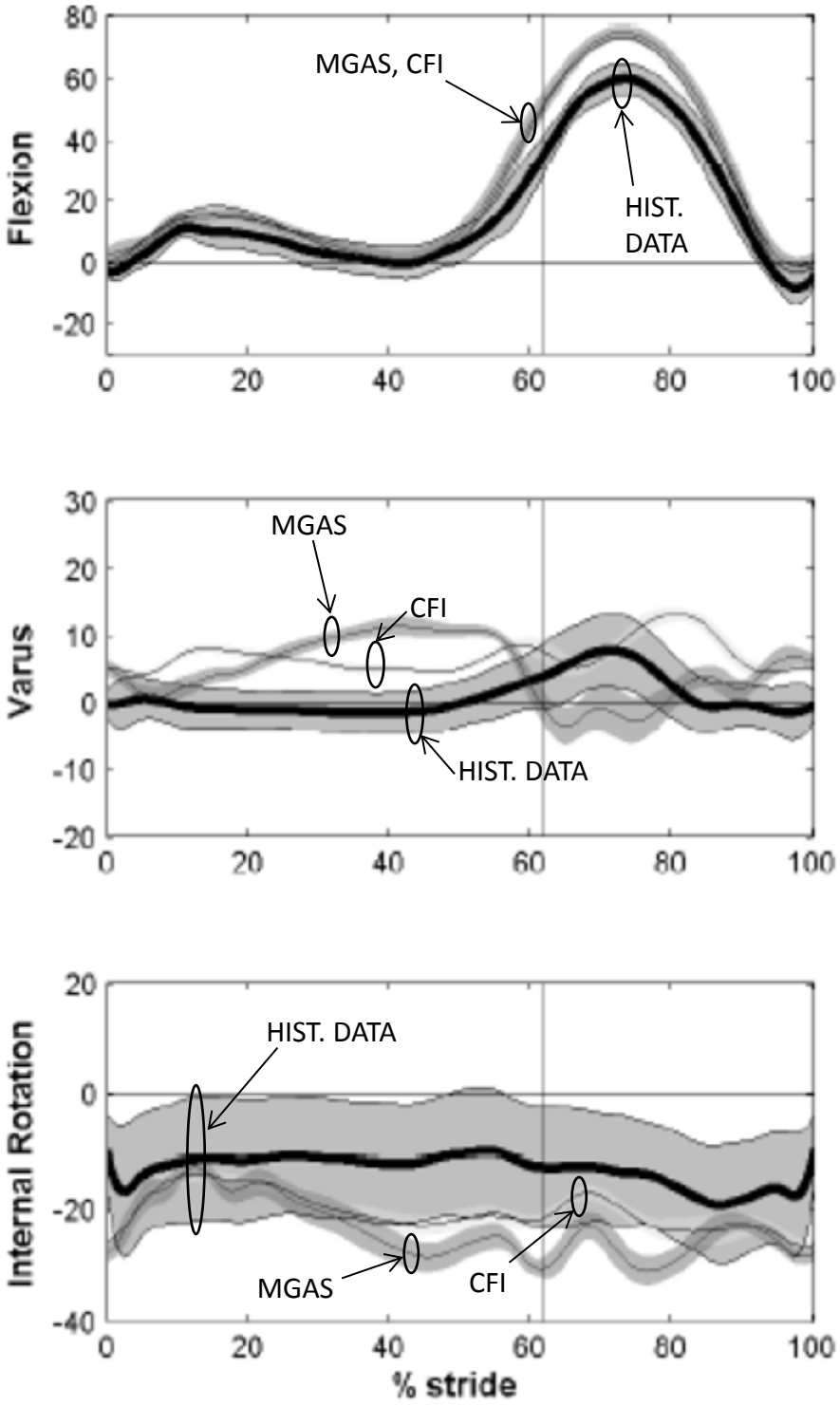
Flexion
80
60
40
20
0
-20
0
20
40
60
80
100
MGAS, CFI
HIST.
DATA
Varus
30
20
10
0
-10
-20
MGAS
CFI
HIST. DATA
Internal Rotation
20
0
-20
-40
HIST. DATA
MGAS
CFI
% stride

FIG. 30

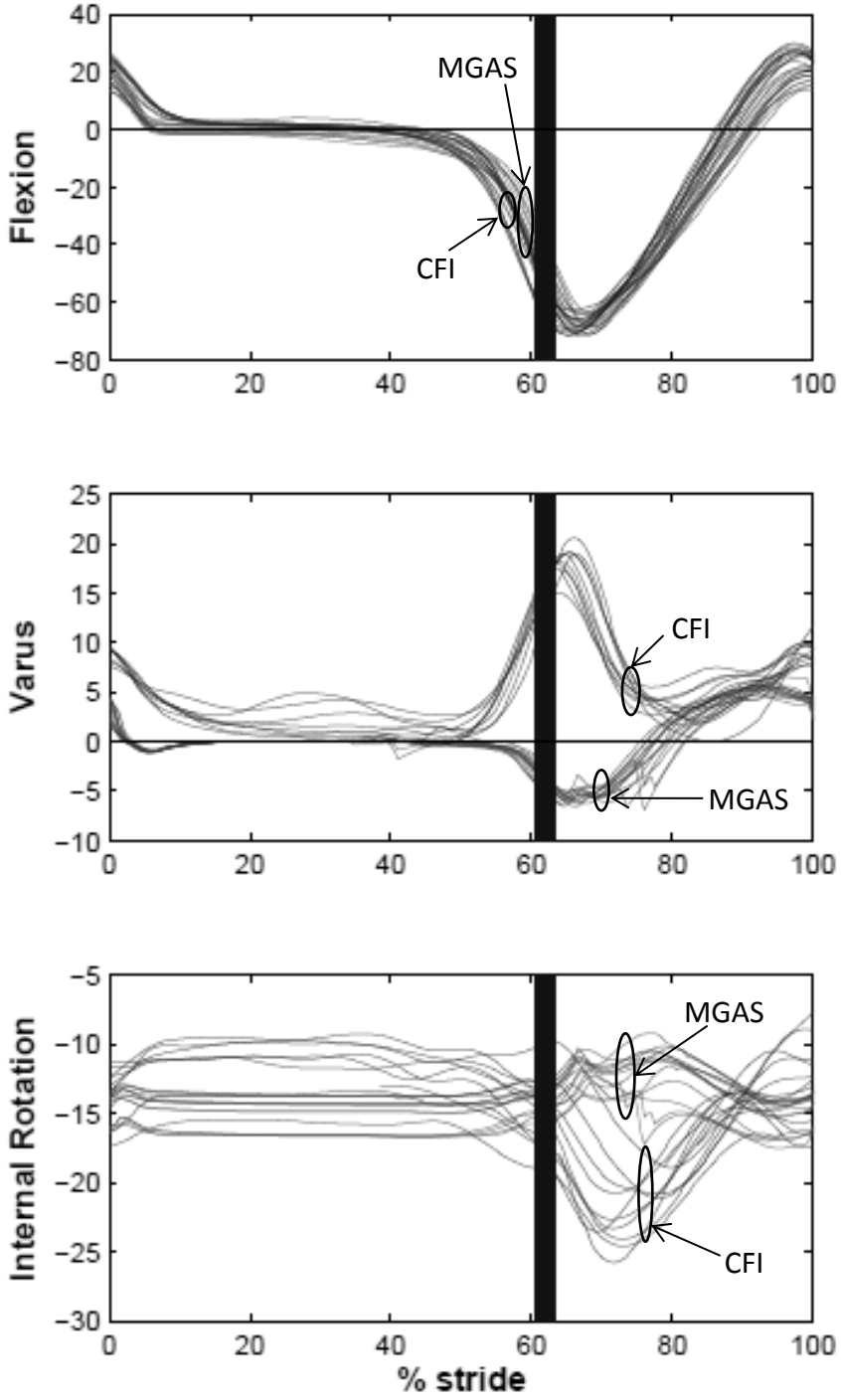
Flexion
MGAS
CFI
Varus
CFI
MGAS
Internal Rotation
MGAS
CFI
% stride

FIG. 31

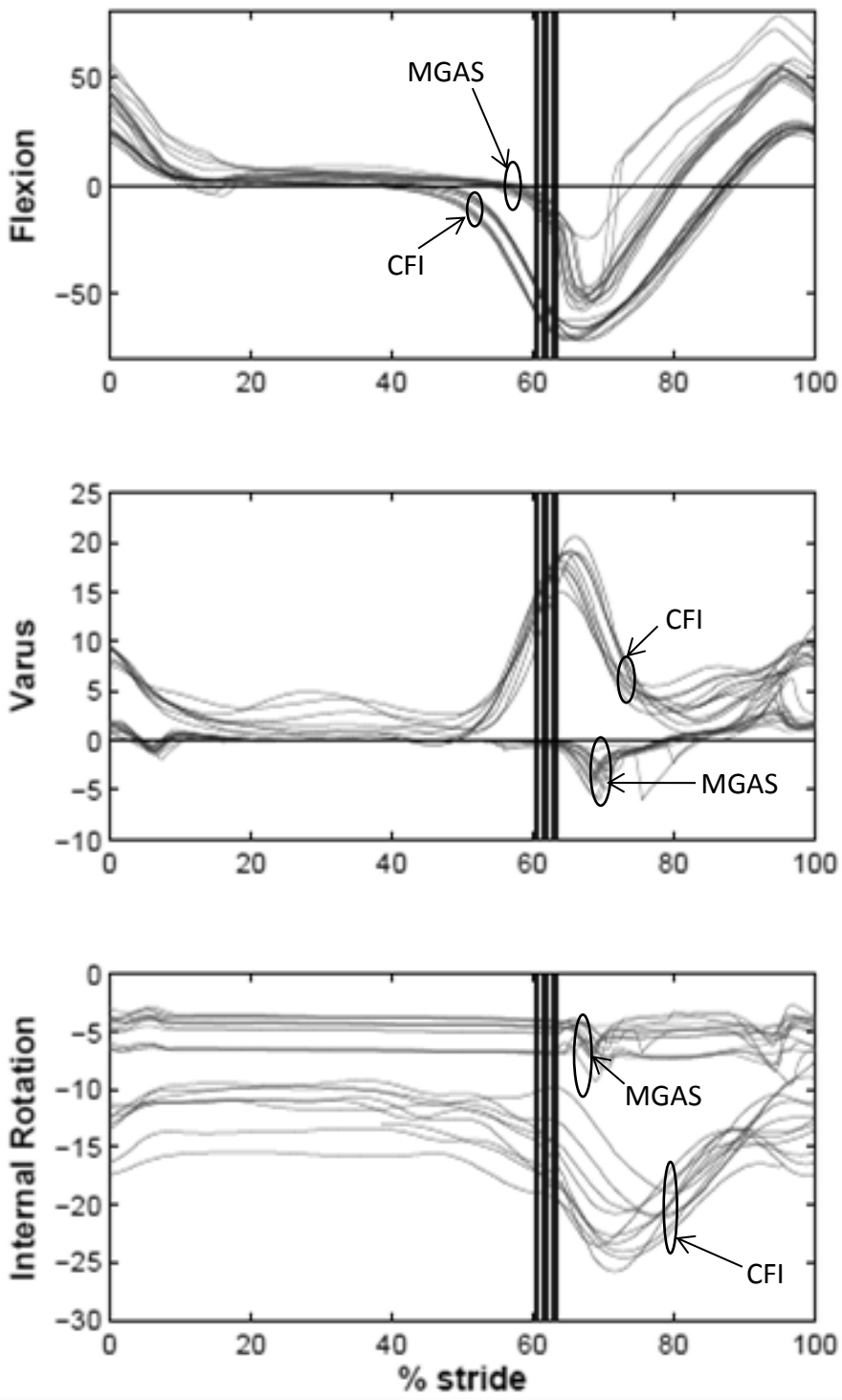
Flexion
50
0
−50
MGAS
CFI
0
20
40
60
80
100
Varus
25
20
15
10
5
0
−5
−10
CFI
MGAS
Internal Rotation
0
−5
−10
−15
−20
−25
−30
MGAS
CFI
% stride

FIG. 32

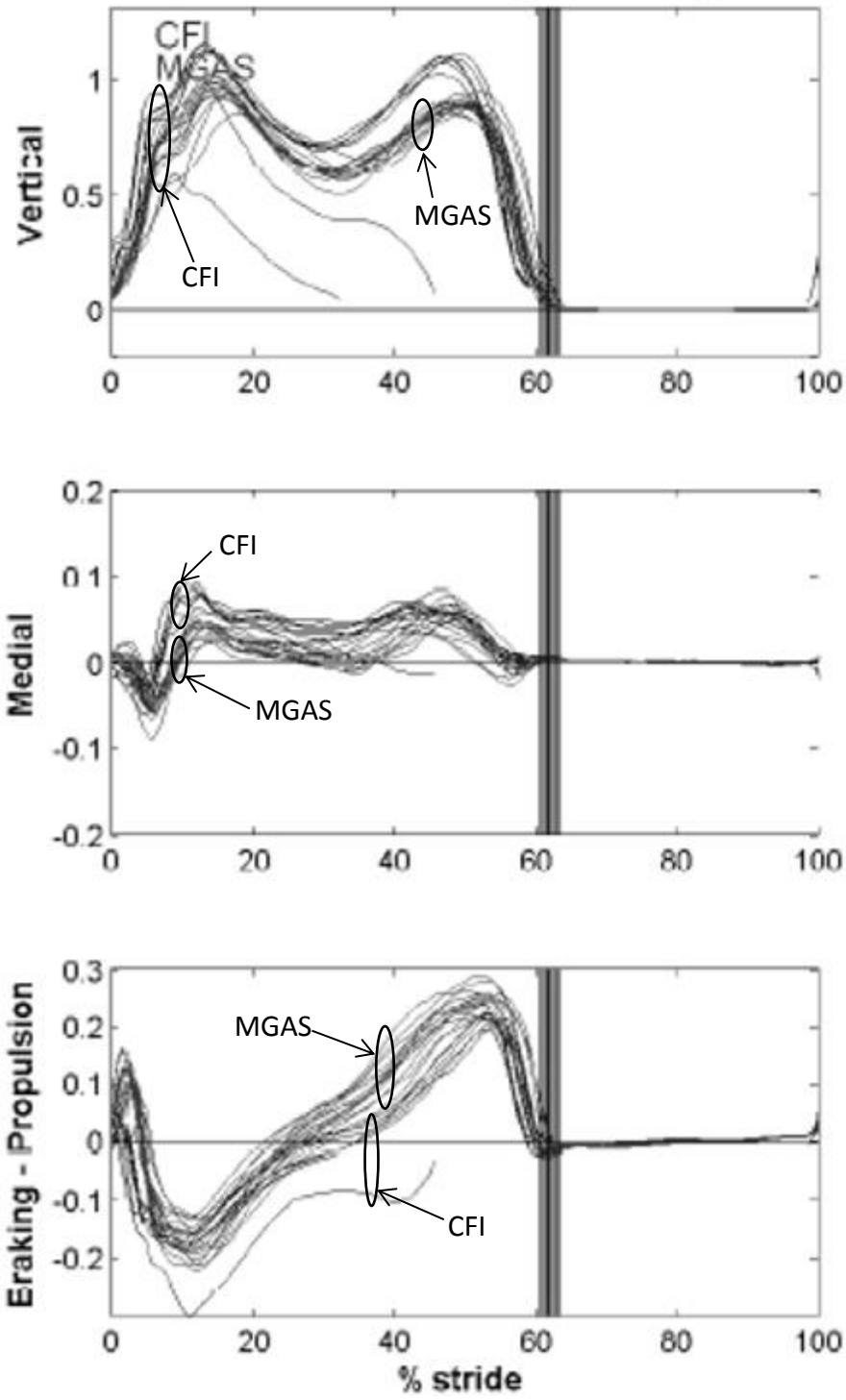
CFI
MGAS
Vertical
1
0.5
0
MGAS
CFI
0
20
40
60
80
100
0.2
0.1
0
-0.1
-0.2
Medial
CFI
MGAS
0.3
0.2
0.1
0
-0.1
-0.2
Eraking - Propulsion
MGAS
CFI
% stride

FIG. 33

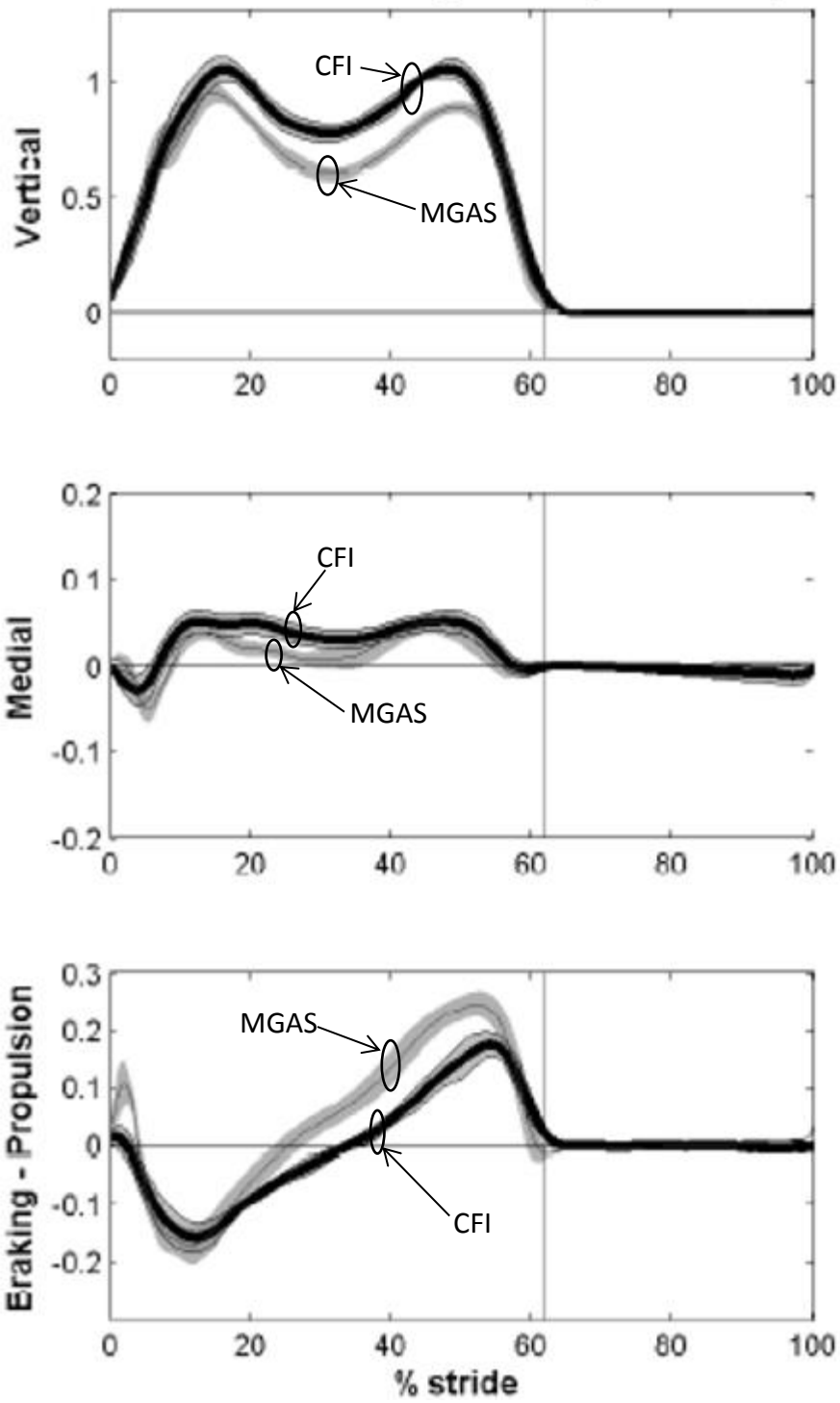
Vertical
1
0.5
0
CFI
MGAS
0
20
40
60
80
100
Medial
0.2
0.1
0
-0.1
-0.2
CFI
MGAS
Eraking - Propulsion
0.3
0.2
0.1
0
-0.1
-0.2
MGAS
CFI
% stride

FIG. 34

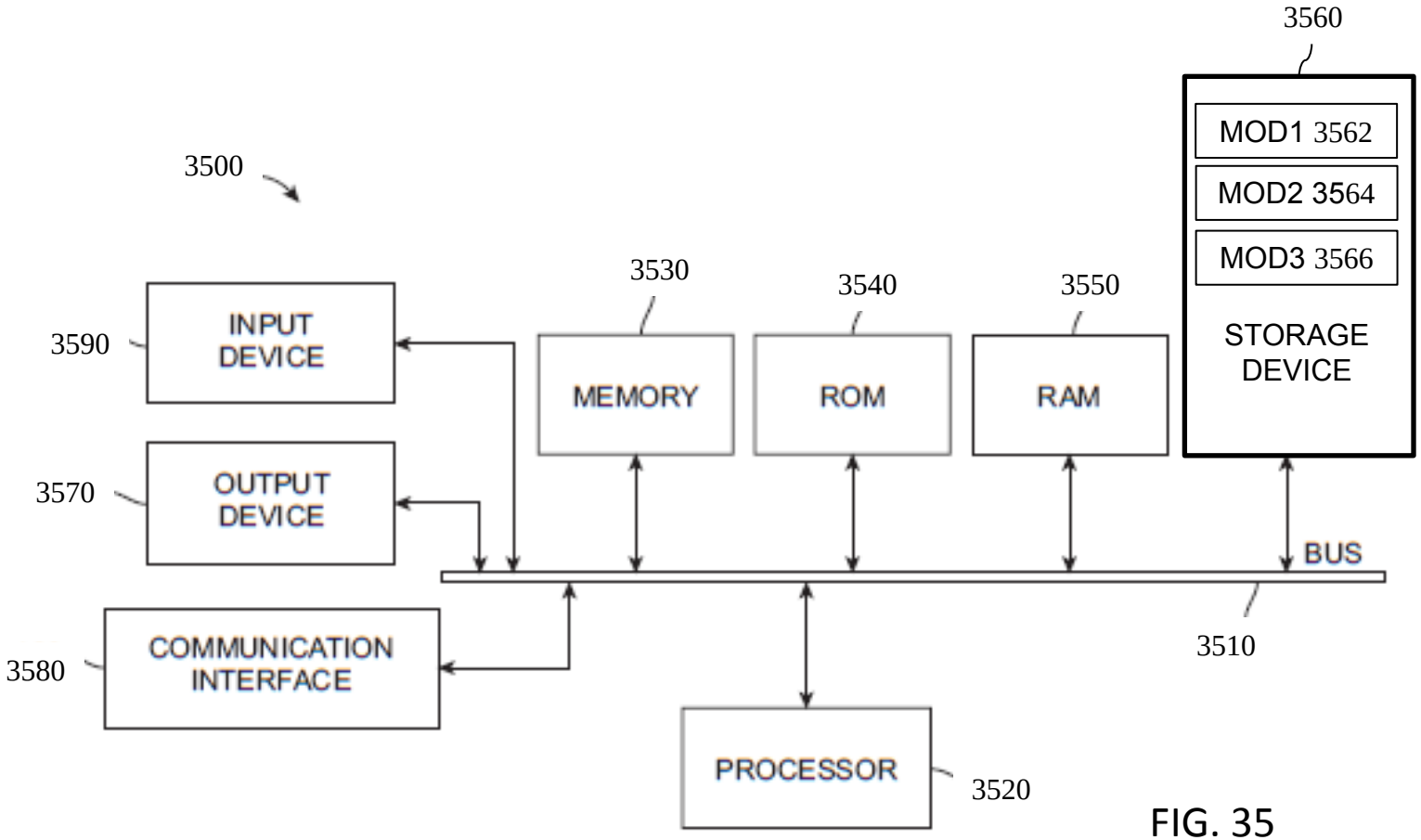
3500
3560
MOD1 3562
MOD2 3564
MOD3 3566
STORAGE DEVICE
3530
3540
3550
3590
INPUT DEVICE
MEMORY
ROM
RAM
3570
OUTPUT DEVICE
BUS
3510
3580
COMMUNICATION INTERFACE
PROCESSOR
3520

FIG. 35

MOBILE GAIT FORCE AND MOTION ANALYSIS SYSTEM

GOVERNMENT LICENSE RIGHTS

This invention was made with government support under contract No. 2095-V215-10 awarded by the U.S. Army Medical Material Command. The government has certain rights in the invention.

FIELD OF THE INVENTION

The various embodiments relate to methods for quantifying biomechanical data, and more specifically to biomechanical data related to a mobile gait force associated with a lower limb prosthesis.

BACKGROUND

American military healthcare system has improved treatment of combat casualties- increase from 76% to 87% survival since Vietnam. As a result of these improvements in survivability, there has been an influx of soldiers dealing with lifelong major injuries attributed to roadside bombs and Improvised Explosive Devises (IEDs). For example, such injuries result in the amputation (transtibial or transfemoral) of a lower limb for a large number of soldiers. In addition to such military amputees, there are also about 100,000 lower limb amputations occurring per year in the general population. As a result, many of these patients are typically fitted with lower limb prostheses. In the case of military personnel, these individuals are typically otherwise healthy and the lower limb prosthesis allows them to engage in an active lifestyle.

However, lower limb prosthetic patients are generally at risk for injury and chronic disease in their unaffected leg, including their healthy joints. A culprit for this increased for injury and chronic disease in unaffected legs and healthy joints is the asymmetric gait generally resulting from the use of some prosthetic lower limb devices. An asymmetric gait can cause increased joint loading and higher energy consumption. Such increased energy consumption can limit the amputee's participation in various activities and work functions. More importantly, if injuries and chronic diseases develop in the unaffected leg or healthy joints, this may permanently limit the amputee's ability to function. Table 1 summarizes peak ground reaction force between intact and prosthetic legs in transtibial amputees at various speeds:

Table 1			
Speed (m/s)	Prosthetic legs Fz (BW)	Intact legs Fz (BW)	ASI (%)
0.5	1.16 (0.07)	1.40 (0.23)	17.54 (19.40)
0.9	1.17 (0.05)	1.40 (0.23)	16.96 (18.49)
1.2	1.18 (0.08)	1.47 (0.20)	22.59 (18.44)
Max	1.23 (0.08)	1.68 (0.32)	29.34 (19.70)

(From L. Nolan et al., "Adjustments in gait symmetry with walking speed in trans-femoral and trans-tibial amputees." Gait and Posture 17 (2003) 142-151.) For at least these reasons, a need exists to limit asymmetric gait by better fitting of prosthetic devices.

Typically, fitting is performed by a trained prosthetist or physical therapist during one or more office visits. Prosthetists have training and experience that allows them to adjust the prosthetic based on feedback from the patient and their observation of the patient's gait. This type of traditional fitting is typically an iterative process requiring multiple sessions. During a session, the prosthetist makes observations to determine the required adjustments. First, the patient walks for an interval of time while the prosthetist

observes. The prosthetist then makes an adjustment, and the process is repeated until the prosthetist and the patient are satisfied with the operation of the prosthesis. In most prosthetic devices, the adjustments can be made to a stump/device interface, any 6-degrees of freedom (DOF) joints, a prosthetic foot, or any combination thereof.

In general, the data collected is typically limited to the prosthetist's observations, which are, of course subjective and variable from one prosthetist to another. This subjectivity can lead to inconsistent results across the plurality of patients and also to counterproductive results if one patient visits a plurality of prosthetists.

In some cases, it is possible to obtain quantifiable biomechanical data for a patient's gait in a so-called "gait laboratory." Unfortunately, the process of obtaining biomechanical data in a gait laboratory is expensive and time-consuming. Accordingly, such methods are not generally available to most prosthetists and therapists. Additionally, a problem exists in translating any quantifiable biomechanical data collected in a gait laboratory into clinically meaningful data which can be used by a prosthetist or a therapist to make actual adjustments to prostheses.

Therefore, a need exists for a mobile gait analysis system which can accurately determine biomechanical data, including joint angles and ground reaction forces, in the lower limb amputee patient and also return clinically meaningful results to a prosthetist. Satisfying this need, would allow for better fitting prosthetic devices, which would in turn limit problems associated with and caused by an asymmetric gait.

SUMMARY

Various system embodiments measure the full lower limb kinetics and kinematics of subjects outside of a motion capture gait laboratory. The system can determine the torques and forces at any of the joints in the body or in any of the limb segments. The system can be used for rehabilitation of patients experiencing injury to the lower extremity or amputee subjects. The system can also be used in the analysis and improvement of amputee prosthetics or joint replacement components. This system can also be used for the optimization of biomechanics in an athletic environment. Various embodiments can be employed a variety of commercial applications, including but not limited to rehabilitation, prosthesis evaluation and design, athletic performance, video game development and/or control.

Various embodiments satisfy the aforementioned need for a mobile gait analysis system which can accurately determine biomechanical data, including joint angles and ground reaction forces, in the lower limb amputee patient and also return clinically meaningful results to a prosthetist. Various embodiments, therefore, allow for better fitting prosthetic devices, and limit problems associated with and caused by an asymmetric gait.

In one embodiment, a method of performing gait analysis of a subject is provided. The method includes obtaining a plurality of measurement sets for a subject, each of the plurality of measurement sets including inertial measurements obtained from a sensor device associated with a different one of a plurality of segments of the subject. The segments can include a trunk or torso of the subject as well as limb segments. The method also includes calculating a sensor orientation for the sensor device associated

with each of the plurality of segments based at least on a portion of a corresponding one the plurality of measurement sets and computing a segment orientation for each of the plurality of segments based on a data fusion process applied to each of the plurality of segments. The data fusion process includes combining at least a one of the plurality measurement sets and the corresponding sensor orientation to estimate the segment orientation. The method also includes determining joint angles based on the estimate of the segment orientation for each of the plurality of segments. Optionally, ground reaction forces can be obtained based force measurements.

In a second embodiment of the invention, there is provided a system for performing gait analysis. The system includes a processor and a communications interface configured for receiving a plurality of measurement sets, each of the plurality of measurement sets including inertial measurements obtained from a sensor device associated with different one of a plurality of segments of a subject. The system also includes a computer-readable medium having stored thereon a plurality of instructions for causing the processor to perform steps. The steps include calculating a sensor orientation for the sensor device associated with each of the plurality of segments based at least on a portion of a corresponding one the plurality of measurement sets and computing an estimate of a segment orientation for each of the plurality of segments based on a data fusion process applied to each of the plurality of segments, the data fusion process including combining at least a one of the plurality measurement sets and the corresponding sensor orientation to estimate the corresponding segment orientation. The steps also include determining joint angles based on the estimate of the segment

orientation for each of the plurality of segments. Optionally, the steps can include computing ground reaction forces can be obtained based force measurements.

In a third embodiment of the invention, there is provided a sensor for analyzing gait and ground reaction forces. The sensor includes a forefoot portion removably attachable to a sole of a subject's forefoot and including at least one force sensor. The sensor also includes a heel portion removably attachable to a sole of the subject's heel and including at least one force sensor. The sensor further includes a processing unit communicatively coupled to the forefoot portion and the heel portion and configured for transmitting sensor signals from the forefoot portion and the heel portion to a remote computing device. In the sensor, at least one of the forefoot portion, the heel portion, and the processing unit includes at least one inertial measurement sensor. The sensor can be utilized with the systems and methods described herein.

BRIEF DESCRIPTION OF THE DRAWINGS

These and other features, aspects, and advantages of the present invention will become better understood with reference to the following description and appended claims, and accompanying drawings where:

FIG. 1 shows a system in accordance with the various embodiments for improving gait in a lower limb amputee fitted with a lower limb prosthesis;

FIG. 2 shows a block diagram of a configuration for IMU 106 in accordance with an embodiment of the invention;

FIG. 3 shows an exemplary configuration for the internal circuitry of an IMU in accordance with an embodiment of the present invention;

FIG. 4 shows an exemplary configuration for an IMU including an enclosure can be provided to house the circuitry of IMU;

FIG. 5A shows a top isometric view of forefoot portion in accordance with an embodiment of the present invention;

FIG. 5B shows a side view of a forefoot portion in accordance with an embodiment of the present invention;

FIG. 5C shows a top, disassembled view of forefoot portion in accordance with an embodiment of the present invention;

FIGs. 6A, 6B, and 6C illustrate exemplary embodiments of a heel portion of a footpad in accordance with an embodiment of the present invention;

FIG. 7 shows a footpad in accordance with an embodiment of the present invention;

FIG. 8 illustrates the exemplary configuration for footpad 114 of FIG. 7, that includes a forefoot portion and a heel portion, strapped to an athletic shoe, via one or more straps;

FIG. 9 shows an FPU coupled to footpad for purposes of providing power and data signals in accordance with an embodiment of the present invention;

FIG. 10, there is shown an exemplary configuration of footpad, that includes a forefoot portion and heel portion 60 in accordance with an embodiment of the present invention;

FIGs. 11 and 12 show operation of IMUs in accordance with an embodiment of the present invention;

FIGs. 13A and 13B schematically illustrate the operation of an algorithm in accordance with an embodiment of the invention.

FIG. 14 shows a schematic illustration of a method for utilizing sensor information for IMUs 106 to calculate knee angle in accordance with the various embodiments of the present invention;

FIG. 15 is a flowchart of steps in an exemplary method for adjusting a prosthesis in accordance with an embodiment of the invention;

FIG. 16 is a flow chart of steps in a method for evaluation of the sensors and the algorithms of the various embodiments of the present invention;

FIG. 17 illustrates an exemplary walking pattern evaluated using the sensors and the algorithms of the various embodiments of the present invention;

FIG. 18 shows the results of a sample trial of Walk A orientation angles from IMU data(MGAS values) and orientation angles calculated by the kinematic model (Robot values) for the “thigh” segment of the robot;

FIG. 19 shows the results of a sample trial of Walk A orientation angles from IMU data(MGAS values) and orientation angles calculated by the kinematic model (Robot values) for the “shank” segment of the robot;

FIG. 20 shows the results of a sample trial of Walk A calculated knee flexion angles (MGAS values) and knee flexion angles calculated by the kinematic model (Robot values);

FIG. 21 shows a sample trial of Walk A knee flexion angles from IMU data (MGAS values) and knee flexion angles from the kinematic model (Robot values) from one simulated gait cycle;

FIG. 22 shows a sample trial of Walk B calculated knee flexion angles (MGAS values) and knee flexion angles calculated by the kinematic model (Robot values);

FIG. 23 shows a sample trial of Walk B knee flexion angles from IMU data (MGAS values) and knee flexion angles from the kinematic model (Robot values);

FIG. 24 shows a sample trial of Stair Climb calculated knee flexion angles (MGAS values) and knee flexion angles calculated by the kinematic model (Robot values);

FIG. 25 shows a sample trial of Stair Climb knee flexion angles from IMU data (MGAS values) and knee flexion angles from the kinematic model (Robot values) from one simulated gait cycle;

FIG. 26 shows the flexion error from the different robot motions;

FIG. 27 shows plots of angle in three physiological planes for a thigh for conventional measurements and measurements in accordance with the various embodiments;

FIG. 28 shows plots of angle in three physiological planes for a shank for conventional measurements and measurements in accordance with the various embodiments;

FIG. 29 shows plots of angle in three physiological planes for a knee for conventional measurements and measurements in accordance with the various embodiments;

FIG. 30 shows plots of average angle in three physiological planes for a knee for conventional measurements and measurements in accordance with the various embodiments;

FIG. 31 shows plots of angle in three physiological planes for a heel for conventional measurements and measurements in accordance with the various embodiments;

FIG. 32 shows plots of angle in three physiological planes for a toe for conventional measurements and measurements in accordance with the various embodiments;

FIG. 33 shows plots of ground reaction forces for conventional measurements and measurements in accordance with the various embodiments;

FIG. 34 shows plots of average ground reaction forces for conventional measurements and measurements in accordance with the various embodiments; and

FIG. 35 shows an exemplary computing device for carrying out the various embodiments.

Some of the figures illustrate diagrams of the functional blocks of various embodiments. The functional blocks are not necessarily indicative of the division between hardware circuitry. Thus, for example, one or more of the functional blocks (e.g., processors or memories) may be implemented in a single piece of hardware (e.g., a general purpose signal processor or a block or random access memory, hard disk or the like). Similarly, the programs may be standalone programs, may be incorporated as subroutines in an operating system, may be functions in an installed imagining software package, and the like.

It should be understood that the various embodiments are not limited to the arrangements and instrumentality shown in the drawings.

DETAILED DESCRIPTION

The present invention may be understood more readily by reference to the following detailed description of preferred embodiments of the invention as well as to the examples included therein. All numeric values are herein assumed to be modified by the term "about," whether or not explicitly indicated. The term "about" generally refers to a range of numbers that one of skill in the art would consider equivalent to the recited value (i.e., having the same function or result). In many instances, the term "about" may include numbers that are rounded to the nearest significant figure.

As noted above, a need exists for a mobile gait analysis system which can accurately determine biomechanical data, including joint angles and ground reaction forces, in the lower limb amputee patient and also return clinically meaningful results to a prosthetist. In view of the limitations of conventional methods, a novel mobile gait analysis system (MGAS) is provided, which can accurately determine biomechanical data, including joint angles and ground reaction forces, in the lower limb amputee patient. Further, the new MGAS can be used to return clinically meaningful results to the prosthetist, who can then determine how to adjust or modify a prosthetic lower limb device.

In particular, the various embodiments are directed to systems and methods for mobile gait analysis, force balancing, and alignment system to determine limb segment positioning, forces, and moments. The systems and methods are not limited solely to analysis of an affected limb, but to analysis of the intact limb. In the various embodiments, in order to mathematically determine joint moments and forces for purposes of adjusting and fitting a prosthesis, knowledge of several kinematic

components is required. A first is knowledge of the ground reaction forces. The second is knowledge of limb orientation. Finally, knowledge of velocity and acceleration for the limb components, both linear and angular, is also required. The mobile gait analysis system of the various embodiments such data to be collected.

Although the various embodiments will be described with respect to human subjects with transtibial prostheses, this is solely for illustrative purposes. Rather, the systems and methods described herein can be utilized with either human or non-human subject having transfemoral or transtibial lower limb prostheses. Further, the systems and methods described herein are also not limited solely to use with prosthetic devices. Rather, the systems and methods described herein can also be used with orthotic or robotic devices and systems.

In the various embodiments, the mobile gait analysis system allows quality kinetic and kinematic data to be measured without the infrastructure investment of a camera-based motion capture gait analysis facility. Moreover, as a laboratory setting is not needed, the mobile gait analysis system allows measurement of biomechanics data in any environment. That is, it can be utilized in the actual locations and activities that any subject or clinician desires to record or analyze biomechanics data. This allows rehabilitation or examination of the actual activities of daily living (ADL) subjects expect to regularly encounter. Further, a software system can be provided to assist with data interpretation. This software system will help assess component fit and alignment as well as patient biomechanics. However, analyses can also be performed manually in the various embodiments.

Beyond the known alignment systems based on force plates, this system represents a new approach to prosthesis alignment, fitting, and patient rehabilitation and will allow subjects to experience more natural and efficient function from their prosthetic limbs and reduce secondary disabilities. This approach will enhance the maintenance and performance of long-term prosthesis and socket performance/fit by increasing the ease of measurement of prosthesis performance. Mobile gait analysis also represents an evidence-based approach to prosthesis fitting and will allow wider use of evidence-based rehabilitation techniques. More natural function will allow patients to return to a higher level of activity, and the reduction in secondary disabilities includes chronic lower back pain, hip and knee pain, as well as osteoarthritis of the knee(s), hips or lower back.

Turing first to FIG. 1, there is shown a system 100 in accordance with the various embodiments for improving gait in a lower limb amputee 102 fitted with a lower limb prosthesis 104. As shown in FIG. 1, an amputee 102 can be fitted with a plurality of inertial measurement units (IMUs) 106 on a torso segment (i.e., trunk segment) and various limb segments of the amputee 102. The IMUs 106 are configured to provide and communicate measurements of velocity (linear and/or angular), acceleration (linear and/or angular), orientation, gravitational forces, or any combinations thereof, at their respective locations using accelerometers, gyroscopes, magnetometers, geolocation devices (e.g., GPS), altimeters, or any combinations thereof. Thus, each IMU can consist of a single electronic component integrating features for conducting all necessary measurements in some embodiments. However, in other embodiments the IMU can be assembled from a collection of discrete devices. In some embodiments, the IMUs can be based on microelectromechanical system (MEMS) devices. However, the various

embodiments are not limited in this regard and the IMUs 101 can be configured to utilize any other type of devices or combination of devices to provide the necessary elements.

As noted above, the amputee 100 is fitted with a prosthesis 104. In the exemplary embodiment of FIG. 1, the prosthesis 104 includes a socket 108 for interfacing with the amputee 102, one or more adapters 110, one or more IMUs 106, and a prosthetic foot 112. The prosthetic foot 112 can be substantially resilient or flexible in the various embodiments.

In some embodiments, the foot 112 can be connected to the remainder of the prosthesis 104 via a passive or powered ankle joint. Further, although the various embodiments will be discussed primarily with respect to below-the-knee amputees, the various embodiments are not limited in this regard and are equally applicable to above-the-knee amputees. Thus, in some embodiments, a passive or powered knee joint can also be included between the socket 108 and the remainder of prosthesis 104. Thus, prosthesis 104 can include a knee joint, an ankle joint, or both, each of which can be powered or passive.

The system 100 can also include a footpad 114 that is secured to the amputee's 102 healthy limb. The footpad 114 can comprise a plurality of force/moment (F/M) sensors. That is, sensors that measure loads and torques in one or more axes. For example, the footpad 114 can have an F/M sensor on a forefoot portion and can have an F/M sensor on a heel portion thereof. The F/M sensors can measure ground reaction forces (GRS) for the healthy limb. The F/M sensors can also determine the orientation of the foot or other portions of the healthy limb. In some embodiments, the footpad can include components similar to IMUs 106 to communicate measurements. In other

embodiments, the footpad 114 can operate in conjunction with a foot processor unit 115, where the foot processor unit (FPU) 115 is configured to communicate with the footpad 114 and communicate measurements on behalf with footpad 114.

In some embodiments, the prosthetic foot 112 can be configured to operate in a manner substantially similar to footpad 114. Further, the IMU 106 in prosthetic leg 104 can also provide a FPU for the sensors in the prosthetic foot. However, in other embodiments, the prosthetic foot 112 can also be fitted with a footpad and, optionally, a FPU to collect measurements. The footpad 114 and IMU 106 may be integrated into a prosthetic foot with force and orientation measurement or feedback. The footpad may also be integrated into a shoe that can provide propulsive force and torque quantity and direction information. The data from the IMU is combined with the data from the footpad such that propulsive forces and torques, foot orientation, and propulsive force vector directions, with respect to a selected reference frame, are measured.

System 100 also includes a computing device 116 for communicating with various elements of system 100, such as IMUs 106, footpad 114, FPU 115, or any other components for providing sensor information. The communications links between computing device 116 and the various elements of system 100 can be wireless, wired, or a combination of both.

In operation, data from the IMUs 106 or from the footpad 114 can be transmitted as a signal 118 to computing device 116. The computing device 116 can also send a signal 120 to the IMUs 106 and/or footpad 114 (or FPU 115). In the exemplary configuration of FIG. 1, the signals 118 and 120 are transmitted wirelessly. However, the

various embodiments are not limited in this regard and such data can be exchanged via wired connections or a combination of wireless and wired connections, as noted above.

Referring to now to FIG. 2, a block diagram of a configuration for IMU 106 is shown. As illustrated in FIG. 2, an IMU can include a microcontroller 202 for controlling the operation of the IMU 106, a clock module 204, a battery module 206, a power management module 208, a transceiver 210, memory 212, and inertial measurement sensors 214.

Referring now to FIG. 3, an exemplary configuration for the internal circuitry of an IMU 106 is shown. In particular, FIG. 2 shows the internal circuit of a microelectromechanical system (MEMS) IMU. In the exemplary configuration of FIG. 3, the IMU 106 is configured to include a computer-on-module 302, an expansion board 304, and a battery 306. The computer-on-module 206 can include an ARM processor running Minix and software written in C++, or any operating system and any suitable language. Further, this exemplary computer-on-module 204 can include Wi-Fi connectivity, Bluetooth connectivity, and/or microSD. However, the various embodiments are not limited in this regard and any other type of connectivity can be supported in the various embodiments. The expansion board 200 can include battery management circuits, an MSP430 microcontroller, a 3 axis IMU, a USB port, and/or a connection to a foot sensor. However, the various embodiments are not limited solely to the architecture described above and an IMU 106 can be configured with comparable functionality in a variety of other ways.

To provide IMUs 106 for the torso and limb segments, the IMUs 106 can be configured to allow their attachment to the body of amputee 102. For example, the IMUs

106 can be configured to be strapped to a plurality of limb segments at various points on an amputee's body. Referring to FIG. 4, an exemplary configuration for an IMU 106 is shown including an enclosure 402 can be provided to house the circuitry of IMU 106. The IMU 106 can be provided with a strap 404 as shown in FIG. 5. In this exemplary embodiment, the strap 404 can include adjustment rings 406 and hook and loop fastening portions 408. However, the various embodiments are not limited in this regard and other configurations for an IMU 106 can be provided to allow the IMUs 106 to be secured to an amputee 102 at various locations as shown in FIG. 1. For example, belts, clips, pins, and other methods of attachment are equally suitable.

Referring now to FIGs 5A-5C, 6A-C, and 7, one exemplary configuration for a footpad 114 is illustrated. In particular, FIGs. 5A-5C show an embodiment of a forefoot portion 500 of a footpad 114 (as illustrated in FIG. 1). FIG. 5A shows a top isometric view of forefoot portion 500. FIG. 5B shows a side view of forefoot portion 500. FIG. 5C shows a top, disassembled view of forefoot portion 500. As shown in FIGs. 5A-5C, the forefoot portion 500 can include a top plate 501 and a bottom plate 502. One or more cleats 503 can be secured to the top plate 501. The cleats 503 can serve to align the forefoot portion 500 with a wearer's foot or shoe. The top plate 501 can include one or more top sensor enclosures 504. The bottom plate 502 can include one or more bottom sensor enclosures 505. The top plate 501 can be secured to the bottom plate 502 by one or more fasteners (not shown). In the various embodiments, fasteners can include screws, nuts and bolts, clips, straps, adhesives, or any other device, material, or combination thereof for securing the top plate 501 to the bottom plate 502. The forefoot portion 500 is assembled by aligning and connecting one or more top sensor enclosures 504 to one or

more bottom sensor enclosures 505 and securing via any fasteners. Additional structural support 506 can be provided to connect top plate 501 to bottom plate 502, such as a washer, spacer, or the like. As shown in FIG. 5B, the forefoot portion 500 of the footpad 105 can be enclosed in a padding material 507, which can provide support and comfort to the wearer. A tread 508 can be secured to the bottom of the padding material 507, such that the forefoot portion 500 closely mirrors the sole of the prosthetic foot or the sole of a shoe placed thereon. The forefoot portion 500 can include 6 DOF Force Sensors (3 Loads, 3 Moments or Torques) to measure ground reaction forces.

Referring now to FIGs. 6A, 6B, and 6C, these illustrate embodiments of a heel portion 600 of a footpad 114 (as illustrated in FIG. 1). The structure of the heel portion 600 can be similar to that of forefoot portion 500. That is, the heel portion 600 can include a top plate 601 and a bottom plate 602. Further, one or more cleats 603 can be secured to the top plate 601. The cleats 603 can serve to align the heel portion 600 with a wearer's foot. Additionally, the top plate 601 can also include one or more top sensor enclosures 604 and the bottom plate 602 can include one or more bottom sensor enclosures 605. As in forefoot portion 500, the top plate 601 can be secured to the bottom plate 602 by aligning and connecting one or more top sensor enclosures 604 to one or more bottom sensor enclosures 605. Fasteners (not shown) can then be used to secure the plates 601 and 602 together. Additional structural support 606 can be provided to connect top plate 601 to bottom plate 602. As shown in FIG. 6B, the heel portion 600 of the footpad 105 can be enclosed in a padding material 607, which can provide support and comfort to the wearer. A tread 608 can be secured to the bottom of the padding material 607, as in forefoot portion 500.

Together, forefoot portion 500 and heel portion 600 can be utilized to define the footpad 114 for foot 602, as shown in FIG. 7. Although FIG. 7 shows that the forefoot portion 500 and the heel portion 600 are physically separated, the various embodiments are not limited in this regard. In some embodiments, the portions 500 and 600 can be physically connected or incorporated into a same sole attachable to a foot or shoe. Thus, the footpad 114 can be formed using one or more components.

Now referring to now to FIG. 8, there is illustrated the exemplary configuration for footpad 114 of FIG. 7, that includes a forefoot portion 500 and a heel portion 600, strapped to an athletic shoe 804, via one or more straps 802. The straps 802 can be secured to the cleats 503, 603 of the forefoot portion 500 and the heel portion 600 via strap anchors 806. Each of the strap anchors 806 can comprise a fastener 808 for attaching a strap anchor 806 to one of cleats 503, 603. Further, each of strap anchors can also include a ring member 803 through which the strap 801 can be fed. The straps 802 can be arranged so that a friction fit keeps the footpad 114 attached to shoe 804. Alternatively, the straps 806 can be further arranged using one or more fasteners (not shown) to secure the straps 806 in place. For example, laces, hook and eye fasteners, fabric (elastic and non-elastic), cords (elastic and non-elastic), snaps, or buckles, to name a few. However, any other types of devices or methods useful for straps, belts, string, or rope can be used in the various embodiments.

Although a specific arrangement of straps and anchors is illustrated in FIG. 8, the configuration can vary in the various embodiments. Further, other types of fasteners can be utilized in the place of straps 801. For example, clips, clamps, belts, or any other

fastening devices can be used in the various embodiments. Additionally, the footpad 114 can be incorporated directly into shoe 804 in some embodiments.

As noted above, the footpad 114 can be configured in a manner similar to IMU 106 or can include a FPU 115 that operates with footpad 114 and that can also be removably attached to the foot (healthy or prosthetic) of the subject. Regardless of the configuration, the block diagram of FIG. 9 illustrates an exemplary configuration for the circuitry of the footpad 114 or footpad 114 with FPU 115. For ease of illustration, FIG. 9 will be discussed in terms of a footpad 114 and an FPU 115.

Referring to FIG. 9, there is shown an FPU 115 coupled to footpad 114 for purposes of providing power and data signals. Specifically, FPU 115 is coupled to forefoot portion 500 via a first link or connection 920 and FPU 115 is coupled to heel portion 600 via a second link or connection 930. These connections 902, 904 can each include one or discrete links for providing data and/or power. FPU 115 can be configured in substantially a same manner as IMU 106 in FIG. 2. That is FPU 115 can include a microcontroller 902, a clock 904, a battery module 906, a power management module 208, a transceiver 210, and a memory 212.

Some elements of each of forefoot portion 500 and heel portion 600 have already been described above. However, to allow operation with FPU 115, additional elements can be provided. For example, as show in in FIG. 9, forefoot portion 500 includes a controller 922 for controlling operation in forefoot portion 500 and receiving instructions from FPU 115. The forefoot portion 500 also includes a power regulation module 924 for receiving power signals from the FPU 115 and providing appropriate power to other components of forefoot portion 500. To provide an output signal, the forefoot portion

500 includes signal conditioning electronics 927 and an analog to digital (A/D) converter 926 to convert the analog signals from the sensors 928 to digital signals for use by the FPU 115 and components beyond. A similar configuration can be provided for heel portion 600. Thus components 932, 934, 936, 937, and 938 in heel portion 600 operate in substantially a same manner as components 922, 924, 926, and 928 in forefoot portion 500.

In the various embodiments, it can be advantageous to provide inertial measurement sensors at the foot. For example, for purposes of gait analysis, it may be useful to obtain the orientation of a foot (healthy or prosthetic). Thus, in some embodiments the FPU 115 at the foot can be configured in substantially the same way as an IMU 106. That is, the FPU 115 can include inertial measurement sensors 914. However, in other embodiments, inertial measurement sensors, or any other type of sensor, can be provided within the footpad 114 as well. For example, inertial measurement sensors 929 and 939 can be configured for measuring orientation for at least one of the forefoot portion 500 and the heel portion 600, respectively.

Now referring to FIG. 10, there is shown an exemplary configuration of footpad 114 that includes a forefoot portion 500 and heel portion 600, as described above. In the configuration of FIG. 10, there is shown the FPU 115 within forefoot portion 500. As noted above, the FPU 115 can be used to power and/or control one or more sensors, to store data from the one or more sensors, and/or two transceivers data from one or more sensors. A connector 1000 can be used connect the FPU 115 in forefoot portion 500 to the heel portion 600. The connector 1000 can include one or more wires to communicatively connect with the sensors and other devices in footpad 114. However,

the configuration of FIG.10 is provided solely for illustrative purposes. That is, FPU 115 can be coupled to a footpad 114 in a variety of ways, including using one or more wired connections, one or more wireless connections, or any combination thereof.

Now turning to FIGs. 11 and 12, the operation of IMUs 106 discussed above is described. Each of the IMUs 106 can include one or more three axis gyroscopes to measure angular rates of change and one or more 3 axis accelerometers to measure acceleration. As noted above, such an IMU can be fabricated using MEMS devices. In operation, the signals from the gyroscope can be integrated to calculate orientation of the IMU 106 in space. The force of gravity, as shown in FIG. 12B, can be used to determine the pitch and roll of each IMU 106. Thereafter, this information for each of IMUs 106 (each of which is associated with a segment) can be individually processed using a data fusion technique to then provide information for each corresponding segment. In some embodiments, the data fusion techniques or processes can include Kalman Filtering processes, such as Extended Kalman Filtering (EKF). Such data processing allows for the extraction of better results than by relying solely on accelerometer or gyroscope measurements alone.

Although exemplary embodiments below will be described with respect to an algorithm based on an extended Kalman filter process, the various embodiments are not limited in this regard. Rather, in the various embodiments, any other type of data fusion techniques or processes can be utilized.

Generally, pitch and roll angles can be calculated by estimating the direction of gravity using the accelerometer signals. Alternatively, the gyroscope signals can be integrated to determine pitch, roll and yaw (heading). However, these calculations are

subject to drift and noise which cause increasing error as the signal is integrated over time. Individually, these respective angle calculations are inaccurate. Accordingly, an extended Kalman filter process was developed in the various embodiments to fuse the accelerometer and gyroscope data to generate covariance data that can be used to estimate segment orientation while accounting for noise and drift.

In one particular embodiment, the filter uses a 14-element state vector (1)

$$x = \begin{bmatrix} v_{\text{int}} \\ a_{\text{int}} \\ \omega_{body} \\ b_{gyr} \\ r \\ p \end{bmatrix} \quad (1)$$

where v_{int} and a_{int} are velocity and acceleration in three axes transformed to an intermediate reference frame, ω_{IMU} and b_{gyr} are the gyroscope signals and the gyroscope bias in three axes, and r and p are roll and pitch of the segment. The intermediate reference frame can be initially aligned with a laboratory reference frame but rotates about the gravity vector and is propagated outside of the roll and pitch EKF. The rotations from the laboratory reference frame to the IMU frames can be represented using direction cosine matrices so pitch and roll rotations can be isolated while rotations about the gravity vector are ignored.

The orientation about the gravity vector (internal/external rotation, heading or yaw) can be calculated through a second EKF that assumes the yaw rotation is minimal and about 0 degrees. This is a valid assumption when the relative rotation between segments (joint rotations) is being examined as opposed to the absolute rotation in global space.

The velocity at step k+1, in the intermediate frame are found by numerically integrating a_{int} (2) over timestep Δt.

$$v_{\text{int},k+1} = v_{\text{int},k} + a_{\text{int},k}\Delta t \,. \tag{2}$$

Accelerations, angular rates and angular biases are modeled by using the value at the previous time step, adding noise, w^a, w^ω, w^{gyr} to acceleration, gyroscopes and bias and, for the acceleration model subtracting a factor multiplied by velocity, γv_p, to stabilize the velocity calculation (3)

$$\begin{aligned} a_{\text{int},k+1} &= a_{\text{int},k} + w_k^a - \gamma v_{p,k} \\ w_{body,k+1} &= \omega_{body,k} + w_k^\omega \\ b_{gyr,k+1} &= b_{gyr,k} + w_k^{gyr} \end{aligned} \tag{3}$$

Angles of the segments in the laboratory reference frame can then be calculated by transforming the gyroscope signals to the laboratory reference frame (4)

$$\begin{aligned} \dot{r} &= \omega_x + (\omega_z \cos r + \omega_y \sin r)\tan p \\ \dot{p} &= (\omega_y \cos r - \omega_z \sin r) \\ \dot{y} &= (\omega_z \cos r + \omega_y \sin r)\sec p \end{aligned} \tag{4}$$

representing the time derivative of roll, pitch and yaw, $\dot{r}$, $\dot{p}$, and $\dot{y}$, then numerically integrating the angular velocities (5)

$$\begin{aligned} r_{k+1} &= r_k + \dot{r}_k \Delta t \\ p_{k+1} &= p_k + \dot{p}_k \Delta t \,. \\ y_{k+1} &= y_k + \dot{y}_k \Delta t \end{aligned} \tag{5}$$

Here, y is yaw, which is not included in the pitch and roll EKF state equations and represents the rotation of the intermediate reference frame about the gravity vector.

The measurement vector (6) consists of the three signals from the accelerometer, a_{IMU} which include the gravity vector in the IMU frame, three signals from the gyroscope in the IMU frame and any drift associated with the gyroscope, w_{IMU} and b_{gyr}. An estimate of roll and pitch, r_{est} and p_{est}, respectively, is calculated using the direction of gravity from the accelerometer signals, basic trigonometry and sequential rotations. The filtered measurement vector, v_k can then be defined by:

$$v_k = \begin{pmatrix} a_{IMU,k} \\ \omega_{IMU,k} + b_{gyr,k} \\ r_{est} \\ p_{est} \end{pmatrix} + w_k^{meas}, \tag{6}$$

where w_k^{meas} is the measurement noise at time k.

The process covariances were calculated using the ideal signals calculated with a kinematic model. Only covariances for a_{int}, ω_{body}, and b_{gyr} were used. All other covariances were set to zero. The angle calculated using the gravity signal from the accelerometers is only accurate during low linear acceleration (when the IMU is not in motion). Therefore, the measurement covariances were optimized so that the algorithm weights the gyroscope measurements more heavily than the accelerometer and estimated angle measurements. The covariances may also be adjusted in real time based on the IMU data or by using data from the force sensors on the feet. During times of low linear acceleration the covariances can be adjusted so as to weight the accelerometer measurements and the pitch and yaw calculations from gravity more heavily than the gyroscope measurements.

In the various embodiments, the gravity vector can be obtained in a variety of ways. One method is to use accelerometers, such as those in the IMUs. Accelerometers

use a “proof mass” which experience forces when the sensor is subjected to acceleration. This can cause a movement of the mass and a strain in the members that support the mass. Typically MEMS devices, like those described above, use capacitive components supported on flexures with integrated capacitive elements to measure the deflection of the proof mass. The changes in capacitance can be measured as a change in acceleration or a feedback voltage can be used to maintain the proof mass at a constant location. The amount of voltage required to hold the proof mass in place is proportional to the acceleration.

If a single axis accelerometer is stationary and oriented such that the measurement axis is perfectly vertical, the mass will deflect due to gravity and the accelerometer will detect an acceleration that equals 9.81 m/s2 or 1 g. The three axis accelerometers used herein can consist of three single axis accelerometers placed orthogonal to each other. Therefore, when the sensor is not moving or experiencing no inertial acceleration, the only signal the accelerometer senses is that of gravity deflecting the proof masses. If one of the three axes is perfectly aligned to vertical it will sense 1 g of acceleration and the other axes will read 0 g. If the accelerometer is randomly oriented and no single axis is aligned with gravity, then the proof masses in the other axes will also deflect and the gravity component in each of the axes will be detected. Assuming that the sensor is not moving, the orientation of the sensor can therefore be calculated using the known magnitude of gravity, the gravity component in each axes, and trigonometric functions arcsine and arccosine.

Depending on the amount of motion, the covariance values can be adjusted for the gyroscope signals and the accelerometer signals. That is, the angle values are either

calculated primarily based on a direction of gravity calculated by the accelerometers or by using the gyroscope signals. During motion, an algorithm can be weighted to consider the gyroscope signals more and the angle calculated from gravity less, because using the accelerometers is less accurate when an IMU is in motion. When the IMU is not moving, the covariance values can be adjusted to consider the angle calculated from gravity using the accelerometers more, because that calculation should be of higher accuracy.

As noted above data fusion methods, such as the EKF methods described above, provide only a portion of an overall algorithm in accordance with the various embodiments. For example, the overall algorithm provides parameters that are input to the data fusion portion and also determines when motion is occurring and when motion has ceased.

In operation, the parameters that are input to the data fusion portion of the overall algorithm can be divided into recursive-type and non-recursive-type parameters. The overall algorithm is configured to provide initial values for both types of parameters. New values for the recursive-type parameters are then calculated by the data fusion portion during a sampling/calculation period and fed back into the data fusion portion as an input for the next sampling/calculation period. The non-recursive-type parameters, such as the measurement covariance values, are also fed into the data fusion portion but remain unchanged by the data fusion portion. However, the overall algorithm may change these non-recursive-type parameter values over time.

The overall algorithm determines when motion starts by using a threshold value for the gyroscope signal of each respective IMU. Also, depending on what portion of the gait activity (stance phase or swing phase) the particular limb is experiencing, the overall

algorithm can change the measurement covariance and can determine how the data fusion algorithm for each segment will weigh the various measurement signals. For covariances for the thigh, shank, and trunk segments, only the IMU data is used as a measure to adjust the measurement covariances. For the foot segments, the force measurements are used to determine when the foot is on the ground and in a stance phase. However, these force measurements are only used to adjust the measurement covariances outside of the data fusion segment and are not used in the orientation calculation.

Other parameters that the overall algorithm calculates for input to the data fusion segment include an initial gyroscope bias which is taken from an average of a static data collection from the respective IMUs. The standard deviations of the gyroscope signals from these static trials are also used as the basis for some of the measurement covariance values.

The operation of the overall algorithm is described below in greater detail with respect to FIGs. 13A and 13B. FIGs. 13A and 13B schematically illustrate the operation of the overall algorithm in accordance with an embodiment of the invention. The overall algorithm can begin with an initialization process 1302. The initialization process begins with a loading of the initial gyrometer bias at 1304. Based on the initial gyrometer bias, EKF parameters for inputting to the EKFs for each segment are generated. These include initial values for:

Q: Process noise covariance. In some embodiments, this can be set to 0.

R: Measurement noise covariance matrix. This is square matrix, such as an 8x8 matrix. The values along the diagonal of R are the covariances and determined

using a combination of measurements (static gyroscopic standard measurements) and factors that are determined empirically.

f: State function which takes measurements and turns them into states.

hyxz: Measurement function which relates states back to the measurements using a yxz rotation sequence.

Once the initial gyrometer bias and initial EKF parameters are obtained, these values are passed to a loop 1308 that is performed to generate EKF output data.

Loop 1308 first begins with a determination that motion has started. In particular, at 1310, a determination is made that motion was started if gyrometer measurements exceed a threshold value for motion start. If motion start is determined at 1310, initial angles for the segments are generated at 1312. In particular, IMU data before motion, specifically acceleration data (A_{norm}), is used at 1312 to calculate initial angles using yaw = 0. The loop 1308 can then utilize EKFs to get data for each of the segments.

In particular, at 1314. the current IMU data, force data, and old EKF data (if available) is received. The IMU data can then be organized by segment at 1314. Further, a determination of whether a current phase is a stance or a swing phase can be made at 1314. Once the IMU data is organized and a current phase (swing or stance) is determined, the EKF process can be performed by an EKF engine 1316.

The EFK engine 1316 receives as inputs current IMU data, old or previous EKF data (if available), and the current phase information (i.e., swing or stance). The old or previous EKF data can include x, the 14 state vector of equation (1), and P, prior variance estimates for the states. Initially, P can be initialized as a square (14x14) matrix of

zeroes. In the data fusion portion, the following is then performed at a configuration stage 1318:

(1) Any EKF parameters not yet initialized are initialized

(2) Covariance values are adjusted based on the current activity (i.e., swing or stance phase)

(3) Parameters are forwarded to EKF filters for processing.

As noted above, two types of EKFs are run, a pitch and roll EFK 1320 and a yaw EKF 1322. For the pitch and roll EKF 1320, it is passed data that include the IMU data for the segment of interest and the current pitch/roll EKF parameters for the segment (x, P). In response, the EKF 1320 generates new values for these EKF parameters. For the yaw EKF 1322, it is passed current yaw data (z), mean yaw data, and old or current yaw EKF parameters for the segment. For example, yzwx and yzwP. In response, the EKF 1322 generates updated yaw data and updates the yaw EKF parameters.

Thereafter, the updated EKF parameters from EKFs 1320 and 1322 are passed back to loop 1308 at 1314 and the updated EKF parameters and states of the segments (i.e., the updated segment orientations) are then provided. The updated data can then be stored at 1324. Further, the updated data can be passed back into loop 1308 to provide the old or current EKF data for a next iteration performing 1314 and 1316. The stored data can then be plotted or otherwise presented to the user at 1326. Finally, all EKF data generated by loop can be stored at 1328.

The filtering process described above can be used to carry out the methods of FIGs. 14 and 15. Turning first to FIG. 14, there is shown a schematic illustration of a method 1400 for utilizing sensor information for IMUs 106 to calculate knee angle in

accordance with the various embodiments. The method begins at step 1402 in which an IMU 106 associated with a thigh, for which knee angle is to be calculated, generating and delivering accelerometer and gyroscope data. Thereafter at step 1404, the angle of x, y, and z axes are calculated with respect to a direction of gravity (G), as discussed above with respect to FIG. 12B. The angle information from step 1404, along with accelerometer and gyroscope data from step 1402 is then fed into the extended Kalman Filter at step 1406 to compute a current pitch and roll of the thigh. Additionally, at step 1408, the heading for the thigh can be calculated based on the heading angular speed obtained from the Kalman filter. Together, the heading (i.e., yaw), the pitch, and the roll therefore provide the orientation of the thigh. The processes at 1404-1408 can be carried out as described above with respect to FIGs. 13A and 13B.

The shank orientation can be computed in a substantially similar way. In particular, steps 1410, 1412, 1414, and 1416 can be performed for the data from an IMU 106 associated with a shank, for which the knee angle is to be calculated, in substantially a same way as steps 1402, 1404, 1406, and 1408, respectively. Steps 1410-1416 can be performed at a same or different time as steps 1402-1408. However, for purposes of reducing errors, it is preferable to perform these steps concurrently so that the calculated orientation is based on corresponding measurements of the thigh and shank. Once the orientation of each of the thigh and shank is obtained at steps 1406, 1408, 1414, and 1416, the associated knee angle can be calculated at step 1418. The method 1400 can then be repeated to capture development of the knee angle over time. Further, the method 1400 can be performed for both legs, concurrently. Additionally, a similar process can also for the individual segments of the footpad (i.e., the forefoot and heel).

Thus, in addition to capturing knee angle, angles for the ankle and angle associated with the foot can also be captured. In such configurations, the ground reaction forces can be considered

As a result, the kinematics of the legs of the amputee can be captured without the need for a conventional gait laboratoryoratory setup. Therefore, together with other information regarding the prosthesis and the amputee and without the need of a gait laboratoryoratory, the prosthetist can perform adjustments to improve the gait of the amputee until such kinematics are within acceptable tolerance limits. For example, a method of carrying out such adjustments is presented below with respect to FIG. 15.

FIG. 15 is a flowchart of steps in an exemplary method 1500 for adjusting a prosthesis in accordance with an embodiment of the invention. The method 1500 begins at step 1502 and proceeds to step 1504. At step 1504, the amputee can be fitted with a prosthesis. At this step, the prosthesis can be initially adjusted based on patient data (e.g., height, weight, previous prosthesis configuration), manufacturer recommendations for configuring the prosthesis, and any initial observation of the prosthetist with regards to operation of the prosthesis or to adjust cosmetic issues with the prosthesis or the patient's gait.

Once the initial configuration of the prosthesis is completed, the method 1500 can proceed to step 1506 to collect additional patient data using the MGAS systems described herein. For example, the amputee/patient can be outfitted as described above with respect to FIG. 1. Thereafter, the patient can walk while data is collected from the various sensors. Once the patient data is collected at step 1506, the kinematic data can be

computed at step 1508. This kinematic data can be computed as described above as described above with respect to FIGs. 13A, 13B, and 14.

The prosthetist, manually or programmatically, can then evaluate the kinematic data. In particular, at step 1510, the kinematic data for the patient can be evaluated to determine whether or not if falls within acceptable limits. For example, to provide a proper gait for the user, it may be preferred that the development of knee angles on both the healthy and affected legs be symmetric. Further, it may also be preferred that the overall stride of the healthy and affected legs also be similar as possible. Thus, a determination is made whether there are any unbalanced or irregular aspects of the patient's gait for the current prosthesis configuration.

If the kinematic data is within acceptable limits at step 1510, the method 1500 can end at step 1512. If the kinematic data is not within acceptable limits at step 1510, the method 1500 can proceed to step 1514. At step 1514, further adjustments can be made to the prosthesis, based on the kinematic data and other data. Such adjustments can be determined manually or automatically based on the kinematic and other data. Thereafter, the method can repeat steps 1506, 1508, 1510, and 1514 until the kinematic data is within acceptable limits.

Although the various embodiments have been described with respect to evaluating gait with respect to the development of the knee angle over time, the various embodiments are not limited in this regard. Substantially similar methods can be utilized for purposes of evaluating the kinematics of any of the other joints of the amputee and/or the prosthesis. For example, similar methods can be applied to adjust the gait of below-the-knee amputees by using measurements of ankle angle to determine how to adjust the

prosthesis. In another example, similar methods can be applied to adjust a prosthesis including both knee joints and ankle joints.

EXAMPLES

Although examples of various aspects of the present invention are discussed in detail below, the various embodiments are not limited in this regard. Rather, these examples are provided solely for illustrating or clarifying the various embodiments of the present invention.

In the following examples, the method of extended Kalman filtering of the various embodiments was evaluated conducting experiments to confirm whether the data collected by the IMUs and the kinematic data obtained using the extending Kalman filtering corresponded to actual kinematic data. In particular, these experiments employed using a Mitsubishi Heavy Industry (Tokyo, Japan) PA-107C robot arm with IMUs and a data processing system, as described above. The difference between applying the EKF algorithm to data from a robot and data from a human subject is adjusting the measurement covariance values, or adjusting how much the EKF weighs one signal over another. The robot was controlled with a personal computer which moved the arm through a repeatable motion sequence while simultaneously recording the encoder data from the robot. A separate personal computer recorded the gyroscope and accelerometer data from the IMUs.

The overall process for the experiment is shown in FIG. 16. FIG. 16 is a flow chart of steps in a method 1600 for evaluation of the sensors and the algorithms of the various embodiments. First, at step 1602, the robot was programmed and actuated to

simulate the motion of a human leg using joint angle data from gait analyses of a healthy subject. The human leg has nine rotational degrees of freedom (DOF) including the hip, knee and ankle while the robot can only represent six, thus, three DOF are excluded from the robot motion. The angles represented by the robot included hip flexion/extension, hip abduction/adduction, knee flexion/extension, abduction/adduction and internal/external rotation and foot flexion/extension. The motions evaluated for these experiments consist of two different walking patterns, Walking A (illustrated in FIG. 17) and Walking B. Walking B is slightly faster than Walking A, but simulates a smaller range of motion. The speed of the motions is limited by the capabilities of the robot arm. A slow stair climb motion was also simulated and called Stair Climb for the purposes of this study.

In the experiments, an IMU was attached to the "thigh" and "shank" segments of the robot. The goal was to determine the orientation of the segments and the angle between them, or the "knee" angle. These IMUs were attached to the robot "thigh" and "shank" segments using custom holders designed to put the IMUs in the same place for each trial. For this study the IMU data was collected using a MSP430 (Texas Instruments, Inc., Dallas, TX) microcontroller and stored on a computer for post processing using MATLAB (The Mathworks, Inc. Natick, MA). Three trials were performed for all three activities. The root mean-squared-error (RMSE) between the MGAS orientation angles and the robot orientation angles were calculated.

A mathematical model of the robot was created using the Matlab (The Mathworks, Natick, MA) programming environment. The position and orientation of the IMUs relative to the robot segments, the robot joint angle data, and the robot segment lengths were the inputs for the model. The outputs were the position and orientation of

the IMUs as well as calculated accelerometer and gyroscope "signals" used as the ground truth when determining the accuracy of the IMU signals. The calculated IMU data was used to synchronize the robot and IMU data, evaluate IMU performance and develop the algorithm used to calculate joint angles from IMU data.

Referring back to FIG. 16, the actuating of the robot was followed by collecting of encoder data from the robot at step 1604 for actuating the robot and collection of IMU data at step 1606. Thereafter, the model of the robot was used to compute "ideal" IMU data from the encoder data at step 1608. At step 1610, the "ideal" and collected IMU data was then be synchronized and/or resampled for subsequent comparisons. These comparisons include a comparison of IMU data at step 1610 and, after performing the extended Kalman filtering at step 1612 to obtain orientation information for the robot, a comparison of the orientation results at step 1614.

Although specific IMUs were utilized in these experiments, a range of IMU sensors were evaluated using these robotic procedures. The IMU chip used herein, that consists of a three-axis accelerometer and a three-axis gyroscope, was selected based on performance, cost, size, form factor, communication interface and ease of implementation. This chip was incorporated to an expansion board for a commercially available computer-on-module device that uses an ARM reduced instruction set processor that runs the Linux operating system, runs compiled. This configuration is substantially similar to that described above with respect to FIGs. 2, 3, and 9-10.

The expansion board for these IMUs was designed for two applications. The first application is to control and manage data from a portable force/moment (F/M) foot sensor which is strapped to the bottom of the shoe, as discussed above with respect to

FIGs. 9 and 10. The foot sensor consists of a toe and heel nodes incorporating load cells that isolate loads in the cardinal directions to eliminate cross talk. These nodes are capable of very accurate force measurements in three dimensions that can be resolved to propulsive or braking forces, vertical load forces (SI), anterior/posterior (AP) and medial-lateral (ML) ground reaction forces (GRF) and moments or torques in each node about a vertical axis. The toe and heel node each contain a circuit board consisting of signal conditioning and 16-bit (effective resolution of greater than 14.5 bits) analog to digital conversion (ADC) circuitry for 10 channels and the selected IMU sensor.

The second application of the expansion board is as a limb segment (e.g. thigh, shank) IMU sensor, as discussed above with respect to FIGs. 2 and 3. In this case the MSP430 microcontroller controls the IMU and on hardware clock. The battery only powers the expansion board and computer-on-module device which has the same function as the foot sensor application but only stores and transmits inertial data from the IMU on the expansion board. In both applications, the expansion board manages the battery charge/discharge with power management circuits. A means to charge the battery, and command line access to the computer-on-module device, is provided through micro-USB on the expansion board.

FIGs. 18-21 show the results for Walk A. FIG. 18 shows the results of a sample trial of Walk A orientation angles from IMU data (MGAS values) and orientation angles calculated by the kinematic model (Robot values) for the “thigh” segment of the robot. FIG. 19 shows the results of a sample trial of Walk A orientation angles from IMU data (MGAS values) and orientation angles calculated by the kinematic model (Robot values) for the “shank” segment of the robot. The pitch RMSE and maximum pitch angle error

are also displayed for this trial. FIG. 20 shows the results of a sample trial of Walking A calculated knee flexion angles (MGAS values) and knee flexion angles calculated by the kinematic model (Robot values). The knee flexion RMSE and maximum knee flexion angle error are also displayed for this trial. FIG. 21 shows a sample trial of Walking A knee flexion angles from IMU data (MGAS values) and knee flexion angles from the kinematic model (Robot values) from one simulated gait cycle. As shown in each of these figures, there is generally good agreement between the "ideal" IMU results ("Robot") and the actual IMU results ("MGAS") for all measurements and calculations.

These are average results of six trials of Walk A, in which the thigh segment pitch RMSE was 0.2 degrees (standard deviation=0.1 degrees), shank segment pitch RMSE was 0.5 degrees (standard deviation =0.0 degrees), and the knee flexion calculation RMSE was 0.5 degrees (standard deviation =0.1 degrees) with a max error of 1.5 degrees (standard deviation =0.2 degrees) of knee flexion. The RMSE of the out of sagittal plane angles were not calculated but by inspection are within one or two degrees throughout the trials.

FIGs. 22 and 23 show the results for Walk B. FIG. 22 shows a sample trial of Walk B calculated knee flexion angles (MGAS values) and knee flexion angles calculated by the kinematic model (Robot values). The knee flexion RMSE and maximum knee flexion angle error are also displayed for this trial. FIG. 23 shows a sample trial of Walk B knee flexion angles from IMU data (MGAS values) and knee flexion angles from the kinematic model (Robot values) from one simulated gait cycle. Again, there is generally good agreement between the "ideal" IMU results ("Robot") and the actual IMU results ("MGAS") for all measurements and calculations.

The average results of the three trials of Walk B were the thigh segment pitch RMSE was 0.1 degrees (standard deviation =0.0 degrees), the shank segment pitch RMSE was 0.3 degrees (standard deviation =0.1 degrees) and the knee flexion RMSE was 0.8 degrees (standard deviation =0.2 degrees). Similar to the Walk A data, by inspection the out of sagittal plane orientation data appeared to be within one or two degrees by visual inspection of the plots.

FIGs. 24 and 25 show the results for the Stair Climb activity. FIG. 24 shows a sample trial of Stair Climb calculated knee flexion angles (MGAS values) and knee flexion angles calculated by the kinematic model (Robot values). FIG. 25 shows a sample trial of Stair Climb knee flexion angles from IMU data (MGAS values) and knee flexion angles from the kinematic model (Robot values) from one simulated gait cycle. Again, there is generally good agreement between the "ideal" IMU results ("Robot") and the actual IMU results ("MGAS") for all measurements and calculations.

The average slow Stair Climb activity segment pitch RMSE for the thigh segment was 0.3 degrees (standard deviation =0.1degrees), for the shank segment was 0.1 degrees (standard deviation=0.1degrees) and for knee flexion 0.4 degrees (standard deviation=0.0 degrees). Similar to the previous two activities the error of out of sagittal plane motion appeared to be within a few degrees by visual inspection of the data.

The average maximum knee flexion errors per trial were 1.5 degrees (standard deviation =0.2 degrees), 3.1 degrees (standard deviation =0.2 degrees) and 1.2 degrees (standard deviation =0.3 degrees) for Walk A, Walk B and Stair Climb activities, respectively. The flexion error from the different robot motions are shown in FIG. 26.

As noted above, the results from these kinematic tests show generally good agreement. The RMSE values for sagittal plane orientations are within 1 degree RMSE, which was a loose goal set for the kinematic portion of the system. The out of sagittal plane motions are also accurate to within a few degrees. There is no additional reference for the yaw component of the limb orientation; therefore this calculation is dependent purely on the gyroscope signal and vulnerable to drift errors. This may be a factor in real world testing of the system when soft tissue artifact and inconsistent motion comes into play. However, with additional processing, a stable estimate of yaw orientation, or heading, can be made without the use of additional sensors such as magnetometers. By avoiding using magnetometers, the concern over ferrous perturbations is avoided and this system will work in any setting.

These trials demonstrate that portable, inexpensive inertial sensors can be used to accurately track complicated repeated biomechanical motion. Incorporating this into the proposed MGAS will result in a tool that will give prosthetists, clinicians and researchers more information to improve the performance of lower leg prosthesis and the overall quality of life of amputee.

To further evaluate the effectiveness of the analysis system of the various embodiments, a study was conducted in which measurements from a system in accordance with the various embodiments (labeled “MGAS” in the following figures) was compared to measurements obtained from a conventional gait laboratory system (labeled “CFI” in the following figures). The measurements were obtained for a healthy subject walking at normal speed.

Thigh and shank angle measurements are compared in FIGs. 27 and 28. FIG. 27 shows plots of angle in three physiological planes for the thigh. FIG. 28 shows plots of angle in three physiological planes for the shank. For each of FIGs. 27 and 28, sagittal angles (flexion and extension rotation) presented in the first row, coronal angles (varus and valgus rotation) are presented in in the second row, and transverse angles (internal and external rotation) are presented in the third row. The horizontal axis is percent gait cycle or stride from heel strike to heel strike. The solid vertical lines are toe off for each of the strides. Therefore, everything to the right of the vertical lines is stance phase, or when the foot is on the ground, and everything to the right is swing phase. The y axis is angle.

As shown in FIGs. 27 and 28, there is generally good agreement in sagittal angle measurements (first row) and poor agreement between coronal angle measurements (second row). As to the transverse angle measurements (third row), there is some agreement, but only during certain portions of the gait cycle.

Knee angle measurements are compared in FIGs. 29 and 30, where the knee angle is obtained from a combination of the thigh and shank data. FIGs. 29 and 30 show plots of angle in three physiological planes for the knee (sagittal, coronal, and transverse), as described above with respect to FIGs. 27 and 28. FIG. 29 shows the measurements for the individual strides, similar to FIGs, 27 and 28. FIG. 30 shows the average (solid line) and standard deviation (shaded) for each set of data and historical averages for data from healthy patients.

As shown in FIGs. 29 and 30, there is generally good agreement in sagittal angle measurements (first row) and poor agreement between coronal angle measurements

(second row). As to the transverse angle measurements (third row), there is some agreement, but only during certain portions of the gait cycle.

Heel and toe measurements are compared in FIGs. 31 and 32. FIGs. 31 and 32 shows plots of angle in three physiological planes for the heel and toe, respectively (sagittal, coronal, and transverse), as described above with respect to FIGs. 27 and 28. As shown in FIGs. 31 and 32, there is again generally good agreement in sagittal angle measurements (first row), but poor agreement between coronal angle measurements (second row) and transverse angle measurements (third row).

FIGs. 33 and 34 show measurements of ground reaction forces. In particular, these include vertical load, medial or lateral loads, and braking (propulsion) ground reaction forces. For the system of the various embodiments, the ground reaction force measurements were obtained by combining the force data from the heel and toe foot sensors with the orientations from FIGs. 31and 32 to transform the forces back into the ground reference frame to match the force plate data of the gait laboratoryoratory. FIG. 33 is the data for all the individual strides. FIG. 34 shows average and standard deviation data. The data for the gait laboratory system is incomplete since it excludes data for foot strikes that did not completely hit the force plate that is embedded in the floor. Thus, this highlights an advantage of the system of the various embodiments in that every foot strike is measured. As shown in FIGs. 33 and 34, the data collected is in generally good agreement,

Various embodiments of the present technology are carried out using one or more computing devices. With reference to FIG. 35, an exemplary system 3500 includes a general-purpose computing device 3500, including a processing unit (CPU or processor)

3520 and a system bus 3510 that couples various system components including the system memory 3530 such as read only memory (ROM) 3540 and random access memory (RAM) 3550 to the processor 3520. The system 3500 can include a cache 3522 of high speed memory connected directly with, in close proximity to, or integrated as part of the processor 3520. The system 3500 copies data from the memory 3530 and/or the storage device 3560 to the cache 3522 for quick access by the processor 3520. In this way, the cache provides a performance boost that avoids processor 3520 delays while waiting for data. These and other modules can control or be configured to control the processor 3520 to perform various actions. Other system memory 3530 may be available for use as well. The memory 3530 can include multiple different types of memory with different performance characteristics. It can be appreciated that the disclosure may operate on a computing device 3500 with more than one processor 3520 or on a group or cluster of computing devices networked together to provide greater processing capability. The processor 3520 can include any general purpose processor and a hardware module or software module, such as module 35 3562, module 2 3564, and module 3 3566 stored in storage device 3560, configured to control the processor 3520 as well as a special-purpose processor where software instructions are incorporated into the actual processor design. The processor 3520 may essentially be a completely self-contained computing system, containing multiple cores or processors, a bus, memory controller, cache, etc. A multi-core processor may be symmetric or asymmetric.

The system bus 3510 may be any of several types of bus structures including a memory bus or memory controller, a peripheral bus, and a local bus using any of a variety of bus architectures. A basic input/output (BIOS) stored in ROM 3540 or the

like, may provide the basic routine that helps to transfer information between elements within the computing device 3500, such as during start-up. The computing device 3500 further includes storage devices 3560 such as a solid state hard disk drive, a magnetic disk drive, an optical disk drive, tape drive or the like. The storage device 3560 can include software modules 3562, 3564, 3566 for controlling the processor 3520. Other hardware or software modules are contemplated. The storage device 3560 is connected to the system bus 3510 by a drive interface. The drives and the associated computer readable storage media provide nonvolatile storage of computer readable instructions, data structures, program modules and other data for the computing device 3500. In one aspect, a hardware module that performs a particular function includes the software component stored in a non-transitory computer-readable medium in connection with the necessary hardware components, such as the processor 3520, bus 3510, display 3570, and so forth, to carry out the function. The basic components are known to those of skill in the art and appropriate variations are contemplated depending on the type of device, such as whether the device 3500 is a small, handheld computing device, a desktop computer, or a computer server.

Although the exemplary embodiment described herein employs the hard disk 3560, it should be appreciated by those skilled in the art that other types of computer readable media which can store data that are accessible by a computer, such as magnetic cassettes, solid state memory devices, digital versatile disks, cartridges, random access memories (RAMs) 3550, read only memory (ROM) 3540, a cable or wireless signal containing a bit stream and the like, may also be used in the exemplary operating

environment. Non-transitory computer-readable storage media expressly exclude media such as energy, carrier signals, electromagnetic waves, and signals per se.

To enable user interaction with the computing device 3500, an input device 3590 represents any number of input mechanisms, such as a microphone for speech, a touch-sensitive screen for gesture or graphical input, keyboard, mouse, motion input, speech and so forth. An output device 3570 can also be one or more of a number of output mechanisms known to those of skill in the art. In some instances, multimodal systems enable a user to provide multiple types of input to communicate with the computing device 3500. The communications interface 3580 generally governs and manages the user input and system output. There is no restriction on operating on any particular hardware arrangement and therefore the basic features here may easily be substituted for improved hardware or firmware arrangements as they are developed.

For clarity of explanation, the illustrative system embodiment is presented as including individual functional blocks including functional blocks labeled as a "processor" or processor 3520. The functions these blocks represent may be provided through the use of either shared or dedicated hardware, including, but not limited to, hardware capable of executing software and hardware, such as a processor 3520, that is purpose-built to operate as an equivalent to software executing on a general purpose processor. For example, the functions of one or more processors presented in Figure 35 may be provided by a single shared processor or multiple processors. (Use of the term "processor" should not be construed to refer exclusively to hardware capable of executing software.) Illustrative embodiments may include microprocessor and/or digital signal processor (DSP) hardware, read-only memory (ROM) 3540 for storing software

performing the operations discussed below, and random access memory (RAM) 3550 for storing results. Very large scale integration (VLSI) hardware embodiments, as well as custom VLSI circuitry in combination with a general purpose DSP circuit, may also be provided.

The logical operations of the various embodiments are implemented as: (1) a sequence of computer implemented steps, operations, or procedures running on a programmable circuit within a general use computer, (2) a sequence of computer implemented steps, operations, or procedures running on a specific-use programmable circuit; and/or (3) interconnected machine modules or program engines within the programmable circuits. The system 3500 shown in Figure 35 can practice all or part of the recited methods, can be a part of the recited systems, and/or can operate according to instructions in the recited non-transitory computer-readable storage media. Such logical operations can be implemented as modules configured to control the processor 3520 to perform particular functions according to the programming of the module. For example, Figure 35 illustrates three modules Mod1 3562, Mod2 3564 and Mod3 3566, which are modules configured to control the processor 3520. These modules may be stored on the storage device 3560 and loaded into RAM 3550 or memory 3530 at runtime or may be stored as would be known in the art in other computer-readable memory locations.

Although the present invention has been described in considerable detail with reference to certain preferred versions thereof, other versions are possible. Therefore, the spirit and scope of the appended claims should not be limited to the description of the preferred versions contained herein.

The reader's attention is directed to all papers and documents which are filed concurrently with this specification and which are open to public inspection with this specification, and the contents of all such papers and documents are incorporated herein by reference.

All the features disclosed in this specification (including any accompanying claims, abstract, and drawings) may be replaced by alternative features serving the same, equivalent or similar purpose, unless expressly stated otherwise. Thus, unless expressly stated otherwise, each feature disclosed is one example only of a generic series of equivalent or similar features.

Any element in a claim that does not explicitly state "means for" performing a specified function, or "step for" performing a specific function, is not to be interpreted as a "means" or "step" clause as specified in 35 U.S.C §112, sixth paragraph. In particular, the use of "step of" in the claims herein is not intended to invoke the provisions of 35 U.S.C §112, sixth paragraph.

CLAIMS

What is claimed is:

1. A method of performing gait analysis of a subject, comprising:

obtaining a plurality of measurement sets for a subject, each of the plurality of measurement sets comprising inertial measurements obtained from a sensor device associated with a different one of a plurality of segments of the subject;

calculating a sensor orientation for the sensor device associated with each of the plurality of segments based at least on a portion of a corresponding one the plurality of measurement sets;

computing a segment orientation for each of the plurality of segments based on a data fusion process applied at each of the plurality segments, the data fusion process comprising combining at least a one of the plurality measurement sets and the corresponding sensor orientation to estimate the corresponding segment orientation; and

determining joint angles based on the estimate of the segment orientation for each of the plurality of segments.

2. The method of claim 1, wherein the determining further comprises calculating each one of the joint angles by subtracting the pitch for each of the different segments associated the one of the joint angles.

3. The method of claim 1, wherein the computing comprises performing a Kalman filtering process.

4. The method of claim 3, wherein each of the plurality of measurement sets comprises accelerometer measurements and gyroscope measurements.

5. The method of claim 5, wherein the Kalman filtering process comprises applying a weighting to covariances associated with each of the accelerometer measurements and the gyroscope measurements during the computing based on a motion of the subject, wherein covariances associated with the gyroscope measurements are weighted more heavily if the subject is in motion, else convariances associated with the accelerometer measurements are weighted more heavily.

6. The method of claim 1, further comprising:

obtaining a plurality of additional measurement sets for the subject, the plurality of additional measurement sets comprising load and moment measurements from at least one footpad attached to a sole of a foot of the subject; and

combining the plurality of additional measurement sets to determine limb forces and joint torques for at least one of the plurality of segments.

7. The method of claim 6, wherein the plurality of the additional measurements further comprises inertial measurements for each of a forefoot and a heel of the subject, and wherein the method further comprises repeating the calculating and computing for each of the forefoot and the heel based at least on the plurality of additional measurements.

8. A system for performing gait analysis, comprising:

a processor;

a communications interface configured for receiving a plurality of measurement sets, each of the plurality of measurement sets comprising inertial measurements obtained from a sensor device associated with different one of a plurality of segments of a subject; and

computer-readable medium having stored thereon a plurality of instructions for causing the processor to perform the steps of:

calculating a sensor orientation for the sensor device associated with each of the plurality of segments based at least on a portion of a corresponding one the plurality of measurement sets,

computing a segment orientation for each of the plurality of segments based on a data fusion process applied at each of the plurality of segments, the data fusion process comprising combining at least a one of the plurality measurement sets and the corresponding sensor orientation to estimate the corresponding segment orientation, and

determining joint angles based on the estimate of the segment orientation for each of the plurality of segments.

9. The system of claim 8, wherein the determining further comprises calculating each one of the joint angles by subtracting the pitch for each of the different segments associated the one of the joint angles.

10. The system of claim 8, wherein the computing comprises performing a Kalman filtering process.

11. The system of claim 10, wherein each of the plurality of measurement sets comprises accelerometer measurements and gyroscope measurements.

12. The system of claim 11, wherein the plurality of instructions further comprises instructions for causing the process to perform the Kalman filtering process by applying a weighting to covariances associated with each of the accelerometer measurements and the gyroscope measurements during the computing based on a motion of the subject, wherein covariances associated with the gyroscope measurements are weighted more heavily if the subject is in motion, else covariances associated with the accelerometer measurements are weighted more heavily.

13. The system of claim 8, wherein the communications interface is further configured for receiving a plurality of additional measurement sets for the subject, the plurality of additional measurement sets comprising force and moment measurements from at least one footpad attached to a sole of a foot of the subject; and

wherein the plurality of instructions further comprise instructions for causing the processor to perform the step of combining the plurality of additional measurement sets in a kinematic and kinetic model to determine limb forces and joint torques for at least one of the plurality of segments.

14. The system of claim 13, wherein the plurality of the additional measurements further comprises inertial measurements for each of a forefoot and a heel of the subject, and,

wherein the plurality of instructions further comprise instructions for causing the processor to perform the step of repeating the calculating and computing for each of the forefoot and the heel based at least on the plurality of additional measurements.

15. A sensor for analyzing gait and ground reaction forces, comprising:

a forefoot portion removably attachable to a sole of a subject's forefoot and comprising at least one force sensor;

a heel portion removably attachable to a sole of the subject's heel and comprising at least one force sensor; and

a processing unit communicatively coupled to the forefoot portion and the heel portion and configured for transmitting sensor signals from the forefoot portion and the heel portion to a remote computing device to perform an analysis of the gait of the subject and to compute the ground reaction forces,

wherein at least one of the forefoot portion, the heel portion, and the processing unit comprises at least one inertial measurement sensor.

16. The sensor of claim 15, wherein the at least one sensor of the forefoot portion and the at least one sensor of the heel portion each comprise a multi-axis load and moment sensor.

17. The sensor of claim 15, wherein at least one of the forefoot portion and the heel portion comprises the at least one inertial measurement sensor.

18. The sensor of claim 17, wherein the processing unit is removable attached to the foot of the subject and comprises the at least one inertial measurement sensor.

ABSTRACT

Systems and methods for performing gait analysis of a subject are provided. A method includes obtaining a plurality of measurement sets for a subject, each of the plurality of measurement sets including inertial measurements obtained from a sensor device associated with a different one of a plurality of segments of the subject and calculating a sensor orientation for the sensor device associated with each of the plurality of segments based at least on a portion of a corresponding one the plurality of measurement sets. The method also includes computing an estimate of a segment orientation for each of the plurality of segments based on a data fusion process applied at each of the plurality of segments, where the data fusion process includes combining at least a one of the plurality measurement sets and the corresponding sensor orientation to estimate the segment orientation.